Master Thesis, Department of Geosciences

Petrology and Sedimentary Provenance of Mesozoic and Cenozoic sequences in the Mandawa Basin

Kristine B. Nerbråten

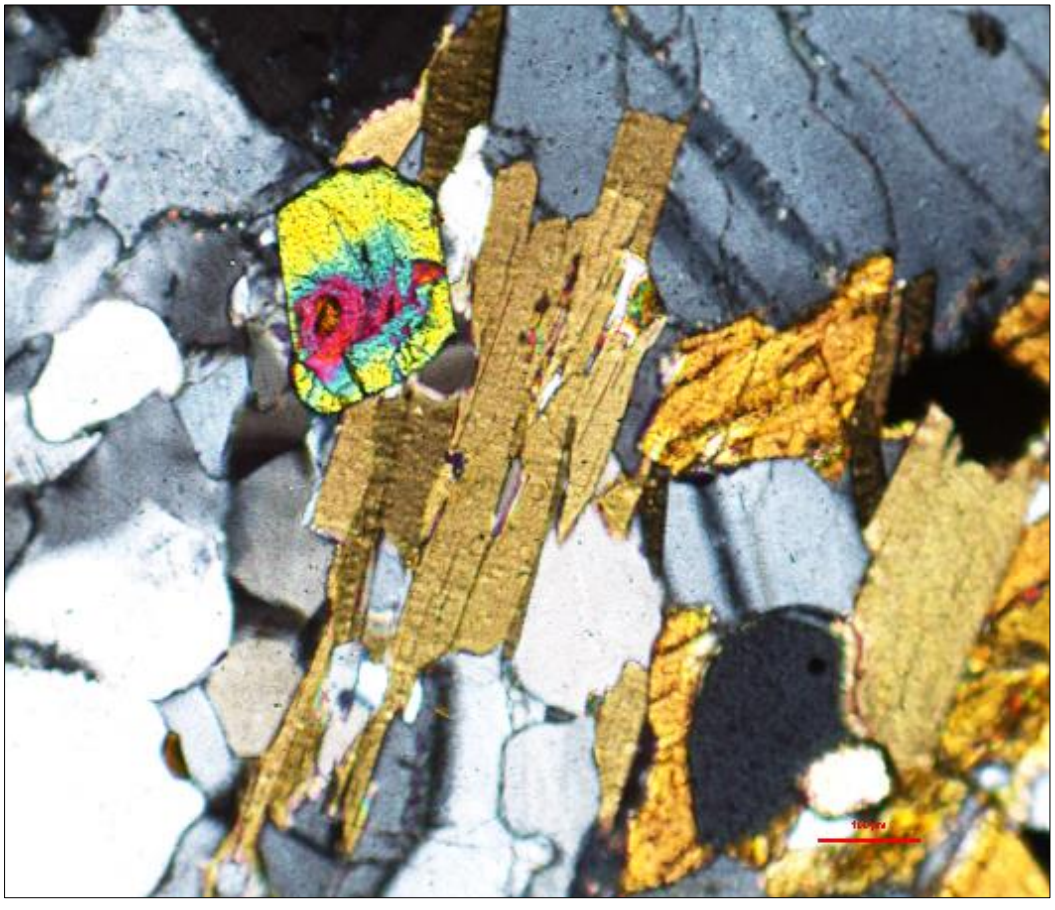

UNIVERSITY OF OSLO

FACULTY OF MATHEMATICS AND NATURAL SCIENCES

Petrology and Sedimentary Provenance of Mesozoic and Cenozoic sequences in the Mandawa Basin

Kristine B. Nerbråten

Master Thesis in Geosciences

Discipline: Geology

Department of Geosciences

Faculty of Mathematics and Natural Sciences

University of Oslo

June 2nd, 2014

Acknowledgement

First, I would like to thank my supervisor, Henning Dypvik, for his support throughout this thesis and for letting me take part of the Mandawa Basin Project. You have guided me in the right directions and motivated me when I needed it. You have always triggered my scientific curiosity and inspired me to learn more.

I would also express my gratitude to everyone involved in Mandawa Basin Project and especially my co- supervisor Arild Andresen and PhD student, Katrine Fossum. Katrine has been a great help through this thesis with her assistance during field work and her help and guidance during the following analysis. Thanks to Ellen Gundersveen and Orhan Mahmic for good teamwork and helpful input and contributions.

I would like to thank Mogens Ramm and Statoil International for financial support for the Mandawa Basin Project, for showing interest in our work and giving us access to samples from Block 2.

Erik Holtar in Statoil Tanzania also deserves thanks for his great expertise and help during our stay in Tanzania.

Thanks to Maarten Aerts for running XRD analysis, Berit Løken Berg for her good help when carrying out SEM analysis, Muriel Marie Laure Erambert for her great expertise end assistance during EMP analysis and the following calculations and thanks to Andrew Morton for conducting the convential heavy mineral analysis and for helping me with all my questions.

Finally I would like to thank my supportive family and my wonderful partner, Erik Zakariassen. He has been really helpful during this year, making geological maps for the project, reading through and correcting my thesis and for being patient and supportive at all times.

Abstract

Mandawa Basin in coastal Tanzania was formed as a result of tensional forces related to the Gondwana break-up and the opening of the Indian Ocean. Mandawa Basin has been influenced by transgressive and regressive phases which have led to deposition of various sedimentary sequences from Late Triassic to recent age. These sedimentary sequences have been deposited in different depositional environments, from alluvial fans proximal to source area to deep marine, distal environments. The sedimentary sequences display various mineralogical and textural compositions and heavy mineral contents. Offshore sediments from Statoil, Block 2, display comparable petrography and heavy mineral content to corresponding onshore sediments.

Conventional heavy mineral analysis, heavy mineral ratios and electron microprobe analysis are all tools for reconstructing the provenance of a sedimentary sequence. The heavy mineral assemblages in Mandawa Basin are influenced by several different processes, such as transport, weathering and diagenesis, which can alter the compositions of the heavy minerals assemblages to the point where they no longer reflect the true composition of the source area. The composition of heavy minerals then indicate the stability of different heavy minerals and the different degrading processes acting on the sediment, thus complicating the interpretation and identification of provenance. Heavy mineral ratios and single grain analysis are tools which provide a better reflection of the true source rock mineralogy and are to a less degree affected by processes that alter the heavy mineral assemblages. Heavy mineral assemblages and the electron microscope analysis of garnet point towards a sedimentary input from the Mozambique Belt, west of Mandawa Basin.

To provide a link between the sedimentary sequences and the source areas, information regarding source rock mineralogy is needed. Samples from different basement lithologies as well as sediments from rivers draining specific source areas are necessary if such a link is to be made.

Large river systems in Tanzania which drain and transport sediments from several source areas, and the possibility of reworked sediments, provide a further challenge when trying to reconstruct the sedimentary provenance.

Contents

1 Introduction

This master thesis addresses questions of sedimentary provenance in Mandawa Basin and the offshore areas of Statoil, Bock 2. The main goal is to give a petrographical description of selected sedimentary formations from and to identify the provenance of these sedimentary units by using heavy mineral analysis. Sedimentological description will be presented and discussed briefly to provide a more complete context of the analyzed sedimentary sequences. The study contributes to the questions concerning the source to sink relationship in the Mandawa Basin.

This thesis is part of a four year (2013- 2017) international research project, named Mandawa Basin Project (MBP). The Mandawa Basin Project is organized by University of Dar Es Salaam (UDSM), Department of Geosciences at University of Oslo (UiO) and Tanzania Petroleum Development Corporation (TPDC) in cooperation with Statoil. The aim of the project is to disclose the sedimentary and structural history of the Mandawa Basin in order to better understand the stratigraphical developments, sediment formation and transportation as well as sediment provenance. The final goal of the project is to compare onshore studies with available core material from offshore sites (Statoil), to tie land and offshore geology. Scientist from UDSM, UiO and TPDC along with master students and PhD students from both universities are involved in this project.

During two weeks of fieldwork, five outcrops and six cores were logged, studied and sampled. Key samples from both outcrops and cores has been selected and studied in detail to provide information related to sedimentology, petrography and sedimentary provenance in the Mandawa Basin. Two offshore samples from Statoil, Block 2, were studied and compared with samples from Mandawa Basin to better understand the offshore- onshore relations.

1.1 Study area

The Mandawa Basin is located in the southern part of coastal Tanzania (Figure 1.1). The basin evolved during Permian age, when Madagascar was drifting away from the African continent (Hudson, 2011). Mbede (1991) studied and categorized the sedimentary basins in Tanzania in an attempt to synthesize a geodynamic model of the basins and their origin related to the tectonic setting. She classified the Mandawa Basin as a coastal basin based on the tectonic setting, form and basin infill. She also suggested that the subsidence of the basin was mainly controlled by isotactic subsidence during the rifting stage and by thermal subsidence as the newly generated crust cooled down.

1.2 Previous work

Mandawa Basin has been explored by several oil companies and research groups since the early 1900`s. The different oil companies which have been active in the Mandawa Basin since the 1950`s have acquired much geological information from well drillings and seismic surveys, but their studies are often confidential and in restricted internal reports (Hudson, 2011). The open scientific studies that have been published on the other hand, have resulted in a better understanding of the geological evolution of the Mandawa Basin. Early fossil studies in the Tendaguru area contributed to establishing the stratigraphy in the basin. Kent et al. (1971) conducted a detailed study of the coastal basins in Tanzania which provided further information with regards to the sedimentary history and tectonic evolution. The Tanzania Drilling Project (TDP) was a project which focused on marine sediments of Cretaceous and Paloegene age (Pearson et al., 2006). The TDP studies involved drilling and coring of several boreholes in the Mandawa Basin and some of these cores have been subjects of study during this master thesis.

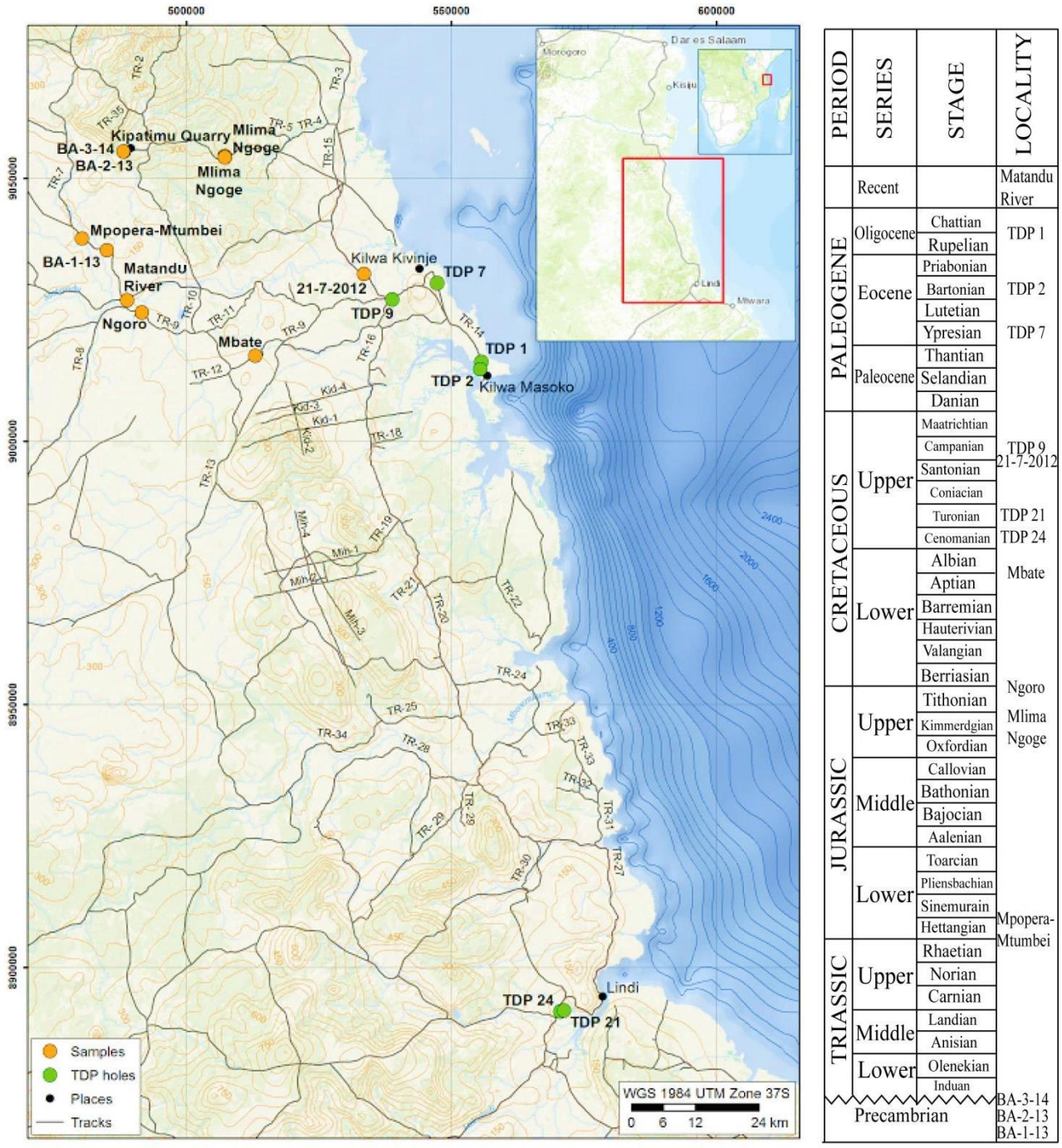

Figure 1.1: *Map of the study area with stratigraphic column. The marked localities in the map and stratigraphic column represent sedimentary formations which are emphasized in this thesis. Mpopera Mtumbei locality represents Karoo sedimentary sequences, Mlima Ngoge is the locality of Upper Kipatimu Member, Ngoro represent Upper Mitole Member and Mbate is the locolaity of Makonde Formation. TDP localities represent well sites of logged TDP cores. Matandu River is a locality were recent river sediments were sampled. Locality BA-1-13, BA-2-13 and BA-3-14 represent basement samples while locality 21-7-2012 represents a sample from Nangurukuru Formation. Modified by Zakariassen (2014) from Esri (2014).*

2 Geological setting

The geological history of East Africa and Tanzania is highly influenced by the extensional tectonic style created by the drifting of continental plates. Continental drifting lead to rifting along the east African coast and the development of sedimentary basins in Tanzania (Mpanda, 1997). A small introduction to the formation and development of the basement rocks during Precambrian age in Tanzania is presented in chapter 2.2. The tectonic and sedimentary evolution of the east African coast and the Mandawa basin is presented in chapter 2.3.

2.1 Geology of Tanzania- formation of basement rocks

Archaean

The Precambrian of Tanzania comprises rocks of igneous, sedimentary and metamorphic origin and is called the Tanzania Craton (Figure 2.2). Tanzania Craton is essentially composed of Archaean rocks with distinct schist belts surrounded by a large granitoid-migmatite-gneiss terrane. The schist belts that are incorporated in the Tanzania Craton are the Dodoman, Nyanzian and Kavirondian System (Schlüter and Hampton, 1997).

The *Dodoman System* comprises the Dodoma schist belt and the surrounding granitiod rocks (Figure 2.2). The granitoid rocks have been dated with K:Ar and Rb:Sr isotopes that indicated ages between 2230 and 3700 My (Figure 2.1) (Schlüter and Hampton, 1997). The rocks comprising the Dodoman System have experienced metamorphism ranging from amphibolite to granulite facies (Schlüter and Hampton, 1997) and are located in the western part of central Tanzania. The Dodoma schist belt is a series of elongated greenstone belts and located east of the granitoid rocks of Tanzania Craton. This belt is highly metamorphosed and consists of metasediments and metavolcanics (Bell and Dodson, 1981). The Dodoma Schist Belt is considered to be older than 2700- 2300 My according to McConnell (1972), but detailed isotope dating of the components of the Dodoma Schist belt have not been obtained.

The *Nyanzian System* is located in areas east of Lake Victoria and occurs as irregular, rounded or horseshoe- shaped areas (Schlüter and Hampton, 1997). The rocks of the Nyanzian System consist of basic and siliceous volcanics with banded ironstone. These rocks have been exposed to a lower degree of metamorphism unlike the older rocks of the Dodaman System

(Bell and Dodson, 1981). The age of the Nyanzian System is considered to range between 3000 and 2500 My (Figure 2.1) (Schlüter and Hampton, 1997).

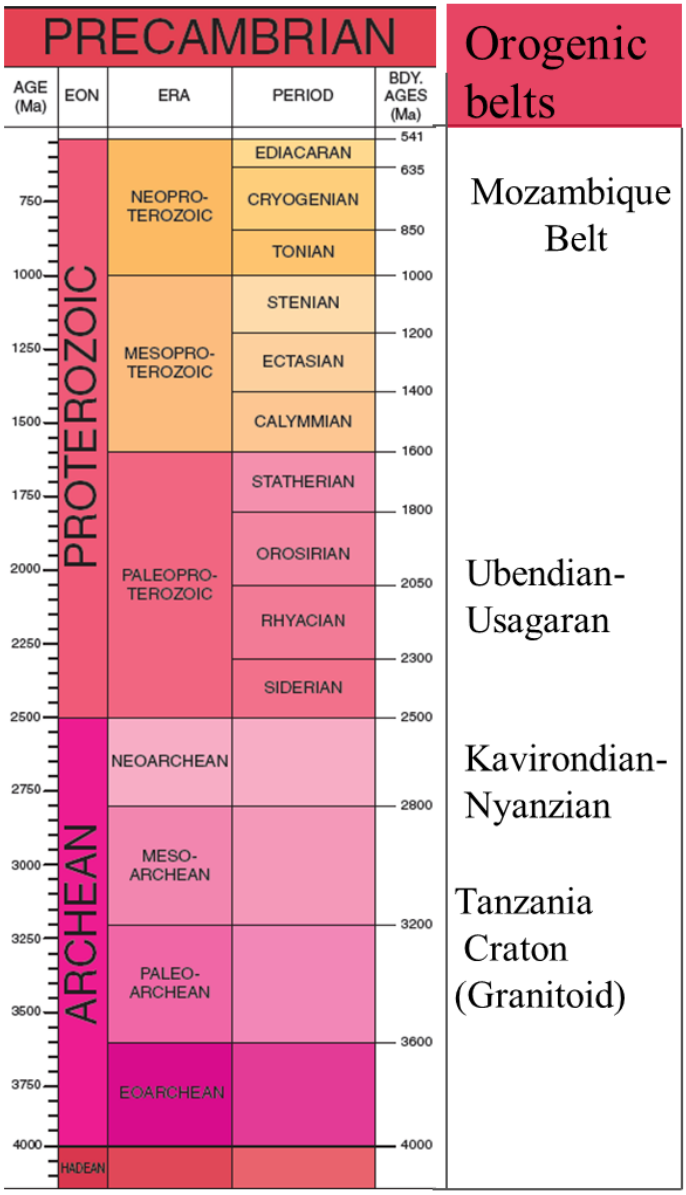

***Figure 2.1**: Stratigraphical overview of the Precambrian orogenic belts in Tanzania. The ages of Dodoman Schist Belt are not known, but are believed to be older than 2700 and 2300My according to McConnell (1972). Ages of the orogenic belts are based on K:Ar and Rb:Sr dating by different researchers, discussed in Schlüter and Hampton (1997). Modified from GSA (2012).*

The rocks of the *Kavirondian System* are essentially of sedimentary nature and appear as a coarse and conglomeratic unit. These rocks lie unconformably over the Nyanzian System and their outcrops are limited to the Musoma region east of Lake Victoria (Schlüter and Hampton, 1997). Cahen and Snelling (1984) suggested a ~2500 My age of the Kavirondian rocks based on K:Ar dating of mica (Figure 2.1).

Proterozoic

The *Ubendian Belt* is a part of a large Paleoproterozoic orogen developed around the Archean Tanzania Craton (Lenoir et al., 1994). The orogenic belt has a NW-SE trend and forms the southwestern margin of the craton (Figure 2.2) (Schlüter and Hampton, 1997). It has undergone different phases of deformation and is characterized by high- grade metamorphic rocks such as biotite and granitic gneisses and schist containing garnet and mica (Lenoir et al., 1994). The peak of the Ubendian metamorphism is estimated at being 2050 My old (Figure 2.1), while the entire cycle of metamorphism occurred from 2500 to 1800 Ma (Schlüter and Hampton, 1997).

The *Usagaran Belt* forms the southeastern part of the Tanzania Craton, adjacent to the Mozambique Belt in the north (Figure 2.2). It is composed of two major lithological units; the sedimentary- volcanic Konse Group and the gneissic- amphibolitic Ismani (Schlüter and Hampton, 1997). The eclogite facies rocks in the Ismani Suite marks the area of an ancient subduction zone in East Africa during the Paleoproterozoic age (Möller et al., 1995). The deformation in the Usagaran Belt is considered to fall in the same general time range as the rocks involved in the Ubendian Belt (Figure 2.1) (Schlüter and Hampton, 1997).

The mobile *Mozambique Belt* is located around the eastern part of the Tanzania Craton (Figure 2.2). This belt represents the most extensive zone of crustal mobility in the African continent. The rocks comprising the Mozambique Belt were subjected to metamorphism during a continent- continent collision of Late Paleoproterozoic age (Muhongo and Lenoir, 1994). There are a wide variety of lithologies present in the Mozambique Belt, ranging from granulite to greenschists facies (Schlüter and Hampton, 1997). Andriessen et al. (1985) suggested that the main high grade deformation occurred around 750 My ago (Figure 2.1)

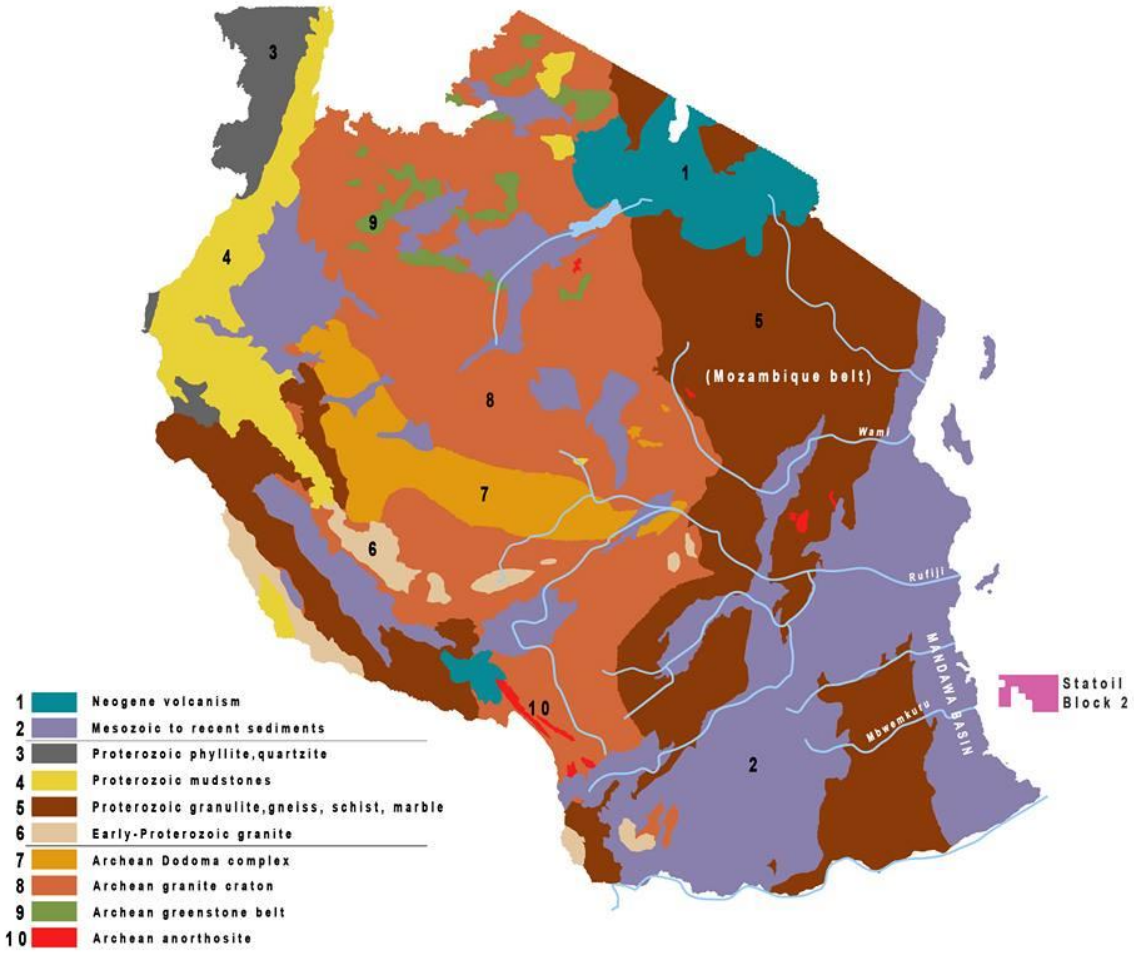

Figure2.1*: Geological map of Tanzania. Tanzania Craton comprises the Archean granites (8), Arcean greenstone belt (9) and Archean Dodoma complex (7). Ubendian Belt comprises the Proterozoic granulite, gneiss, schist and marble (5) which is located southwest of the Tanzania Craton. Usagaran Belt comprises similar lithologies (5), but is located southeast of the Tanzania Craton and adjacent to the Mozambique belt. Modified from (GOVERNMENT OF THE UNITED REPUBLIC OF TANZANIA) by Mahmic (2014).*

2.2 Tectonic evolution and sedimentary infill sequences of Mandawa Basin

Upper Carboniferous- Lower Jurassic- Karoo rifting event

The break-up of the Gondwana continent was preceded by a long period of continental rifting (Hankel, 1994). This rifting event started in the Late Carboniferous (Mpanda, 1997) and

tensional conditions developed along the coast of Tanzania during Permian time (Kent et al., 1971). The rifting initiated as a result of a regional doming caused by thermal expansion and convective upwelling. This tectonic activity resulted in faults, grabens and basinal structures which controlled the deposition of sediments during this period (Mbede, 1991). The first cycle of sedimentation created the sedimentary successions described as Bobukan rocks and was deposited in basinal depressions during the Precambrian to Early Paleozoic age (Figure 2.2). Apart from this early cycle of sedimentation, the sedimentary successions of Tanzania are considered to have started with the deposition of the Karoo. The Karoo sediments (Figure 2.4 and 2.5) are the oldest sediments encountered in the Mandawa Basin and include sediments deposited during Late Carboniferous to Early Jurassic age (Kreuser et al., 1990). The continued doming and heating of the lithosphere contributed to thinning of the crust (Mpanda, 1997) and episodes of igneous activity at a later stage (Cox, 1992). The elevated areas were eroded and the sediments were deposited in the adjacent basins by a number of sedimentary cycles.

Mid Jurassic to Late Cretaceous – Gondwana breakup

The age of the Gondwana break-up has been highly debated and many studies have been dedicated to reconstructing the timing and location of this event (Norton and Sclater, 1979, Coffin and Rabinowitz, 1987, Gaina et al., 2013). The Karoo rifting event, which preceded the Gondwana break -up, created zones of weaknesses which are assumed to have influenced the locations of rifting during the breakup of the Gondwana continent (Mpanda, 1997). The separation of the continents contributed to a marine influence and restricted marine environments in the Mandawa Basin during Late Triassic to Early Jurassic. According to Coffin and Rabinowitz (1987), Madagascar, India and Antarctica started to drift apart from the African continent during Mid Jurassic age, along spreading axes (Figure 2.3). The sea transgressed further into the Mandawa Basin and created a shallow marine environment where sequences of carbonates were deposited. Fluvial sequences such as Upper Kipatimu Member (Mb), Upper Mitole Member (Mb). and Makonde Formation (Fm) (Figure 2.4 and 2.5) were deposited in the basin during Late Jurassic to Mid Cretaceous before the transgression created fully marine conditions (Hudson, 2011). The Indian plate started to drift northwards along the eastern Madagascar margin during Mid Cretaceous (Gaina et al., 2013). According to Mpanda (1997) the movement of Madagascar relative to Africa ceased in late Cretaceous while the Indian plate continued to move relative to Madagascar.

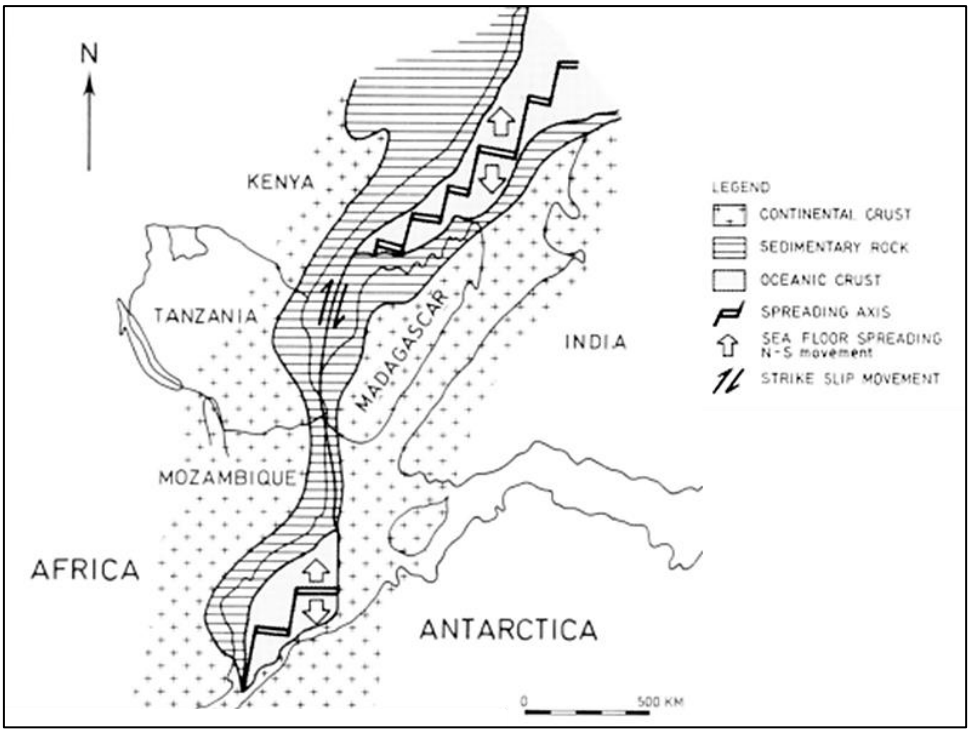

***Figure 2.3**: The positions of continental plates during Late- Mid Jurassic and the opening of the Indian Ocean during an early stage of the Gondwana breakup. The rifting took place along a strike- slip fault called the Davie Fracture Zone (DFZ) and the drifting of the continents took place along spreading axes (Mpanda, 1997).*

Upper Kipatimu Mb. (Figure 2.4 and 2.5) was, according to Hudson (2011), deposited during Late Jurassic age. He suggested a fluvial/deltaic depositional environment for the Late Kipatimu Mb. where the large river systems of Rufiji and Matandu River may have acted as transport agents.

Upper Mitole Mb. (Figure 2.4 and 2.5) is a fluvial sedimentary succession which was deposited during Late Jurassic to Early Cretaceous age. The Upper Mitole Mb. was deposited above shallow marine sediments of the Lower Mitole Mb., indicating a phase of regression during Late Jurassic age (Hudson, 2011).

Makonde Fm. was deposited during Mid Cretaceous contemptuously with Kiturika Fm. and Kihuluhulu Fm. (Figure 2.4 and 2.5). The Makonde Fm. was, according to Hudson (2011), deposited in a fluvial/ deltaic environment, while Kiturika Fm. was deposited in a shallow marine environment during the same time period. Kihuluhulu Fm. consists of clay and represents a shelf environment during the same time period as the deposition of Makonde and Kiturika Fm. (Hudson, 2011).

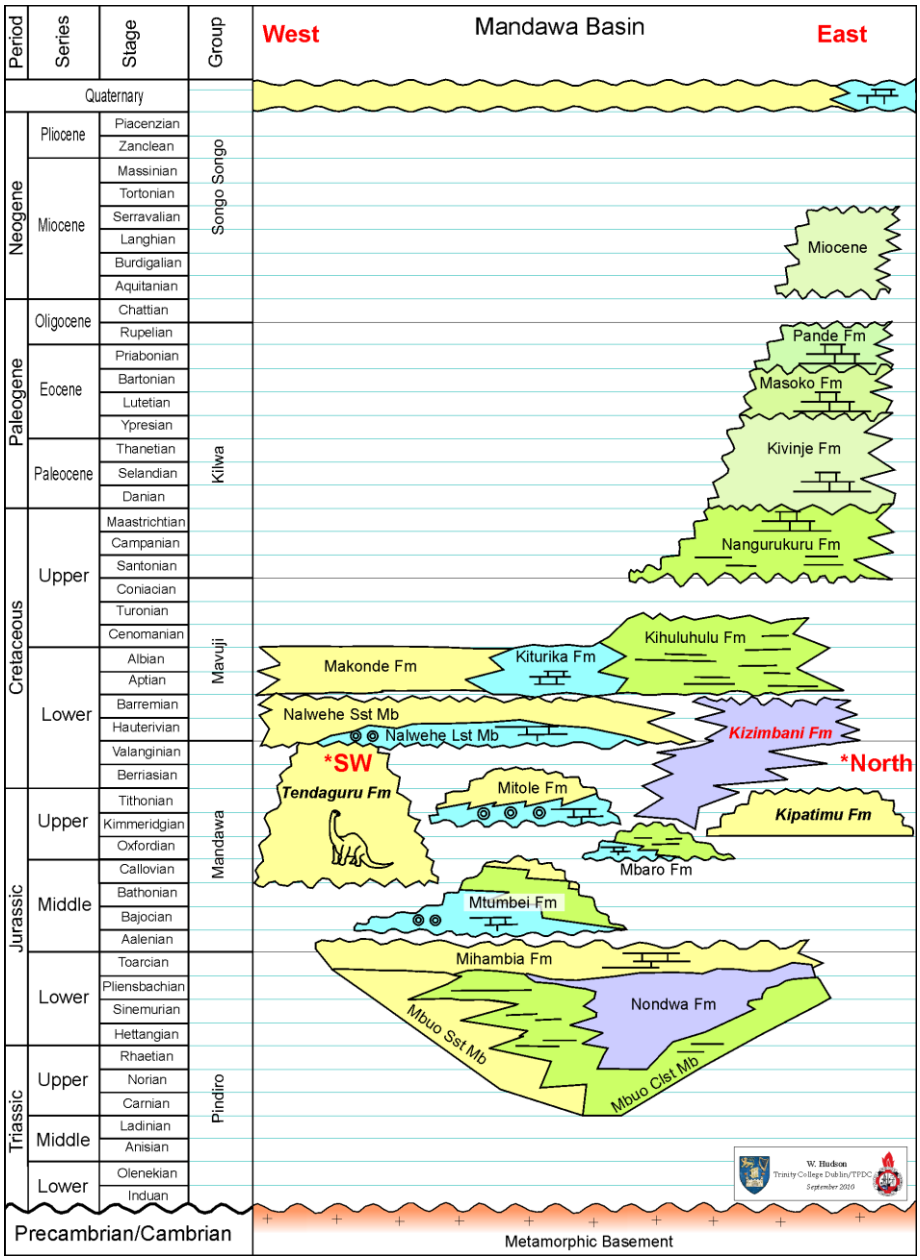

***Figure 2.4**: Stratigraphical sequences in Mandawa Basin. The Pindiro group comprises sequences which are referred to as Karoo deposits (Hudson, 2011).*

Late Cretaceous to Early Oligocene- Marine conditions

Late Cretaceous to Oligocene age was characterized by marine conditions in the Mandawa Basin. This was a calm period where large sequences of marine clays with reef carbonates were deposited. Four sedimentary formations were deposited during this time period (Nangurukuru, Kivinje, Masoko and Pande Fm.) which represent the Kilwa Group (Figure 2.4 and 2.5) (Hudson, 2011). The present East African Rift System was initiated during Early Tertiary age (Mpanda, 1997) and contributed to an increased subsidence of the Mandawa

Basin. This led to a renewal of accommodation space and deposition of thick clay sequences (Nicholas et al., 2007).

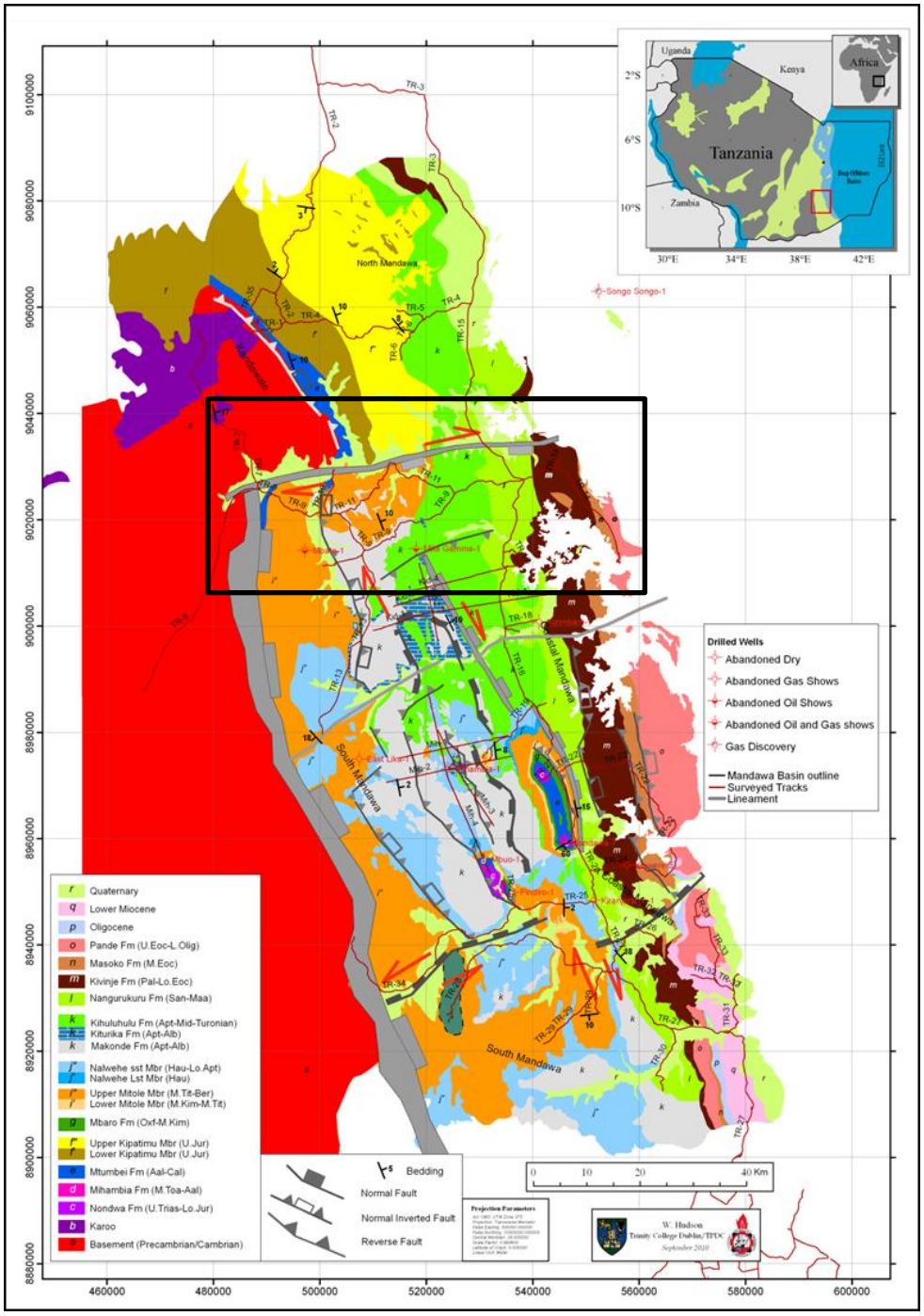

Figure 2.5*: Map of stratigraphical units in the Mandawa Basin. Marked section indicates the studied part of the basin during field work in 2013. Modified from Hudson (2011).*

Early Oligocene to Recent – Regression and igneous activity

The time period from late Oligocene to Recent age represent a regressive phase in the Mandawa Basin (Hudson, 2011). The East African Rift System contributed to a period of volcanism during Neogene age, in the northern part of Tanzania (Figure 2.1). The rifting also led to a significant uplift and erosion of the Tanzania Craton.

Offshore Tanzania

The coastal areas of Tanzania and the Somali basin are characterized by extensional tectonics and are dominated by faults oriented parallel to the present coast line. The normal faults which dominate the offshore regions are considered to be of post- Karoo age and rejuvenated by older faults (Mpanda, 1997). During the formation of the Indian Ocean, extensive volumes of sediments were transported from the African Craton and deposited in the newly formed accommodation space (Bourget et al., 2008). These sediments were deposited in depression structures in the basement and form finely stratified sedimentary sequences in the abyssal plain in the southern part of Western Somali Basin (Bunce et al., 1967).

3 Method

3.1 Core logging and sampling

Core logging was executed from 18.09.13- 24.09.13 at the TPDC storage unit in Dar es Salaam. The cores were logged and studied in collaboration with two master students from University of Oslo, Ellen Gundersveen and Orhan Mahmic, a PhD student from University of Oslo, Katrine Fossum and a PhD student of University of Dar es Salaam, Justina Saroni. The logging was supervised by Henning Dypvik. Cores from six TDP well sites were logged on standard log sheet at a scale of 1:50. The cores were divided by TDP into sections of 1 m (Figure 3.1). The well sites were logged from the deepest core and up towards the present day sediments. The deepest part of the well site is marked as the baseline in the logs. The maximum "depth" in the logs therefore represents present day sediments. The samples were named as follows: TDP core site/ Core- Section- Meter within section. Example: TDP 7B/45/2- 20-22cm.

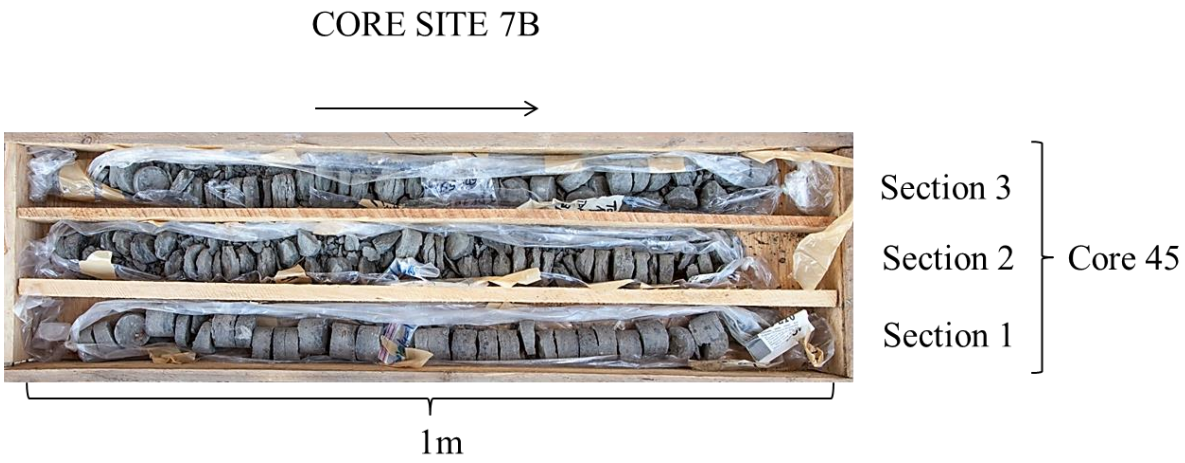

Figure 3 .1*: This figure is an example displaying 3 individual 1m length sections of core 45, well site 7B.*

3.2 Field work and sampling

The field work was executed from 26.09.13- 29.09.13, in the northern and central parts of the Mandawa Basin (Figure 1.1 and 2.4). The field work was conducted in collaboration with the same group as previously mentioned, with additionally two master students from TPDC. Henning Dypvik and Charles Kaaya supervised the logging and sampling conducted by the

group. Six localities were logged and sampled during the field work and only key localities are presented in this study. In some localities, two sections were logged; section 1 was located stratigrafically below section 2 (Figure 3.2). The sections were logged by different groups, to provide a more extensive coverage of the stratigrafical unit. At the Mlima Ngoge locality (Figure 1.1), section 1 was located strategraphically above section 2 due to the order with which they were logged. Some sedimentary formations were studied at two different localities. The logged sections from these localities are included in the same log; section 1 is located stratigraphically below section 2. The age gap between the two sections can be unknown. Samples taken from field localities are named as follows: Initials of locality- section- number of sample- year. The first sample from the first section at Ngoro locality (Figure 1.1 and 3.2) is named NG-1-1-13. Two of the samples in this study were sampled during previous field trips in 2012 and 2014. BA- 3- 13 was sampled in February 2014 by Arild Andresen during fieldwork near the Kipatimu Quarry locality (Figure 1.1). Sample 21-7-2012 was sampled by Henning Dypvik and Arild Andresen during a reconnaissance field trip in 2012.

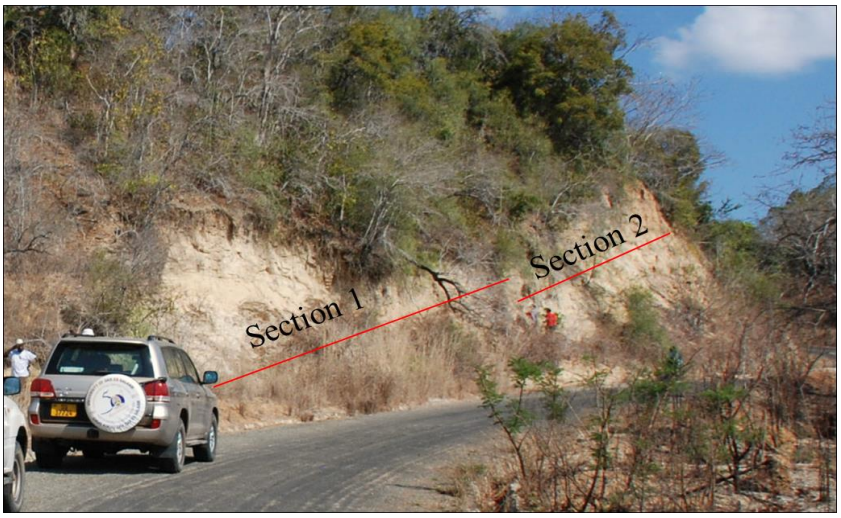

Figure 3.2: *The locality of the Upper Mitole Mb. was divided into two sections to provide a more extensive coverage of the stratigraphical unit. Section 1 is located stratigraphically below section 2.*

3.3 Offshore samples

The offshore samples studied in this thesis derive from Statoil, Block 2, approximately 80 km off the coast of southern Tanzania (Figure 3.3) (Statoil, 2014). The studied samples comprise sand of Cenomanian and Paleocene age.

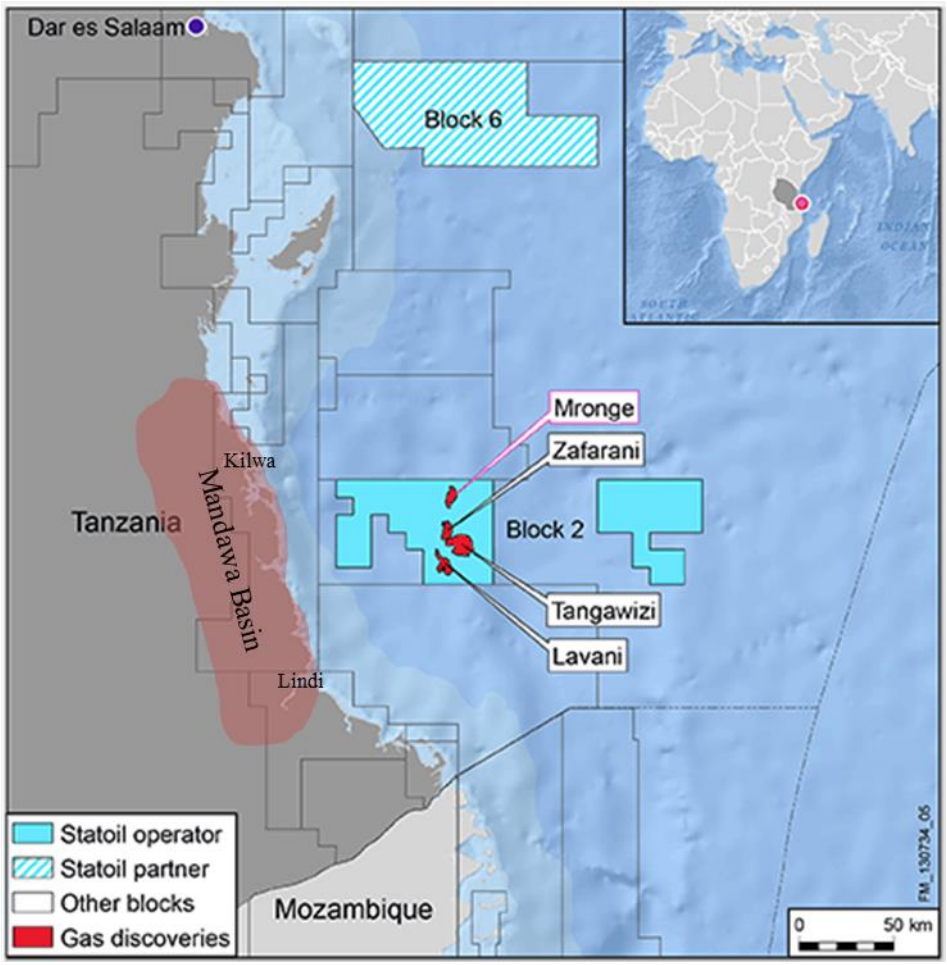

***Figure 3.3**: Statoil, Block 2 is located approximately 80 km off the coast of Mandawa Basin. Samples from Block 2 of Cenomanian and Paleocene age were studied and compared with samples from Mandawa Basin. Modified from Statoil (2014).*

3.4 Facies and facies association

Facies are bodies of rocks characterized by specific features which differentiate them from bodies of rocks above, below and laterally adjacent. The specific features of a facies consist of a combination of lithological, physical and biological structures. When several facies are

genetically related to one another they form a facies association (Walker, 1992). Observations during core logging, field work and laboratory analysis of thin sections were used to define facies and facies associations based on lithology and sedimentary and biogenic structures. The facies and facies association are divided between field outcrops and cores. The field outcrops have been subjected to sub- aerial weathering which has altered the mineralogy and the appearance of the rocks. Samples from TDP well sites have not been subjected to similar weathering processes and structures and minor lithological changes are more easily identified in these well preserved cores. Samples from TDP well sites were deposited in marine environments while sediments from selected field outcrops represent alluvial deposition. The differences in appearance, depositional environments and processes acting on the sediments form the basis of the division between core and outcrop facies. This thesis only describes the facies and facies associations for selected sections of the sedimentary logs. The Wentworth grain size classification (Table 3.1) was used to determine the grain sizes.

3.5 Digitalizing of sedimentary logs

The sedimentary logs from field outcrops and cores were digitalized in collaboration with Gundersveen (2014) and Mahmic (2014). The logs were digitalized by the use of Adobe Illustrator.

3.6 Petrographical and mineralogical analysis

26 key samples were selected for heavy mineral analysis (Table 3.4). These samples were analyzed by XRD and optical microscope to provide mineralogical and petrographical information which could, in combination with heavy mineral analysis, enhance our understanding of the provenance of Mandawa Basin sediments. This thesis only present the petrological and mineralogical composition of these selected samples and results associated with these.

***Table 3.1**: Wenthworth grain size classification for clastic sediments (Wentworth, 1922).*

Size range (mm)	Phi unit	Wentworth size class
>256	-8	Boulder
64-256	-6	Cobble
4-64	-4	Pebble
2-4	-2	Granule
1-2	-1	Very coarse sand
0.5-1	0	Coarse sand
0.25-.05	1	Medium sand
0.125-0.25	2	Fine sand
0.063-0.125	3	Very fine sand
0.004-0.063	4	Silt
<0.004	8	Clay

3.6.1 Thin sections

A total of 98 thin sections, from field and core samples, were produced by Lars Kirksæther at IFE Petrosec. The samples were impregnated with blue epoxy and glued to a 2,5cm* 4,5cm slide. The slide was then polished down to a thickness of 30μm. Four thin sections were produced by Salahalldin Akhaven at Department of Geoscience, University of Oslo.

3.6.2 Point counting and petrographical descriptions

25 of the total 102 thin section were point counted and described in detail with regards to petrography. Point counting was performed with a Nikon light microscope and a Swift automatic counter. 400 points were counted in each thin section. The mineralogy encountered during point counting was separated into twelve main categories; 1) Quartz, 2) K-feldspar, 3) Plagioclase, 4) Clay matrix, 5) Carbonate cement, 6) Porosity, 7) Pyrite, 8) Heavy minerals, 9) Mica, 10) Rockfragments, 11) Overgrowth, 12) Fe-Oxide. The category of quartz was

differentiated further based on crystallinity and extinction. The category of K- feldspar and plagioclase were also classified based on the degree of preservation (Table 3.2). Point counting was performed in collaboration with Gundersveen (2014). Table with complete point counting results are presented in Appendix B.

***Table 3.2**: Five categories of feldspar preservation. Examples display the characteristic features in plan polarized light (PPL) and cross polarized light (XPL) for the five categories.*

Category	**1**	**2**	**3**	**4**	**5**
Description	Fresh, has not been subjected to weathering	Subjected to some weathering. Twins are almost fully preseved	Twins start to look blurry. Grain surface show evidence of etching	Very rough surface. Twins are difficult to recognize	Twins are absent. Only parts of the grain is preserved. Difficult to recognize the mineral.
Example PPL	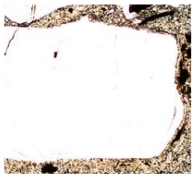	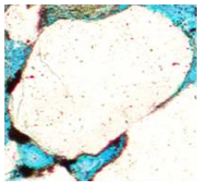	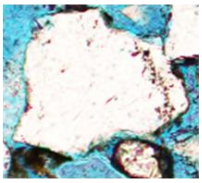	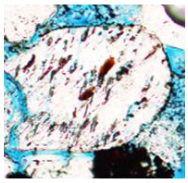	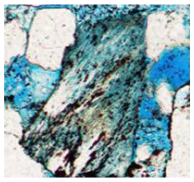
Example XPL		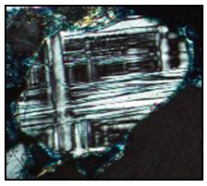	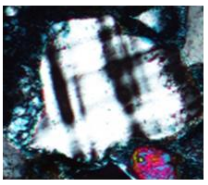	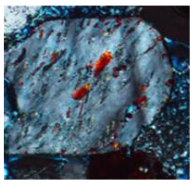	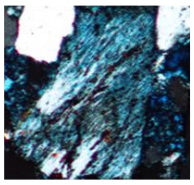

The 25 thin sections were studied in a Nikon light microscope to provide petrographical descriptions of the samples. When studying the thin sections, characteristic textural features were described. The mineral content was identified and a quantitative estimation of the different components in the thin section was performed. Minerals were separated between authigenic and detrital origin. Results and products of weathering and diageneitic processes were identified and the relations between the different minerals and mineral phases were attempted established. Diagenetic processes and relations between mineral phases are less emphasized in this study, but are more thoroughly described by Gundersveen (2014). The preservation of the minerals was noted and feldspar grains were classified by the degree of preservation (Table 3.2). The grain size was estimated by measuring the average of ten grains.

Further, sorting, shape, porosity and the nature of the grain contacts were described. Grain shape was determined by Power`s (1953) terminology for degree of grain roundness (Figure 3.3). The range of sorting proposed by Compton (1962) was used to determine the sorting of the sediment (Figure 3.4).

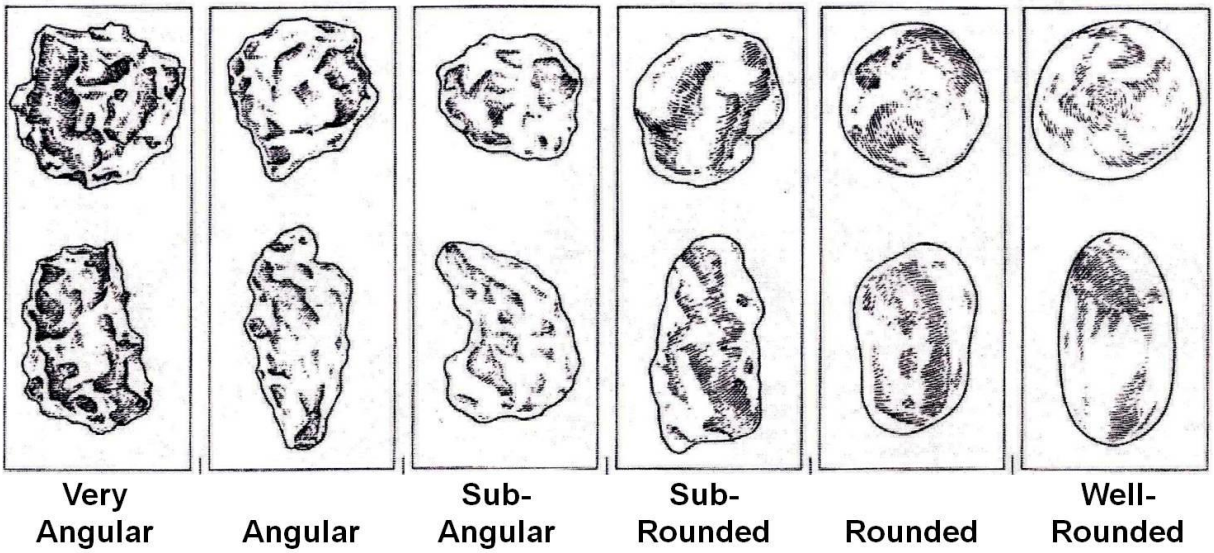

***Figure 3.3**: Roundness scale terminology for sedimentary particles (Powers, 1953).*

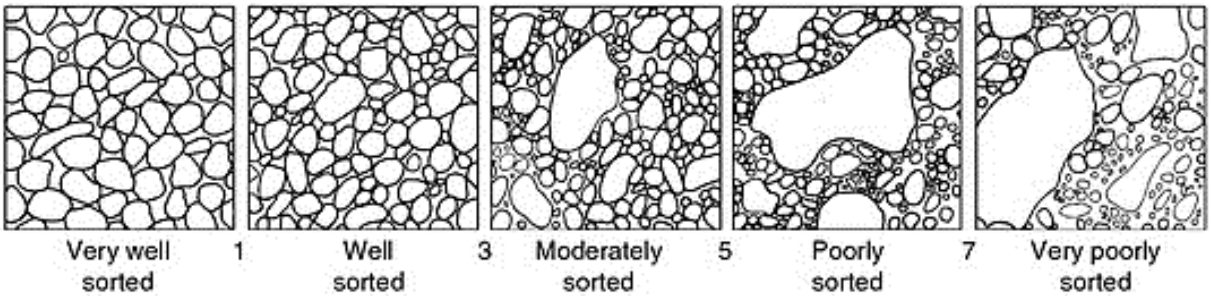

***Figure 3.4**: The range of sorting proposed by Compton (1962)*

The point counted samples were classified in a classification diagram by Miall (2003), based on the mineralogical composition (Figure 3.5). Classification results are presented in Appendix C.

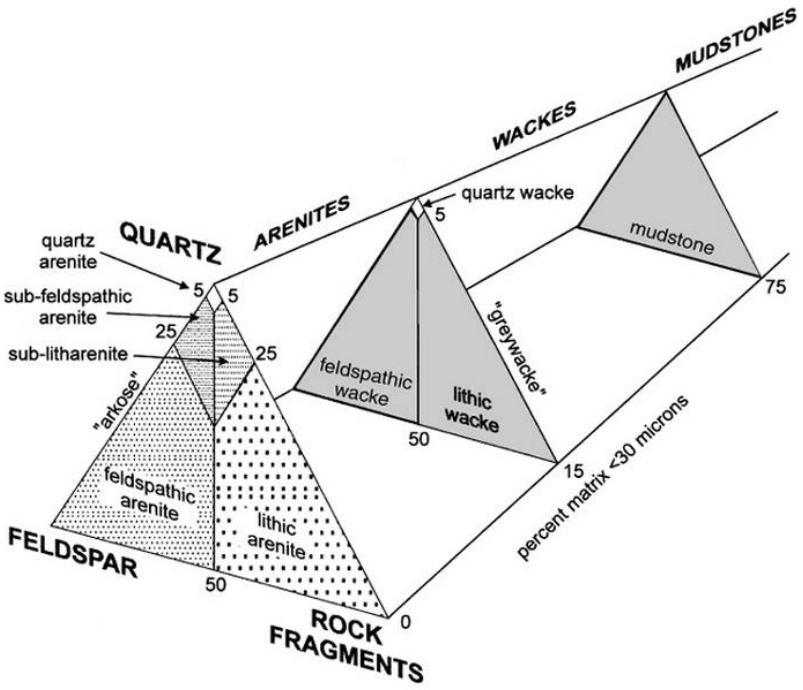

Figure 3.5*: Classification of sand and sandstone according to composition. The classification diagram is modified from Dott (1964) by Miall (2003).*

3.6.3 Scanning Electron Microscopy (SEM)

Twenty thin sections from key samples were studied using scanning electron microscope (SEM) at Department of Geoscience, University of Oslo. The scanning electron microscope was used to identify heavy minerals and to get more detailed observations of surface structures on the grains. The SEM analysis was conducted using a JEOL JSM-6460LV Scanning Electron Microscope, with LINK INCA Energy 300 (EDS) from Oxford Instruments, and was supervised by Berit Løken Berg. The JEOL JSM-6460 LV uses a standard wolfram filament (15Kv). The microscope has detectors for secondary-electron images (SEI), back-scattered electron images (BEI), cathodoluminescens (CL) and X-Ray detectors for element determination and element mapping.

3.6.4 X-ray diffractometry (XRD)

75 core samples and 52 field samples were analyzed by XRD at Department of Geoscience, University of Oslo. The analyses were conducted by Maarten Aerts with a Bruker D8 Advance, equipped with a Lynxeye linear PSD detector. The samples were prepared for

analysis in collaboration with Gundersveen (2014) and Mahmic (2014). A slinging mill and a McCrone micronizer were used to crush the samples to powder. The slinging mill and micronizer were carefully cleaned with ethanol between each sample. The detection limit of the different minerals depends on several factors, but considered to be in the order of 1-2% in multiphase geological mixtures. The mix of minerals present in the sample has a significant effect on the detection limits as the different peaks of minerals could overlap to some degree. The number of phases present in the sample will also affect the detection limit of the different minerals (Aerts, 2014).

The powder of each sample was put in a suitable holder and placed in a beam of monochromatic x-rays. The small assemblages of crystals in the powder are oriented so every set of lattice planes are capable of diffraction. The different crystals have a specific distance between the mineral lattices which produce characteristic angles of diffraction. The diffraction occurs when Bragg`s law is satisfied (Equation 3.1). The detected angles from the crystals are recorded as peaks in a diffractogram. A qualitative and a semi- quantitative analysis of the diffracted peaks were performed using Diffrac EVA. This analysis was followed by a quantitative analysis conducted with the software Siroquant. Field samples and samples from TDP well site 21 and 24 were analyzed in collaboration with Gundersveen (2014). Samples from TDP well site 1, 2, 7B and 9 was analyzed by Mahmic (2014). The two offshore samples (2/1/14 and 2/2/14) and the recent sediment sample were analyzed by PhD student, Katrine Fossum.

$$n\lambda = 2d \sin \theta$$

Equation 3.1*: Bragg`s law of diffraction. n represent an integer, λ is the wavelength of the incident ray, d equals the spacing in the crystal lattice and θ is the angle between the incident ray and the scatter plane (Bragg and Bragg, 1913).*

3.6.4.1 Diffrac. EVA

The qualitative analysis of the bulk mineral content was conducted by the use of Diffrac. EVA. The mineral peaks in the diffractogram were identified manually by the use of d- values presented by Chen (1977) (Table 3.3). Identification of mineral phases was also conducted using the search and match function in EVA.

The semi- quantitative analysis was conducted by measuring the count intensity in the diffractograms. The count values were calculated to percentages for each sample.

Table 3.3: *Utilized d-values in qualitative and semi- quantitative analysis (Chen, 1977).*

Mineral	d- values (Å)
Quartz	4.25
K-feldspar	3,24
Plagioclase	3,19
Mica	10,08
Hornblende	8,4
Mixed layer clay	10-13
Kaolinite	3,58
Chlorite	3,54
Calcite	3,04
Dolomite	2,89
Aragonite	3,39
Pyrite	2,71
Anatase	3,7

3.6.4.2 Siroquant

A qualitative XRD analysis was conducted using Siroquant software. This software uses the Rietveld instrumental parameters to quantify the different minerals in the sample. The full profile of the XRD pattern is analyzed, which provides a more accurate quantification than the quantification of particular peaks in the diffractrogram. The Rietveld formula calculates the intensity at any points in the scan by refining relevant crystal structures and instrumental parameters with a least-squares analysis (Ruan and Ward, 2002). The different parameters used to provide a better fit for the analyzed minerals in this study was preferred orientation, asymmetry and unit-cell parameters. A table of complete quantitative XRD results is presented in Appendix A1 and A2.

3.7 Heavy mineral analysis

26 samples were analyzed by different heavy mineral analyses. These samples are referred to as key samples in this study. The different analyses conducted on these samples are presented in Table 3.4.

***Table 3.4**: Analysis performed on key samples. Samples from offshore Tanzania are marked with red.*

Age	Stratigraphical unit	Key sample	Conventional heavy mineral analysis	Garnet chemistry	Rutile chemistry
Recent		Matandu River	X	X	
Oligocene	Pande Fm	TDP1/20/1	X		
		TDP1/18/1	X	X	
Eocene	Masoko Fm	TDP2/14/2	X	X	
	Kivinje Fm	TDP7B/12/2	X	X	
Paleocene	?	**2/1/14**	X	X	
Late Cretaceous	Nangurukuru Fm	TDP9/13/1	X	X	
		21-7-2012	X	X	
Mid Cretaceous	Kihuluhulu Fm	TDP21/17/2	X	X	
		TDP21/22/2	X		
		TDP21/21/1	X		
		TDP24/16/3	X		
		TDP/24/28/1	X	X	
	?	**2/2/14**	X	X	
	Makonde Fm	MB-1-4-13	X		X
		MB-1-7-13	X		
Late Jurassic	Mitole Fm	NG-1-2-13	X		
		NG-1-5-13	X		
	Kipatimu Fm	MN-1-3-13	X		
		MN-1-6-13	X		
		MN-2-1-13	X		X
Triassic-Jurassic	Karoo	MP-2-1-13	X	X	
		MP-2-0-13	X		
Precambrain	Basement (Mozambique Belt)	BA-3-14		X	
		BA-2-13	X		
		BA-1-13	X		

3.7.1 Electron microprobe analysis (EMP)

Twelve thin sections were analyzed by electron microprobe at Department of Geoscience, University of Oslo. The analysis was conducted using a Cameca SX100 instrument fitted with five wavelength-dispersive spectrometers and was supervised by Muriel Marie Laure Erambert.

Electron microprobe analysis (EMP) is a technique used for chemically analyzing small areas of a solid sample. It has been proven useful in many areas and is commonly used in petrological description and identification, mineral identification and age determination. When a solid is bombarded with electrons from an electron gun in EMP, X-rays are produced. A characteristic X-ray spectrum is obtained in EMP, as a result from a transition between energy levels in the electrons. The spectrum contains lines that are characteristic for the elements present in the sample. By identifying these lines a qualitative analysis can be obtained. A quantitative analysis can also be obtained by the microprobe by comparing the intensities of the lines from the sample with lines from pure elements of known composition. This makes the electron microprobe a more accurate method than the related Scanning Electron Microscope (Reed, 2005). EMP quantitative analysis was conducted on samples containing garnet and rutile to identify their chemical composition. Rutile and garnet grains were identified in thin section by the criterias determined by Mange and Mauer (1992) before EMP analysis. Anatase was separated from rutile, its polymorph, by the presence of authigenic features, such as euhedral crystal surfaces. Heavy minerals were also identified by optical and backscatter images obtained from a Cameca SX100.

When analyzing major elements in garnets, an accelerating voltage of 15 kV was used. The focused beam current was 15 nA and the counting time per site was 10 seconds. The elements were calibrated by Muriel Marie Laure Erambert before each round of analysis.

A 20 kV acceleration voltage and a 100 nA, 5μm beam current was used when analyzing trance elements in rutile grains. The counting time per site was 10 seconds. The different elements analyzed by EMP have varying detection limits based on the accelerating voltage and beam current (Table 3.5).

The results of the quantitative EMP analysis are expressed as elemental mass concentrations (weight per cent). The total sum of oxides should be close to 100 % and a total sum lower than 98.0 % was discarded in these analyses. A low total sum can occur as a result of different

factors. A drift in the beam- current, poor spectrometer calibration, presence of water and elements not included in the analysis can all cause a low total sum of oxides (Reed, 2005).

***Table 3.5**: Detection limits in weight percent (Wt %) for major and trace elements in rutile and garnet analysis. The detection limits for trace elements in rutile analysis are lower due to higher accelerating voltage and stronger beam current.*

Detection limit; rutile analysis		**Detection limit; garnet analysis**			
Elements	**Wt %**	**Elements**	**Wt %**	**Elements**	**Wt %**
Zr	0,00485	Si	0,031	Cr	0,050
Cr	0,0032	Al	0,029	Mg	0,032
Nb	0,0058	Ca	0,043	Na	0,037
Si	0,0023	Fe	0,070	K	0,022
Fe	0,0083	Mn	0,060	Ti	0,028

The molar percentages of the different elements in the garnet formula were calculated from the initial values on the basis of 24 oxygen (Deer et al., 2013) (Appendix E1) and the results were plotted in triangular diagrams. The triangle end members were based on element values in garnet, obtained by EMP. Calcium (Ca), Iron (Fe), Magnesium (Mg) and Manganese (Mn) displayed the highest values in the analyzed garnets, thus making grossular ($Ca_3Al_2Si_3O_{12}$), pyrope ($Mg_3Al_2Si_3O_{12}$) and almandine ($Fe_3^{2+}Al_2Si_3O_{12}$) + spessartine ($Mn_3Al_2Si_3O_{12}$) suitable end members. Low values of Titanium and Chromium in the analyzed garnets eliminate uvarite ($Ca_3Cr_2Si_3O_{12}$) and andradite ($Ca_3(Fe^{3+},Ti)_2Si_3O_{12}$) as possible variables. Spessartine and almandine were plotted together since almandine is the main substituent for spessartine (Deer et al., 2013). This study does not differentiate between low and high values of Mn in the almandine + spessartine component since the author has been emphasizing overall provenance signal, and since there are generally low values of Mn in all the analyzed garnets. Garnets from the two offshore samples, 2/1/14 and 2/2/14 were analyzed by Katrine Fossum and supervised by Muriel Marie Laure Erambert. 50 grains from each sample should be analyzed to represent all chemical variations within one sample (Morton, 1985). Due to the varying content of garnet grains in the analyzed thin section, the acquired amount of 50 analyzed grains was not obtained.

The weight percent (wt%) of the different elements from rutile analyses were converted to parts per million (PPM) though multiplication by a factor of 10 000 (Appendix E2). The

values of Chromium (Cr) and Niobium (Nb) were plotted in a diagram from Meinhold et al. (2008) which separate between rutile derived from metamafic rock and rutile derived from metapelitic rocks (Figure 3.6).

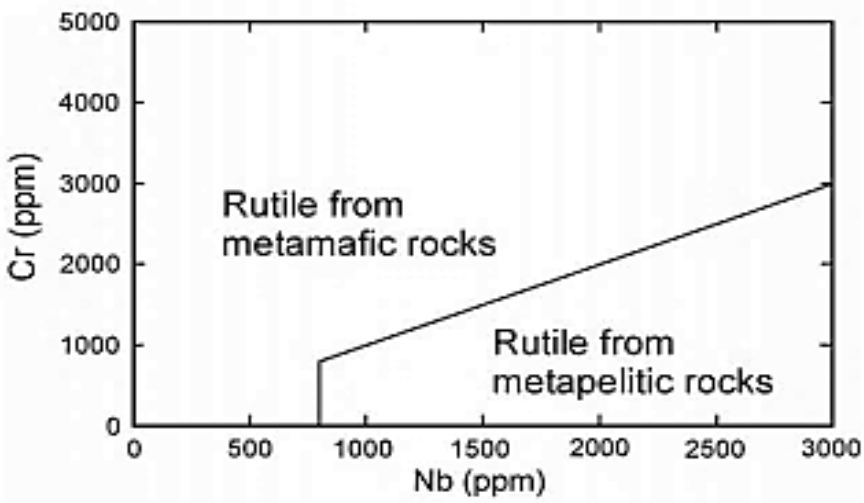

***Figure 3.6**: Diagram which separates between rutile derived from metamafic rocks and rutile from metapelitic rocks. Rutile with Cr < Nb combined with Nb > 800 ppm are interpreted as rutile derived from a metapelitic rock while rutile with Cr > Nb and Nb < Cr where Nb < 800 ppm are interpreted as derived from metamafic rocks (Meinhold et al., 2008).*

3.7.2 Conventional heavy mineral analysis

Sample preparation was conducted by Lee Clark in Aberdeen, Scotland at Palyno Services Ltd. The samples were gently disaggregated by the use of pestle and mortar. Disaggregation was followed by an immersion of the samples in water and cleaned by an ultrasonic probe to remove any remaining clay on the grain surfaces. The samples were then washed through a 63 μm sieve and resubmitted into ultrasonic treatment until no clay particles passed into suspension. The cleaning procedure was followed by wet sieving through 125 μm and 63 μm sieves. The resulting >125 μm and 63-125 μm fractions were dried in an oven at 80 ℃. The heavy minerals were separated in the 63-125 μm fractions by using bromoform with a specific gravity of 2.8 g/m^3. The heavy mineral residue was mounted under Canada Balsam for optical study.

Conventional heavy mineral data were acquired by Andrew Morton (HM Research Associates Ltd, UK) using a polarizing microscope. 200 heavy mineral grains were counted and identified by the criteria from Mange and Maurer (1992).

Selected provenance-sensitive heavy mineral indices as defined by Morton and Hallsworth (1994) were also calculated. The indices contain heavy mineral pairs with similar behavior during transport, deposition and diagenesis (Table 3.5)

Samples with comparable heavy mineral content were grouped into heavy mineral assemblages to provide the overall characteristics of the samples.

Selected heavy mineral indexes are plotted against each other to provide further provenance information. The heavy minerals included in each mineral pair have similar chemical stability, mechanical stability, grain size, density and shape. When comparing heavy minerals ratios which fulfill these criteria, the result are more likely to reflect the true composition of source area.

There are several factors which can cause problems with determination and interpretation of mineral ratios. A prerequisite for an accurate ratio determination is correct identification of the heavy minerals, but similar appearance and optical properties can make identification a difficult procedure. The mineral identification manual by Mange and Maurer (1992) and SEM or EMP analysis can be used when in doubt. Additionally, secondary overgrowths and apatite dissolution can affect the determination of heavy mineral indexes and should be considered when interpreting the results. The ratio values are determined by a separate count with minimum 100 grains per mineral pair (Morton and Hallsworth, 1994).

***Table 3.5**: Heavy mineral indices determined by Morton and Hallsworth (1994). The heavy mineral pairs have similar hydraulic and diagenetic behavior to more likely reflect the true composition of the source area (Morton and Hallsworth, 1994).*

Index	Mineral pair	Index determination
ATi	apatite-tourmaline index	100 * apatite count/ (apatite plus tourmaline)
GZi	garnet-zircon index	100* garnet count/ (garnet plus zircon)
RuZi	rutile-zircon index	100* rutile count/ (rutile plus zircon)
MZi	monazite-zircon index	100* monazite count/ (monazite plus zircon)
CZi	chrome spinel-zircon index	100* chrome spinel count/ (chrome spinel plus zircon)

4 Result

During two weeks of field work, six cores and five outcrops were logged and sampled. This chapter presents the sedimentology and petrography of selected sections and 26 key samples from the Mandawa Basin and offshore Tanzania. The samples were derived from six field outcrops and six cores, and range from Precambrian to recent age. The key samples consist of sand or silt, and are analyzed in regard to provenance studies. They were selected for this study based on their heavy mineral content in attempt to cover a large geological time span by typical lithologies. The sedimentological, mineralogical and petrographic descriptions concern only the key samples from each sedimentary unit. Complete sedimentological and mineralogical results are presented in Appendix.

4.1 Sedimentological and petrographic description

The sedimentological descriptions are presented briefly in chapter 4.1.1. The petrographical descriptions are presented from Precambrian to recent age, and subdivided by analyzed stratigraphical units. Offshore samples are presented at the end of this chapter.

4.1.1 Facies and facies association

Eleven facies from field outcrops (Table 4.1) and seven facies from cores (Table 4.2) were identified in this study. The facies have been divided between field outcrops and cores due to the differences in appearance, deposition environment and processes acting on the sediments. The facies and facies associations are described briefly in this chapter, while a more detailed and thorough description of the facies and facies associations can be found in the theses of Gundersveen (2014) and Mahmic (2014). Descriptions and figures of facies and facies associations are presented in sedimentological logs together with associated stratigraphical units, in chapter 4.1.2.

Facies classification and description

Classification and a short description of facies identified in field outcrops, Karoo sedimentary sequences, Upper Kipatimu Mb., Upper Mitole Mb. and Makonde Fm. (Figure 2.4 and 2.5) are presented in Table 4.1. Classification and short description of facies identified in cores from TDP well sites, 24, 21, 9, 7B, 2 and 1 (Figure 1.1), which comprises Kihuluhulu Fm, Nangurukuru Fm., Kivinje Fm., Masoko Fm and Pande Fm. (Figure 2.4 and 2.5), are presented in Table 4.2.

***Table 4.1**: Classification and descriptions of facies identified in the field outcrops of Karoo sedimentary sequences, Upper Kipatimu Mb., Upper Mitole Mb. and Makonde Fm (Figure 2.4 and 2.5).*

Facies nr.	Facies	Grain size	Characterization
A	Mudstone to silty mudstone	Clay to silt	Silt content varying from 0-50%, clay clasts.
B	Massive sandstone	Medium to coarse sand	No apparent bedding, with mud clasts. Light grey/orange.
C	Massive sandstone	Fine	No apparent bedding, erosive bed.
D	Conglomerate	Very coarse	Matrix supported, polymict conglomerate.
E1	Laminated siltstone	Silt to very fine sand	Parallel laminated / weakly laminated.
E2	Laminated/bedded sandstone	Fine to very coarse sand	Parallel laminated or bedded, varying silt content from 0-20%. Occasional clay rip up clasts.
F	Conglomerate	Coarse to granule/pebble	Upwards fining sequence.
G1	Cross stratified sandy siltstone	Silt to coarse sand	Cross bedded, with occasionally mud clasts. Often upwards fining sequences.
G2	Cross straified sandstone	Medium to coarse sand	Highly cross bedded with mud couplets. Light grey/orange.
G3	Cross stratified conglomerate	Coarse to pebble	Cross bedded. Upwards fining.
H	Through cross stratified sandstone	Fine to very coarse	Through cross bedded, occasional clay rip up clasts and erosive beds.

***Table 4.2**: Classification and description of facies identified in cores from TDP well sites, 24, 21, 9, 7B, 2, 1 (Figure1.1) which comprises Kihuluhulu Fm, Nangurukuru Fm., Kivinje Fm., Masoko Fm and Pande Fm. (Figure 2.4 and 2.5).*

Facies nr.	Facies	Grain size	Characterization
1	Claystone to silty claystone	Clay to silt	Silt content varying from 0-40%. No lamination. "Beef" can occur. Varying degree of bioturbation and shell and plant fragments.
2	Siltstone to sandstone	Silt to very fine sand	Varying clay content between 0-40%. Varying degree of bioturbation, with some shell and coal fragments. Rip up clasts and erosive beds can occur.
3	Laminated clay to siltstone	Clay to very fine sand	Parallel or weakly laminated, varying silt content from 0-50%. Scattered bioturbation.
4	Inverse graded siltstone	Silt to very fine sand	Varying content of sand, from 0-50%. Upwards coarsening sequences.
5	Soft sediment deformed silt- and sandstone	Very fine to medium	Soft sediment deformation and water escape structures. Some coal and shell fragments.
6	Cross stratified sandstone	Very fine to coarse	Varying silt content of 0-20%. Occasionally erosive beds. Upwards fining sequences.
7	Limestone	Meduin to very coarse	Occasional large fossils / fossil fragments (3-7 mm). Poorly sorted. Clay rip-up clasts may be present.

Facies associations

The classification of facies associations are presented in Table 4.3. Description of facies association only includes facies association 1 (FA-1) in this thesis. The description of facies association 2-8 can be read in the theses of Gundersveen (2014) and Mahmic (2014).

***Table 4.3**: Classification of facies associations which were identified in the stratigrphical units, Karoo sedimentary sequences, Upper Kipatimu Mb., Upper Mitole Mb., Makonde Fm. Kihuluhulu Fm, Nangurukuru Fm., Kivinje Fm, Masoko Fm. and Pande Fm. Detailed description of facies associations 2-8 can be read in the thesis of Gundersveen (2014)and Mahmic (2014).*

Facies association	Facies	Stratigraphical unit	Locality	Figure
1	B, E2, F	Karoo	Mpopera Mtumbei	4.3
2	A, C, E1, E2, G1	Upper Kipatimu Mb.	Mlima Ngoge	4.7
3	B, E1, E2, G1, G2	Upper Mitole Mb.	Ngoro	4.10
4	A, B, C, D, E1, E2, H	Makonde Fm.	Mbate	4.13
5	1, 2, 3, 4, 5, 6	Kihuluhulu Fm.	TDP well site 21 and 24	4.17, 4.19
6	1, 2, 3	Kivinje Fm, Nangurukuru Fm. and Kihuluhulu Fm.	TDP well site 7B, 9 and 24	4.17, 4.21, 4.23
7	1, 3, 7	Masoko Fm.	TDP well site 2	4.25
8	1, 2, 3, 7	Pande Fm.	TDP well site 1	4.26

Facies association 1 (FA-1)

Facies association 1 (Figure) was identified in Karoo sedimentary sequences at the Mpopera Mtumbei locality (Figure 1.1). This facies association is dominated by facies E2 which comprises bedded, fine to very coarse sandstone. Massive, very coarse sandstone and an upwards fining conglomerate are also present in FA-1. A trunk of silicified wood was observed at 14-15 in the upper part of the sedimentary sequence (14-15 m in sedimentary log, Figure 4.3)

4.2.1 Precambrian

Three Precambrian basement samples (Figure 1.1) from the Mandawa basin were analyzed in this study. The samples were analyzed to get an improved knowledge of the possible sediment sources, which are used to compare and discriminate the sedimentary units in this study. Sample BA-1-13 and BA-2-13 were analyzed with conventional heavy mineral analysis while

sample BA-3-14 was analyzed with regard to the chemical composition of garnets with EMP (Table 3.4).

BA-1-13

BA-1-13 (Figure 4.1.A) was sampled from a granitic gneiss sampled near Mpopera-Mtumbei Village (Figure 1.1). The sample was derived from a large granulite complex (Mozambique Belt) west of the Mandawa Basin (Figure 2.1 and 2.2).

BA-2-13

BA-2-13 was sampled from a granitic gneiss near the Kipatimu quarry locality (Figure 1.1, Figure 4.1 B). BA-2-13 represents the same orogenic system (Mozambique belt) as sample BA-1-13 (Figure 2.1 and 2.2). This basement sample is characterized by a higher content of amphibole (Figure 4.1 C and D) then sample BA-1-1.

BA-3-14

This sample derives from the same orogenic system as the previous basement samples BA-1-13 and BA-2-13. It differs from the other samples by the content of garnet (Figure 4.1 E), which makes it valuable as a source rock indicator in the study of garnet provenance.

4.2.2 Upper Triassic to Early Jurassic

The Upper Jurassic to Early Jurassic time period is represented by the Karoo sequence in this study (Figure 1.1, 2.1 and 2.5).

Karoo sedimentary sequences

Karoo is the oldest formation studied in the field. The age of this sequence is uncertain, but Upper Jurassic to Early Jurassic was proposed by Hudson (2011). The sequence is poorly exposed with small scattered outcrops (Figure 4.2).

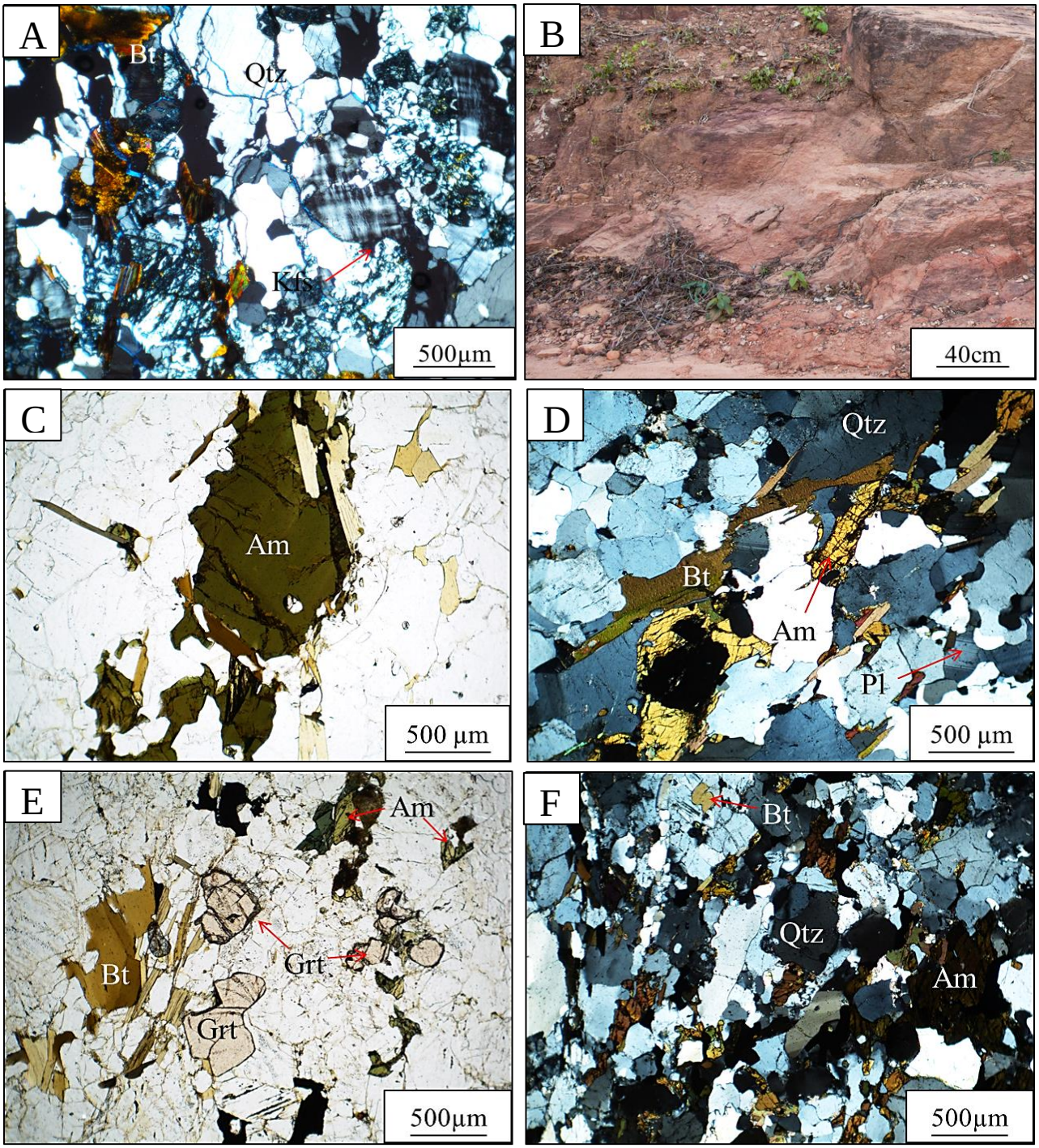

***Figure 4.1**: A) Micrograph of sample BA-1-13 in cross polarized light. The sample is dominated by quartz (Qtz), K- feldspar (Kfs), and biotite (Bt). B) The field outcrop where sample BA-2-13 was sampled. C) Sample BA-2-13 in plan polarized light. The sample is abundant in amphibole (Am). D) Micrograph of sample BA-2-13 in cross polarized light, displaying biotite, quartz, plagioclase and amphibole. E) Micrograph of sample BA-3-14 in plan polarizing light, showing biotite, amphibole and garnet. F) Micrograph of sample BA-3-14 in cross polarized light. Amphibole, quartz and biotite are present in the sample.*

The exposed outcrop is located near the village Mpopera- Mtumbei (Figure 1.1) in the Kandawale region (Figure 2.5) and it has previously been studied by Wellington Hudson in 2009. The Karoo sedimentary sequence is dominated by coarse, carbonate cemented sandstone (Facies E2) (Figure 4.3, Table 4.3). Matrix dominated conglomerate (Facies F) was also present in the logged outcrop (Figure 4.3 and 4.3 C). Within the studied locality, pieces of silicified wood were found (Figure 4.3 B).

Figure 4.2*: An overview of the locality where Karoo deposits were logged and sampled. Only scattered exposures of the formation are present, as indicated by red arrows and in log of Figure 4.3.*

Mineralogical composition

Two samples (MP-2-1-13 and MP-2-0-13) from the Karoo locality were analyzed by XRD (Figure 4.5). The complete XRD results from all Karoo samples are represented in Appendix. The samples comprise the lower part of the Karoo section (Figure 4.3). Sample MP-2-0-13 was sampled from an outcrop approximately 20 m below the logged section. The sample contains almost 20% mixed layer clay and has the highest content of clay minerals of both samples from the Karoo unit. Quartz and plagioclase dominate the sample, comprising 60% of the bulk composition. K-feldspar and mica are present in the sample with 10 and 15% of the mineral content respectively. Sample MP-2-1-13 is dominated by quartz (40%) and calcite (40%). K-feldspar and plagioclase are present in the sample in almost equal amount with 9 and 12% respectively. Table of complete XRD results are presented in Appendix A2.

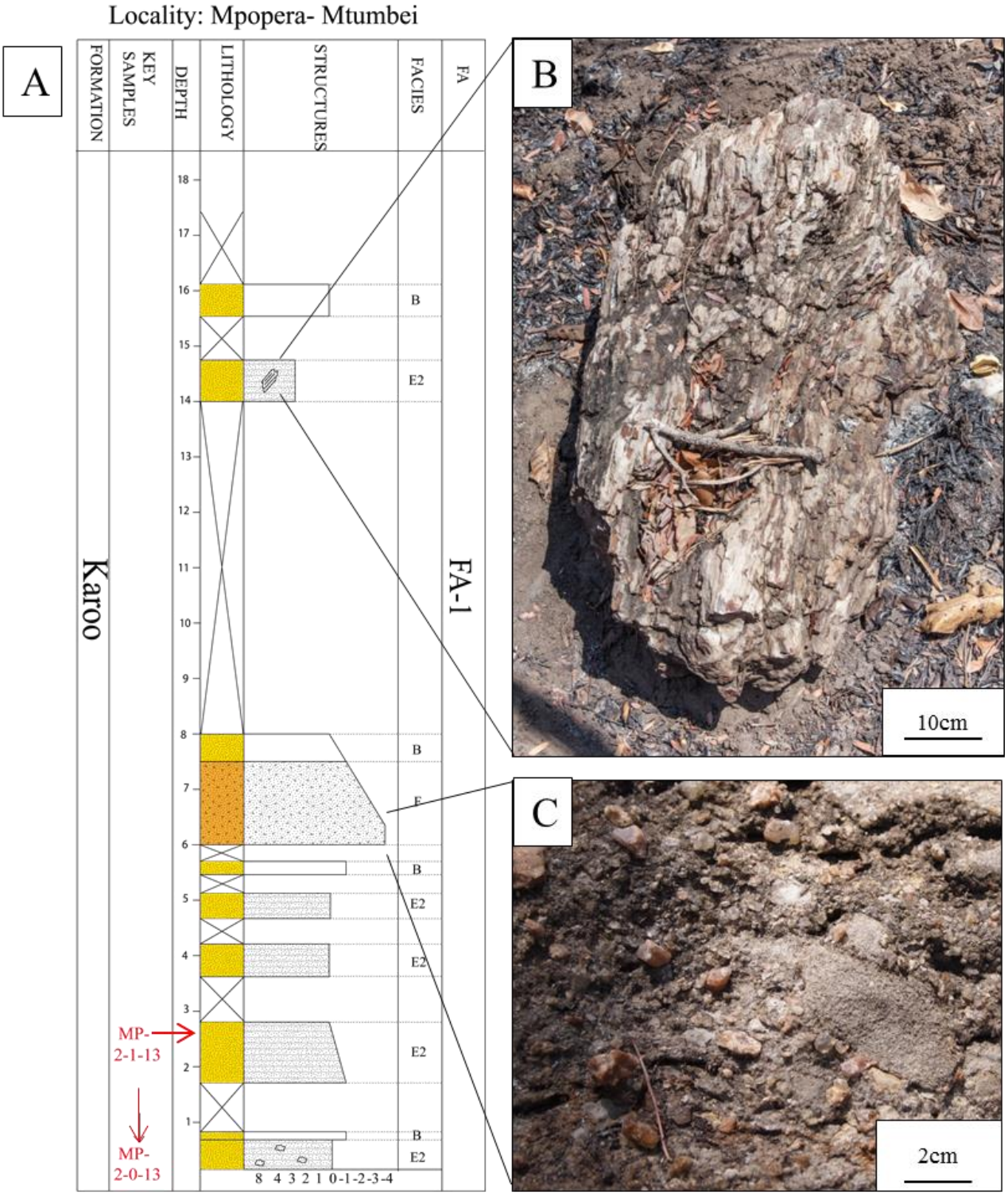

***Figure 4.3**: A) Logged section of the Karoo Formation. Key samples (MP-2-1-13 and MP-2-0-13) are marked in red, and arrows indicate where the samples were taken (sample MP-2-0-13 was sampled approximately 20 m below the logged section). B) Silicified trunk of wood found at the Karoo locality. C) Matrix dominated, polymict conglomerate.*

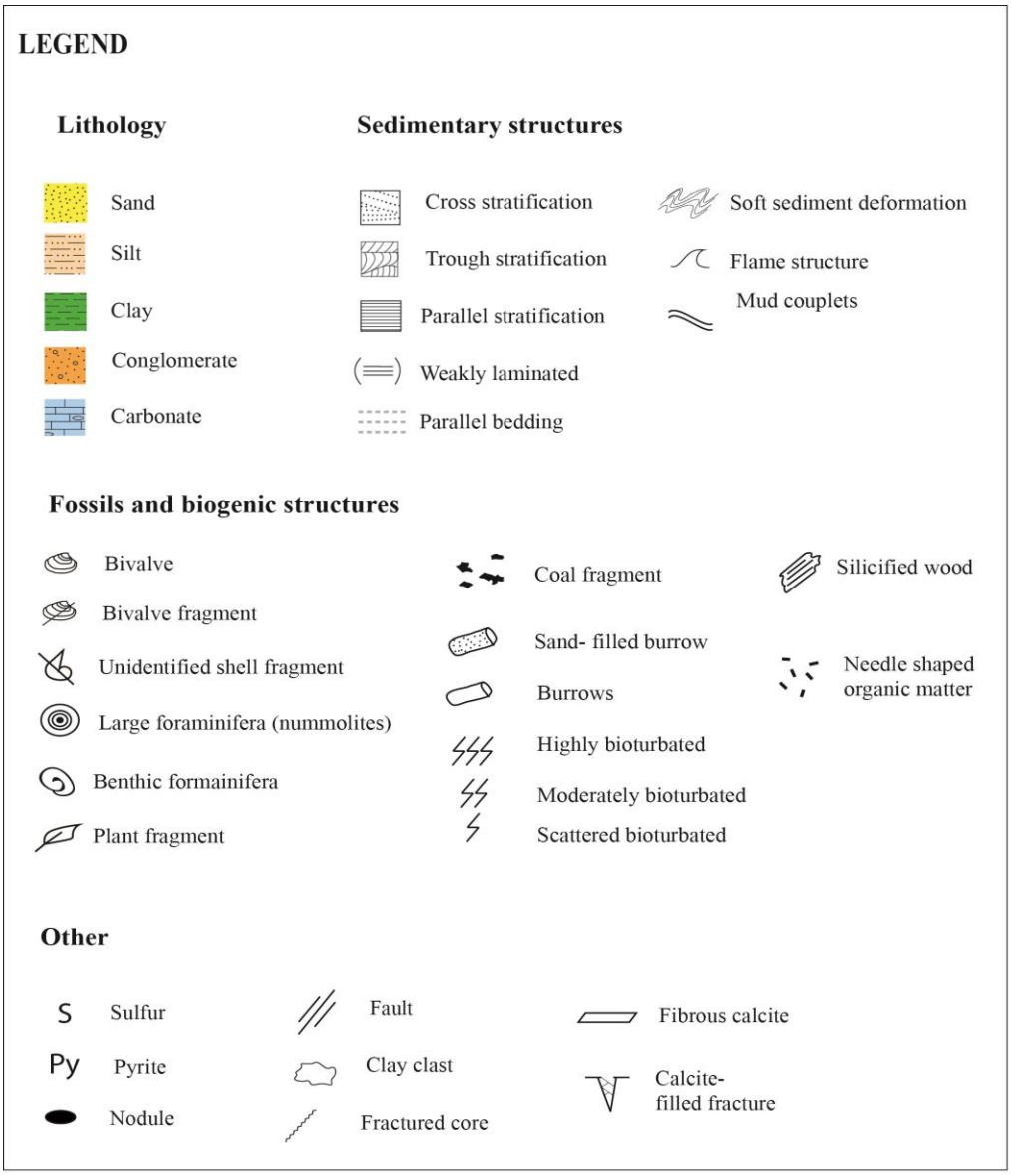

***Figure 4.4**: Legend explaining the symbols used in all sedimentary logs in this study.*

Petrographic description

The samples (MP-2-1-13 and MP-2-0-13) from the Karoo sediments were studied in thin section. Sample MP-2-0-13 consists of poorly sorted fine sand in a clay matrix. It is characterized by monocrystalline and polycrystalline quartz, highly weathered feldspars (category 4-5 (Table 3.2)), and mica and clay matrix. The fraction of quartz is dominated by grains of monocrystalline character with straight extinction. Quartz grains with undulose extinction comprise 12% of the total quartz fraction, while 7% of the quartz grains are of

polycrystalline character. The grains are angular to sub angular with long and tangential contacts. With almost 60% clay matrix, and a dominance of quartz and feldspar, this sample classifies as a feldspatic wacke according to the classification diagram modified by Dott (1964) (Figure 3.5). Sample MP-2-1-13 consists of poorly sorted coarse sand in recrystallized calcite cement. It is characterized by quartz and highly weathered feldspar, mostly from category 4 and 5 on the preservation scale (Table 3.2). The quartz fraction is dominated by monocrystalline grains which comprises 88% of the total quartz fraction. Quartz grains with undulose extinction make up 18% of the quartz composition. Overgrowths on K-feldspar and clay clasts were observed in light microscope and by SEM. The grains are sub rounded with a dominance of long contacts between the grains. Point counting of this sample classifies the sediments in MP-2-1-13 as an arkose (Appendix C).

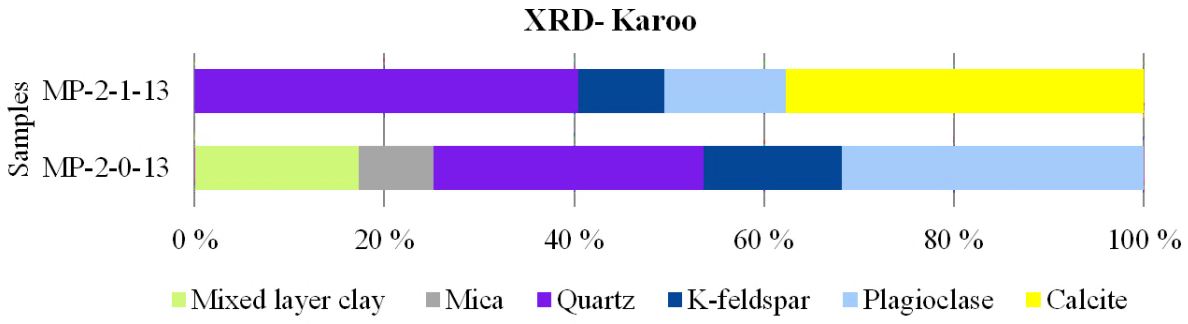

***Figure 4.5**: Mineralogical composition of the two key samples, MP-2-1-13 and MP-2-0-13, from the Karoo locality.*

4.2.3 Upper Jurassic

The Upper Jurassic time period is represented by the Upper Kipatimu Member (Kimmeridgian to Tithonian) and Upper Mitole Member (Tithonian to Berriasian) in this study (Figure 1.1, 2.4, 2.5).

Upper Kipatimu Member

Upper Kipatimu Mb was exposed at two outcrops approximately 289 m apart, near the Mlima-Ngoge village (Figure 1.1) in the North Mandawa region (Figure 2.5). The first outcrop was located at a quarry (Figure 4.6), and was logged and sampled as Section 1 (Figure 4.7). The second outcrop is located stratigraphically below the first section and was

exposed at a road section, and was logged and sampled as Section 2 (Figure 4.7). Upper Kipatimu Mb. has previously been studied by Wellington Hudson during a field season in 2007 (Hudson, 2011).

Upper Kipatimu Mb. is characterized by poorly to moderate sorted, medium to coarse sand. The sand is cross bedded with clay clasts and has a brick red colour (Figure 4.7). Parts of the formation are dominated by parallel lamination (Figure 4.7 C).

Figure 4.6*: An overview of the brick red sand comprising the Upper Kipatimu Mb. The exposed outcrop was located at a quarry (Figure 1.1).*

Mineralogical composition

The bulk mineral composition of three samples from Upper Kipatimu Mb. was analyzed by XRD (Figure 4.8). The formation is dominated by quartz comprising 80% of the bulk composition. Almost equal amounts of kaolinite and K-feldspar (about 10%) are present in the samples. Sample MN-2-1-13 contains 3% anatase unlike sample MN-1-6-13 and MN-1-3-13. Table of complete XRD results are presented in Appendix A2.

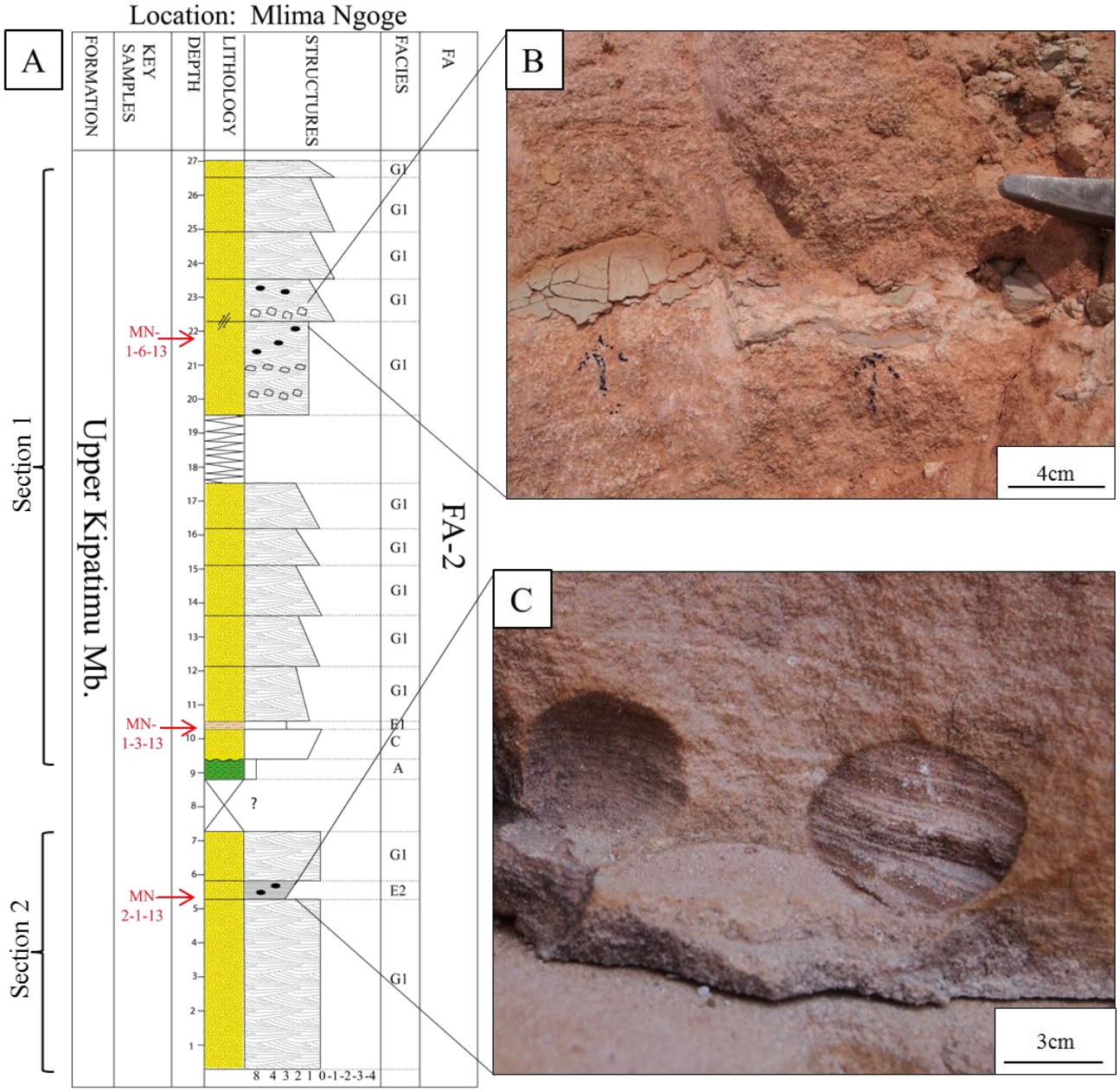

Figure 4.7: *A) Logged section of the Upper Kipatimu Mb. Cross bedded medium to coarse sand in upwards fining sequences dominates the formation. Key samples are marked in red. B) Clay clasts found in the upper part of the logged section. C) Parallel lamination is observed within the cavity of nodules.*

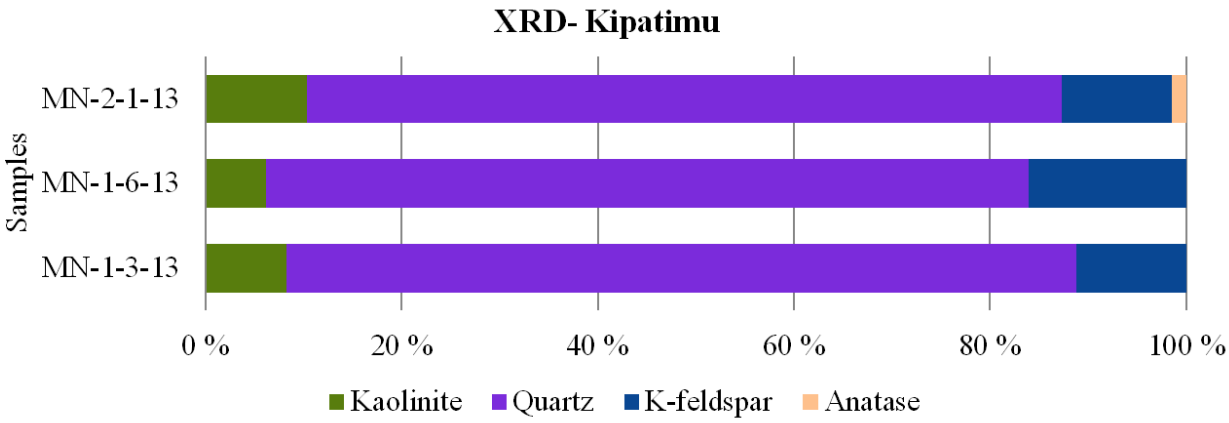

***Figure 4.8**: Bulk mineral composition of key samples from the Upper Kipatimu Mb.*

Petrographic description

The petrography of three samples from Upper Kipatimu Mb. was studied in thin section (MN-1-3-13, MN-1-6-13 and MN-2-1-13). They show a high abundance of quartz and weathered K-feldspar. Feldspar grains are poorly preserved with the majority of grains being classified as category 4-5 (Table 3.2). Monocrystalline quartz with straight extinction is the most dominant quartz type (80%), but both undulatory (6-14%) and polycrystalline (7-13%) quartz and chert was observed. The grains are surrounded by kaolinite booklets and iron oxides which is a typical feature throughout the formation (Figure 4.11 B). The grains are moderate to poorly sorted, subrounded with tangential and long contacts. Sample MN-2-1-13 was sampled from a parallel laminated part of the formation (Figure 4.11 A, C). The lamination consists of alternating heavy and light minerals (Figure 4.11 C). Zircon, apatite and anatase were identified when studying the lamination in SEM. Point counting results classify the key samples from Upper Kipatimu Mb. as arkosic sandstones and feltspatic wacke (Appendix C).

Upper Mitole Member

Upper Mitole Mb. was studied in a 20 m thick outcrop (Figure 4.9), a cliff section close to the Ngoge village (Figure 1.1) in the South Mandawa region (Figure 2.5). The sedimentary unit was logged in two sections (Figure 4.12) where section 1 is located stratigraphically below section 2. The outcrop was studied by Wellington Hudson in 2008 and 2009 (Hudson, 2011). The exposure of Upper Mitole Mb. is dominated by cross- and parallel bedded sandstone with

mud couplets and mud clasts (Figure 4.12 B). The sandstone member consists of medium sized sand, which is well sorted.

***Figure 4.9**: The Late Mitole Mb. was exposed in a 20 m section close to the road at Ngoro locality (Figure 1.1, 2.4, and 2.5).*

Mineralogical composition

The bulk mineralogical composition of two key samples (NG-1-2-13 and NG-1-5-13) from Upper Mitole Mb. was analyzed by XRD (Figure 4.10). The two sand samples are dominated by quartz which makes up almost 80% of the mineral composition. Approximately equal amounts of K-feldspar and plagioclase make up the remaining 20% of the bulk composition. Table of complete XRD result is presented in Appendix A2.

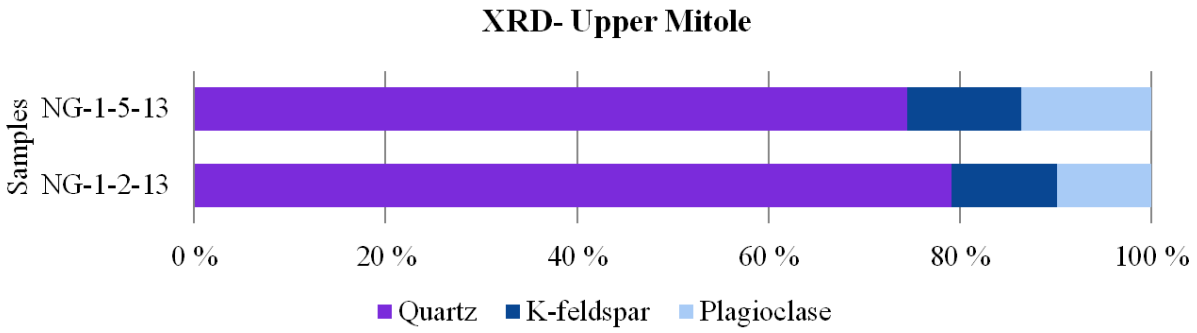

***Figure 4.10**: Bulk mineral composition of the two key samples, NG-1-2-13 and NG-1-5-13, of the Upper Mitole Mb, Ngoro locality (Figure 1.1, 2,4 and 2,5).*

Petrographic description

The petrography of two key samples (NG-1-2-13 and NG-1-5-13) from the Late Mitole Mb. was studied in thin section. The two samples consist of medium sized, well sorted sand. The samples are dominated by quartz of monocrystalline character with straight extinction which comprises 90- 92% of the total quartz composition. Undulose quartz (4-7%), polycrystalline quartz (3-4%) and chert were also observed. The feldspar grains are highly weathered with an abundance of grains in category 4-5 (Table 3.2). Mixed smectite-chlorite coating (Gundersveen, 2012) and authigenic kaolinite booklets are a common feature in the key samples (Figure 4.11 D). Authigenic anatase is present in some pores and partly dissolved ilmenite and titanite were observed in SEM. The grains are sub rounded and dominated by long and tangential contacts (Figure 4.11 E). Results from point counting classify the Upper Mitole sandstone as arkosic sand and feltspatic wacke (Appendix C).

Figure 4.11*: A) Scanned thin section of sample MN-2-1-13. The scanned picture displays the lamination within the sediment. B) A backscatter image taken in SEM of sample MN-2-13. The image shows a section of the laminated part of the thin section. The lamination consists of a separation between light and heavy minerals. Zircon (Zr) and anatase (Ant) are identified in these layers. C) Plan polarized Image of sample MN-1-6-13.The sample is characterized by pore filling authigenic kaolinite (Kln). Pyrite and Fe- oxide are abundant in the sample. D) A backscatter image of sample NG-1-5-13 from the Upper Mitole Member taken with SEM. Mixed smectite- chlorite coating (Sme/Chl) surrounding the grains are a common feature in the samples from this Upper Mitole Member. Authigenic kaolinite is present in the pores. E) A plan polarized image of sample NG-1-5-13 from the Upper Mitole Member. The sample displays good sorting and an abundance of long and tangential contacts. F) A plan polarized image of sample MB-1-7-13 of the Makonde Formation. The sample display good sorting and the contacts between the grains are mostly of long and tangential character. G) A backscatter image of sample MB-1-7-13 form Makonde Formation. The sample is dominated by mixed smectite/ chlorite coating surrounding the grains.*

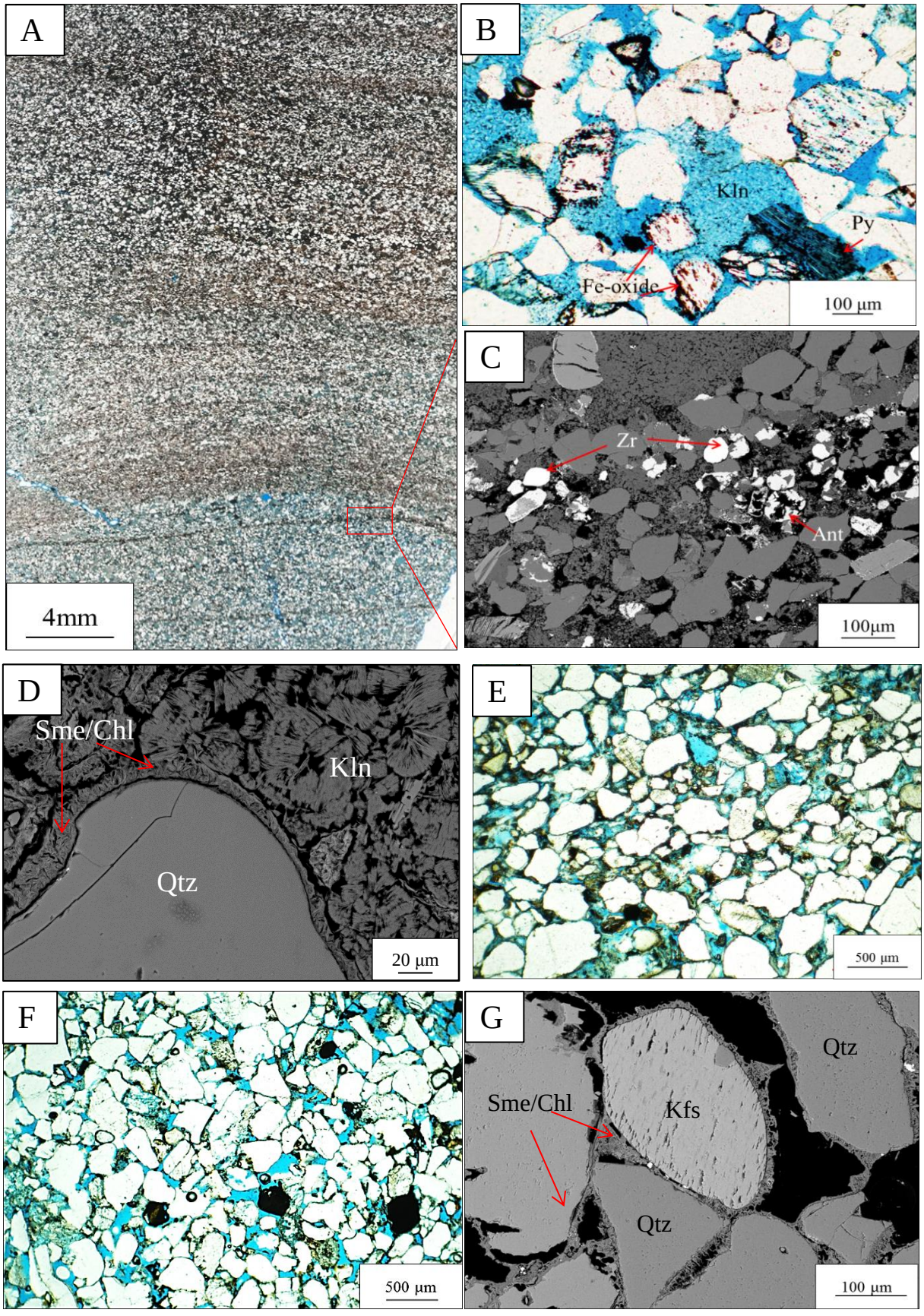
A
4mm
B
Kln
Py
Fe-oxide
100 µm
C
Zr
Ant
100µm
D
Sme/Chl
Kln
Qtz
20 µm
E
500 µm
F
500 µm
G
Qtz
Sme/Chl
Kfs
Qtz
100 µm

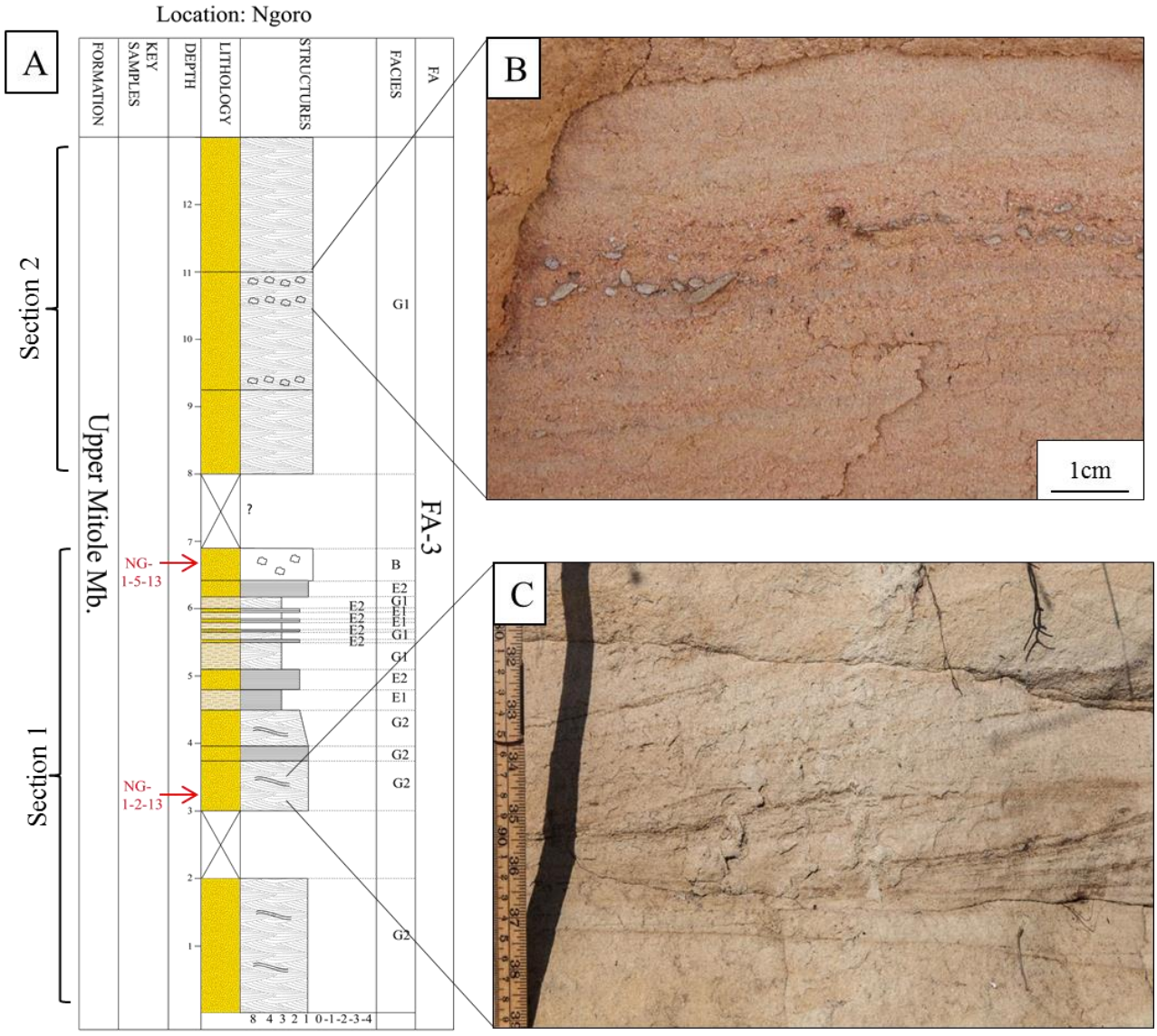

***Figure 4.12**: A) Logged section of the Upper Mitole Mb. at Ngoro locality (Figure 1.1, 2, 2 and 2, 5) Key samples are marked in red. B) Imbricated clay clasts oriented in a layer in section 2. C) Mud drapes in cross stratified sandstone in section 1. Mud drapes is a common feature throughout section 1.*

4.2.4 Mid Cretaceous

The Mid Cretaceous time period is represented by the Makonde Formation (Aptian to Albian), TDP 24 (Cenomanian to Turonian) and TDP 21 (Cenomanian to Coniacian) in this study (Figure 1.1, 2.4 and 2.5).

Makonde formation

The Makonde Formation was studied in two field locations about 1 km apart, near the Mbate village (Figure 1.1) in the South Mandawa region (Figure 2.5). The first section was logged and sampled at an exposure located in a ditch near the road (Figure 4.13). The second section was logged at an outcrop located by a water hole. These localities were studied by Wellington Hudson in 2008 and 2009 (Hudson, 2011). The first section is characterized by an upwards coarsening trend with clay cemented, medium sized sand (Figure 4.14). The sand is typically parallel and trough stratified (Figure 4.14 and 4.14 C). The second section is dominated by coarse trough stratified sand units with erosive base (Figure 4.13 B).

***Figure 4.13**: The exposed outcrop of Makonde Formation (Section 1), at Mbate locality is located in a ditch near the road (Figure 1.1, 2.4 and 2.5)*

Mineralogical composition

The bulk mineral composition of two key samples, MB-1-4-7 and MB-1-7-13, were analyzed by XRD (Figure 4.15). The samples are dominated by high percentages of quartz (65-62%). Plagioclase comprises 20- 25% of the bulk composition while the remaining 15% consists of K-feldspar. Table of complete XRD results are presented in Appendix A2.

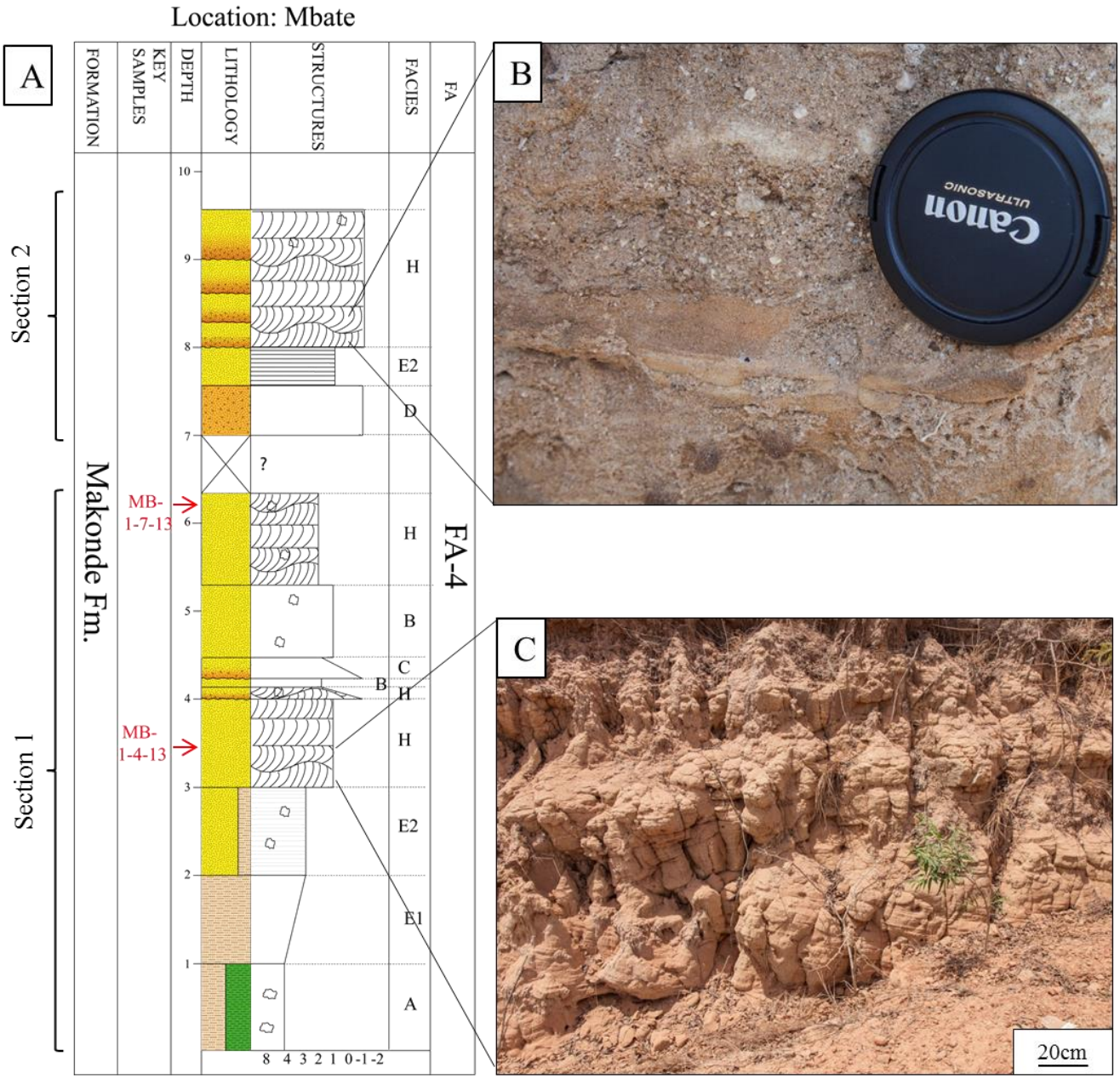

***Figure 4.14**: A) Logged sections of Makonde Fm at Mbate locality. The formation displays an upwards coarsening trend. Key samples are marked in red. B) Erosive base in trough bedded section 2. C) Trough stratification displayed in section 1.*

Petrographic description

The petrography of two key samples from the Makonde Formation (MB-1-4-13 and MB-1-7-13) was studied in thin section. The samples are dominated by monocrystalline quartz with instantaneous extinction which makes up 85-91% of the total quartz composition. Only 3-4% of the total fraction of quartz consists of polycrystalline grains and 4-7% display undulose

character. Plagioclase and K-feldspar are poorly preserved with a dominance of category 4 and 5 (Table 3.2). Mica and rock fragments of medium size were observed. The two samples, MB-1-4-13 and MB-1-7-13 consist of medium sand with sub angular shape and good sorting. The grains are dominated by tangential and long contacts (Figure 4.11 F). SEM analysis displayed a high abundance of mixed smectite- chlorite coating around the grains (Gundersveen, 2012) (Figure 4.11 G) and authigenic anatase filling pores in the sediment. Partly dissolved ilmenite and titanite were observed in SEM. Results from point counting classify Makonde samples as arkosic sand and feltspatic wacke (Appendix C).

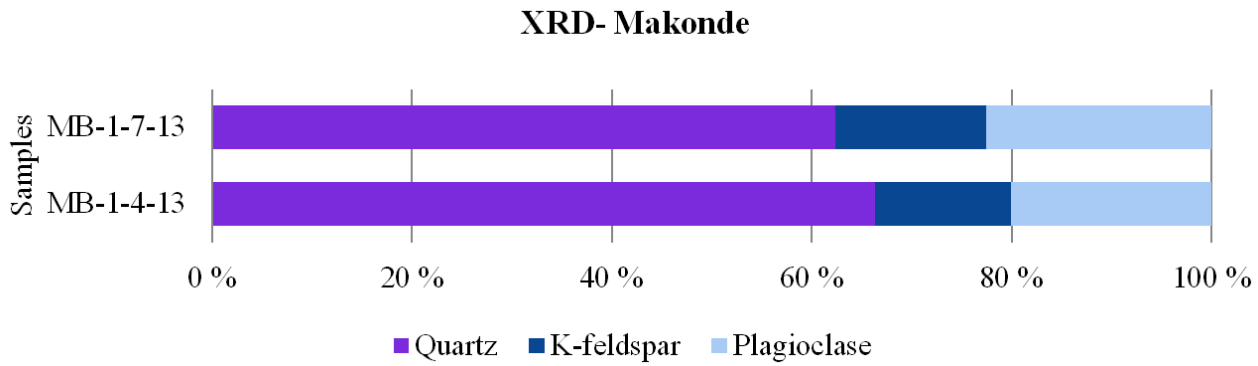

***Figure 4.15**: Bulk mineral composition of two key samples from the Makonde Formation. The key samples include sample MB-1-4-13 and sample MB-1-7-13.*

TDP well site 24- Kihuluhule Fm.

Cores from TDP well site 24 was studied and logged at the TPDC storage unit. The cores were drilled in the Lindi area (Figure 1.1) in the southern part of the Mandawa Basin and comprise sediments from Kihuluhulu Fm. The core comprises 90m of mainly alternating clay and carbonate cemented sand (Figure 4.17 A, B and C).

Mineralogical composition

The bulk mineral composition of two key samples from TDP well site 24, TDP 24/28/1 and TDP 24/16/3 was analyzed by XRD (Figure 4.16). Sample TDP 24/28/1 is dominated by quartz, which makes up 60% of the total mineral composition. It contains over 30% ankerite while plagioclase and K-feldspar are less abundant with 2 and 5 % of the total mineral composition of this sample. Sample TDP 24/16/3 is dominated by similar amounts of quartz and calcite which makes up 80% of the total mineral composition of this sample. Almost

equal amounts of plagioclase and K-feldspar form the remaining 20% of the mineral composition. Table with complete XRD results are presented in Appendix A1.

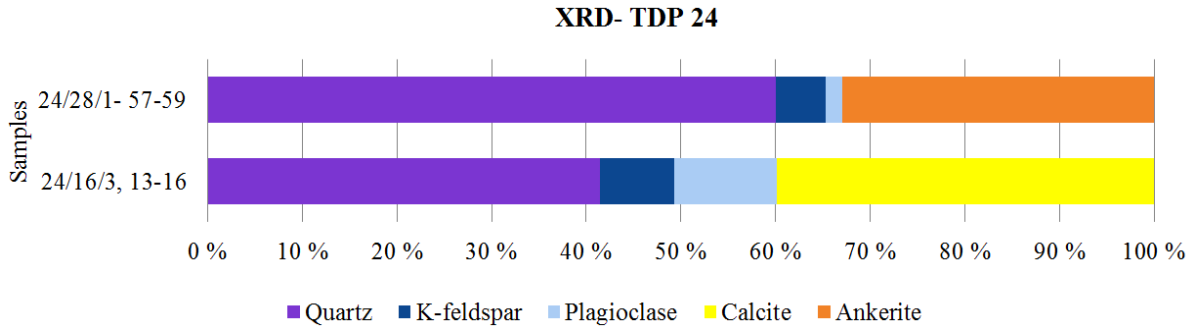

***Figure 4.16**: Bulk mineral composition of the key samples, TDP 24/28/1 and TDP 24/16/3, from TDP well site 24.*

Petrographical description

The petrography of two sand samples (TDP 24/28/1 and TDP 24/16/3) from TDP well site 24 was studied in thin section. The samples consist of fine to medium sized sand and the grains are well rounded (Figure 4.19 A). The sand is well sorted and the grains generally display mostly long and tangential contacts. The samples are characterized by quartz surrounded sparitic calcite or rhombic ankerite cement. The quartz grains are dominated by monocrystalline grains with instantaneous extinction which make up 78-85% of the quartz composition. Polycrystalline quartz comprises 7-8% of the quartz grains while undulose quartz grains are more abundant with 16- 20%. The feldspar grains are poorly preserved in these samples and display a preservation dominated by category 4 (Table 3.2). Overgrowth of K- feldspar is present on some of the K-feldspar grains. Authigenic kaolinite booklets is observed filling up some of the pores. The sand samples from TDP 24 are classified as arkosic sands based on results from point counting (Appendix C).

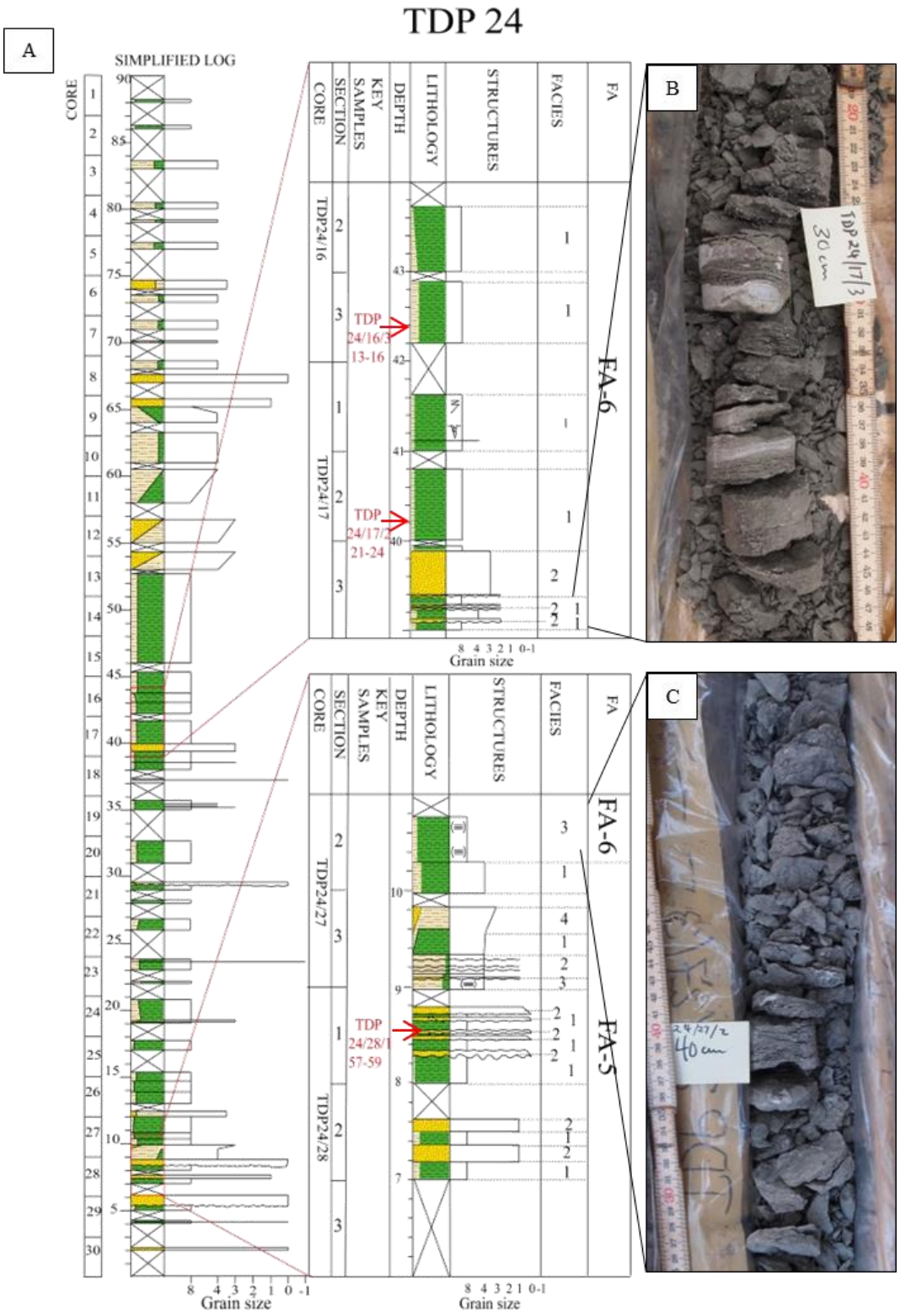

***Figure 4.17**: A) Simplified sedimentological log of cores from TDP well site 24, Kuhiluhulu Fm. (Figure 1.1, 2.4 and 2.5). The parts where key samples were taken (marked in red) are displayed in more detail. B) Thin alternating layers of sand and clay from within section 17. C) Slightly parallel laminated clay within section 27. Complete sedimentological log is presented by Gundersveen (2014).*

TDP well site 21- Kihuluhulu Fm.

Cores from TDP well site 21 was drilled in the Lindi area in the southern part of the Mandawa Basin and comprises sediment from Kihuluhulu Fm. (Figure 1.1, 2.4 and 2.5). The core comprises 75m of clay with medium sized sand intervals (Figure 4.20). The sand intervals are characterized by soft sediment deformation structures (Figure 4.20 C) and sand beds with erosive base and mud clasts (Figure 4.20 B) are common.

Mineralogical composition

The bulk mineral composition of three key samples (TDP 21/17/2, TDP 21/21/1 and TDP 21/22/2) from the lower part of TDP well site 21 (Figure 4.20) was analyzed by XRD (Figure 4.18). Samples TDP 21/17/2 and TDP 21/22/2 display similar mineral composition. They are dominated by quartz (54-59%) and calcite (32-36%). Feldspar makes up less than 10% and is dominated by K-feldspar (6-8%). Sample TDP 21/21/1 differs from the previous key samples from TDP well site 21 by the high content of clay minerals. Mixed layer clay makes up 35% of the total mineral composition in this sample. Clay separation analysis of clays in Kilwa Group (Figure 2.4), conducted by Mahmic (2014) revealed a mixture of smectite, kaolinite, chlorite and vermiculite of varying combination of these, within the mixed layer clay. Quartz comprises 40% of the sample while K-feldspar and plagioclase makes up 21 %, with 13% and 8 % respectively. Sample TDP 21/21/1 also differs from the other key samples by the content of pyrite, which makes up nearly 3 % of the mineral composition. Table with complete XRD results are presented in Appendix A1.

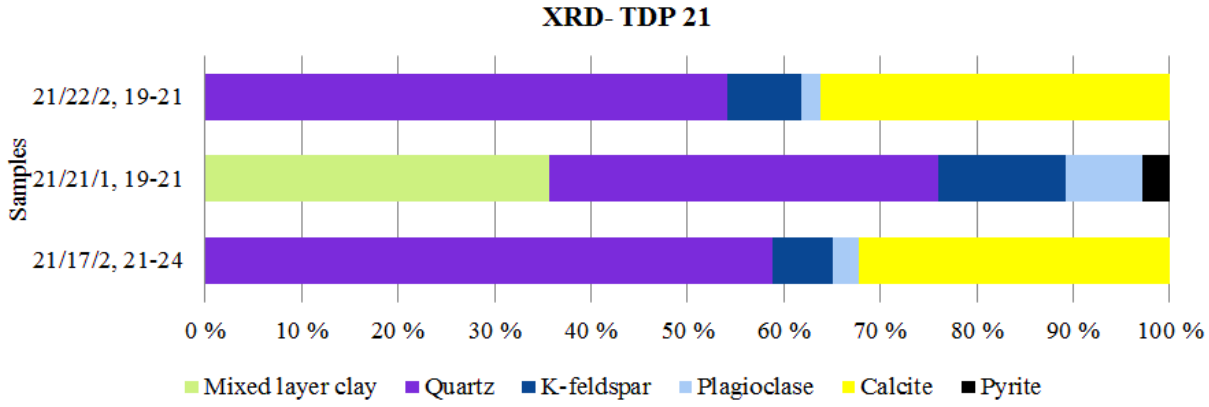

***Figure 4.18**: Bulk mineral composition of three key samples, TDP 21/22/2, TDP 21/21/1 and TDP 21/17/2, from TDP well site 21, Kihuluhulu Fm. (Figure 1.1, 2.4 and 2.5).*

Petrographic description

The petrography of three key sand samples from TDP well site 21 (TDP 21/22/2, TDP 21/21/1 and TDP 21/17/2) was studied in thin section. Sample TDP 21/22/2 and TDP 21/17/2 are dominated by monocrystalline quartz with straight extinction which makes up 90% of the quartz composition. Polycrystalline quartz (5%) and quartz with undulose extinction (9%) are less abundant. The grains are surrounded by sparitic calcite cement in sample TDP 21/17/2 while micritic calcite cement and possible recrystallized calcite cement is more abundant in sample TDP 21/22/2. Although the two samples display similar mineral content their appearance are quite different. Sample TDP 21/17/2 consists of well rounded, coarse, well sorted sand. Feldspar grains in this sample are poorly preserved with an abundance of feldspar from category 4 and 5 (Table 3.2). Authigenic kaolinite booklets were observed within dissolved grains (Figure 4.19 B). Sample TDP 21/22/2 contains sub rounded medium sand with moderate sorting. Feldspar grains are slightly better preserved in this sample with the majority of grains classified as category 4. The calcite cement in sample TDP 21/21/1 includes clay minerals which were observed and analyzed by SEM. Sample TDP 21/21/1 are dominated by a clay rich matrix and subrounded grains with moderate sorting. Monocrystalline quartz with instantaneous extinction dominates the quartz composition with 87%. Only 4% of the quartz grains display polycrystalline character while 10% of the quartz grains have an undulatory extinction. A majority of the feldspar grains in this sample display a preservation classified as category 4. Results from point counting classify sample TDP 21/22/2 and TDP 21/17/2 as arkosic sand and sample TDP 21/21/1 as a feltspatic wacke (Appendix C).

4.2.5 Upper Cretaceous

The Late Cretaceous time period is represented by cores from TDP well site 9 (Campanian – Maastrichtian) and sample 21-7-2012 (Campanian), both comprising sediments from Nangurukuru Fm (Figure 1.1, 2.4 and 2.5).

TDP well site 9-Nagurukuru Fm

Cores from TDP well site 9 was logged and studied at the TPDC core storage. Of the total 140m, 90m of the core was logged. The core is dominated by silty clay (Figure 4.22 A and B) and bioturbation (Figure 4.22 C). Burrows and foraminifera are abundant.

***Figure 4.19**: A) Cross polarized micrograph of rounded grains in sample TDP 24/28/1 from TDP well site 24. The grains are well sorted with long and tangential contacts, and are surrounded by sparitic calcite cement. B) A backscatter image taken in SEM, displaying authigenic kaolinite (Kln) within a dissolved quartz grain (Qtz) in sample TDP 21/17/2 from TDP well site 21. Sparitic calcite cement (Cal) surrounds the grains. C) Plan polarized micrograph of sub rounded grains within a clay matrix in sample TDP 9/13/1, TDP well site 9. The sample is moderately sorted and fossils of foraminifera (marked with red arrow) are abundant in the sample. D) Cross polarized micrograph of sub rounded grains in sample 21-7-2012. The sand displays good sorting and grain contacts are mainly of tangential character. Sparitic calcite cement surrounds the grains. E) Plan polarized micrograph of sample TDP 7B/12/2 from TDP well site 7B. The sample is moderately sorted with an abundance of Numolites (marked with red arrow). F) Cross polarized micrograph of sample TDP 2/14/2 from TDP well site 2. The sand display moderate sorting with sub rounded and sub angular grains. Grain contacts are of tangential character. Heavy minerals (marked with red) are abundant in this sample.*

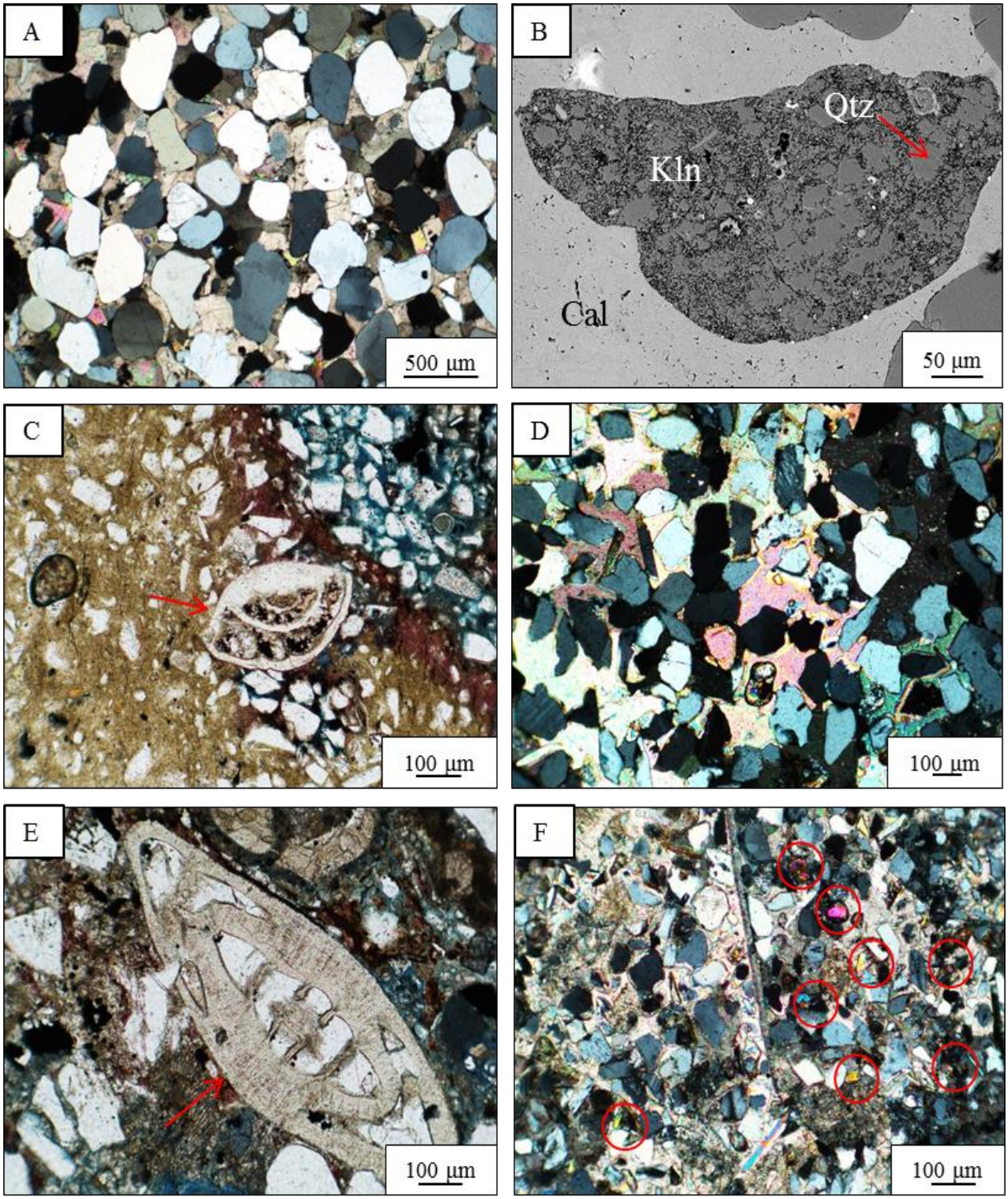
A
500 µm
B
Qtz
Kln
Cal
50 µm
C
100 µm
D
100 µm
E
100 µm
F
100 µm

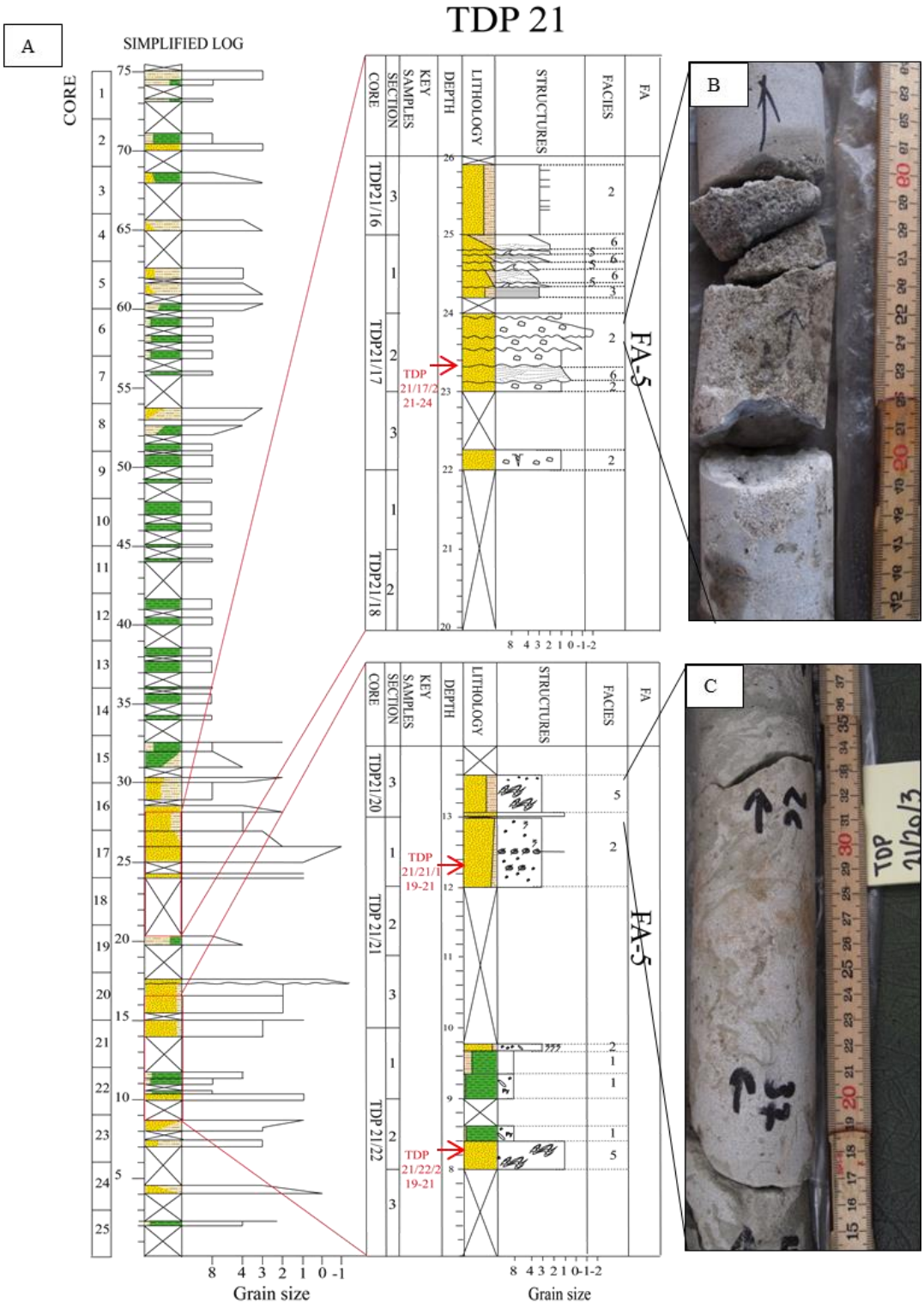

***Figure 4.20**: A) Simplified sedimentological log of cores from TDP well site 21 which comprises sediments from Kihuluhulu Fm. (Figure 1.1, 2.4 and 2.5) Parts of the log where key samples are taken from (marked in red) are displayed in more detail. B) Erosive beds displayed in sand from section 17. C) Soft sediment deformation structures in section 20. Complete sedimentological log is presented by Gundersveen (2014).*

Mineralogical composition

The bulk mineral composition of one clay rich key sample from TDP well site 9 (TDP 913/1) was analyzed by XRD (Figure 4.21). The sample is dominated by quartz (21%) and calcite (29%). Plagioclase comprises 14% of the bulk mineralogy and is more abundant than K-feldspar which makes up 10%. The remaining bulk composition consists of a variety of clay minerals. Mixed layer clay comprises 7% of the bulk mineralogy, and mica comprises 6%, while kaolinite and chlorite make up 5% each. Mixed layer clay comprises smectite, illite chlorite, kaolinite and vermiculite or varying combination of these (Mahmic, 2014). Table of complete XRD results are presented in Appendix A1.

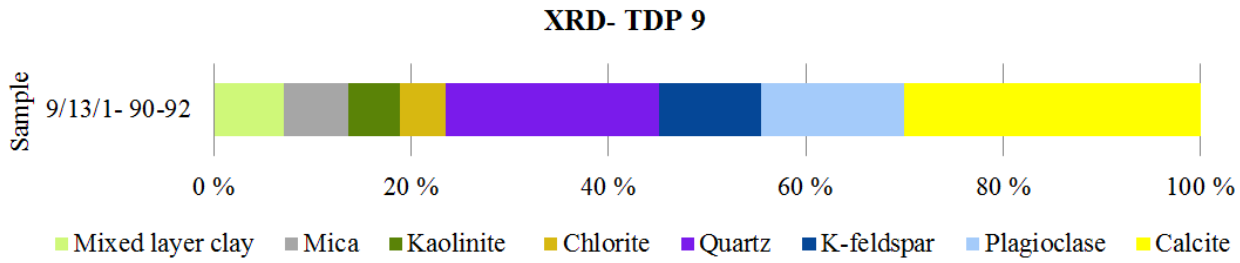

***Figure 4.21**: Bulk mineral composition of the key sample TDP 9/13/1 from TDP well site 9. The sample comprises sediments from Nangugrukuru Fm. (Figure 2.4and 2.5)*

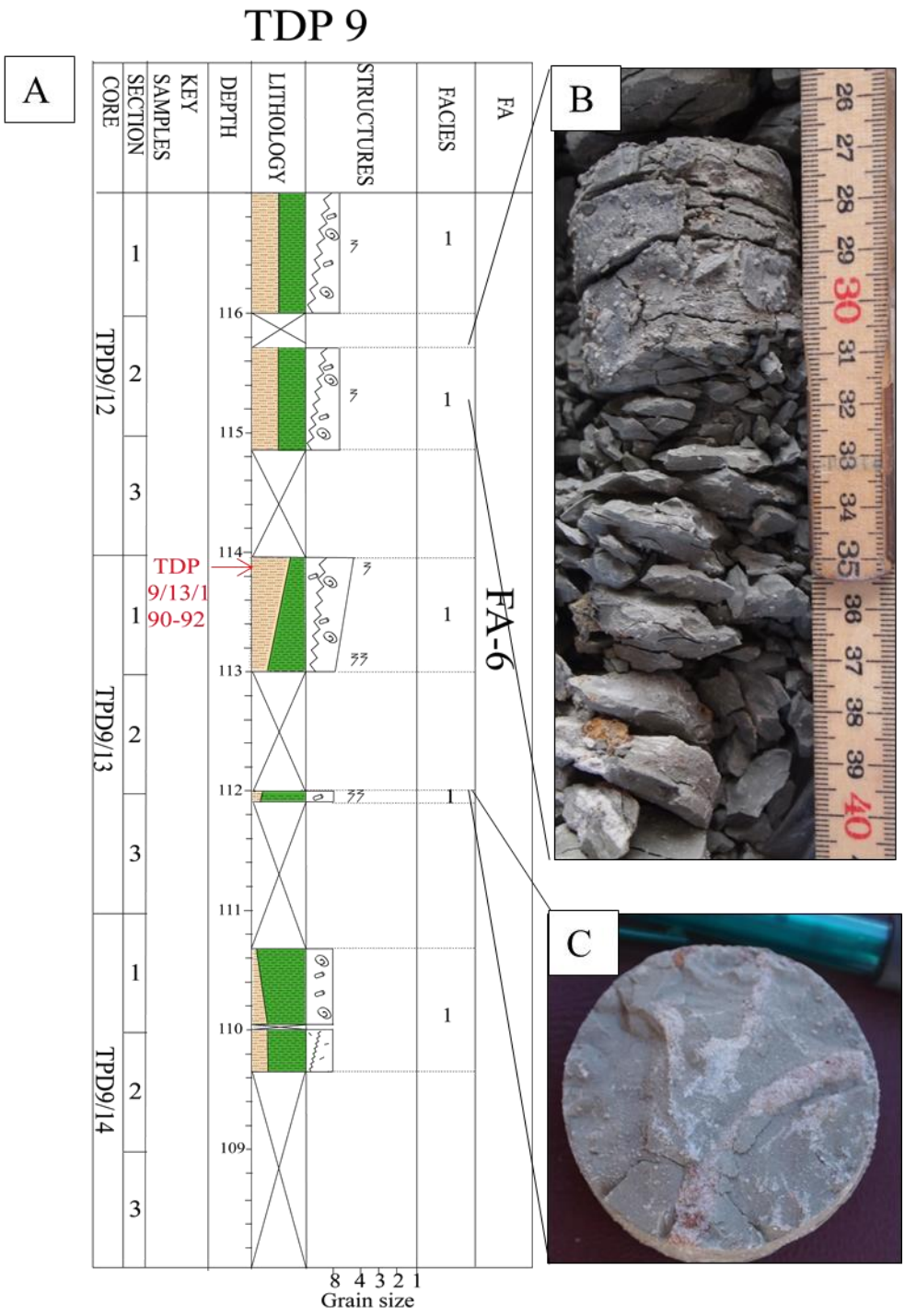

***Figure 4.22**: A) A 9m section from TDP well site 9 (Figure 1.1). Key sample and sampled position are marked with red. TDP well site comprises sediments from Nangurukuru Fm. (Figure 2.4 and 2.5) B) Silty clay (facies 1) dominates throughout the core. C) A cross section through core 13, section 3, where bioturbation is abundant. Complete sedimentological log is presented by Mahmic (2014).*

Petrographic description

The petrography of one key sample from TDP well site 9, sample TDP 9/13/1, was studied in thin section. This sample consists of very fine sand with subrounded grains and moderate sorting. The grains are surrounded by a matrix contains both clay minerals and micritic calcite (SEM analysis). The presence of matrix in the sample leads to a minimum of grain contacts but the few that are present are of tangential character. Sample TDP 9/13/1 is abundant in monocrystailline quartz with straight extinction which makes up 85% of the quartz composition. Polycrystalline quartz is sparse and comprises only 4% of the quartz content. Quartz grains with undulatory extinction are more abundant with 11%. The feldspar grains are moderately to poorly preserved with an abundance of feldspar classified as category 3-4 (Table 3.2). Pyrite and fossils of foraminifera are abundant in the thin section (Figure 4.19 C). Results from point counting show a matrix content of 75%, which classifies sample 9/13/1 between a feltspatic wacke and a mudstone (Appendix C).

21-7-2012- Nangurukuru Fm.

Sample 21-7-2012 was taken by Arild Andresen and Henning Dypvik during a reconnaissance field in 2012 and comprises sediments from Nangurukuru Fm. (Figure 1.1, 2.4 and 2.5). The petrography of the sample was studied in thin section and SEM and the mineralogical composition was analyzed by point counting.

Mineralogical composition and petrographic description

Sample 21-7-2012 consists of fine, well sorted sand. The grains are subrounded and consist mostly of tangential contacts between the grains (Figure 4.19 D). The sample is dominated by quartz which makes up 50% of the total mineral composition. 95% of the quartz grains are of monocrystalline character with straight extinction. Only 4 % of the quartz grains display undulose extinction while polycrystalline grains are even less abundant comprising 2% of the total quartz composition. The grains are surrounded by sparitic calcite which makes up 40% of the total mineral composition. Feldspar grains are sparse in sample 21-7-2012 and make up less than 7% of the mineral composition with 4, 5% K- feldspar and 2 % plagioclase. The feldspar grains are poorly preserved with a majority of grains classified as category 4. Mica and pyrite were observed in the sample by light microscope and heavy minerals were

recognized by the use of SEM. Results from point counting classify sample 21-7-2012 as arksoic sandstone (Appendix C).

4.2.6 Eocene

The Eocene successions is represented by TDP well site 7B (Lower Eocene) and TDP well site 2 (Lower to Mid Eocene) in this study. Cores from TDP well site 7B comprises sediments from Kivinje Fm., while cores from TDP well site 2 consist of sediments from Masoko Fm. (Figure 2.4 and 2.5)

TDP well site 7B- Kivinje Fm.

Cores from TDP well site 7B was retrieved from the Kilwa area near Kilwa Kivinje (Figure 1.1). The core comprises 160m of silty clay (facies 1) (Figure 4.24 A and B) with occasional sandy intervals (facies 2).

Mineralogical composition

The bulk mineral composition of one key sample from TDP well site 7B (TDP 7B/12/2) was analyzed by XRD (Figure 4.23). The sample is dominated by calcite, which makes up 60% of the bulk composition. Quartz comprises 18% of the minerals while feldspar makes up 13%, with 5% K-feldspar and 8% plagioclase. Clay minerals make up 8% of the bulk composition, with 4% mica, 3% mixed layer clay and 1 % kaolinite. Mixed layer clay comprises smectite, illite chlorite, kaolinite and vermiculite or varying combination of these (Mahmic, 2014). Aragonite and pyrite both comprise 2, 5% of the bulk mineral composition. Table of complete XRD results are presented in Appendix A1.

Petrographic description

The petrography of one key sample (TDP 7B/12/2) from TDP 7B was studied in thin section. The sample is characterized by fine sand with sub angular grains and moderate sorting. It is dominated by bioclastic calcite where fossils of Nummulites (Figure 4. 19 E) and other foraminifera are common (Figure 4.23 A). Micritic and possibly recrystallized calcite cement are also abundant in the sample. The majority of the quartz grains are monocrystalline with instantaneous extinction (88%) but undulatory and polycrystalline quartz grains are also

present comprising 6% and 5% respectively. The feldspar grains are poorly preserved, and are dominated by grains classified as category 4-5 (Table 3.2). Pyrite is present in this sample and rock fragments were observed. Results from point counting classify sample TDP 7B712/2 as arkosic sand (Appendix C).

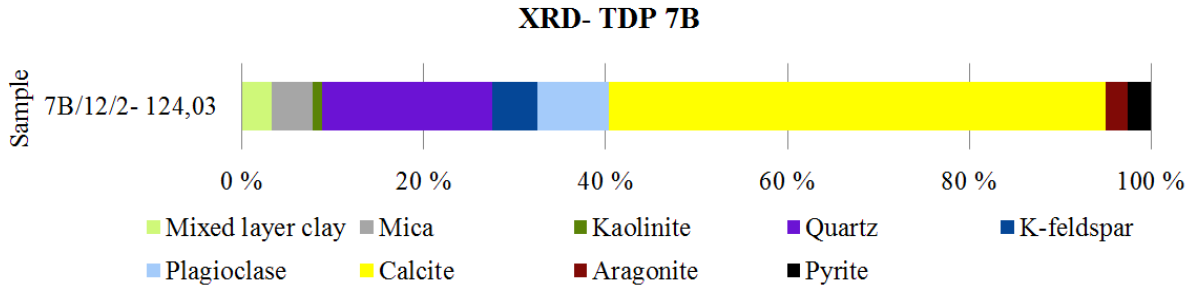

Figure: 4.23*: Bulk mineral composition of key sample (TDP 7B/12/2) from TDP well site 7B (Figure 1.1). The sample comprises sediments from Kivinje Fm. (Figure 2.4 and 2.5).*

TDP well site 2- Masoko Fm.

Cores from TDP well site 2 was drilled in the Kilwa area near the town Kilwa Masoko (Figure 1.1) and comprises sediments from Masoko Fm.(Figure 2.4 and 2.5). TDP 2 is dominated by silty clay (facies 1) with carbonate intervals rich in Nummulites (facies 7) (Figure 4.25).

Mineralogical description

The bulk mineral content of one key sample (TDP 2/14/2) from TDP well site 2 was analyzed by XRD (Figure 4.24). Calcite is the most abundant mineral comprising 36% of the bulk mineral composition. Quartz comprises 29% of the sample while feldspar makes up 26%, with 16% plagioclase and 10 % K-feldspar. The remaining 9% consist of equal amounts of mica and aragonite. Table of complete XRD results are presented in Appendix A1.

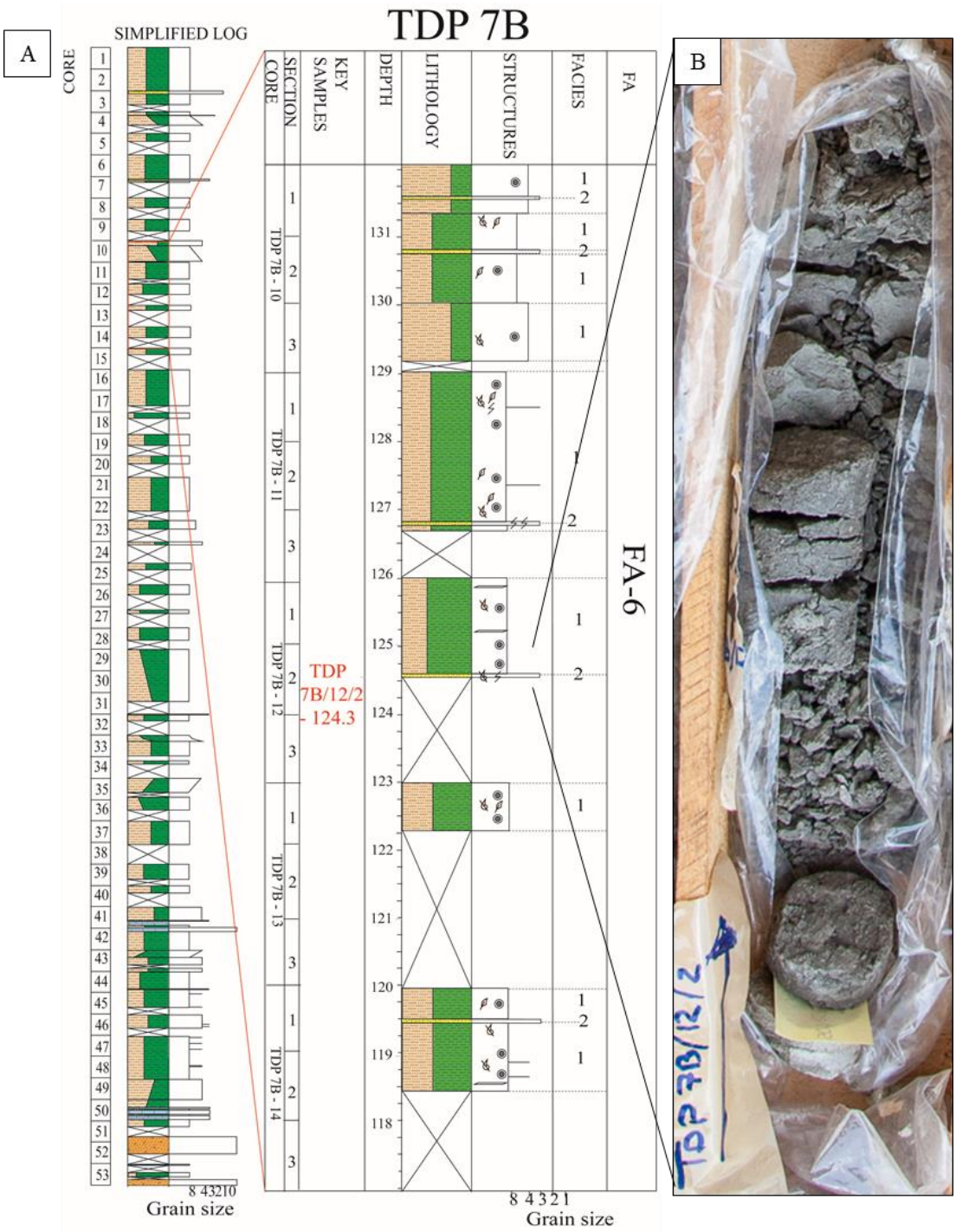

***Figure 4.23**: A) simplified log of TDP well site 7B, Masoko Fm., with a more detailed section showing where the key sample (marked in red) sampled. B) Image of section 12 with silty clay (facies 1), which dominates throughout the core. Complete sedimentological log is presented by Mahmic (2014).*

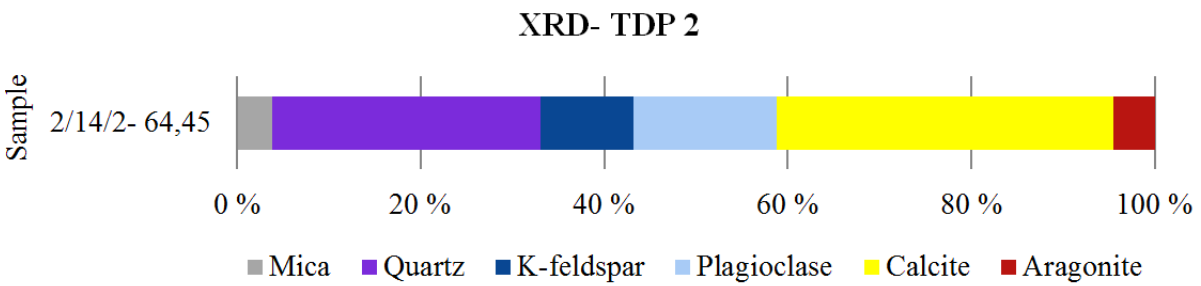

***Figure 4.24**: Bulk mineral composition of sample TDP 2/14/2 from TDP well site 2. The sample comprises sediments from Masoko Fm. (Figure 2.4 and 2.5).*

Petrographic description

The petrography of one key sample (TDP 2/14/2) from TDP well site 2 was studied in thin section. The sample consists of fine and medium sized sand with medium sorting. The few grain contacts in the sample are of tangential character and the grains are generally subrounded to subangular. The sample is dominated by bioclastic calcite and Nummulites and other foraminifera were observed in light microscope. The quartz content is characterized by monocrystalline grains with straight extinction (86%) while polycrystalline grains (3%) are less abundant. Quartz grains with undulose extinction make up 13% of the quartz composition. Feldspar grains are moderately preserved with a majority of grains classified as category 3-4 (Table 3.2). Lamination is present in the sampled section (Figure 4.25 B) and within the thin section. The lamination consists of the separation between very fine sand and fine to medium sized bioclastic sand. Pyrite and mica was observed in light microscope and by SEM. Heavy minerals are also abundant in this sample (Figure 4.19 F). Result from point counting classify the sediments in sample TDP 2/14/2 as an arkose (Appendix C).

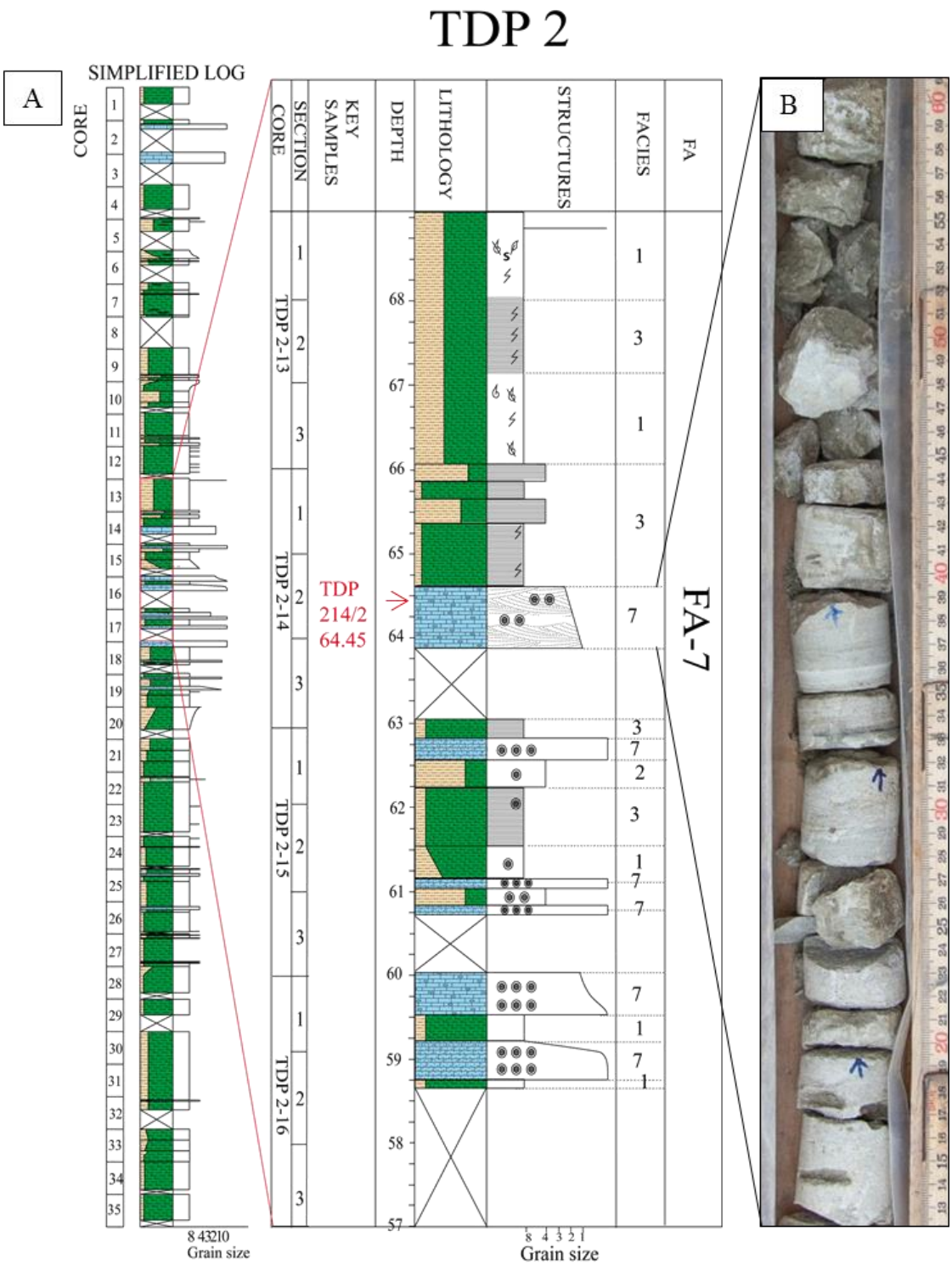

***Figure 4.25**: Simplified logs of TDP well site 2 with detailed section where the key sample (marked in red) was sampled. Cores from TDP well site 2 comprises sediments from Masoko Fm. (Figure 2.4 and 2.5) B) Carbonate layer displaying cross lamination. Complete sedimentological log is presented by Mahmic (2014).*

4.2.7 Oligocene

Oligocene time period is represented by TDP well site 1 (Lower Oligocene) in this study and comprises sediments from Pande Fm. (Figure 11, 2.4 and 2.5).

TDP well site 1

Cores from TDP well site 1 was retrieved from the Kilwa area, close to Kilwa Masoko (Figure 1.1) and comprises sediments from Pande Fm. (Figure 2.4 and 2.5). TDP well site 1 is dominated by silty and sandy clay (facies 1) (Figure 4.27 A and B) and parallel laminated intervals (facies 3). Intervals with very fine or carbonate rich sand occur (Figure 4. 27).

Mineralogical composition

The bulk mineral composition of two key samples (TDP 1/18/1 and TDP 1/20/1) from TDP well site 1 was analyzed by XRD (Figure 4.26). Sample TDP 1/18/1 is dominated by quartz, which makes up 61% of the bulk composition. Feldspar comprises 31% with 22% K-feldspar and 9% plagioclase. The remaining 8% of the mineral composition consists of equal amounts of mica and calcite. Sample TDP 1/20/1 is also dominated by quartz (44%) but contain a variety of other minerals which are absent in sample 1/18/1. Different clay minerals make up 25% of the sample with mixed layer clay as the dominating constituent (19%). Mixed layer clay comprises smectite, illite chlorite, kaolinite and vermiculite or varying combination of these (Mahmic, 2014). Mica comprises 5% of the total composition while kaolinite and chlorite are less abundant comprising only 1% each. Feldspar makes up 24% of the total mineral composition with 18% K-feldspar and 6% plagioclase. The remaining 6% of the sample consist of aragonite. Table of complete XRD results are presented in Appendix A1.

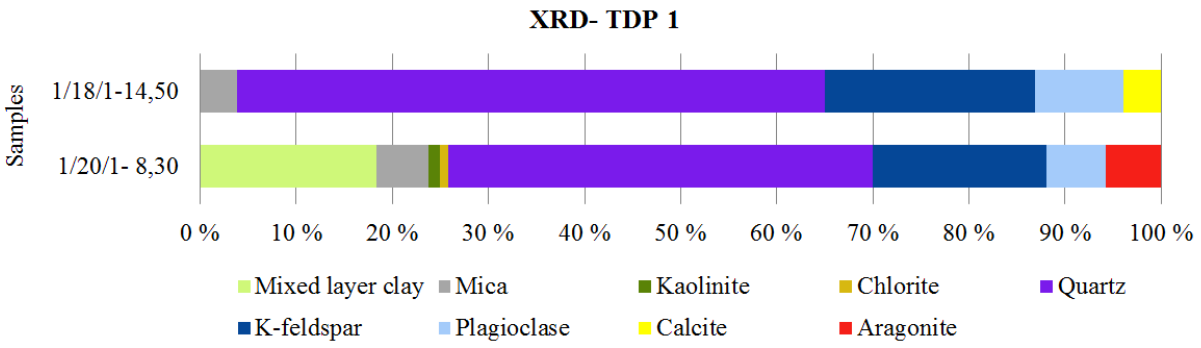

Figure 4.26: Bulk mineral composition of two key samples, TDP 1/18/1 and TDP 1/20/1, from TDP well site 1.

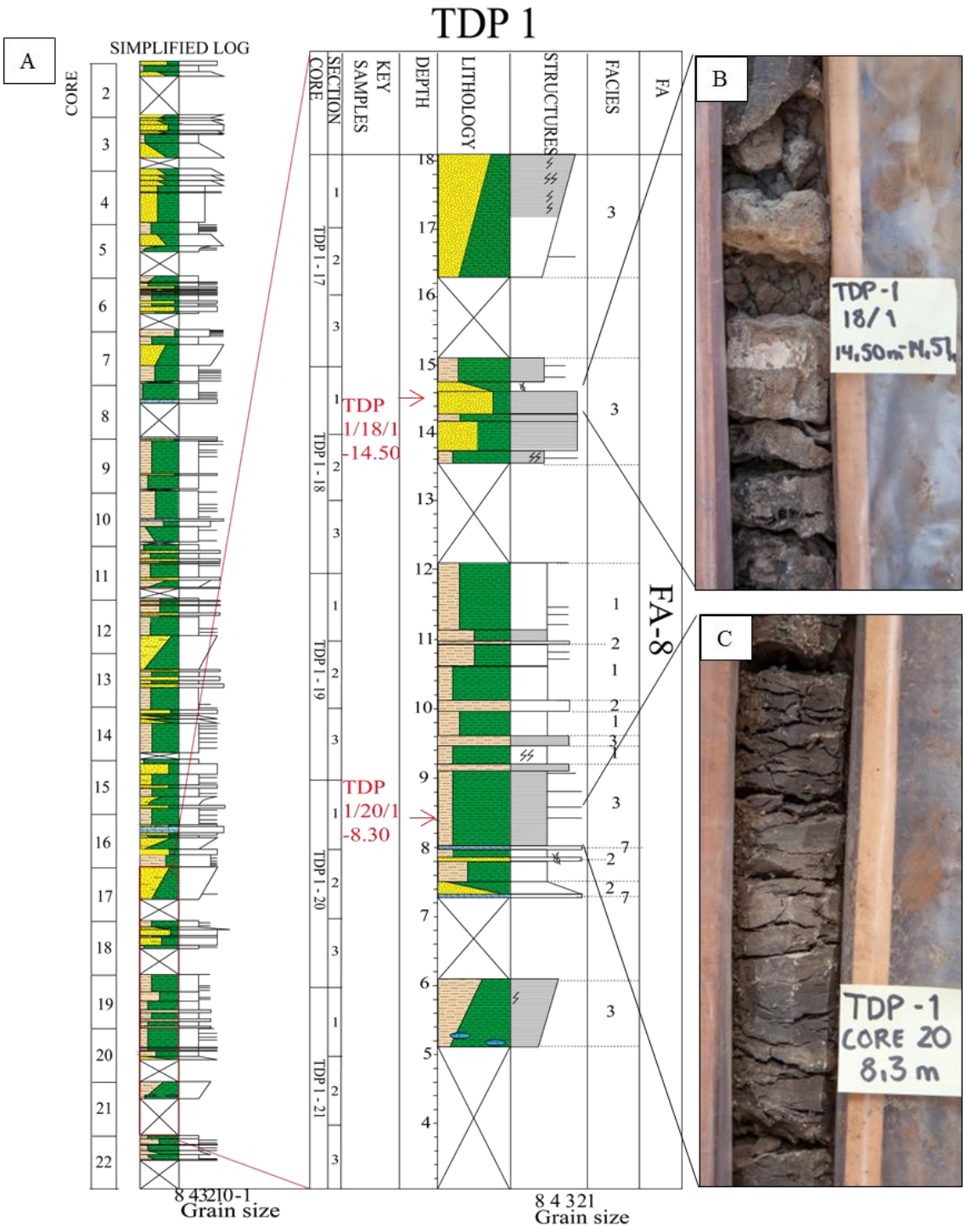

***Figure 4.27**: A) Simplified logs of TDP well site 1 with a more detailed section where the key samples (marked in red) were sampled B) Clayey sand in core 18, section 1. C) Silty clay in core 20, section 1. Complete sedimentological log is presented by Mahmic (2014).*

Petrographic description

The petrography of two key samples from TDP well site 1, TDP 1/18/1 and TDP 1/20/1, was studied in thin section. Sample TDP 1/18/1 consists of fine sand with moderate sorting. The grains are subangular. The few grain contacts in the sample are of tangential character. The quartz fraction is dominated by monocrystalline grains with straight extinction (89%). Quartz grains with undulose extinction makes up 7% of the quartz composition while polycrystalline grains comprise 5% of the quartz grains. Feldspar grains are moderate to poorly preserved in the sample with the majority of grains being classified as category 3-4 (Table 3.2). The calcite occurs as bioclasts or clasts of recrystallized calcite. Mica, present in the sample is poorly preserved. Sample TDP 1/20/1 consists of coarse silt in a matrix consisting of clay and aragonite. The grains are subangular and display moderate sorting. There are few contacts between the grains due to the clayey matrix present in the sample. The sample is dominated by monocrystalline quartz with straight extinction which comprises 90% of the quartz composition. The remaining 10% of the quartz fraction consist of grains which display undulose extinction. The feldspar grains are moderately to poorly preserved with a majority of grains classified as category 3-4 (Table 3.2). Results from point counting classify sample TDP 1/20/1 as feltspatic wacke and sample 1/18/1 as arkosic sand (Appendix C).

4.2.8 Recent

The recent time period is represented by sediments from Matandu River in this study.

Matandu River

A sample from Matandu River was taken from a dry river bed near the Mpopera-Mtumbei locality (Figure 1.1).

Mineralogical composition

The bulk mineral composition of a recent sediment sample from Matandu River (Figure 1.1) has been analyzed by XRD (Figure 4.28). Table of complete XRD results are presented in Appendix A2.

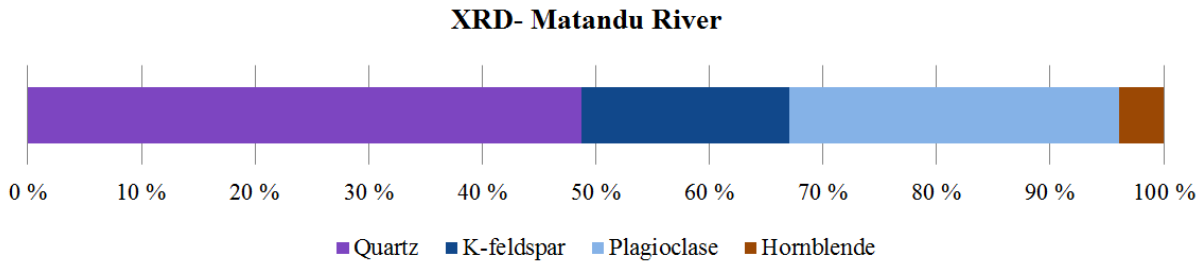

***Figure 4.28**: Bulk mineral composition of a recent sediment sample from Matandu River.*

The Matandu River sample is dominated by quartz, comprising 49% of the mineral composition. Plagioclase comprises 29% of the composition, while K-feldspar makes up 18% of the sample. Hornblende is less abundant and comprises 4% of the bulk mineral composition.

Petrographic description

The petrography of one recent sediment sample, Matandu River, has been analyzed in thin section. The sample consists of very coarse, well sorted sand with subangular grains. Monocrystalline quartz with straight extinction dominates the quartz composition by 89%. Quartz with polycrystalline character makes up 7% of the quartz composition while undulose quartz comprises 5% of the total quartz composition.

Feldspar grains are poorly preserved with an abundance of grains classified as category 4-5 (Table 3.2). Amphibole is abundant in the sample and the grains are partly dissolved. Rock fragments are observed in thin section. Result from point counting classify Matandu River sample as a lithic subarkose (Appendix C).

4.2.9 Offshore samples

Two sand samples, 2/2/14 and 2/1/14 from Statoil, Block 2 (Figure 2.6) represent the offshore sediments in this study.

Cenomanian

Cenomanian age are represented by the offshore sample 2/2/14.

Mineralogical composition

The bulk mineralogy of one offshore sample, 2/2/14 of Cenomanian age was analyzed by XRD (Figure 4.29). The sample is dominated by quartz, which make up 84% of the total mineral composition. K-feldspar comprises 10% of the bulk mineralogy while plagioclase makes up the remaining 6%. Table of complete XRD results are presented in Appendix A2.

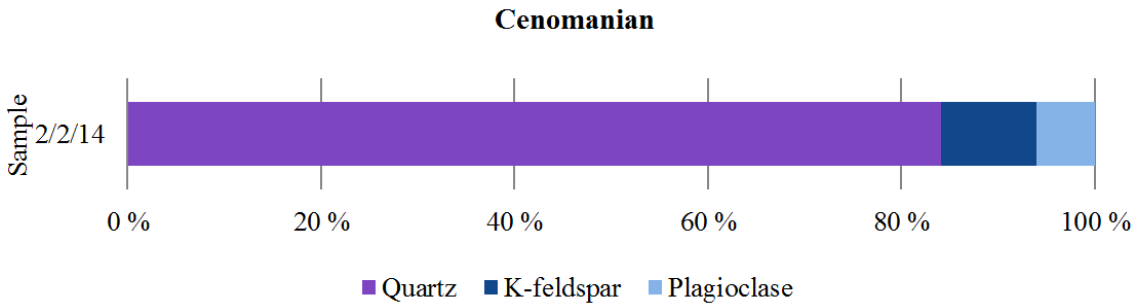

***Figure 4.29**: Bulk mineral composition of sample 2/2/14 from offshore Tanzania.*

Petrographic description

The petrography of the offshore sample 2/2/14, of Cenomanian age was studied in thin section. The sample consists of well sorted, medium to coarse sand with rounded to subrounded grains. The grain contacts are dominated by long, tangential and convex- concave character. Sample 2/2/14 is dominated by monocrystalline quartz grains with straight extinction which makes up 83% of the quartz composition. Quartz with undulatory character comprises 14% while polycrystalline quartz is less abundant with 5% of the total quartz composition. The majority of feldspar grains display a preservation classified as category 4-5 (Figure 3.2). Minor amounts of mica end rock fragments are observed in thin section. Results from point counting classify the sediments in sample 2/2/14 as arkosic sand (Appendix C).

Paleocene

Paleocene age are represented by the offshore sample 2/1/14

Mineralogical composition

The bulk mineral composition of one offshore sample of Paleocene age, 2/1/14 was analyzed by XRD (Figure 4.30). The sample is dominated by quartz which comprises 91% of the bulk composition. Equal amounts of K- feldspar and plagioclase makes up 8% of the mineralogy while calcite only comprises 1% of the total bulk composition. Table of complete XRD results are presented in Appendix A2.

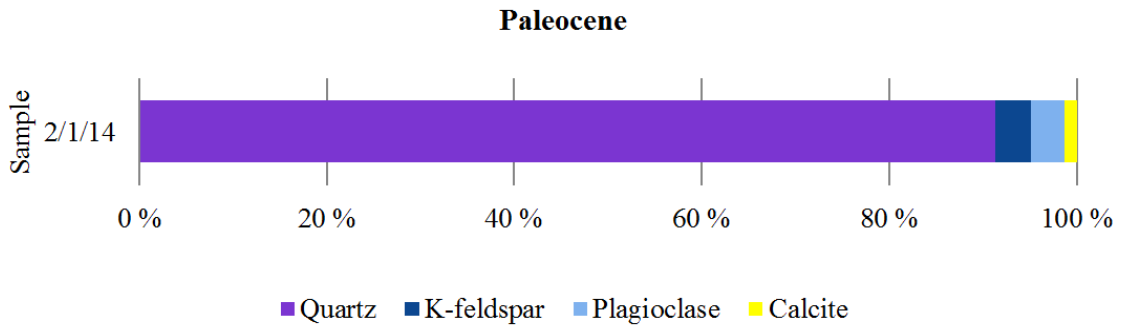

***Figure 4.30**: Bulk mineral composition of sample 2/1/14 from offshore Tanzania.*

Petrological description

The petrography of one offshore sample, 2/1/14 of Paleocene age was studied in thin section. The sample consists of moderate sorted, medium to coarse sand with subangular grains. The grains display mostly long and tangential contacts. Sample 2/1/14 is dominated by monocrystalline quartz with straight extinction which comprises 78% of the quartz composition. Quartz with undulatory character makes up 16% of the quartz faction while quartz of polycrystalline character is less abundant with 8%. Feldspar grains display moderate preservation with the majority of grains being classified as category 3-4 (Figure 3.2). Foraminifera and rock fragments are observed in thin section. Results from point counting classify the sediments in sample 2/1/14 as arkosic sand (Appendix C).

4.3 Heavy mineral analysis

Selected heavy mineral analyses have been conducted to provide provenance information of the sedimentary formations in the Mandawa Basin and offshore Tanzania.

4.3.1 Heavy mineral assemblage

Conventional heavy mineral analysis has been conducted by Andrew Morton at HM Research Associates Ltd, UK (Figure 4.30). See chapter 3.7.2 for more details on methods and classification. Table with complete results of conventional heavy mineral analysis are presented in Appendix D.

Assemblage 1

Heavy mineral assemblage 1 comprises the heavy mineral content of the analyzed basement sample BA-2-13 (Table 4.4). Assemblage 1 is characterized by a high content of calcic amphibole. Apatite is also present in this assemblage making up of 10% of the heavy mineral content. Zircon and clinopyroxene only constitute less than 3% of the heavy mineral content (Table 4.4, Figure 4-31).

Assemblage 2

Assemblage 2 includes heavy minerals of basement sample BA-1-13 and is characterized by a high percentage of zircon (Table 4.4). Apatite makes up just over 10% while garnet, rutile, epidote and monazite only represent a small part of the heavy mineral content (Table 4.4, Figure 4.31)

Assemblage 3

Heavy mineral assemblage 3 includes two samples, MP-2-0-13 and MP-2-1-13, from Karoo sedimentary sequences, of Triassic/Jurassic age (Table 4.4). Sample MP-2-0-13 is dominated by zircon which comprises almost 50% of the heavy mineral content. Approximately equal amounts of garnet, titanite and apatite dominate the remaining 50% while epidote and rutile comprise less than 3% of the heavy mineral fraction. Sample MP 2-1-13 is dominated by

garnet which makes up 65% of the heavy mineral content. Apatite titanite and zircon comprise 30% of the sample while rutile and monazite make up the remaining 5%.

Assemblage 4

Assemblage 4 includes samples from Upper Mitole Mb., Upper Kipatimu Mb. and Makonde Fm. (Figure 2.4 and 2.5), of Late Jurassic to Mid Cretaceous age (Table 4-4). The assemblage is characterized by a high content of zircon and tourmaline, which make up over 80% of the heavy mineral composition. Rutile and monazite are also present but make up less than 20% of the assemblage. Anatase garnet and staurolite are present in minor amounts (Table 4.4, Figure 4.31).

Assemblage 5

Heavy mineral assemblage 5 includes samples from Kihuluhulu Fm., Nangurukuru Fm., and Kivinje Fm. (Figure 2.4 and 2.5), of Mid Cretaceous to Eocene age (Table 4-4). The assemblage is dominated by garnet which comprises 30-70% of the mineral composition. Apatite, kyanite, titanite, zircon and tourmaline are less abundant and make up 40% of the heavy minerals. Rutile, staurolite and epidote are present in minor amounts (Table 4.4, Figure 4.31).

Assemblage 6

Assemblage 6 includes samples from Masoko Fm. and Pande Fm. (Figure 2.4 and 2.5), of Eocene and Oligocene age (Table 4-4). The assemblage is characterized by a high content of epidote (40-50%) which is almost absent in the other assemblages. Apatite, garnet and titanite make up 35- 55% while zircon, tourmaline, staurolite and kyanite are less abundant (Table 4.4, Figure 4.31

Figure: 4.31*: Heavy mineral assemblages in the Mandawa Basin (onshore) and offshore Tanzania. Samples with similar characteristic heavy mineral content are grouped into assemblages (Table 4.4).*

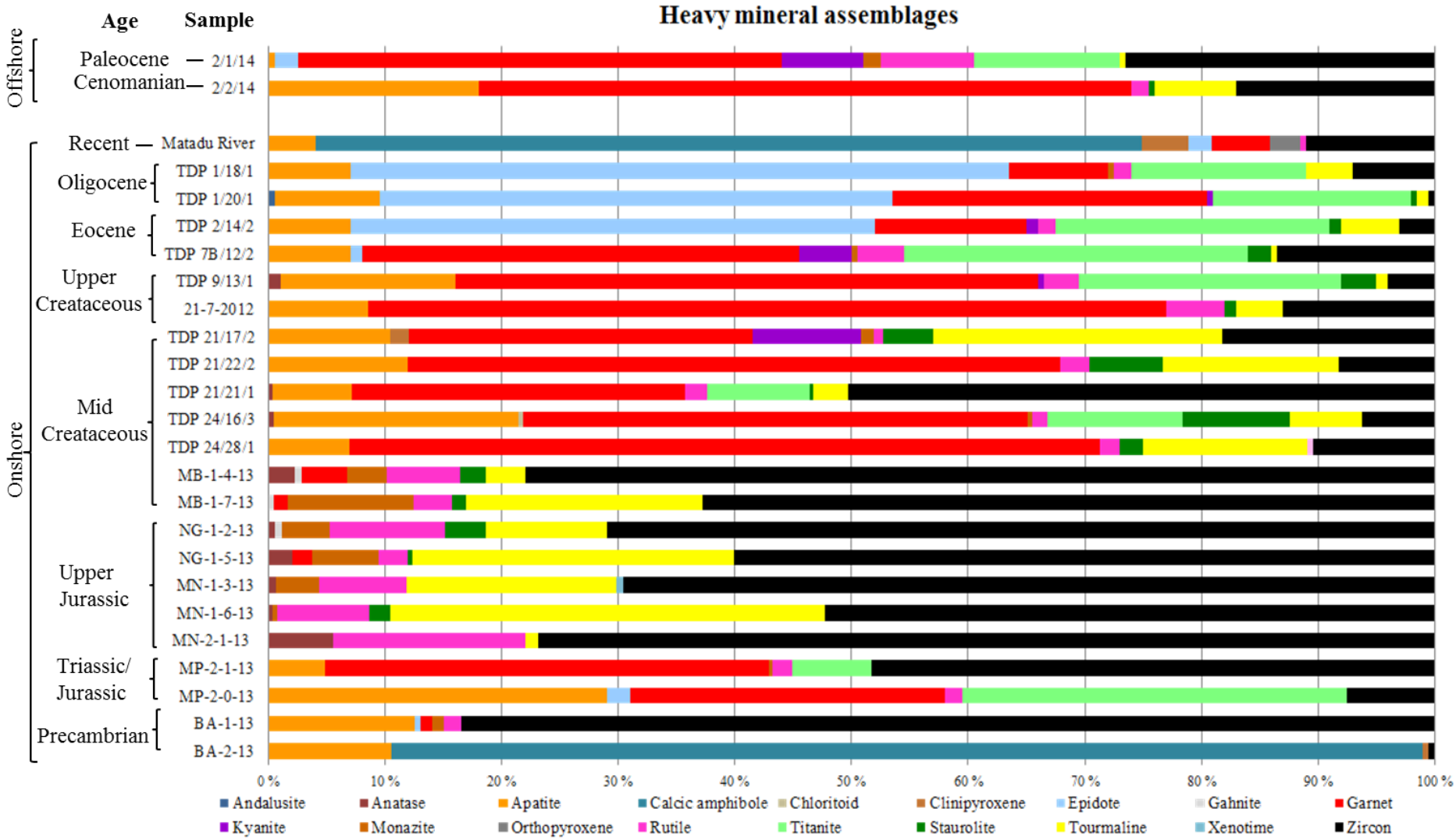
Heavy mineral assemblages
Age
Sample
Offshore
Onshore
Paleocene — 2/1/14
Cenomanian — 2/2/14
Recent — Matadu River
Oligocene
TDP 1/18/1
TDP 1/20/1
Eocene
TDP 2/14/2
TDP 7B/12/2
Upper Creataceous
TDP 9/13/1
21-7-2012
Mid Creataceous
TDP 21/17/2
TDP 21/22/2
TDP 21/21/1
TDP 24/16/3
TDP 24/28/1
MB-1-4-13
MB-1-7-13
Upper Jurassic
NG-1-2-13
NG-1-5-13
MN-1-3-13
MN-1-6-13
MN-2-1-13
Triassic/ Jurassic
MP-2-1-13
MP-2-0-13
Precambrian
BA-1-13
BA-2-13
0 %
10 %
20 %
30 %
40 %
50 %
60 %
70 %
80 %
90 %
100 %
Andalusite
Anatase
Apatite
Calcic amphibole
Chloritoid
Clinipyroxene
Epidote
Gahnite
Garnet
Kyanite
Monazite
Orthopyroxene
Rutile
Titanite
Staurolite
Tourmaline
Xenotime
Zircon

Table 4.4: *Table of ages, samples and heavy mineral content included in the different heavy mineral assemblages.*

	Age	Samples	Heavy mineral content	Heavy mineral assemblage	Depositional environment
Onshore	**Precambrian**	BA-2-13	Calcic amphibole Apatite	1	Basement
		BA-1-13	Zircon	2	Basement
	Triassic/Jurassic	MP-2-0-13 MP-2-1-13	Garnet Titanite Apatite	3	Alluvial fan
	Upper Jurassic	MN-2-1-13 MN-1-6-13 MN-1-3-13 NG-1-5-13 NG-1-2-13	Zircon Tourmaline Rutile Monazite	4	Coastal
					Tidal
	Mid Cretaceous	MB-1-7-13 MB-1-4-13 TDP 24/28/1 TDP 24/16/3 TDP 21/22/2 TDP/21/21/1 TDP 21/17/2	Garnet Apatite Tourmaline Zircon Titanite		River delta
				5	Upper slope/ outer shelf
	Upper Cretaceous	21-7-2012 TDP-9/13/1			Outer shelf (TDP 9)
	Eocene	TDP 7B/12/2 TDP 2/14/2			Outer shelf
			Epidote Titanite Garnet Apatite	6	Carbonate slope
	Oligocene	TDP 1/20/1 TDP 1/18/1			Prodelta/ interdistributary bay
	Recent	Matandu River	Calcic amphibole Zircon Garnet Apatite	7	Fluvial
Offshore	**Cenomanian**	2/2/14	Garnet Apatite Zircon Tourmaline	8	Unknown
	Paleocene	2/1/14	Garnet Zircon Titanite Rutile Kyanite	9	Unknown

Assemblage 7

Heavy mineral assemblage includes the recent sediment from Matandu River (Figure 1.1) (Table 4-4). The assemblage is dominated by calcic amphibole which makes up 70% of the heavy mineral content. Zircon and apatite make up 17% while clinopyroxene, epidote, garnet, rutile and orthopyroxene comprise the remaining 13% (Table 4.4, Figure 4.31)

Assemblage 8

Assemblage 8 is represented by an offshore sample of Cenomanian age (Table 4-4). The heavy mineral content of this assemblage is very similar to assemblage 5 but differs with the absence of titanite. Over 50% of the heavy mineral fraction consists of garnet while 34% consists of equal amounts of apatite and zircon. Tourmaline, staurolite and rutile make up the remaining 16% (Table 4.4, Figure 4.31).

Assemblage 9

Heavy mineral assemblage 9 includes an offshore sample of Paleocene age (Table 4-4). This assemblage is dominated by garnet (40%) and zircon (25%). Titanite rutile and kyanite make up 20% while apatite, epidote, clinopyroxene and tourmaline are less abundant and make up the remaining 15% of the heavy mineral content (Table 4.4, Figure 4.31).

4.3.2 Heavy mineral ratios

To minimize the effect of hydraulic sorting and burial diagenesis, which can overprint the provenance signal, the heavy mineral ratios have been analyzed. Mineral pairs which make up the mineral index were suggested by Morton and Hallsworth (1994) and are based on the similar hydraulic behavior of the different minerals (Table 3.5).

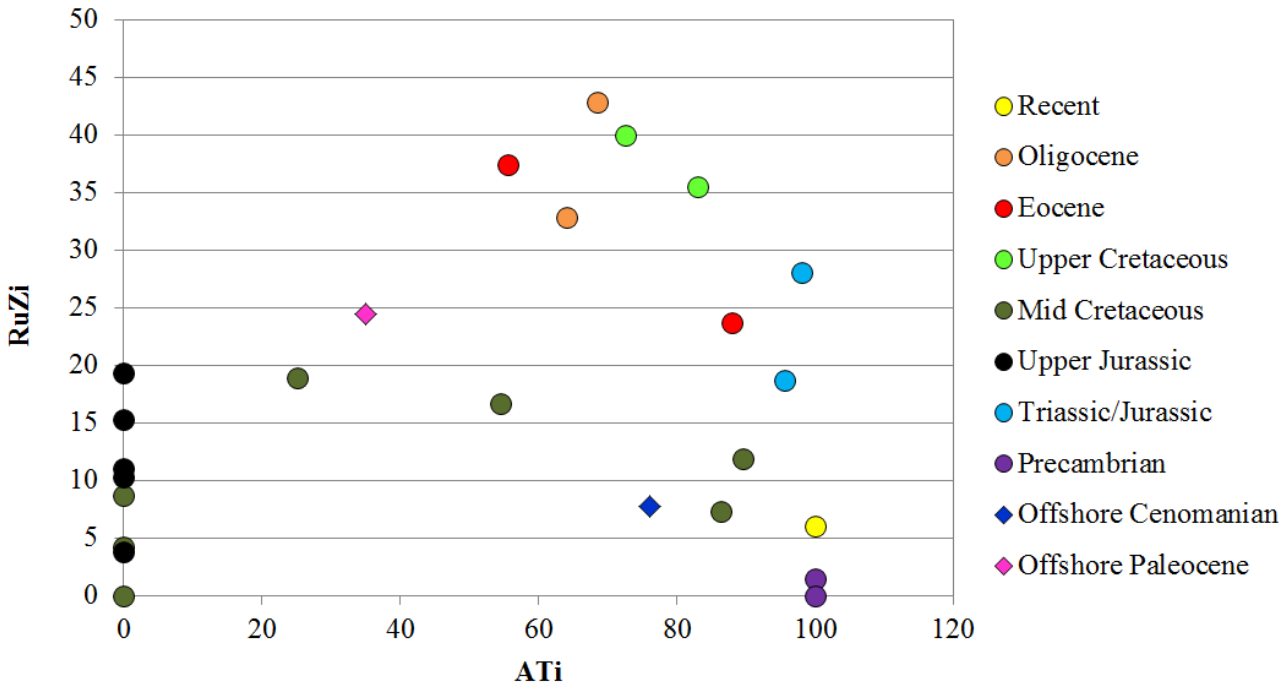

Figure 4.32: Two heavy mineral ratios, RuZi (Rutile, Zircon) and ATi (Apatite, Tourmaline), are plotted.

RuZi-ATi ratio

Rutile-zircon index (RuZi) is plotted against apatite-tourmaline index (ATi) in Figure 4.32. The RuZi index displays an abundance of samples from the Precambrian to the Mid Cretaceous in the lower part of the diagram (RuZi values below 20). The younger samples are abundant in the upper part of the diagram (RuZi values between 25 and 45) with the exception of recent sediments. The apatite–tourmaline index (ATi) is plotted in Figure 4.32. This index displays extremely low values for Upper Jurassic samples and for some samples from the Mid Cretaceous time period. Apart from these extremely low ATi values, a wide distribution is seen for the remaining samples.

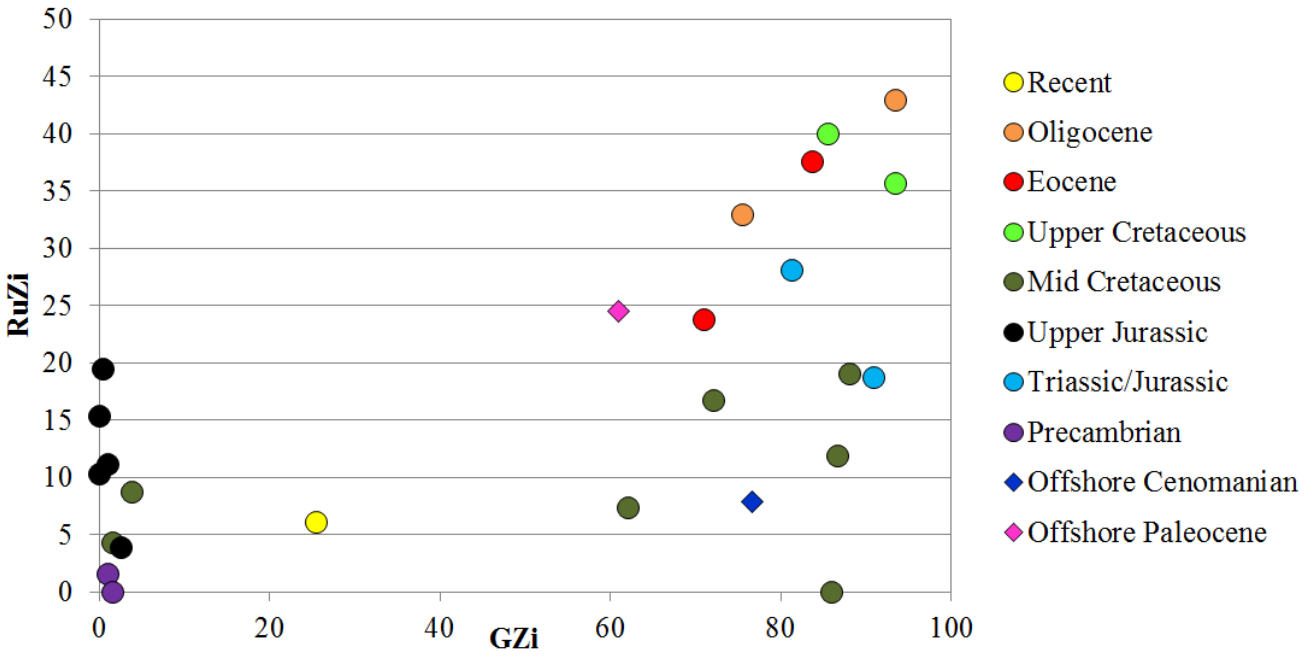

Figure 4.33: Two heavy mineral indexes, RuZi (Rutile, Zircon) and GZi (Garnet, Zircon), are plotted.

RuZi-GZi ratio

The Rutile–Zircon index (RuZi) is plotted against the garnet-zircon index (GZi) in Figure 4.33. The RuZi index display a separation between Precambrian to the Mid Cretaceous samples and samples of Late Cretaceous to recent age, as described in previous section. The GZi index display low values for samples from Precambrian to Late Jurassic age. Samples from Mid Cretaceous to Recent age display variable values, but has generally higher GZi values than Precambrian to Upper Jurassic samples

4.3.3 Electron Microprobe analysis

12 samples from basement, Karoo sedimentary sequence, Kihuluhulu Fm., Nangurukuru Fm. Kivinje Fm., Masoko Fm., Pande Fm. and recent sediments were analyzed in regard to the chemical composition of garnet by the use of electron microprobe analyses. 11 of the samples are of sedimentary origin while one sample represents the basement and is used for comparison and discrimination. Two samples (MN-2-2-13 and MB-1-4-13) from Upper Kipatimu Mb. and Makonde Fm., of Late Jurassic and Mid Cretaceous age were analyzed for

the chemical composition of rutile. Table with complete results of electron microprobe analysis are presented in Appendix E1 and E2.

Geochemical composition of rutile

Electron microprobe analysis has been conducted on two sand samples, one from the Upper Kipatimu Member (MN-2-2-13) and one from the Makonde Formation (MB-1-4-13) (Figure 2.4 and 2.5), regarding the chemical composition of rutile (Figure 4.34). The samples are highly weathered and do not display a large variation in of detrital heavy minerals. Rutile is among the most stable heavy minerals and one of the few heavy minerals that are preserved in these samples. Rutile was analyzed in thin section and the number of analyzed rutile grains is therefore inconsistent. Table of data are presented in Appendix E2.

Rutile with Cr < Nb combined with Nb > 800 ppm are interpreted as rutile derived from a metapelitic rock, based on the diagram introduced by Meinhold et al. (2008) (Figure 3.6). Rutile with Cr > Nb and Nb < Cr where Nb < 800 ppm are interpreted as deriving from metamafic rocks (Meinhold et al., 2008). The two analyzed samples both contain rutile with metamafic and metapelitic chemistry (Figure 4.34). There is an abundance of rutile within the metapelitic field of chemistry and rutile from sample MN-2-1-13 are characterized by lower Nb values than rutile from sample MB-1-4-13.

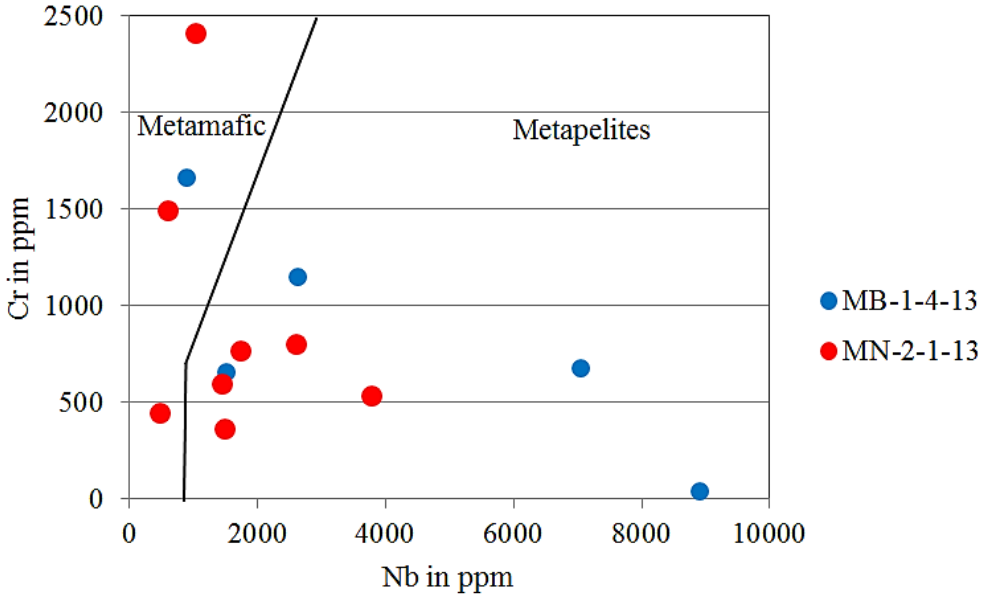

Figure 4.34: *Rutile composition in sample MN-2-2-13 and sample MB-1-4-13. The composition is plotted based on the content of Chromium (Cr) and Niobium (Nb) in parts per million (ppm).*

Geochemical composition of garnet

The chemical garnet composition is analyzed in 11 samples ranging from Precambrian to recent age (Table 3-4). Table of data are presented in Appendix E1. The offshore samples 2/1/14 and 2/2/14 (Figure 4.38) were analyzed by the PhD student, Katrine Fossum. Prochaska and Pohl (1983) analyzed garnets deriving from a metagabbro in northern Tanzania and their result is plotted in figure 4.38. Garnet was analyzed in thin section and in varying number of grains. To minimize the source of error by garnet zonation, some grains were analyzed several times at different areas to detect any changes in the chemical composition (Figure 4.36). The analyzed garnets did not display any significant internal chemical variations.

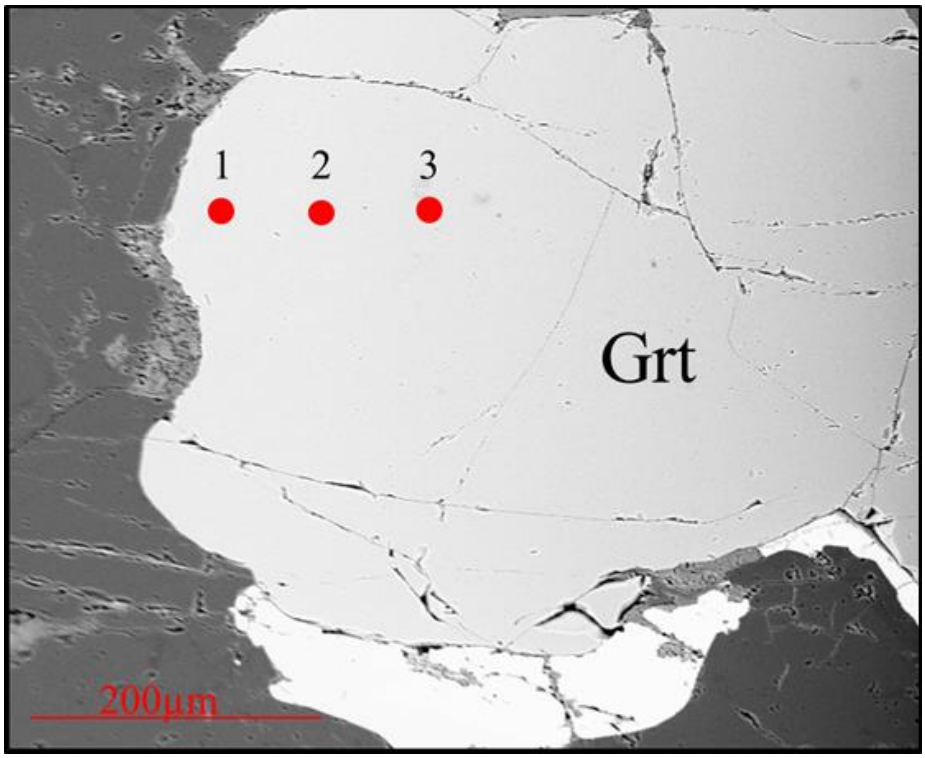

Figure 4.36: *Backscatter image of an analyzed garnet grain. The red areas indicate the different sites which were analyzed to detect the possibility of zonation within the grain.*

The analyzed garnet composition is presented in Figure 4.37 with the end members pyrope, grossular and almandine+ spessartine. Pyrope is a garnet rich in magnesium (Mg), grossular is rich in calcium (Ca), almandine is the iron (Fe) rich garnet and spessartine is rich in manganese (Mn) (Deer et al., 2013).

The analyzed garnet grains (Figure 4.37) display varying chemical compositions. The basement sample BA-3-14 (Figure 1.1) consists of a type of garnet which lies within a field of 10-30% grossular, 10-20% pyrope and 80-75% almandine+ spessartine.

Sample MP-2-13, from the Jurassic to Triassic time period shows a wide variety of garnet composition. Although the garnet composition is spread, the grains all contain over 50% almandine + spessartine, 40% pyrope and between 40-50% grossular (Figure 4.34).

Sample TDP 24/28/1 and TDP 21/17/2 (Figure 1.1) from Kihuluhulu Fm. (Figure 2.4 and 2.5) and represent the Mid Cretaceous time period and display a similar distribution of garnet compositions (Figure 4.34). The samples are characterized by two populations of garnets. One of the populations (population 1) contains Ca- poor garnets with 0-10% of the grossular constituent, 50-60% almandine+ spessartine and around 30% of the pyrope constituent. The other population (population 2) has a higher Ca- content with 15-30% of the grossular constituent. The pyrope (Mg) content varies between 0-30% and the almandine+ spessartine values vary between 50-80% (Figure 4.37).

Sample 21-7-2012 and TDP 9/13/1 (Figure 1.1) from Nangurukuru Fm. (Figure 2.4 and 2.5) represent the Late Cretaceous time period (Figure 4.34). Sample 21-7-2012 contains garnet grains with similar composition as population 2, seen in samples of Mid Cretaceous age. The sample 21-7-2012 also contains Ca- poor garnets as seen in population 1 of Mid Cretaceous age and garnets which are rich in the almandine+ spessartine constituent and poor when it comes to pyrope content. Sample 9/13/1 shows similar characteristics as sample 21-7-2012, but contains garnets which have lower almandine+ spessartine content (Figure 4.37).

Sample TDP 7B/12/2 (Figure 1.1) from Kivinje Fm. (Figure 2.4 and 2.5) and TDP 2/14/2 (Figure 1.1) from Masoko Fm. (Figure 2.4 and 2.5) represent Eocene time period (Figure 4.34). Sample TDP 7B/12/2 displays similar characterization as Mid Cretaceous samples. The sample contains two populations of garnets with similar compositions as the population seen in the Mid Cretaceous samples. Sample TDP 2/14/2 has a narrower distribution of garnet

composition but has similar chemical compositions as garnets from population 2 in the Mid Cretaceous samples (Figure 4.37).

Oligocene time period is represented by sample TDP 1/18/1(Figure 1.1) from Pande Fm. (Figure 2.4 and 2.5). This sample has a wide distribution of garnet compositions much like the sample from the Triassic to Jurassic time period.

The garnets in sample TDP 1/18/1 all contain between 5-40% of the pyrope constituent, 0-40% grossular and 50-90% of the almandine+ spessartine constituent (Figure 4.37).

Sediments from the Matandu River represent the recent time period. Only one garnet grain was present in thin section and available for microprobe analysis. The composition of this garnet grain has a similar chemical composition as the garnets seen in population 2 present in Mid Cretaceous samples (Figure 4.37).

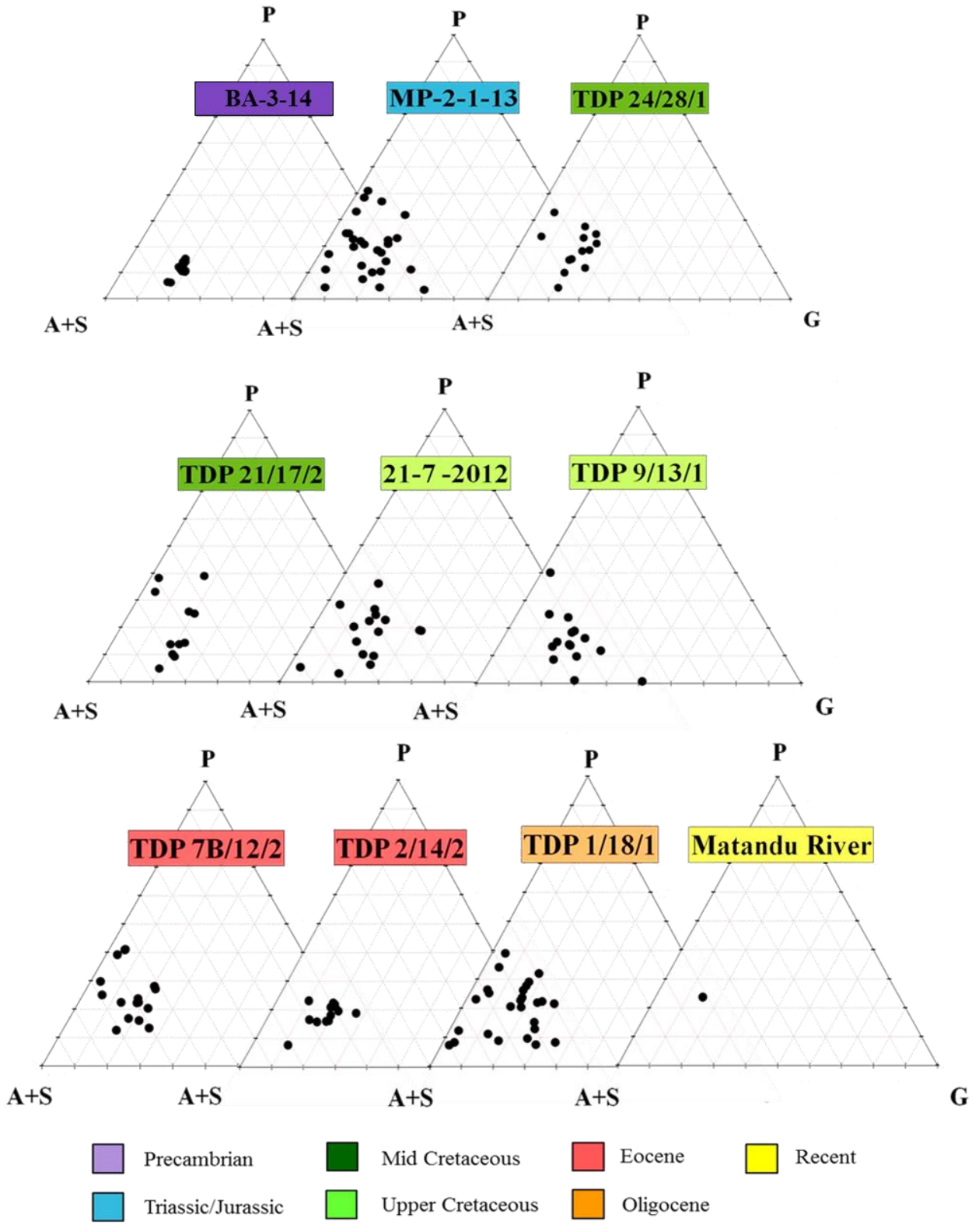

***Figure 4.37**: Chemical composition of garnet grains from Precambrian to recent from onshore Tanzania. The composition is plotted with the end members Pyrope (P), Grossular (G) and Almandine (A) + Spessartine (S).*

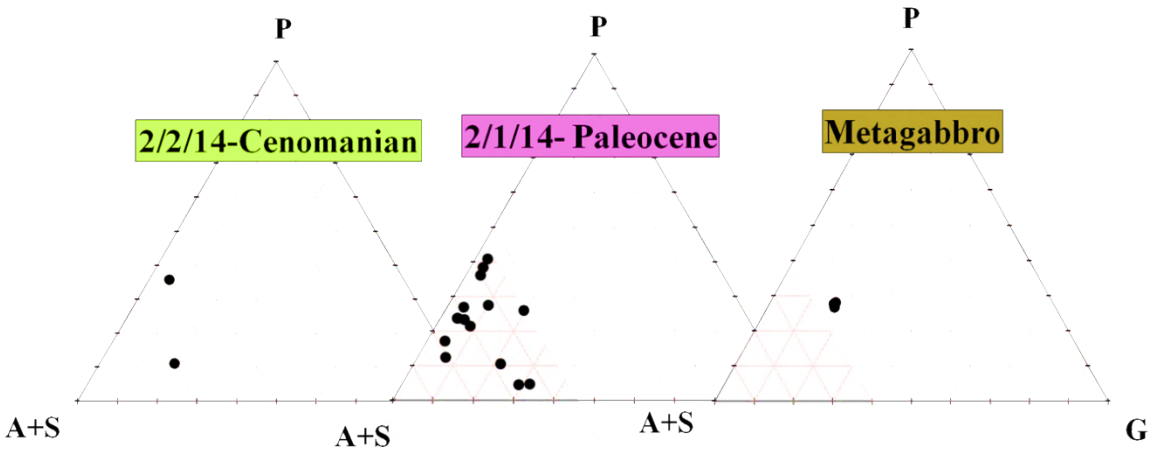

***Figure 4.38**: Chemical composition of garnet from offshore Tanzania samples (2/1/14 and 2/2/14). The plot of garnets deriving form a metagabbro in northern Tanzania are based on EMP results from Prochaska and Pohl (1983). The composition is plotted with the endmembers pyrope (P), grossular (G) and almandine + spessartine (A+S).*

Only two garnets were analyzed from the Cenomanian sample, 2/1/14 (Figure 4.38). One of the garnets consists of 5 % grossular, 40% almandine+ spessartine and 60% of the pyrope constituent. The other analyzed garnet grain contains higher values (70%) of Fe+ Mn (almandine+ spessartine), 20% grossular and 40% of the pyrope constituent.

The Paleocene sample, 2/2/14 display an abundance of garnets with low (less than 10%) Ca content (grossular) (Figure 4.38). The sample also contains garnets with 20- 40% of the grossular constituent, 5-30% pyrope and 30-50% of the almandine+ spessartine constituent.

5 Discussion

5.1 Facies associations

The facies associations FA-2 to FA-8 are briefly discussed in this chapter. More thorough interpretations of the sedimentary environments of these facies associations are discussed by Gundersveen (2014) and Mahmic (2014).

FA- 1

FA-1 is dominated by facies E2 (Table 4.1) and is present in the Karoo sediments (Figure 2.4 and 2.5), studied at Mpopera Mtumbei locality (Figure 1.1). Facies E2 is characterized by very coarse laminated sand and the overall coarse characterization indicates deposition close to the sediment source. FA-1 also includes a grain supported, polymict conglomerate of facies F. The presence of silicified wood within this section reinforces the interpretation of a proximal and alluvial depositional environment. The trunk of wood (Figure 4.3 B) was probably silicified by silica rich groundwater (Buurman, 1972) which percolated through the rock prior to the calcite cementation. The coarse nature of the sediments in FA-1 indicates alluvial fans as the main depositional environment (Galloway and Hobday, 1983).

The very coarse, bedded sand in facies E2 may indicate a distal fan deposition dominated by streamflow. Streamflows occur as unchannelized flows and follows intense periods of rainfall. and typically deposits planar laminar, pebbly sand. Sheetflooded deposits are typical for the distal fringe of a fan (Galloway and Hobday, 1983).

The grain supported conglomerate of facies F indicates a proximal deposition and may be deposited by a debris flow at a steeper and proximal part of the fan (Galloway and Hobday, 1983).

The different characterizations of the deposits in FA-1 all indicate a depositional environment in an alluvial fan system (Galloway and Hobday, 1983).

The Karoo deposits may represent a period of initial rifting during the opening of the Mandawa Basin during Late Triassic to Early Jurassic age. This time period was characterized by rifting, prior to the Gondwana break-up (Chapter 2.1). The high content of calcite present

in the section (Figure 4.5) may have been derived from leaching of the overlying limestone unit (Hudson, 2011).

FA-2

FA-2, seen in the Upper Kipatimu Mb. (Figure 2.4 and 2.5) at Mlima Ngoge locality (Figure 1.1), is dominated by facies G1 (Table 4.1). Facies G1 is characterized by upwards fining sequences with cross stratified sand and clay clasts. FA-2 also includes facies E1 which is characterized by parallel laminated sand. All facies included in FA-2 display a characteristic brick red colour.

Facies G1 indicates a fluvial dominated environment based on the cross stratification which is typical for ancient channel deposits (Collinson, 1986). The parallel lamination in facies E2, with a separation of heavy and light minerals (Figure 4.11 A and C), indicates an influence of wave activity. The lamination might have formed as a result of grain segregation during wave backwash (Clifton, 1969), but could also have developed within fluvial channels with hydrodynamic sorting (Hjellbakk, 1997). The regular, nearly parallel lamination is a characteristic sedimentary structure of beach foreshore deposits (Thompson, 1937). The brick red colour throughout the Upper Kipatimu Mb. may indicate an alluvial influence at the time of deposition (Besly and Turner, 1983), but could also reflect present day weathering as Walker (1967) claims that alteration of iron-bearing grains may occur wherever grains are in contact with interstitial water. There were no observed marine fossils in the samples from Upper Kipatimu Mb., which may indicate an alluvial depositional environment and minimizing the possibility of coastal deposition.

FA-3

FA-3 is present in the Upper Mitole Mb. (Figure 2.4 and 2.5), studied at Ngoro locality (Figure 1.1), and is dominated by facies G1 and G2 (Table 4.1). Facies G1 is characterized by cross stratified sand with mud couplets and is dominating section 2 in Upper Mitole Mb. (Figure 4.10 A). However, Upper Mitole Mb. does not display the same brick red colour as FA-2.

A tidal dominated depositional environment is proposed for FA-3. The high abundance of mud couplets and the cross stratified sand (Figure 4.12 A and C) is the basis for this interpretation (Klein, 1985). Clay clasts, as found in facies G1, can be found in both fluvial

and tidal channel deposit (Collinson, 1986). There were no marine fossils in the analyzed samples from Upper Mitole Mb., but the lack of marine fossils does not need to imply a non-marine environment or absence of marine influence (Williams, 1989).

FA-4

FA-4 is present in Makonde Fm. (Figure 2.4 and 2.5), studied at Mbate locality (Figure 1.1), and is dominated by facies E2 and H (Table 4.1). Facies H is characterized by fine to coarse sand with trough cross stratification (Figure 4.14 A and C) while facies E2 is characterized by parallel laminated sand (Figure 4.14 A).

The upwards coarsening trend and the facies included in FA-4 may indicate a depositional environment within a river dominated delta system. A terminal distributary channel within a delta system deposits coarse sediments and commonly contains trough cross stratified sand and clay rip up clasts. The delta front gives rise to upward coarsening deposits and the parallel bedded fine grained sediments indicate a mouth bar deposit (Olariu and Bhattacharya, 2006).

FA-5

FA-5 is present within cores from TDP well site 21 and 24 (Figure 1.1), from Kuhuluhulu Fm. (Figure 2.4 and 2.5) and includes facies 1-6 (Table 4.3). Facies 2 and 6 is the most abundant sandstone facies in FA-5 and is characterized by erosive beds and soft sediment deformation structures (Figure 4.20). Facies 1 includes silty and bioturbated clay and appears irregularly in FA-5.

An upper slope environment is suggested for the sediments in FA-5. The upwards fining, sandy intervals with erosional base (Figure 4.20) could represent high-energy events originating from turbulent flows (Browne et al., 2000). Soft sediment deformation structures in facies 6 reflects a rapid sedimentation rate typical for different slope processes (Mills, 1983). Intervals dominated by silty clay represent periods of lower energy between the high energy events where the suspended material has time to settle (Berrocoso et al., 2010). No marine fossils were observed in the analyzed samples from FA-5, but fossils of bivalves and bivalve fragments were observed when logging (Figure 4.12 A). Although no marine fossils were observed in thin section and SEM, samples within FA-5 are cemented with carbonate minerals which may have been derived from dissolved carbonate shells (Pettijohn et al., 1972b)

FA-6

FA-6 is present in cores from TDP well sites 24, 9 and 7B (Figure 1.1) and is dominated by facies 1 (Table 4.3). Cores from TDP well site 24 comprise sediments from Kihuluhulu Fm. (Figure 2.4 and 2.5), cores from TDP well site 9 represent Nangurukuru Fm. (Figure 2.4 and 2.5), while cores from TDP well site 7B consists of sediments from Kivinje Fm. (Figure 2.4 and 2.5). Thin sandstone intervals (facies 2) are occasionally interbedded with the otherwise clay dominated lithology (Figure 4.23 A).

An outer shelf environment is proposed for FA-6. The high abundance of clay and silt facies and the sparse occurrence of sedimentary structures indicate sedimentation in a calm environment below the storm wave base (Berrocoso et al., 2010). The thin, sandy intervals may originate from bottom currents transporting sediments from the inner shelf (Pearson et al., 2006). The proposed theory of an outer shelf environment is supported by the open marine microfossil assemblage, studied in TDP well site 7B by Pearson et al. (2006).

FA-7

FA-7 is present in cores from TDP well site 2 (Figure 1.1), comprises sediments from Masoko Fm. (Figure 2.4 and 2.5) and includes facies 1, 3 and 7 (Table 4.3).

The abundant limestone intervals (facies 7) present in this facies association indicate transportation from a shallow carbonate environment. The limestone intervals may represent turbiditic currents or debris deposits related to a carbonate slope (Conigilo and Dix, 1992). The transport of carbonate deposits could be triggered by several different factors. Sea level fluctuation, topography and tectonic activity and local marine conditions are processes that influence the sedimentation in a slope apron environment (Stow et al., 1983). Although FA-7 is characterized by carbonate sequences, the facies association is dominated by silty, partly laminated clay (facies 1 and 3). This indicates a more calm sedimentary environment and may represent the lower part of a carbonate slope were clay can settle and where the limestone intervals represent distal turbidities (Conigilo and Dix, 1992).

FA-8

FA-8 is present in TDP well site 1 (Figure 1.1) and comprises sediments from the Pande Fm. (Figure 2.4 and 2.5) FA-8 is characterized by alternating laminated silty and sandy mudstone

to sandstone units (facies 3), and structureless silty mudstone and siltstone intervals (facies 1, 2).

The relatively coarse nature of the sediments in FA-8 indicates a shallow depositional environment. Sediments with parallel lamination and high silt content can be typical for deposits within an upper prodelta or interdistributary bays and flats above the delta front (Wright, 1985). Additionally, samples included in FA-8 contain minor amounts of carbonate cementation compared to previous marine facies associations. The low carbonate content may indicate a higher input of terrigenous clastic sediment in FA-8 which would "drown out" the carbonate contribution (James and Kendall, 1992).

5.2 Petrography

The mineralogy, texture and the sedimentary structures are essential factors when studying a sedimentary rock. The petrography of the Mandawa Basin stratigraphic units are discussed in the following chapter.

Karoo sequences

Karoo sedimentary sequences (Figure 2.4 and 2.5), studied at Mpopera Mtumbei locality (Figure 1.1), are represented by two Late Triassic to Early Jurassic samples, MP-2-0-13 and MP-2-1-13. Sample MP-2-0-13 is characterized by poorly sorted, fine sand in a clay matrix (chapter 4.2.2). The poorly sorted, angular to sub angular grains and clay content indicate a low textural and mineralogical maturity of this sediment (Pettijohn et al., 1972a). Sample MP-2-1-13 is characterized by poorly sorted, coarse sand in sparitic calcite cement. The petrological characteristic of this sample indicates low textural maturity. The studied Karoo sequences are located stratigraphically below a limestone unit which might have contributed to the calcite cement in sample MP-2-1-13 (Hudson, 2011). The carbonate shells in this overlying limestone sequence may have been dissolved when being subjected to acidic pore water and reprecipitated as cement in the studied sediment (Pettijohn et al., 1972b). The texturally and mineralogically immature samples of Karoo sedimentary sequences support the theory of a proximal depositional environment (Pettijohn et al., 1972a), as suggested in chapter 5.1.

Upper Kipatimu Member

Upper Kipatimu Mb. (Figure 2.4 and 2.5), studied at Mlima Ngoge locality (Figure 1.1) is represented by 3 Late Jurassic samples, MN-2-1-13, MN-1-3-13 and MN-1-6-13. Samples from Upper Kipatimu Mb. are characterized by moderate to poorly sorted, medium to coarse sand with an abundance of authigenic kaolinite booklets and iron oxides (chapter 4.2.2) (Figure 4.11 B). The poorly preserved K-feldspar and the absence of plagioclase in these samples indicate a chemical weathering process acting on the sediment (Pettijohn et al., 1972c). According to Nesbitt and Young (1984), plagioclase is the most abundant mineral in unweathered continental crust. Plagioclase has a lower stability and higher weathering rate than K-feldspar (Nesbitt and Young, 1996) and has likely been depleted and altered by weathering processes in the analyzed samples from Upper Kipatimu Mb. Kaolinite is the most common weathering product of plagioclase, K-feldspar and mica in tropical environments (Tardy et al., 1973). The abundance of kaolinite booklets and the absence of plagioclase in samples from Upper Kipatimu Mb., thus indicate an alternation process of plagioclase to kaolinite (Nesbitt and Young, 1984). The alternation takes place when plagioclase grains are subjected to water containing carbon dioxide (Pettijohn et al., 1972b). The high abundance of iron oxide, which stains the sediments with a red colour, indicates an influence of oxygen as an additional weathering agent. Formation of ferric iron may take place when iron of dissolved ferromagnesian minerals, such as calcic amphibole and orthopyroxene, are taken into solution and oxidized from ferrous to ferric iron (Morton and Hallsworth, 1999). Although some sediment features are recognized as a result of weathering, it can be difficult to distinguish between weathering processes and early diagenetic processes (Pettijohn et al., 1972b).

Upper Mitole Member

Upper Mitole Mb. (Figure 2.4 and 2.5), studied at Ngoro locality (Figure 1.1), is represented by two Late Jurassic samples, NG-1-2-13 and NG-1-5-13. Samples from Upper Mitole Mb. are characterized by well sorted, subrounded, medium sized sand (chapter 4.2.3). Sediments from Upper Mitole Mb. display mixed smectite-chlorite coatings surrounding the grains (Gundersveen, 2014) which indicate an influence of diagenetic processes acting on the sediments during burial (Aagaard et al., 2000). Samples from Upper Mitole Mb. contain authigenic kaolinite booklets, like samples from Upper Kipatimu Mb., although the kaolinite content in Upper Mitole Mb. is too low to appear in bulk mineral analysis (Figure 4.10). The

poorly preserved feldspar grains and the authigenic kaolinite booklets in Upper Mitole Mb. may indicate similar weathering processes acting on the sediments as seen and discussed in Upper Kipatimu Mb. The well sorted sediments with subrounded grains suggest a greater textural maturity in Upper Mitole Mb. compared to sediments from the Karoo sequences and Upper Kipatimu Mb. (Pettijohn et al., 1972a).

Makonde Formation

Makonde Fm. (Figure 2.4 and 2.5), studied at Mbate locality (Figure 1.1), is represented by two Mid Cretaceous samples, MB-1-4-13 and MB-1-7-13. Samples from Makonde Fm. are characterized by well sorted, subangular grains (chapter 4.2.4). A mixed smectite-chlorite coating is seen in analyzed samples from Makonde Fm., as in samples from Upper Mitole Mb. Textural and mineralogical similarities between the two sedimentary sequences, Makonde Fm. and Upper Mitole Mb., may indicate comparable weathering processes acting on the sediments after or during deposition (Pettijohn et al., 1972a).

Kihuluhulu Formation

Kihuluhulu Fm. (Figure 2.4 and 2.5), studied in cores from TDP well site 21 and 24 (Figure 1.1), is represented by 5 Mid Cretaceous samples from both TDP well sites 21 and 24 (Table 3.4). The samples are characterized by well-rounded to subrounded, moderate to well sorted sand (chapter 4.2.4). Berrocoso et al. (2010) reported similar characteristics when studying cores of similar depth from TDP well site 21. Carbonate cement, either as ankerite or calcite cement, is present in the majority of samples from Kihuluhulu Fm. Calcite cement may form when a fluid, saturated with respect to the cement phase, percolates through the sediment. The fluid flow could become saturated with carbonate phase as a result of calcite dissolution (Tucker, 2001). Carbonate cemented sequences in Kihuluhulu Fm. are interpreted as shelf deposits (chapter 5.1) which may indicate a transport of carbonates from shallow marine environments, rather than primary precipitation of carbonates (Nicholas et al., 2006). The analyzed calcite rich samples from these marine sequences consist of coarser sediments than the surrounding clay. Turbuditic sequences or storm deposits are suggested for these coarser layers (chapter 5.1) which supports the idea of transported carbonate grains from a shallow marine environment to deep marine environments. Additionally, calcite precipitation favors warm water with high alkalinity which makes it reasonable to assume that the carbonates seen in the deep water sediments originated from a shallow marine area. (Greensmith, 1978).

Sparitic calcite cement and recrystallized calcite may both consist of grains larger than 10 μm, which makes it difficult to distinguish between the two mineral phases (Greensmith, 1978). Sparitic calcite cement was identified in samples from Kihuluhulu Fm., but some samples also displayed carbonate grains of >10 μm,, in an otherwise micrite dominated sediment, which could indicate recrystallization processes (Tucker, 2001). Sample TDP 24/28/1 contains ankerite cement which is isomorphic with dolomite, and distinguished from dolomite by ionic substitution between magnesium and ferrous iron (Greensmith, 1978). Ankerite tends to form at a later stage in the sequence of cementation compared to calcite, and the presence of ferrous iron in the mineral structure indicates precipitation in reducing conditions. It may precipitate directly or originate from ionic substitution within iron-poor, pre-existing cement (Tucker, 2001).

Nangurukuru Formation

Nangurukuru Fm. (Figure 2.4 and 2.5), studied in cores from TDP well site 9 and in sample 21-7-2012 (Figure 1.1), is represented by two Late Cretaceous samples, TDP 9/13/1 and 21-7-2012. Sample 21-7-2012 is characterized by well sorted, subrounded grains surrounded by sparitic calcite cement while sample TDP 9/13/1 is dominated by moderately sorted, subrounded grains in a micritic and partly sparitic calcite cement (chapter 4.2.4). Sample TDP 9/13/1 also contains an abundance of different clay minerals (Figure 4.21). The micrite cement in sample TDP 9/13/1 may have originated from disintegration of calcareous green algae, bioerosion, mechanical breakdown of skeletal grains or biochemical precipitation. The larger calcite grains may indicate a diagenetic alteration where micrite is replaced by coarser grains (Tucker, 2001). Sample TDP 9/13/1 and 21-7-2012 both comprise sediments from Nangurukuru Fm., but display differences in petrographical and mineralogical composition which may indicate different processes during or after deposition. The well sorted grains of sample 21-7-2012 indicate a more mature sediment than the moderately sorted, clay rich sediments of sample TDP 9/13/1 (Pettijohn et al., 1972a).

Kivinje Formation

Kivinje Fm. (Figure 2.4 and 2.5), studied in cores from TDP well site 7B (Figure 1.1), is represented by an Early Eocene sample, TDP 7B/12/2. This sample is characterized by moderately sorted, subangular grains surrounded by bioclastic calcite, micrite and recrystallized calcite cement (chapter 4.2.6). The characteristic petrographic features in

sample TDP 7B/12/2 indicate an immature sediment, much like sample TDP 9/13/1 from Nangurukuru Fm. Similarities between Kivinje and Nangurukuru formations. were also pointed out by Nicholas et al (2006), based on their faunal assemblages. Samples TDP 7B/12/2 and TDP 9/13/1 both contain authigenic pyrite which is also seen in several other marine sediments in Mandawa Basin, such as in Kihuluhulu Fm. (Figure 4.18) and Masoko Fm. (chapter 4.2.6). Although pyrite in samples TDP 7B/12/2 and TDP 9/13/1 and other marine sediments in Mandawa Basin indicate reducing conditions, trace elements in the clayey sequences of these formations indicate somewhat oxidizing environments (Mahmic, 2014). Sample TDP 7B/12/2 contains, in addition to calcite cement, the more unstable carbonate mineral aragonite. Aragonite alters to the more stable calcite mineral under normal temperature and pressure conditions. The aragonite mineral is usually not present in ancient sediments, but can be preserved locally where water rich in sulphate ions has been trapped within the sediment (Greensmith, 1978). Analyzed samples containing aragonite cement, TDP 7B/12/2, TDP 2/14/2 and TDP 1/20/1, are all dominated by clay matrix or calcite cement which may have trapped sulphate rich fluids, thus preventing alteration of aragonite to calcite (Aplin et al., 1999).

Masoko Formation

Masoko Fm. (Figure 2.4 and 2.5), studied in cores from TDP well site 2 (Figure 1.1), is represented by a Mid Eocene sample, TDP 2/14/2. This sample is characterized by moderately sorted, subangular to subrounded grains with an abundance of calcite bioclasts (chapter 4.2.6). The sample contains authigenic pyrite and preserved aragonite cement as seen in sample TDP 7B/12/2. Although there are distinct similarities between sample TDP 2/14/2 and TDP 7B/12/2, feldspar preservation and the amount of undulatory quartz grains separate the two samples (Appendix B). Sample TDP 2/14/2 displays a somewhat better preservation of feldspar grains than sample TDP 7B/12/2 with the majority of grains being classified as category 3-4 (Table 3.4) compared to a majority of grains classified as category 4-5 in sample TDP 7B/12/2. Undulatory quartz grains comprises 14% of the quartz composition in sample TDP 2/14/2, while they only comprise 6% of the quartz composition in sample TDP 7B/12/2 (chapter 4.2.6). The undulating extinction within quartz grains can be related to the amount of strain subjected to the rock (Blatt, 1967). Blatt and Christie (1963) suggests that the amount of undulatory quartz is controlled by the maturity of the sediments due to a selective destruction of undulating grains during mechanical and chemical weathering. Although sample TDP 2/14/2 and sample TDP 7B/12/2 display different amounts of undulatory quartz,

both samples display low mineralogical maturity based on the ratio between quartz and feldspar of 1,13 and 1,45 respectively (Appendix A1). Additionally, mature sediments from Kihuluhulu Fm. (sample TDP 24/28/1) display the highest amounts of undulatory quartz in all analyzed samples from Mandawa Basin (16,5%), thus indicating a minor effect of destruction of undulatory quartz during mechanical and chemical weathering in the analyzed samples.

Pande Formation

Pande Fm. (Figure 2.4 and 2.5), studied in cores from TDP well site 1 (Figure 1.1), is represented by two Oligocene samples, TDP 1/20/1 and TDP TDP 1/18/1. The samples are characterized by moderately sorted, subangular grains (chapter 4.2.7). Sample TDP 1/18/1 contains calcitic bioclasts and clasts of recrystallized calcite. Sample TDP 1/20/1 contains clay matrix and aragonite cement. Samples from Pande Fm. display comparable characteristics as samples from the underlying Kivinje and Mosoko formations, but differ with the low content of calcite cement. The moderately sorted and the subanglular grains indicate relative low textural maturity, much like sediments from Kivinje and Masoko formations (Pettijohn et al., 1972a). The low carbonate content seen in Pande Fm. may indicate increased terrigenous clastic sediment supply, compared to the underlying sedimentary sequences as discussed in chapter 5.1.

Matandu River

Sediments of recent age are represented by Matandu River sediments in this study (Figure 1.1). The river sample is characterized by very coarse, well sorted, subangular grains (chapter 4.2.8). The sample is also characterized by a high content of rock fragments, unlike the other analyzed sediments from Mandawa Basin. Shiki (1959) discussed the relations between grain size, maturity and the amounts of rock fragments in sandstones, and suggested a higher frequency of rock fragments in immature sediments, especially in grain sizes coarser than 0,25 mm. Sediments from the Matandu River comprise grains with an average size above 1 mm which may explain the high content of rock fragments. The sediments also display a low mineralogical and textural maturity, indicated by the presence of subangular grains and high content of unstable and metastable minerals, such as orthopyroxene, clinopyroxene and calcic amphibole (Figure 4.31) (Morton and Hallsworth, 1999).

Offshore Tanzania

Offshore Tanzania is represented by a Cenomanian sample, 2/2/14, and a Paleocene sample, 2/1/14, from Statoil, Block 2 (Figure 3.3). Sample 2/2/14 is characterized by well sorted, rounded to subrounded grains (chapter 4.2.9). These petrographical features indicate great sediment maturity, much like the samples from Kihuluhulu Fm. from onshore Tanzania. Sample 2/1/14 is characterized by moderately sorted, subangular grains which are also seen in onshore marine sediments from Eocene (Kivinje and Pande Fm.) and Late Cretaceous (Nangurukuru Fm) age. Although there are comparable characteristics between the onshore and offshore sediments, sedimentary sequences should not be compared or discriminated based solely on sorting and grain shape. The offshore samples are not cemented with carbonates, unlike onshore marine sediments, which demonstrate petrographical differences between onshore and offshore sediments. Statoil, Block 2 is located at a water depth of 2500 m (Statoil, 2014) which may explain the absence of carbonate cement in offshore sediments. Carbonates dissolves at a higher rate with increased hydrostatic pressure and decreasing temperatures, thus carbonates dissolve more actively in deep marine environments (Volat et al., 1980).

5.3 Sedimentary provenance

Provenance analysis is an important tool for reconstructing the history of the sediment from the initial erosion of the source area to the site of deposition. The provenance signal is a function of different factors such as climate, relief, transportation and tectonic setting. To reveal the provenance history of the sediment, one could study the composition of the deposit, detrital minerals and rock fragments (Pettijohn et al., 1972d). Provenance data plays an important part when reconstructing aspect of the lithospheric history, such as characterizing crust that is no longer exposed. When studying sedimentary provenance, the sedimentological and petrographical analysis contribute to improved knowledge of the sedimentary context, thus enhancing the provenance interpretation. When the depositional environment, textural composition and bulk mineralogy is known one can easier recognize and distinguish between provenance signals which reflect the true source rock composition and signals which result from different alternating and degrading processes.

5.3.1 Conventional heavy mineral analysis

There are many techniques available for sedimentary provenance analysis. Heavy mineral analysis is one of the most widely used techniques within this field and shows a great sensitivity in constraining the source rock lithology. Many of the heavy minerals have a restricted paragenesis which provides crucial provenance information (Morton and Hallsworth, 1999). Some minerals are characteristic for various igneous rocks, such as zircon, tourmaline and rutile, while other minerals such as kyanite and garnet are formed during metamorphism (Deer et al., 2013).

The different heavy mineral assemblages present in the Mandawa Basin and offshore Tanzania (Figure 4.31) can be used to discriminate the sedimentary units and give an indication of the sediment source area. Different sedimentary processes and environments can influence the assemblages and must be taken into account when interpreting these data.

The heavy minerals in the Mandawa Basin and offshore Tanzania are plotted in Figure 4.31, which displays distinct groups of similar heavy mineral content (Table 4.4, Figure 4.31). The groups with a characteristic heavy mineral content are grouped together as assemblages (Table 4.4). There are seven heavy mineral assemblages identified in the analyzed samples from the Mandawa Basin, and two assemblages which represent offshore Tanzania (Table 4.4).

Heavy mineral assemblages 1 and 2 comprise the heavy mineral content of the two analyzed basement samples BA-1-13 and BA-2-13. Assemblage 1 is represented by sample BA-2-13 which is characterized by a high content of calcic amphibole (Figure 4.31). Assemblage 2, which includes sample BA-1-13, is characterized by a high percentage of zircon (Figure 4.31). The two basement samples are derived from two different localities but within the same orogenic system. The large variation between assemblages 1 and 2 shows the great mineralogical differences even within small regions in the same orogenic system. This illustrates the challenges of trying to characterize basement mineralogy based on in-situ samples. Analyzing modern stream sediments, shed from specific source regions, may be the best approach to characterize a basement terrain (Morton et al., 2004). The heavy mineral content in these samples will be compared with the other heavy mineral assemblages in the Mandawa Basin.

Heavy mineral assemblage 3 includes samples from the Late Triassic to Jurassic unit, Karoo. The assemblage is dominated by garnet, apatite and titanite (Table 4.4, Figure 4.31). Garnet is absent in the two basement samples BA-2-13 and BA-1-13 and the high content of garnets in assemblage 3 could therefore reflect another source area. Sample BA-3-14 has not been analyzed regarding heavy mineral assemblage but has been proven to contain garnet by the use of light microscope, SEM and microprobe analyzes. The source-sediment link between the garnet bearing basement sample and sediments in the Mandawa Basin will be discussed later. The analyzed basement samples, BA-1-13 and BA-2-13 do not contain any amounts of titanite which is abundant in heavy mineral assemblage 3. This mineral is a widespread accessory mineral in igneous rocks and in intermediate or acid plutonic rocks (Deer et al., 2013). There are large terrains with plutonic rocks, mostly granite and granodiorite, located in the central parts of Tanzania (Figure 2.1). Large river systems, such as The Great Ruhaha River, Rufji River and Wami River drain the central parts of Tanzania, transporting the sediments eastwards through the Mandawa Basin. The titanite in assemblage 3 could derive from granite, granodiorite or other titanite bearing rocks (Deer et al., 2013) being transported by these river systems.

Assemblage 4 comprises samples from Late Jurassic units, Upper Kipatimu Mb. and Upper Mitole Mb. to Mid Cretaceous unit, Makonde Fm. (Table 4.4). The assemblage is characterized by a high content of zircon and tourmaline. Rutile and monazite are also present but make up less than 20 % of the heavy mineral composition. The high content of zircon and tourmaline in this assemblage could indicate an input of sediment from a source area most likely composed of granite or granitic pegmatite (Deer et al., 2013). A low grade metamorphic rock could also act as a source of zircon, demonstrated by the high zircon content in basement sample BA-1-13 (Figure 4.31). Zircon, tourmaline and rutile are among the most stable heavy minerals and will accumulate in mature sediments where other heavy minerals are no longer stable (Morton and Hallsworth, 1994). The high content of these minerals may therefore reflect an influence of degrading processes and not solely reflect the composition of the source area. High percentages of stable heavy minerals could indicate an influence of several processes acting on the sediment and modifying the original composition.

The sedimentary units included in assemblage 4 are field outcrops which display a great textural maturity with good sorting and a high content of quartz (Figure 4.7, 4.10 and 4.13). Although these sediments display a good textural maturity, there are other sedimentary units in the Mandawa Basin, such as samples from TDP well site 24 and 21, with similar

characteristics which contain a higher abundance of less stable heavy minerals. The heavy mineral content may therefore not solely depend on mineralogical and textural maturity.

The absence of apatite in assemblage 2 could indicate an influence of acidic conditions (Morton, 1984, Morton and Hallsworth, 1999). Heavy mineral experiments conducted by Friis (1974) and Morton (1984) demonstrates the stability patterns among the heavy minerals, when subjected to acidic weathering. According to these studies, apatite is one of the least stable heavy minerals in acidic environments together with amphibole, epidote and titanite. Garnet displays a higher persistence than apatite but has a lower stability than monazite, staurolite, rutile, tourmaline and zircon. The unstable heavy minerals which dissolve when subjected to acidic fluids are absent in assemblage 4 and thus indicate an influence of acidic weathering. Titanite minerals, which were almost completely dissolved, were observed in SEM analysis and support the indication of acidic weathering. Climatic conditions in Tanzania contribute to a great diversity of vegetation and affect the weathering process by the generation of organic acids in the soil (Drever, 1994). High annual rain fall in Tanzania will affect the weathering process further by percolation of acidic water through the rocks and sediments (Carroll, 1970). The high percentages of stable heavy minerals such as zircon and tourmaline, seen in assemblage 4, may be an effect of the depletion of less stable heavy minerals.

Heavy mineral assemblage 4 also contains small amounts of authigenic anatase. They are recognized as authigenic minerals by the distinct crystal surfaces that extend into the pore space. Anatase could occur as an alteration product of other Ti-bearing minerals such as titanite and ilmenite (Deer et al., 2013). Titanite subjected to acidic water percolation will lose most of its constituent, leaving Ti as the remaining component (Bain, 1976). Anatase can be formed by TiO_2 at moderate to low temperatures and mildly acid solution (Deer et al., 2013). Titanite is absent or partly dissolved in assemblage 4 and may have been altered to anatase by hydrothermal circulation.

Heavy mineral assemblage 5 includes samples from Mid Cretaceous to Eocene age, (Kihuluhulu Fm., Nangurukuru Fm. and Kivinje Fm. (Figure 2.4 and 2.5)), and is characterized by a high content of garnet (Table 4.4, Figure 4.31). Assemblage 5 displays a higher diversity of heavy minerals than assemblage 4 and contains a higher abundance of less stable heavy minerals such as kyanite and clinopyroxene (Morton and Hallsworth, 1999). The high percentages of garnet in heavy mineral association 5 could indicate a change in the

sedimentary input during Mid Cretaceous age. Samples MB-1-7-13 and MB-1-4-13 (assemblage 4) also contain Mid Cretaceous sediments but these are almost absent in garnet and other unstable heavy minerals. If the high content of garnet in assemblage 5 is associated with a change in provenance during Mid Cretaceous, one would expect to see similar changes in sample MB-1-7-13 and MB-1-4-13 (assemblage 4). The differences between assemblage 4 and 5 could therefore indicate different processes acting on the sediments. The high abundance of stable heavy mineral in assemblage 4 indicates an exposure to processes which have disintegrated and altered the composition of the heavy minerals. Assemblage 5 contains more of the unstable heavy minerals and does not show the same indications of depletion.

Assemblage 5 contains very similar heavy minerals to those seen in assemblage 3. The main difference between these two assemblages is the content of tourmaline and kyanite which is absent in assemblage 3. Tourmaline is considered to be one of the most stable heavy minerals when subjected to processes such as physical sorting, mechanical abrasion and dissolution (Morton and Hallsworth, 1994). The differences in tourmaline content between assemblage 3 and 5 could therefore be a result of changes in the sedimentary input and not destruction of tourmaline. Both epidote and garnet are considered to be more unstable minerals, compared to tourmaline, under conditions like acidic weathering, burial diagenesis and physical abrasion. The presence of these garnets and epidote in assemblage 3 supports the idea of a change in sedimentary input between the Late Triassic to Jurassic unit (Karoo) and the Mid Cretaceous units (Makonde, TDP well site 21 and TDP well site 24), rather than dissolution of tourmaline. The differences in tourmaline content could, on the other hand, be caused by different sedimentary inputs within assemblage 5 since the highest abundance of tourmaline is restricted to samples deriving from the Lindi Area (Figure 1.1). The Lindi area is located approximately 100 km south of Kilwa and may have received input from river systems draining different areas than the remaining samples in assemblage 5.

A phase of transgression took place in Aptian-Albian age and created a continental shelf along the coast of Tanzania. The relative sea level rise continued to influence the coastal areas into Eocene age (Mpanda, 1997). The samples from heavy mineral assemblage 5 include sediments deposited in a marine depositional environment during this phase of transgression (Table 4.4). These samples are characterized by a high content of cement comprising calcite, ankerite and clay, or a mixture of the three. Could the relative sea level rise and a possible change in sedimentary input, cause the differences seen between assemblages 4 and 5? Or is the higher abundance of garnet in assemblage 5 a result of an improved preservation due to

the presence of cement and clay? Cement creates effective barriers to fluid flow and reduces the percolation of acidic water through the rock (Bjørlykke, 2010). Blatt and Sutherland (1969) investigated the usefulness of silt-sized heavy minerals in shales and sandstones and concluded that heavy minerals post-depositionally dissolved in sandstones could probably be preserved in the impermeable shales. It seems that clay and carbonate cement might prevented the dissolution and depletion of heavy minerals in assemblage 5 by shielding them from being subjected to intrastratal solution. The presence of apatite in assemblage 5 implies a minor influence of weathering processes in these sediments, since apatite is unstable when subjected to acidic groundwater (Morton and Hallsworth, 1994).

There are two different transport directions which could have influenced the marine sediments in heavy mineral assemblage 5. The large river systems in Tanzania drain many different source areas in the central part of the country and transport and distribute sediments towards the coastal areas. According to Hudson (2011) river systems may have acted as major transport agents since Late Jurassic age. These rivers systems were interpreted by Hudson (2011) to have transported the large sand deposits in Upper Kipatimu Mb., Upper Mitole Mb. and Makonde Fm. during Late Jurassic to Mid Cretaceous age. It is possible that the river sediments were transported further out on the shelf, by different mechanisms, and comprise the sand in the analyzed samples included in assemblage 5. The high energy events and turbiditic deposits observed in facies associations 5 and 7 supports the possibility of a transport direction from the mainland of Tanzania towards offshore areas.

Offshore Tanzania is dominated by strong ocean currents which flow parallel to the coast line (Sætre and Da Silva, 1984). Little is known about the paleocurrents along coastal Tanzania during Mid Cretaceous, but one cannot exclude the possibility of a sedimentary transport by coast parallel currents during the phase of transgression. This could explain the different heavy mineral content between assemblage 4 and 5. It could also explain the difference between samples MB-1-4-13 and MB-1-7-13, and the remaining samples in assemblage 5, since samples MB-1-4-13 and MB-1-7-13 are interpreted as deltaic and fluvial deposits while the remaining samples in assemblage 5 are interpreted as marine deposits (Chapter 5.1).

Heavy mineral assemblage 6 includes samples from Eocene and Oligocene age (Masoko Fm. and Pande Fm. (Figure 2.4 and 2.5)) and is characterized by a high content of epidote. Epidote is commonly found in metamorphic rock of greenschist to epidote-amphibolite facies (Deer et al., 2013). It is associated with relatively low stability compared to heavy minerals

like zircon, tourmaline, rutile and garnet (Pettijohn, 1941). According to Pettijohn (1941) an increasing complexity in the heavy mineral content can be associated with the decreasing age of the sediment. Although heavy mineral assemblage 6 consists of younger sediments than the previous assemblages, only a short geological time span separates sample 2/14/2 (Assemblage 6) and sample 7B/12/2 (Assemblage 5). Sample 7B/12/2 comprises sediments from Early Eocene while sample 2/14/2 consists of sediments of Mid Eocene age. The two samples display a significant difference in epidote contents which leads to the assumptions of a changed sediment input, rather than an effect of the minor time span between the assemblages.

The samples included in assemblage 6 could derive from an area near Kilwa Masoko (Figure 1.1) while samples from assemblage 5 derive from areas around Kilwa Kivinje and Lindi (Figure 1.1). It is noteworthy that assemblage 5, with a wide spread in age (~75 My) and geography, displays such similar heavy mineral content while samples taken from a more narrow area with smaller age differences (~10 My) display great differences in heavy mineral content. This may be related to petrological differences between the assemblages which could lead to different epidote preservation, or indicate an influence of another sediment source during Mid Eocene age. The samples included in heavy mineral assemblages 5 and 6 are either cemented with calcite or contain a clay matrix, which would reduce percolation of intrastratal fluids and dissolution of heavy minerals (Blatt and Sutherland, 1969, Morton, 1984).

The varying sediment input during Mid Eocene can be explained by the two possible transport directions as previously discussed in connection with heavy mineral assemblage 5. The marine sediments in assemblages 5 and 6 may have derived from mainland Tanzania and transported by the large river systems. The high epidote content seen in assemblage 6, may therefore reflect an additional input from a smaller local river. There is a minor river, west of Kilwa Masoko, which transport sediments from a limited source area within the Mozambique belt (Figure 2.1) and (Figure 1.1). The Mozambique belt consists of a variety of lithologies with different metamorphic facies and a sedimentary input from a restricted source area could explain the high epidote content. The sediments in heavy mineral assemblage 6 could possibly have been supplied with the comparable source material as assemblage 5 but the local source of epidote dilutes the presence of other heavy minerals.

A regressive phase occurred in the coastal areas of Tanzania from Mid Eocene and Oligocene age (Mpanda, 1997). This is also supported by the observation of coarser sediments in facies associations 7 and 8 (Figure 4.25 and 4.26). If the deep marine sediments in assemblage 5 were distributed by coast parallel currents, a regressive phase during Mid Eocene could explain the greater input of clastic sediments. This could also cause the observed differences in heavy mineral content between assemblages 5 and 6. The differences between deep-marine samples (heavy mineral assemblage 5) and shallow marine samples (heavy mineral assemblage 6), with respect to heavy mineral content, may therefore indicate an influence of different sediment sources.

Heavy mineral assemblage 7 consists of sediments from Matandu River (Figure 1.1) and is characterized by a high content of calcic amphibole (Figure 4.31). Calcic amphibole is a common constituent of plutonic igneous rocks and of metamorphic rocks from greenschist to lower granulite facies (Deer et al., 2013). A high content of calcic amphibole is also found in heavy mineral assemblage 1 (sample BA-2-13) which comprises a granitic gneiss from the Mozambique orogenic belt (Figure 2.1). Areas within the Mozambique belt could therefore act as a sedimentary source of the heavy minerals seen in assemblage 7. The basement sample included in heavy mineral assemblage 2 are sampled closer to the Matandu River locality, but does not display any significant similarities with heavy mineral assemblage 7.

Calcic amphibole is associated with relatively low stabilities according to the studies conducted by Pettijohn (1941), Morton (1984) and Morton and Hallsworth (1999). Calcic amphibole is rarely present within sediments buried more than 600 m in the North Sea, and show a low order of persistence in environments subjected to acidic weathering (Morton and Hallsworth, 1999). The calcic amphibole in Matandu River sediments displayed signs of partial dissolution, and the absence of calcic amphibole in the previous heavy mineral assemblages is therefore assumed to be related to dissolution of this mineral rather than a change of sedimentary source.

Heavy mineral assemblage 8 includes one sample, 2/2/14, from an offshore basin outside Tanzania (Figure 3.3). It consists of sediments of Cenomanian age and is characterized by a high content of garnet. This heavy mineral assemblage show great similarities with samples included in heavy mineral assemblage 5. Samples from TDP well site 21 and TDP well site 24 (assemblage 5) consist of sediments of comparable geological age as sample 2/2/14 (assemblage 8) and these well sites is located in the Lindi area, approximately 90 km south of

Block 2 (Figure 3.3). The resemblance in heavy mineral content between these two assemblages, 5 and 8, indicates a possibility of similar sedimentary input. The two heavy mineral assemblages may have been supplied with sediments from similar source areas, whether it derives from mainland Tanzania or has been transported with coast parallel currents. If the sediments from offshore areas (Block 2, Figure 3.3) were derived from the mainland, it illustrates the extensive distribution of the river systems in Tanzania.

Although the samples included in assemblage 8 display similar heavy mineral content as assemblage 5, there are petrological differences which separate the two assemblages. Sample 2/2/14 (assemblage 8) is not cemented with carbonate minerals and contains no significant amounts of clay matrix which is a common feature in heavy mineral assemblage 5. If the high garnet content in assemblage 5 was a result of improved preservation due to cementation and clay content as previously discussed, it is peculiar that garnet is well preserved in assemblage 8. The preservation of garnet in the offshore sample could be explained by the absence of exposure to the acidic weathering environment associated with vegetation and heavy rainfall (Oliva et al., 2003). It is possible that the samples within assemblage 8 would have displayed a similar heavy mineral content to assemblage 4, which has a high abundance of stable heavy minerals, if it was subjected to alluvial storage on the mainland of Tanzania. Garnets display higher stability patterns during deep burial than in acidic weathering environments (Morton and Hallsworth, 1999) which could explain the high abundance of garnet in heavy mineral assemblage 8. On the other hand, similar garnet content in assemblage 5 and 8, and the significant differences between these assemblages and assemblage 4, could indicate a similar sedimentary input in marine sediments. One can therefore not exclude the possibility of coast parallel sediment transport along the coast.

Heavy mineral assemblage 9 includes one sample (2/1/2) from offshore Tanzania and comprises sediments of Paleocene age. It is characterized by a high content of garnet and zircon with smaller amounts of kyanite, rutile and titanite (Table 4.4, Figure 4.31). Assemblage 9 displays a similar heavy mineral content as sample TDP 7B/12/2 (assemblage 5) which consists of sediments of Eocene age. The similar provenance signal in these two samples could indicate sedimentary input from the same source area. The resemblance between offshore samples (assemblages 8 and 9) and samples from assemblage 5 supports the theory of a similar sedimentary input in samples deposited in a marine environment. Heavy mineral assemblages 8 and 9, both from offshore Tanzania, display somewhat similar heavy mineral content with an abundance of garnet and zircon. The apatite content in assemblage 8

and the kyanite and titanite content in assemblage 9 separate the two assemblages. The two offshore assemblages display greater similarities with comparable onshore samples than with each other, which may indicate sedimentary input from onshore Mandawa rather than sediment input from coast parallel currents.

The questions concerning the provenance and transport direction of these sediments cannot be fully explained by the results of this study. The northern parts of Mozambique comprise similar lithologies as the sampled basement areas in the Mandawa Basin (Pinna et al., 1993) and could act as a sediment source to the coastal areas outside Tanzania.

Heavy mineral ratios

To minimize the effect of hydraulics and diagenesis on the heavy mineral assemblages one can compare the ratios between minerals with the same hydraulic and diagenetic behavior or quantify varietal characteristics within a single heavy mineral group (Morton and Hallsworth, 1994). Different heavy mineral indexes are plotted together in Figures 4.32 and 4.33 in an attempt to provide further information concerning sedimentary provenance and discrimination between the sedimentary formations in the Mandawa Basin.

The RuZi index (Rutile- zircon) is plotted against the ATi index (Apatite-tourmaline) in Figure 4.32. Samples from Precambrian to Mid Cretaceous age have lower RuZi values and dominate the lower part of the diagram in Figure 4.32, while younger samples (Late Cretaceous to Recent) display higher RuZi values. The increase in RuZi values from Mid Cretaceous could indicate a change in provenance where a source rich in rutile became more prominent. It is noteworthy that the change in RuZi values coincides with the phase of transgression during Mid Cretaceous to Mid Eocene age (Mpanda, 1997). Heavy mineral indexes are assumed to provide a good reflection of the source area and are not as vulnerable to alteration during the sedimentary cycle (Morton and Hallsworth, 1994). The results indicate that sediments from Mid Cretaceous to Oligocene age have a different sedimentary source and provenance than the sediments from Triassic to Late Jurassic age. The analyzed sediments from Mid Cretaceous to Oligocene age are deposited in marine environments, during the transgressional phase, while Triassic to Upper Jurassic sediments are deposited in alluvial environments. Since the differences in RuZi index seem to be related to sedimentary environments, it may support the possibility of coast parallel currents transporting sediments along the coastal areas of Tanzania. The recent river sample from Matandu River display

similarly low RuZi values as the samples from Triassic to Late Jurassic and emphasizes the different heavy mineral content between marine and alluvial sediments.

The ATi index (Apatite-tourmaline) displays extremely low values for samples from Late Jurassic formations as well as some of the samples of Mid Cretaceous age (Figure 4.32). The low values could represent present-day weathering, especially since these samples are derived from field outcrops. The effect of alluvial storage on heavy mineral suites was evaluated by Morton and Johnsson (1993). Their study of heavy mineral assemblages from samples from the Apure River system in Venezuela concluded that the apatite-tourmaline ratio was reduced during alluvial storage. There are samples from field outcrops in Mandawa Basin which display higher ATi values, but they typically contain clay matrix or carbonate cement which can prevent the dissolution of apatite (Morton, 1984). Although the heavy mineral ratios should better reflect the composition of the source area, samples display influence of weathering and alteration of the heavy mineral content.

The GZi index (Garnet-Zircon) was plotted against the RuZi index in Figure 4.33. The GZi index display similar characteristics as the ATi index, with increasing values in carbonate cemented or clay dominated samples. It is possible that the low values in outcrop samples are associated with weathering of garnet.

5.3.2 Microprobe analysis

Microprobe analysis was conducted on garnets and rutile to get a better understanding of the link between the source rocks and the sediments. This type of analysis is an accurate and quick approach to determine the chemical composition of a mineral. By using microprobe analysis one can also avoid the risk of errors due to subjective factors, such as the determination of color and shape (Morton, 1985).

Garnet

Garnets of different paragenesis have different chemical composition, which make them a very suitable mineral for provenance studies (Wright, 1938). Morton et al. (2004) demonstrated the usefulness of garnet composition when discriminating sandstones in the North Sea. The relatively high stability of garnet and the wide variety of chemical compositions makes it a suitable mineral for microprobe analysis. Garnets have a narrow total density range from 3.6 to 4.3 which minimizes the effect of hydraulic differentiation.

Although a study of a single mineral group reduces the effect of hydraulic and diagenesis to a minimum, these effects cannot be completely ruled out (Morton, 1985).

It can be difficult to trace the garnet composition directly to the source rock, especially when the composition of the garnet in the basement is poorly known. The garnet bearing basement sample, BA-3-14, were analyzed to provide a better connection between source and sediment. Garnet zoning is a common feature in almost all garnet bearing source areas (Morton 1985). The possibility of zoning was tested by analyzing individual grains on different targets (Figure 4.36). There were no detectable differences within the garnet grain, minimizing the risk of misinterpretation due to zoning.

Garnet has different stabilities depending on the chemical composition. Low Ca-garnets are more stable than high Ca-garnets (Morton, 1987). If apatite is present in the sample it is less likely that the sediment has been exposed to modification related to dissolution during groundwater percolation. Garnets are more stable than apatite in acidic environments and can be used as an indicator for groundwater flushing. Figure 4.31 shows that apatite was present in all samples analyzed regarding garnet chemistry. Although the garnets are more likely to have been unaltered with the presence of apatite, one cannot exclude the possibility of recycling (Morton 1985).

The garnet composition of the analyzed sand samples shows a dominance of high Fe+Mn (Almandine+ Spessartine) content. Almandine is typical of garnet bearing schist of regional metamorphism, argillaceous sediments and basic igneous rocks (Deer et al., 2013). The samples from Mid Cretaceous comprise garnets of two different populations. One population consists of garnets with less than 10% Ca (Grossular) and 5-50% Mg (Pyrope). This population is also apparent in samples from Triassic/Jurassic (Karoo sedimentary sequenses, Eocene (Kivinje and Masoko Fm.) and Oligocene (Pande Fm.) (Figure 4.37). The low content of Ca in this population indicates a source area of high metamorphic grade (Deer et al., 2013). The second population is characterized by a Ca content varying between 15–50% and a Mg content (Pyrope) between 5-40%. All the analyzed samples contain garnets with a similar field of composition to the second population. The two populations of garnets in the analyzed samples might indicate an input of more than one source area since different basement lithologies display characteristic garnet compositions. Although the wide distribution could indicate several sources, some lithologies contain garnets with a wide compositional range and overlapping chemical compositions (Krippner et al., 2014). The garnets in sample BA-3-

14, on the other hand, display a narrow field of composition which supports the suggestion of input from several source areas. It is also possible that periods of recycling have contributed to the mix of garnet compositions that is seen in many of the samples.

The few garnet grains available for analysis in thin sections make it difficult to quantify the chemical variations. 50 grains from each sample should be analyzed to represent all the chemical variations within one sample (Morton 1985). In some cases less than 10 grains were analyzed and the results could give rise to a skewed distribution of chemical variations.

The analyzed basement sample, BA-3-14, displays a garnet composition which can be found in many of the analyzed samples from the Mandawa Basin. This increases the possibility of a westerly sediment transport from the Mozambique belt towards the coast and the possibility of garnet bearing gneiss as a potential source rock.

Parts of the Proterozoic Mozambique belt was analyzed by Prochaska and Pohl (1983) in the northern part of Tanzania. Their study included analysis of a garnet grain from a metagabbro within the Mozambique orogenic belt (Figure 4.38). Only one garnet grain were analyzes in their study, but the analysis included both rim and core of the garnet grain (Prochaska and Pohl, 1983). No significant chemical variations were observed, which reduces the possibility of zonation (Figure 5.1).

The chemistry of the garnet derived from northern Tanzania metagabbro has higher values of the pyrope component than the analyzed sample from granitic gneiss (BA-3-14). Similar garnet chemistry as the one seen in the metagabbro can be seen in many of the analyzed samples from Mandawa Basin. Samples of Late Cretaceous to recent age, which include Nangurukuru Fm., Kivinje Fm., Masoko Fm., Pande Fm and sediments from Matandu River, display garnet grains within the same field of composition as the garnet deriving from the metagabbro within Mozambique belt. This could indicate a more prominent influence of this type of source rock during Late Cretaceous age. The absence of the metagabbro garnet chemistry in Mid Cretaceous samples could possibly be related to the geographical position of the core sites TDP 21 and TDP 24, which are located south in the Mandawa Basin (Figure 1.1).

Rutile

Rutile is among the most stable heavy minerals in the sedimentary system. They provide important provenance information for mature sediments where other detrital minerals are no longer stable(Zack et al., 2004). Most rutile derives from medium to high grade metamorphic rocks and recycled sediment, while it is almost absent in other rock types such as most igneous and low metamorphic rocks (Force, 1980). When it is present in igneous and low metamorphic rocks it occurs as needles within other phases (Zack et al., 2004).

The concentration of trace elements present in rutile can be linked to the source rock which makes it attractive for provenance studies. The concentration of Nb and Cr in rutile can be used to distinguish between an origin of metamafic or metapelitic rocks (Zack et al., 2004). According to the study by Zack et al. (2004) it is apparent that rutile derived from metacumulates are characterized by a high content of Cr. Metamafic rocks contain rutile with low values of Cr and Nd while metapelites are characterized by rutile consisting of low Cr and high Nb values.

The samples analyzed regarding rutile chemistry are mature sediments with no garnet present. Only a few rutile grains were available for analysis, which reduces the possibility to delineate the compositional range in the samples. Additionally, rutile from several geological time periods should be analyzed in order to get a better understanding of any changes in sediment input through time. The basement samples in this study did not contain rutile grains. It is possible that the sampled areas have been exposed to lower metamorphic grade than what is required for rutile formation (Deer et al., 2013). This absence of rutile in the basement samples makes it difficult to provide a link between the analyzed rutile and any possible source rock.

Analysis of rutile from Late Jurassic shows a wide range in chemical composition and rutile of both metamafic and metapelitic origins are present in the samples (Figure 2.34). The analysis of Mid Cretaceous sediments shows a similar wide distribution of rutile chemistry. Since there is no rutile available in the basement samples for comparison one can only speculate about the possible source rocks. There are large schist belts surrounding the Tanzania craton which could provide rutile of metapelitic chemistry (Zack et al., 2004) (Figure 2.1). These belts have undergone a medium to high grade of metamorphism (Schlüter

and Hampton, 1997) and may contain rutile with similar metapelitic chemistry seen from Late Jurassic and Mid Cretaceous.

The metamafic rutile could derive from rocks such as eclogite or other mafic rocks that have undergone a medium to high metamorphic grade. Eclogite is a high grade metamorphic rock which could contain large percentages of rutile (Korneliussen et al., 2000). This type of rock is present in Tanzania but occurs only as small lenses west of the central craton. There are large river systems which transport sediments from the central part of Tanzania, towards the coast. Although large areas are drained by these river systems, it seems unlikely that rutile in the analyzed samples were derived from eclogites as far away as Lake Tanganyika. Scattered areas of metagabbros of Arhean age, located east of the Tanzania could also provide rutile of metamafic composition seen in the analyzed samples. Additionally, since rutile is stable in weathering environments, one should consider recycling of sedimentary sequences as a secondary source of rutile (Zack et al., 2004).

To summarize the previously discussed issues, Figure 5.1 illustrates the main factors which have influenced the analyzed sedimentary sequences.

5.4 Further studies

Further studies are required to provide a better link between the possible source areas and the sedimentary units within the Mandawa Basin. The sparse information about the chemical composition of possible source areas makes it difficult to interpret the provenance of the analyzed samples. The large river systems in Tanzania transport sediments from several source areas and cause a mix of provenance signals in the sediments. River sediments from restricted source areas should therefore be analyzed to be able to differentiate between the provenance signals seen in the analyzed sediments.

Many of the heavy minerals seen in the samples from Mandawa Basin are suitable for single grain analysis. Tourmaline is abundant in many of the samples and could provide further information with the regards to provenance. Many heavy minerals are also suitable for trace elements and isotope analysis. Hafnium (Hf) and Uranium (U) in rutile can indicate different source rock lithologies while zirconium (Zr) could provide information about the temperature during crystallization (Meinhold, 2010). Different trace elements in apatite could provide information about the lithologies of the source area (Belousova et al., 2002). Analysis of Lead

(Pb) and Uranium (U) isotopes in zircon is a widely used tool for age determination of rocks and comparison of zircon ages in source rocks and sediments could provide a stronger link between the two (McLaren et al., 1994).

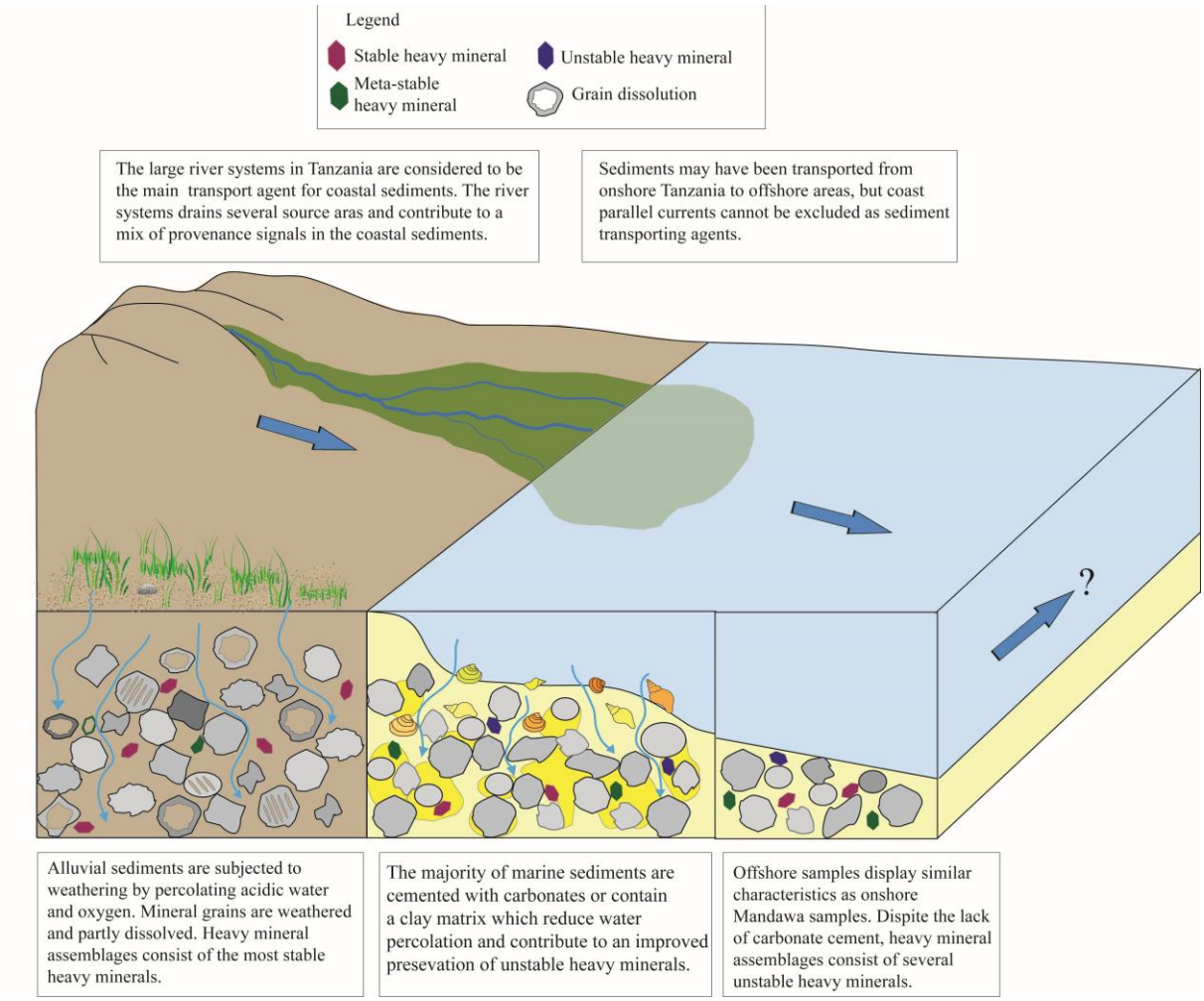

Figure 5.1*: Summarizing figure of the possible factors which may have influenced the analyzed samples from Mandawa Basin and offshore Tanzania. The large river systems in Tanzania are considered to be the main distribution agents for coastal sediments, but it is uncertain whether the offshore sediments from Statoil, Block 2 originate from onshore Tanzania or if the sediments have been transported by coast parallel currents. Alluvial sediments are highly affected by weathering processes which dissolve and alter the mineral composition. Marine sediments are generally cemented with carbonates which reduce water percolation and chemical weathering. Sediments from offshore areas (Block 2) display similarities with comparable onshore sediments.*

5 Conclusion

Sediments from Karoo sedimentary sequences, Upper Kipatimu Mb., Upper Mitole Mb. and Makonde Fm. are characterized by sedimentary facies and facies associations which indicate deposition in different alluvial environments. Sediments from these stratigraphical sequences display petrographical features which indicate a severe influence of chemical weathering.

Sediments from Kihuluhulu Fm., Nangurukuru Fm., Kivinje Fm., Masoko Fm. and Pande Fm. are characterized by sedimentary facies and facies associations which indicate a varying marine depositional environment. Sediments from these formations are generally cemented with different carbonate minerals which may have reduced the percolation of water, thus restricting the effect of chemical weathering.

Upper Kipatimu Mb., Upper Mitole Mb. and Makonde Fm. are characterized by stable heavy minerals which may reflect an influence of weathering rather than a reflection of source area. Marine sediments from TDP well site 1, 2, 7B, 9, 21 and 24 contains relatively high content of unstable heavy minerals. The heavy mineral content in these sediments could reflect a shift in sedimentary input, but could also result from a better preservation of unstable heavy minerals due to carbonate cementation or clay matrix. A change in heavy mineral assemblage is seen in Eocene sediments which may reflect a shift in sedimentary input.

The analyzed sediments from Mandawa Basin display mixed provenance signals which complicate the interpretation and identification of possible source areas. Rufiji, Wami and the Greta Ruaha River are large river systems which drain and transport sediments from several source areas and contribute to the mix of provenance signals seen in the analyzed sediments. Microprobe analysis of garnets and rutile indicate an input of more than one source area. The Mozambique Belt, west of Mandawa Basin, includes varying lithologies and metamorphic facies which may have act as a source of sediments in the analyzed samples.

Offshore samples display petrographical characteristics and a heavy mineral content similar to comparable onshore Mandawa samples which may indicate a sediment transport from onshore Tanzania to offshore areas, although an influence of coast parallel currents cannot be excluded.

References

AAGAARD, P., JAHREN, J., HARSTAD, A., NILSEN, O. & RAMM, M. 2000. Formation of grain-coating chlorite in sandstones. Laboratory synthesized vs. natural occurrences. *Clay Minerals,* 35**,** 261-269.

AERTS, M. 20.05.14 2014.

ANDRIESSEN, P., COOLEN, J. & HEBEDA, E. 1985. K • Ar hornblende dating of late Pan-African metamorphism in the Furua Granulite Complex of southern Tanzania. *Precambrian Research,* 30**,** 351-360.

APLIN, A. C., FLEET, A. J. & MACQUAKER, J. H. 1999. Muds and mudstones: Physical and fluid-flow properties. *Geological Society, London, Special Publications,* 158**,** 1-8.

BAIN, D. 1976. A TITANIUM-RICH SOIL CLAY. *Journal of Soil Science,* 27**,** 68-70.

BELL, K. & DODSON, M. H. 1981. The Geochronology of the Tanzanian Shield. *The Journal of Geology,* 89**,** 109-128.

BERROCOSO, J. Á., MACLEOD, K. G., HUBER, B. T., LEES, J. A., WENDLER, I., BOWN, P. R., MWENEINDA, A. K., ISAZA LONDOÑO, C. & SINGANO, J. M. 2010. Lithostratigraphy, biostratigraphy and chemostratigraphy of Upper Cretaceous sediments from southern Tanzania: Tanzania drilling project sites 21–26. *Journal of African Earth Sciences,* 57**,** 47-69.

BESLY, B. & TURNER, P. 1983. Origin of red beds in a moist tropical climate (Etruria Formation, Upper Carboniferous, UK). *Geological Society, London, Special Publications,* 11**,** 131-147.

BJØRLYKKE, K. 2010. Sandstone and Sandstone Reservoirs. *Petroleum Geoscience: From Sedimentary Environments to Rock Phiysics.* Heidelberg: Springer, 113-141.

BLATT, H. & CHRISTIE, J. M. 1963. Undulatory extinction in quartz of igneous and metamorphic rocks and its significance in provenance studies of sedimentary rocks. *Journal of Sedimentary Research,* 33.

BLATT, H. & SUTHERLAND, B. 1969. Intrastratal solution and non-opaque heavy minerals in shales. *Journal of Sedimentary Research,* 39**,** 591-600.

BOURGET, J., ZARAGOSI, S., GARLAN, T., GABELOTAUD, I., GUYOMARD, P., DENNIELOU, B., ELLOUZ-ZIMMERMANN, N. & SCHNEIDER, J.-L. 2008. Discovery of a giant deep-sea valley in the Indian Ocean, off eastern Africa: The Tanzania channel. *Marine Geology,* 255**,** 179-185.

BRAGG, W. & BRAGG, W. 1913. The reflection of X-rays by crystals. *Proceedings of the Royal Society of London. Series A,* 88**,** 428-438.

BROWNE, G. H., SLATT, R. M. & KING, P. R. 2000. Contrasting styles of basin-floor fan and slope fan deposition: Mount Messenger Formation, New Zealand. *SPECIAL PUBLICATION-SEPM,* 68**,** 143-152.

BUNCE, E. T., LANGSETH, M. G., CHASE, R. & EWING, M. 1967. Structure of the western Somali Basin. *Journal of Geophysical Research,* 72**,** 2547-2555.

BUURMAN, P. 1972. *Mineralization of fossil wood,* Rijksmuseum van Geologie en Mineralogie Leiden.

CAHEN, L., SNELLING, N., DELHAL, J., BONHOMME, M. & LEDENT, D. 1984. *The geochronology and evolution of Africa*, Clarendon Press Oxford.

CARROLL, D. 1970. The Weathering Environment. *Rock Weathering.* Springer, 7-18.

CHEN, P.-Y. 1977. *Table of key lines in x-ray powder diffraction patterns of mineral in clays and associated rocks,* Geological Survey.

CLIFTON, H. E. 1969. Beach lamination: nature and origin. *Marine Geology,* 7**,** 553-559.
COFFIN, M. F. & RABINOWITZ, P. D. 1987. Reconstruction of Madagascar and Africa: Evidence from the Davie fracture zone and western Somali basin. *Journal of Geophysical Research: Solid Earth (1978–2012),* 92**,** 9385-9406.
COLLINSON, J. D. 1986. Ancient sandy fluvial systems *In:* READING, H. G. (ed.) *Sedimentary Environments and Facies.* University of Oxford: Blackwell Scientific Publications, 49-54.

COMPTON, R. R. 1962. Manual of field geology. *Soil Science,* 93**,** 295.
CONIGILO, M. & DIX, G. R. 1992. Carbonate slopes. *In:* WALKER, R. G. & JAMES, N. P. (eds.) *Facies Models; Response to sea level changes.* Ontario: Geological Association of Canada, 349-375.

COX, K. 1992. Karoo igneous activity, and the early stages of the break-up of Gondwanaland. *Geological Society, London, Special Publications,* 68**,** 137-148.
DEER, W. A., HOWIE, R. A. & ZUSSMAN, J. 2013. *An Introduction to the Rock Forming Minerals,* London The Mineralogical Society.
DOTT JR, R. H. 1964. Wacke, Graywacke and Matrix--What Approach to Immature Sandstone Classification? *Journal of Sedimentary Research,* 34.
DREVER, J. I. 1994. The effect of land plants on weathering rates of silicate minerals. *Geochimica et Cosmochimica Acta,* 58**,** 2325-2332.
ESRI. 2014. *Basemaps, Reference Maps, and Specialty Maps*.
FORCE, E. R. 1980. The provenance of rutile. *Journal of Sedimentary Research,* 50**,** 485-488.
FRIIS, H. 1974. Weathered heavy-mineral associations from the young-Tertiary deposits of Jutland, Denmark. *Sedimentary Geology,* 12**,** 199-213.
GAINA, C., TORSVIK, T. H., VAN HINSBERGEN, D. J., MEDVEDEV, S., WERNER, S. C. & LABAILS, C. 2013. The African Plate: A history of oceanic crust accretion and subduction since the Jurassic. *Tectonophysics,* 604**,** 4-25.
GALLOWAY, W. E. & HOBDAY, D. K. 1983. Terrigenous clastic depositional systems. Applications to petroleum, coal and uranium exploration.
GOVERNMENT OF THE UNITED REPUBLIC OF TANZANIA. *Geology*.
GREENSMITH, J. T. 1978. Limstones. *Petrology of the Sedimentary Rocks* London: George Allen & Unwin, 124-155.

GSA. 2012. *GSA Geological Time Scale* [Online]. The Goelogical Society of America. Available: http://www.geosociety.org/science/timescale/.
GUNDERSVEEN, E. 2014. Sedimentology, Petrology and Diagenesis of Mesozoic Sandstones in the Mandawa Basin, Coastal Tanzania. University of Oslo.

HANKEL, O. 1994. Early Permian to middle Jurassic rifting and sedimentation in East Africa and Madagascar. *Geologische Rundschau,* 83**,** 703-710.
HJELLBAKK, A. 1997. Facies and fluvial architecture of a high-energy braided river: the Upper Proterozoic Seglodden Member, Varanger Peninsula, northern Norway. *Sedimentary Geology,* 114**,** 131-161.
HUDSON, W. 2011. *The Geological Evolution of the Petroleum Prospective Mandawa Basin Coastal Tanzania.* PhD, Trinity Collage.
JAMES, N. P. & KENDALL, A. C. 1992. Introductin to carbonate facies models. *In:* WALKER, R. G. (ed.) *Facies Models; Response to sea level change.* Ontario: Geological Association of Canada, 265-277.

KENT, P. E., HUNT, J. A. & JOHNSTONE, D. W. 1971. *The geology and geophysics of coastal Tanzania*, HM Stationery Office.

KLEIN, G. D. V. 1985. Intertidal Flats and Intertidal Sand Bodies. *In:* RICHARD A. DAVIES, J. (ed.) *Coastal Sedimentary Environments.* New York, USA: Springer-Verlag, 187-219.

KORNELIUSSEN, A., MCLIMANS, R., BRAATHEN, A., ERAMBERT, M., LUTRO, O. & RAGNHILDSTVEIT, J. 2000. Rutile in eclogites as a mineral resource in the Sunnfjord region, Western Norway. *NORGES GEOLOGISKE UNDERSOKELSE,* 436**,** 39-48.

KREUSER, T., WOPFNER, H., KAAYA, C., MARKWORT, S., SEMKIWA, P. & ASLANDIS, P. 1990. Depositional evolution of Permo-Triassic Karoo basins in Tanzania with reference to their economic potential. *Journal of African Earth Sciences (and the Middle East),* 10**,** 151-167.

KRIPPNER, A., MEINHOLD, G., MORTON, A. C. & VON EYNATTEN, H. 2014. Evaluation of garnet discrimination diagrams using geochemical data of garnets derived from various host rocks. *Sedimentary Geology,* 306**,** 36-52.

LENOIR, J. L., LIÉGEOIS, J. P., THEUNISSEN, K. & KLERKX, J. 1994. The Palaeoproterozoic Ubendian shear belt in Tanzania: geochronology and structure. *Journal of African Earth Sciences,* 19**,** 169-184.

MAHMIC, O. 2014. Composition and Trace-element Geochemistry of Clays of the Upper Cretaceous to Paleogene Kilwa Group, Tanzania: A Provenance Study. University of Oslo.

MANGE, M. A. & MAURER, H. F. 1992. *Heavy minerals in colour*, Chapman & Hall London.

MBEDE, E. 1991. The sedimentary basins of Tanzania-reviewed. *Journal of African Earth Sciences (and the Middle East),* 13**,** 291-297.

MCCONNELL, R. 1972. Geological development of the rift system of eastern Africa. *Geological Society of America Bulletin,* 83**,** 2549-2572.

MCLAREN, A., GERALD, J. & WILLIAMS, I. 1994. The microstructure of zircon and its influence on the age determination from Pb/U isotopic ratios measured by ion microprobe. *Geochimica et Cosmochimica Acta,* 58**,** 993-1005.

MEINHOLD, G. 2010. Rutile and its applications in earth sciences. *Earth-Science Reviews,* 102**,** 1-28.

MEINHOLD, G., ANDERS, B., KOSTOPOULOS, D. & REISCHMANN, T. 2008. Rutile chemistry and thermometry as provenance indicator: an example from Chios Island, Greece. *Sedimentary Geology,* 203**,** 98-111.

MIALL, A. D. 2003. Sands, gravels, and their lithified equivalents. *Sedimentology.* Springer, 960-966.

MILLS, P. C. 1983. Genesis and diagnostic value of soft-sediment deformation structures—a review. *Sedimentary Geology,* 35**,** 83-104.

MORTON, A. 1984. Stability of detrital heavy minerals in Tertiary sandstones from the North Sea Basin. *Clay minerals,* 19**,** 287-308.

MORTON, A., HALLSWORTH, C. & CHALTON, B. 2004. Garnet compositions in Scottish and Norwegian basement terrains: a framework for interpretation of North Sea sandstone provenance. *Marine and Petroleum Geology,* 21**,** 393-410.

MORTON, A. C. 1985. A new approach to provenance studies: electron microprobe analysis of detrital garnets from Middle Jurassic sandstones of the northern North Sea. *Sedimentology,* 32**,** 553-566.
MORTON, A. C. & HALLSWORTH, C. 1994. Identifying provenance-specific features of detrital heavy mineral assemblages in sandstones. *Sedimentary Geology,* 90**,** 241-256.
MORTON, A. C. & HALLSWORTH, C. R. 1999. Processes controlling the composition of heavy mineral assemblages in sandstones. *Sedimentary Geology,* 124**,** 3-29.
MORTON, A. C. & JOHNSSON, M. 1993. Factors influencing the composition of detrital heavy mineral suites in Holocene sand of the Apure River drainage basin, Venezuela. *Processes Controlling the Composition of Siliciclastic Sediments. Geol. Soc. Am. Spec. Pap,* 284**,** 171-185.
MPANDA, S. 1997. Geological development of the East African coastal basin of Tanzania.
MUHONGO, S. & LENOIR, J.-L. 1994. Pan-African granulite-facies metamorphism in the Mozambique Belt of Tanzania: U-Pb zircon geochronology. *Journal of the Geological Society,* 151**,** 343-347.
MÖLLER, A., APPEL, P., MEZGER, K. & SCHENK, V. 1995. Evidence for a 2 Ga subduction zone: eclogites in the Usagaran belt of Tanzania. *Geology,* 23**,** 1067-1070.
NESBITT, H. & YOUNG, G. 1984. Prediction of some weathering trends of plutonic and volcanic rocks based on thermodynamic and kinetic considerations. *Geochimica et Cosmochimica Acta,* 48**,** 1523-1534.
NESBITT, H. W. & YOUNG, G. M. 1996. Petrogenesis of sediments in the absence of chemical weathering: effects of abrasion and sorting on bulk composition and mineralogy. *Sedimentology,* 43**,** 341-358.
NICHOLAS, C. J., PEARSON, P. N., BOWN, P. R., JONES, T. D., HUBER, B. T., KAREGA, A., LEES, J. A., MCMILLAN, I. K., O'HALLORAN, A. & SINGANO, J. M. 2006. Stratigraphy and sedimentology of the Upper Cretaceous to Paleogene Kilwa Group, southern coastal Tanzania. *Journal of African Earth Sciences,* 45**,** 431-466.
NICHOLAS, C. J., PEARSON, P. N., MCMILLAN, I. K., DITCHFIELD, P. W. & SINGANO, J. M. 2007. Structural evolution of southern coastal Tanzania since the Jurassic. *Journal of African Earth Sciences,* 48**,** 273-297.
NORTON, I. & SCLATER, J. 1979. A model for the evolution of the Indian Ocean and the breakup of Gondwanaland. *Journal of Geophysical Research: Solid Earth (1978–2012),* 84**,** 6803-6830.
OLARIU, C. & BHATTACHARYA, J. P. 2006. Terminal distributary channels and delta front architecture of river-dominated delta systems. *Journal of Sedimentary Research,* 76**,** 212-233.
OLIVA, P., VIERS, J. & DUPRÉ, B. 2003. Chemical weathering in granitic environments. *Chemical Geology,* 202**,** 225-256.
PEARSON, P. N., NICHOLAS, C. J., SINGANO, J. M., BOWN, P. R., COXALL, H. K., VAN DONGEN, B. E., HUBER, B. T., KAREGA, A., LEES, J. A. & MACLEOD, K. 2006. Further Paleogene and Cretaceous sediment cores from the Kilwa area of coastal Tanzania: Tanzania drilling project sites 6–10. *Journal of African Earth Sciences,* 45**,** 279-317.
PETTIJOHN, F. 1941. Persistence of heavy minerals and geologic age. *The Journal of Geology***,** 610-625.
PETTIJOHN, F. J., E.P, P. & SIEVER, R. 1972a. Texture. *Sand and Sandstones* Heidelberg: Sringer-Verlag, 25-63.
PETTIJOHN, F. J., POTTER, P. E. & SIEVER, R. 1972b. Diagenesis. *Sand and Sandstones.* Heidelberg: Springer- Verlag, 383-434.

PETTIJOHN, F. J., POTTER, P. E. & SIEVER, R. 1972c. Mineral and Chemical Composition *Sand and Sandstone*. Heidelberg: Springer-Verlag, 25-63.

PETTIJOHN, F. J., POTTER, P. E. & SIEVER, R. 1972d. Production and Provenance of Sand. *Sand and Sandstones.* Heidelberg: Springer- Verlag, 294-323.

PINNA, P., JOURDE, G., CALVEZ, J., MROZ, J. & MARQUES, J. 1993. The Mozambique Belt in northern Mozambique: Neoproterozoic (1100–850 Ma) crustal growth and tectogenesis, and superimposed Pan-African (800–550 Ma) tectonism. *Precambrian Research,* 62**,** 1-59.

POWERS, M. C. 1953. A new roundness scale for sedimentary particles. *Journal of Sedimentary Research,* 23.

PROCHASKA, W. & POHL, W. 1983. Petrochemistry of some mafic and ultramafic rocks from the Mozambique Belt, northern Tanzania. *Journal of African Earth Sciences (1983),* 1**,** 183-191.

REED, S. J. B. 2005. Electron- specimen interactions. *Electron Microprobe Analysis and Scanning Electron Microscopy in Geology*. Cambridge: Cambridge University Press, 7-20.

RUAN, C.-D. & WARD, C. R. 2002. Quantitative X-ray powder diffraction analysis of clay minerals in Australian coals using Rietveld methods. *Applied Clay Science,* 21**,** 227-240.

SCHLÜTER, T. & HAMPTON, C. 1997. *Geology of East Africa*, Borntraeger Berlin.

SHIKI, T. 1959. Studies on Sandstones in the Maizuru Zone, Southwest Japan I: Importance of some Relations between Mineral Composition and Grain Size. *Memoirs of the College of Science, University of Kyoto. Series B.*, 25**,** 239-246.

STATOIL. 2014. *Statoil's Zafarani reservoir in Tanzania Block 2 successfully tested* [Online]. Available: http://www.statoil.com/en/NewsAndMedia/News/2014/Pages/03Mar_Tazania.aspx.

STOW, D. A., HOWELL, D. G. & NELSON, C. H. 1983. Sedimentary, tectonic, and sea-level controls on submarine fan and slope-apron turbidite systems. *Geo-Marine Letters,* 3**,** 57-64.

SÆTRE, R. & DA SILVA, A. J. 1984. The circulation of the Mozambique Channel. *Deep Sea Research Part A. Oceanographic Research Papers,* 31**,** 485-508.

TARDY, Y., BOCQUIER, G., PAQUET, H. & MILLOT, G. 1973. Formation of clay from granite and its distribution in relation to climate and topography. *Geoderma,* 10**,** 271-284.

THOMPSON, W. O. 1937. Original structures of beaches, bars, and dunes. *Geological Society of America Bulletin,* 48**,** 723-751.

TUCKER, E. M. 2001. Limestones. *Sedimentary Petrology; An Introduction to the Origin of Sedimentary Rocks* United Kingdom: Blackwell Science, 110-151.

VOLAT, J.-L., PASTOURET, L. & VERGNAUD-GRAZZINI, C. 1980. Dissolution and carbonate fluctuations in Pleistocene deep-sea cores: a review. *Marine Geology,* 34**,** 1-28.

WALKER, R. G. 1992. Facies, facies models and modern stratigraphic consepts. *In:* WALKER, R. G. (ed.) *Facies Models; response to sea level change.* Ontario: Geological Association of Canada, 1-15.

WALKER, T. R. 1967. Formation of red beds in modern and ancient deserts. *Geological Society of America Bulletin,* 78**,** 353-368.
WENTWORTH, C. K. 1922. A scale of grade and class terms for clastic sediments. *The Journal of Geology***,** 377-392.
WILLIAMS, H. F. 1989. Foraminiferal zonations on the Fraser River Delta and their application to paleoenvironmental interpretations. *Palaeogeography, Palaeoclimatology, Palaeoecology,* 73**,** 39-50.
WRIGHT, L. D. 1985. River Deltas. *In:* RICHARD A. DAVIES, J. (ed.) *Coastal Sedimentary Environments.* New York: Springer- Verlag, 1-70.

WRIGHT, W. 1938. The composition and occurrence of garnets. *American Mineralogist,* 23**,** 436-449.
ZACK, T., VON EYNATTEN, H. & KRONZ, A. 2004. Rutile geochemistry and its potential use in quantitative provenance studies. *Sedimentary Geology,* 171**,** 37-58.
ZAKARIASSEN, E. 2014.

Appendix

Appendix A1- Table of quantitative XRD result, in %, from TDP core 1, 2,7B, 9, 21 and 24.

Appendix A2 – Table of quantitative XRD result, in %, from Karoo sedimentary sequences, Upper Kipatimu Mb., Upper Mitole Mb., Makonde Fm., Matandu River, basement samples and offshore samples.

Appendix B - Table of point counting results in %.

Appendix C – Classification of samples based on point counting results.

Appendix D – Conventional heavy mineral analysis in %.

Appendix E1 – Electron microprobe analysis of garnet in wt% and mol%.

Appendix E2 - Electron microprobe analysis of rutile in wt% and ppm.

Appendix A1 – Quantitative XRD results (Core)

Sample name	Mixed layer	Illite/Mica	Kaolinite	Chlorite	Quartz	K-Feldspar	Plagioclase	Calcite	Dolomite	Aragonite	Ankerite	Siderite	Pyrite	Gypsum	Chi Squared	R-Factor	Q/F
c1_1,45	0,00	15,30	1,70	0,00	18,60	6,20	3,70	21,10	0,60	8,00	0,00	23,90	0,90	0,00	2,67	0,080	1,88
c1_8,30	18,30	5,40	1,20	0,90	44,20	18,10	6,10	0,00	0,00	5,80	0,00	0,00	0,00	0,00	3,96	0,114	1,83
c1_11,60	27,80	7,50	1,80	1,00	29,00	16,40	9,00	1,90	0,00	4,40	0,00	0,00	1,00	0,00	4,26	0,119	1,14
c1_14,50	0,00	3,80	0,00	0,00	61,10	21,80	9,20	3,90	0,00	0,00	0,00	0,00	0,10	0,00	4,43	0,123	1,97
c1_14,74	13,30	2,70	1,40	0,30	45,40	12,80	10,40	8,70	0,00	4,30	0,00	0,00	0,30	0,00	3,76	0,107	1,96
c1_19,75	12,30	2,50	1,20	0,50	27,10	14,30	5,50	29,30	0,00	4,00	0,00	0,00	1,40	1,90	3,05	0,091	1,37
c1_20,21	0,00	1,40	0,00	0,00	13,10	4,50	3,20	71,10	0,00	4,10	0,00	1,30	1,20	0,00	3,53	0,121	1,70
c1_24,30	23,90	31,10	9,90	0,00	11,50	1,40	17,30	0,00	0,00	0,70	0,00	0,00	3,20	0,90	2,78	0,072	0,61
c1_25,65	17,00	3,20	1,70	0,80	44,40	21,20	9,00	0,00	0,00	2,60	0,00	0,00	0,00	0,00	4,00	0,114	1,47
c1_27.03	21,40	19,20	2,50	1,00	19,20	13,70	6,70	7,70	0,00	4,50	0,00	0,00	2,70	1,10	3,11	0,093	0,94
c1_34,25	7,20	5,00	1,20	0,00	41,20	16,20	5,90	13,30	0,00	7,70	0,00	0,00	0,70	1,50	3,45	0,103	1,86
c1_40,85	0,00	0,00	0,50	0,00	12,80	3,80	2,80	76,70	0,00	2,70	0,00	0,00	0,60	0,00	3,45	0,118	1,94
c1_44,70	13,50	1,40	0,90	0,80	38,90	16,60	6,70	12,00	0,00	7,00	0,00	0,00	0,90	1,30	3,41	0,102	1,67
c1_49,79	26,20	12,00	6,00	0,00	6,50	47,00	0,00	0,50	0,00	0,00	0,00	0,00	0,60	1,20	3,92	0,103	0,14
c1_62,54	18,20	7,70	2,80	0,60	33,60	25,00	9,30	0,70	0,00	2,10	0,00	0,00	0,00	0,00	4,68	0,133	0,98
c2_3,57	17,60	25,40	3,40	1,40	7,80	7,80	10,10	12,00	0,00	12,10	0,00	0,00	1,30	1,00	3,36	0,098	0,44
c2_11,30	17,80	25,50	3,70	3,30	9,20	10,20	11,20	9,50	0,00	7,10	0,00	0,00	1,50	1,10	4,01	0,116	0,43
c2_16,43	22,30	33,10	3,80	2,70	6,20	9,10	9,50	6,10	0,00	5,10	0,00	0,00	1,40	0,70	4,21	0,114	0,33
c2_35,40	13,60	34,40	2,30	1,20	8,10	6,10	10,90	14,90	0,00	7,40	0,00	0,00	0,90	0,30	3,44	0,095	0,48
c2_50,20	14,80	32,70	2,00	1,10	10,40	7,70	10,10	13,10	0,00	5,80	0,00	0,00	1,00	1,40	3,22	0,093	0,58
c2_52,20	21,60	28,10	2,50	0,60	9,40	8,10	13,10	10,20	0,00	5,30	0,00	0,00	0,70	0,30	3,57	0,102	0,44
c2_53,45	0,00	0,00	0,00	0,00	0,80	0,00	0,00	98,40	0,00	0,00	0,00	0,00	0,90	0,00	4,92	0,175	
c2_59,33	0,00	0,00	0,00	0,00	2,00	0,00	4,00	93,90	0,00	0,00	0,00	0,00	0,00	0,00	4,51	0,155	0,50
c2_64,45	0,00	3,80	0,00	0,00	29,00	10,10	15,50	36,40	0,00	4,50	0,00	0,00	0,00	0,00	4,07	0,129	1,13
c2_69_52	16,90	12,20	2,80	1,20	21,70	14,90	11,20	12,30	0,00	4,60	0,00	0,00	1,00	1,20	3,23	0,096	0,83
c2_76,55	21,20	9,10	4,70	2,60	16,60	14,20	12,70	13,20	0,00	4,30	0,00	0,00	1,10	0,40	3,78	0,106	0,62
c2_98,05	0,00	0,00	0,00	0,00	1,40	0,00	0,40	98,20	0,00	0,00	0,00	0,00	0,00	0,00	4,37	0,156	3,50
21/25/1, 5-6	12,90	0,00	0,00	0,00	70,30	9,30	4,70	0,00	0,00	0,00	0,00	0,00	2,80	0,00	4,39	0,127	5,02
21/24/1, 10-12	0,00	0,00	0,00	0,00	53,80	5,40	3,40	37,40	0,00	0,00	0,00	0,00	0,00	0,00	4,52	0,142	6,11
21/23/1, 10-12	11,80	0,00	0,00	0,00	31,30	8,10	3,40	2,90	40,40	0,00	0,00	0,00	2,20	0,00	3,86	0,122	2,72
21/22/2, 19-21	0,00	0,00	0,00	0,00	54,00	7,70	1,90	36,20	0,00	0,00	0,00	0,00	0,00	0,00	3,85	0,117	5,63
21/21/1, 19-21	35,50	0,00	0,00	0,00	40,00	13,20	7,90	0,00	0,00	0,00	0,00	0,00	2,80	0,00	3,98	0,117	1,90
21/20/1,81-83	0,00	0,00	0,00	0,00	29,10	2,50	1,20	67,20	0,00	0,00	0,00	0,00	0,00	0,00	4,05	0,135	7,86
21/20/1, 88-90	0,00	0,00	0,00	0,00	57,70	8,10	2,80	31,40	0,00	0,00	0,00	0,00	0,00	0,00	4,59	0,142	5,29
21/17/3,23-25	0,00	0,00	0,00	0,00	60,00	7,90	2,80	29,30	0,00	0,00	0,00	0,00	0,00	0,00	4,35	0,129	5,61
21/17/2,56-58	0,00	0,00	0,00	0,00	61,50	7,80	5,30	25,30	0,00	0,00	0,00	0,00	0,00	0,00	5,00	0,152	4,69
21/17/2, 21-24	0,00	0,00	0,00	0,00	58,80	6,20	2,70	32,20	0,00	0,00	0,00	0,00	0,00	0,00	5,21	0,162	6,61

Sample name	Mixed layer	Illite/Mica	Kaolinite	Chlorite	Quartz	K-Feldspar	Plagioclase	Calcite	Dolomite	Aragonite	Ankerite	Siderite	Pyrite	Gypsum	Chi Squared	R-Factor	Q/F
24/30/1, 3-5	0,00	0,00	0,00	0,00	80,60	4,50	0,70	0,00	14,30	0,00	0,00	0,00	0,00	0,00	5,60	0,15	15,50
24/28/1, 57-59	0,00	0,00	0,00	0,00	60,00	5,30	1,80	0,00	0,00	0,00	32,90	0,00	0,00	0,00	0,00	0,00	8,45
24/28/3. 5-8	0,00	0,00	0,00	0,00	74,60	4,00	0,80	0,00	20,60	0,00	0,00	0,00	0,00	0,00	4,88	0,14	15,54
24/28/2, 16-18	0,00	0,00	0,00	0,00	72,40	7,10	2,60	0,00	17,90	0,00	0,00	0,00	0,00	0,00	4,78	0,13	7,46
24/27/3, 11-12	0,00	0,00	0,00	0,00	31,90	1,70	0,90	2,90	0,00	0,00	0,00	0,00	62,60	0,00	3,00	0,10	12,27
24/26/3, 9-13	19,20	0,00	0,00	0,00	17,20	6,20	3,00	38,80	15,70	0,00	0,00	0,00	0,00	0,00	3,05	0,10	1,87
24/18/2, 25-26	0,00	0,00	0,00	0,00	80,10	5,20	1,90	12,90	0,00	0,00	0,00	0,00	0,00	0,00	4,58	0,13	11,28
24/17/3, 9-10	0,00	0,00	0,00	0,00	76,20	4,60	1,70	17,50	0,00	0,00	0,00	0,00	0,00	0,00	4,52	0,13	12,10
24/16/3, 13-16	0,00	0,00	0,00	0,00	41,50	7,80	10,80	39,90	0,00	0,00	0,00	0,00	0,00	0,00	4,22	0,13	2,23
24/10/3, 16-18	0,00	0,00	0,00	0,00	5,40	0,90	1,60	92,10	0,00	0,00	0,00	0,00	0,00	0,00	3,17	0,11	2,16
c7B_0,48	0,00	0,00	0,00	0,00	3,00	0,00	2,80	90,60	3,50	0,00	0,00	0,00	0,00	0,00	4,38	0,150	1,07
c7B_5,30	2,40	0,90	1,00	0,00	6,70	1,50	2,70	70,90	13,40	0,00	0,00	0,00	0,50	0,00	3,64	0,119	1,60
c7B_6,13	0,00	0,00	0,20	0,00	2,10	0,00	0,90	89,60	6,60	0,00	0,00	0,00	0,70	0,00	4,56	0,155	2,33
c7B_14,55	8,90	8,90	2,50	1,60	11,20	6,00	9,90	32,70	0,00	17,60	0,00	0,00	0,70	0,00	3,08	0,095	0,70
c7B_15,30	18,30	36,10	5,50	4,70	11,80	6,80	9,30	3,30	0,00	3,20	0,00	0,00	0,90	0,00	3,37	0,096	0,73
c7B_19,99	10,50	18,20	2,80	2,10	13,00	6,50	10,40	28,10	0,00	7,10	0,00	0,50	0,70	0,20	3,25	0,095	0,77
c7B_25,14	0,00	2,20	0,90	0,00	3,80	1,40	2,90	87,50	0,00	0,80	0,00	0,00	0,50	0,00	4,11	0,135	0,88
c7B_26,45	0,00	0,90	0,00	0,00	9,50	1,80	3,20	65,80	0,00	12,00	0,00	0,00	4,00	2,90	3,46	0,116	1,90
c7B_29,70	23,80	14,90	6,30	0,40	10,50	10,60	9,40	11,70	0,00	10,80	0,00	0,30	0,70	0,80	3,10	0,089	0,53
c7B_30,21	0,00	3,80	0,90	0,00	2,70	1,40	2,40	84,80	0,00	3,40	0,00	0,00	0,50	0,00	3,63	0,122	0,71
c7B_37,60	13,20	35,50	5,60	2,60	9,90	8,90	12,00	3,10	0,00	5,80	0,00	0,00	1,20	2,20	4,80	0,127	0,47
c7B_43,60	25,30	18,60	7,90	4,10	14,90	11,60	13,40	0,40	0,00	3,10	0,00	0,00	0,50	4,10	4,76	0,130	0,60
c7B_54,14	0,00	1,70	0,90	0,00	2,00	10,70	2,70	80,00	0,00	0,30	0,00	0,00	0,60	0,00	3,95	0,130	0,15
c7B_56,45	19,40	3,20	2,40	0,00	21,80	6,90	8,70	29,10	0,00	5,50	0,00	0,00	1,10	1,90	2,85	0,085	1,40
c7B_68,53	23,50	35,60	4,70	2,80	7,80	8,80	9,90	1,20	0,00	4,10	0,00	0,00	0,90	0,80	4,28	0,114	0,42
c7B_80,10	20,30	8,50	3,00	0,00	6,40	2,60	5,60	47,10	0,00	3,50	0,00	0,00	1,40	1,70	3,07	0,093	0,78
c7B_113,50	22,50	20,10	4,10	2,90	15,90	11,70	14,30	1,70	0,00	4,40	0,00	0,00	0,90	1,50	4,69	0,127	0,61
c7B_124,03	3,30	4,40	1,10	0,00	18,40	5,00	7,70	54,00	0,00	2,40	0,00	0,00	2,60	1,10	3,25	0,102	1,45
c7B_152,50	7,60	4,40	1,70	0,00	11,10	4,80	6,40	58,20	0,00	2,90	0,00	0,00	1,50	1,40	3,13	0,099	0,99
c9_40-42	20,20	11,70	2,90	4,40	15,30	7,80	9,70	25,00	0,00	2,20	0,00	0,00	0,00	1,00	3,23	0,097	0,87
c9_90-92	7,00	6,30	5,20	4,50	21,20	10,00	14,20	29,40	0,00	1,20	0,00	0,00	0,70	0,40	3,56	0,108	0,88
c9_34-35	17,50	19,60	5,50	1,30	12,60	5,30	7,80	28,40	0,00	0,70	0,00	0,00	0,70	0,80	3,18	0,096	0,96
c9_23-24	15,80	17,90	4,30	2,30	13,00	7,60	9,70	27,70	0,00	0,90	0,00	0,00	0,80	0,00	3,36	0,102	0,75
c9_68-69	19,20	18,80	4,10	1,20	10,30	5,80	8,60	30,30	0,00	0,30	0,00	0,00	0,60	0,80	3,31	0,102	0,72
c9_31-32	20,00	14,30	4,90	3,80	19,90	10,80	13,60	11,10	0,00	0,60	0,00	0,00	0,70	0,30	3,35	0,094	0,82
c9_14-16	0,00	3,00	0,00	0,00	28,50	8,30	20,50	35,40	0,00	4,10	0,00	0,00	0,20	0,00	4,34	0,134	0,99
c9_25-27	19,10	26,00	2,10	2,80	12,30	9,40	12,00	14,10	0,00	1,60	0,00	0,00	0,50	0,00	3,60	0,108	0,57

Appendix A1 – Quantitative XRD results (Field)

Sample	Quartz	Albite	Calcite	Microcline	Kaolinite	Muscovite	Clay Mixed	Pyrite	Biotite	Chlorite	Hornblende	Anatase	Chi ^2	R-factor	Q/F
MP-2-0-13	28,50	31,80	0,00	14,60	0,00	7,90	17,30	0,00	0,00	0,00	0,00	0,00	4,09	0,117	0,61
MP-2-1-13	40,40	12,80	37,70	9,10	0,00	0,00	0,00	0,00	0,00	0,00	0,00	0,00	4,23	0,131	1,84
MP-2-2-13	54,20	23,90	0,00	18,80	0,00	0,00	0,00	0,00	0,00	3,20	0,00	0,00	4,63	0,132	1,27
MP-2-4-13	55,40	9,00	28,10	7,40	0,00	0,00	0,00	0,00	0,00	0,00	0,00	0,00	4,30	0,130	3,38
MP-2-5-13	58,80	5,20	29,20	6,80	0,00	0,00	0,00	0,00	0,00	0,00	0,00	0,00	4,40	0,135	4,90
MP-2-6-13	49,80	9,90	31,00	9,20	0,00	0,00	0,00	0,00	0,00	0,00	0,00	0,00	4,38	0,133	2,61
MP-2-7-13	60,80	8,60	21,10	9,50	0,00	0,00	0,00	0,00	0,00	0,00	0,00	0,00	4,63	0,137	3,36
MP-2-8-13	37,40	10,70	45,00	7,00	0,00	0,00	0,00	0,00	0,00	0,00	0,00	0,00	4,07	0,133	2,11
MP-2-9-13	31,40	24,50	29,10	12,80	2,20	0,00	0,00	0,00	0,00	0,00	0,00	0,00	4,54	0,136	0,84
MP-2-11-13	50,20	18,60	20,10	11,20	0,00	0,00	0,00	0,00	0,00	0,00	0,00	0,00	4,55	0,134	1,68
MP-2-12-13	9,20	0,60	87,20	1,80	1,10	0,00	0,00	0,00	0,00	0,00			4,49	0,158	3,83
NG-1-1-13	75,90	13,50	0,00	10,60	0,00	0,00	0,00	0,00	0,00	0,00	0,00	0,00	4,89	0,135	3,15
NG-1-2-13	79,10	9,80	0,00	11,10	0,00	0,00	0,00	0,00	0,00	0,00	0,00	0,00	5,12	0,138	3,78
NG-1-4-13	72,90	15,20	0,00	11,80	0,00	0,00	0,00	0,00	0,00	0,00	0,00	0,00	5,27	0,143	2,70
NG-1-5-13	74,50	13,60	0,00	11,90	0,00	0,00	0,00	0,00	0,00	0,00	0,00	0,00	5,34	0,147	2,92
NG-2-1-13	70,60	11,40	0,00	10,40	0,00	0,00	7,70	0,00	0,00	0,00	0,00	0,00	5,03	0,135	3,24
NG-2-3-13	71,80	12,30	0,00	11,50	4,50	0,00	0,00	0,00	0,00	0,00	0,00	0,00	5,23	0,141	3,02
MB-1-0-13	43,80	12,10	0,00	10,20	0,00	5,60	28,30	0,00	0,00	0,00	0,00	0,00	3,93	0,112	1,96
MB-1-3-13	55,00	15,70	0,00	11,40	0,00	0,00	17,90	0,00	0,00	0,00	0,00	0,00	4,31	0,119	2,03
MB-1-4-13	66,40	20,10	0,00	13,60	0,00	0,00	0,00	0,00	0,00	0,00	0,00	0,00	4,81	0,137	1,97
MB-1-7-13	62,40	22,50	0,00	15,10	0,00	0,00	0,00	0,00	0,00	0,00	0,00	0,00	5,12	0,144	1,66
MB-2-1-13	82,00	10,20	0,00	7,80	0,00	0,00	0,00	0,00	0,00	0,00	0,00	0,00	5,33	0,143	4,56
MB-2-2-13	59,10	27,00	0,00	13,90	0,00	0,00	0,00	0,00	0,00	0,00	0,00	0,00	5,06	0,144	1,44
MB-2-3-13	70,70	16,90	0,00	12,50	0,00	0,00	0,00	0,00	0,00	0,00	0,00	0,00	5,19	0,143	2,40
MB-2-4-13	75,60	14,10	0,00	10,30	0,00	0,00	0,00	0,00	0,00	0,00	0,00	0,00	5,14	0,139	3,10

Sample	Quartz	Albite	Calcite	Microcline	Kaolinite	Muscovite	Clay Mixed	Pyrite	Biotite	Chlorite	Hornblende	Anatase	Chi ^2	R-factor	Q/F
MN-1-1-13	24,70	0,00	0,00	11,20	3,00	16,70	44,40	0,00	0,00	0,00	0,00	0,00	4,18	0,117	2,21
MN-1-2-13	74,80	0,00	0,00	7,10	12,70	0,00	0,00	5,50	0,00	0,00	0,00	0,00	4,73	0,142	10,54
MN-1-3-13	80,50	0,00	0,00	11,20	8,30	0,00	0,00	0,00	0,00	0,00	0,00	0,00	5,64	0,153	7,19
MN-1-4-13	85,10	0,00	0,00	8,10	6,80	0,00	0,00	0,00	0,00	0,00	0,00	0,00	5,68	0,152	10,51
MN-1-5-13	75,20	0,00	0,00	14,30	10,50	0,00	0,00	0,00	0,00	0,00	0,00	0,00	5,87	0,149	5,26
MN-1-6-13	77,70	0,00	0,00	16,10	6,20	0,00	0,00	0,00	0,00	0,00	0,00	0,00	5,38	0,148	4,83
MN-1-7-13	78,20	0,00	0,00	15,50	6,30	0,00	0,00	0,00	0,00	0,00	0,00	0,00	5,43	0,145	5,05
MN-2-1-13	76,90	0,00	0,00	11,20	10,40	0,00	0,00	0,00	0,00	0,00	0,00	1,50	4,87	0,137	6,87
MN-2-2-13	74,40	0,00	0,00	12,70	11,50	0,00	0,00	0,00	0,00	0,00	0,00	1,40	5,03	0,138	5,86
MN-2-3-13	83,70	0,00	0,00	8,60	7,60	0,00	0,00	0,00	0,00	0,00	0,00	0,00	5,34	0,145	9,73
BA-2-13	33,10	48,00	0,00	10,50	0,00	0,00	0,00	0,00	3,60	0,00	4,80	0,00	6,98	0,184	0,57
BA-1-13	45,40	17,40	0,00	34,70	0,00	0,00	0,00	0,00	2,50	0,00	0,00	0,00	5,33	0,15	0,87
Mtandu Rive	48,5	28,9	0,00	18,2	0,00	0,00	0,00	0,00	0,00	0,00	3,9	0,00	0,00	0,00	1,03
2/2/14	84,1	6	0	9,9	0,00	0,00	0,00	0,00	0,00	0,00	0,00	0,00	0,00	0,00	5,29
2/1/14	91,3	3,6	1,3	3,8	0,00	0,00	0,00	0,00	0,00	0,00	0,00	0,00	0,00	0,00	12,34

Appendix B- Point counting

Sample	Total	Qtz				Total	K-feldspar					Plagioclase					Clay	Carb.	Poro-	Pyrite	HM	Mica	Rock.	Fe
	Qtz	Mono-M	Mono-U	Poly-M	Poly-U	Feld.	1	2	3	4	5	1	2	3	4	5	cement	cement	sity				frag	oxide
Matandu River	73,50	65,50	3,00	4,50	0,50	11,50	0,00	0,00	3,50	0,75	0,00	0,00	1,00	5,00	0,00	0,00	0,00	0,00	0,00	0,00	3,00	0,50	11,50	0,00
TDP 1/20/1 8,3	26,20	23,75	2,50	0,00	0,00	2,00	0,00	0,00	0,00	1,75	0,00	0,00	0,00	0,00	0.25	0,00	53,70	2,00	11,70	3,50	0,50	0,20	0,00	0,00
TDP 1/18/1 14,50	47,50	42,25	2,75	2,00	0,50	8,20	0,00	0,25	3,00	3,00	1,25	0,00	0,00	0,25	0,50	0,00	9,70	6,00	26,00	0,20	0,20	1,20	0,00	0,00
TDP 2/14/2 64,45	24,70	21,00	3,00	0,50	0,25	4,00	0,00	0,00	0,25	2,25	0,50	0,00	0,00	0,75	0,25	0,00	0,00	63,70	5,00	1,20	0,50	0,70	0,00	0,00
TDP 7B/12/2	23,50	20,75	1,50	1,25	0,00	7,20	0,00	0,00	0,75	3,50	1,50	0,00	0,00	0,75	0,50	0,25	3,20	59,20	2,70	3,50	0,00	0,00	0,50	0,00
TDP 9/13/1	17.75	15,00	2,00	0,75	0,00	2,50	0,00	0,00	0,50	1,25	0,50	0,00	0,00	0,00	0,25	0,00	75,00	1,75	1,25	1,50	0,25	0,00	0,00	0,00
21-7-2012	48,70	45,50	1,25	0,25	0,50	5,70	0,00	0,00	0,50	3,00	1,00	0,00	0,00	0,75	0,25	0,25	0,00	40,70	3,70	0,70	0,50	0,50	0,00	0,50
TDP 21/21/1 19-21	22,25	19,25	1,75	0,50	0,50	0,50	0,00	0,00	0,00	0,50	0,00	0,00	0,00	0,00	0,00	0,00	65,75	0,75	7,75	3,25	0,00	0,00	0,00	0,00
TDP 21/17/2 82-84	61,20	55,50	5,25	2,50	0,25	1,20	0,00	0,00	0,75	0,50	0,00	0,00	0,00	0,00	0,00	0,00	0.5	11,00	25,70	0,00	0,00	0,00	0,00	0,00
TDP 21/22/2 19-21	28,70	26,25	1,75	0,75	0,00	1,20	0,00	0,00	0,00	1,25	0,00	0,00	0,00	0,00	0,00	0,00	0,00	61,70	8,20	0,00	0,00	0,00	0,00	0,00
TDP 24/28/1 57-59	66,50	52,00	9,75	3,50	1,25	0,20	0,00	0,00	0,25	0,00	0,00	0,00	0,00	0,00	0,00	0,00	0,00	32,70	0,50	0,00	0,00	0,00	0,00	0,00
TDP 24/16/3 13-16	37,70	32,25	2,75	2,50	0,25	5,00	0,00	0,00	0,75	3,25	1,00	0,00	0,25	0,25	0,00	0,00	0,70	48,20	8,00	0,20	0,00	0,00	0,00	0,00
MB-1-7-13	49,50	45,25	2,50	1,50	0,25	14,70	0,00	1,25	6,00	0,75	2,25	0,00	0,00	0,00	0,00	0,00	1,00	0,00	14,70	0,00	1,50	0,50	0,00	0,00
MB-1-4-13	46,20	39,25	3,25	3,25	0,50	8,20	0,00	0,00	4,25	0,00	3,50	0,00	0,00	0,00	0,00	0,00	7,40	0,00	19,20	0,00	0,20	0,20	0,00	4,20
NG 1/5/13	49,00	44,25	2,50	1,25	1,00	8,50	0,00	0,00	1,25	4,00	2,25	0,00	0,00	0,00	0,25	0,25	20,50	0,00	21,20	0,00	0,20	0,00	0,50	0,00
NG-1-2-13	53,20	49,50	2,00	1,50	0,25	5,20	0,00	0,00	0,00	1,00	0,00	0,00	0,00	2,25	2,00	0,00	2,70	0,00	26,70	0,00	0,00	0,00	0,00	0,50
MN 2/1/13	43,50	40,25	1,75	1,00	0,50	0,75	0,00	0,00	0,00	0,50	0,25	0,00	0,00	0,00	0,00	0,00	24,50	0,00	7,50	0,20	0,50	0,50	0,50	22,00
MN-1-3-13	48,70	40,25	5,75	2,25	1,50	5,20	0,00	0,00	1,75	2,25	1,50	0,00	0,00	0,00	0,00	0,00	21,50	0,00	13,50	0,00	0,00	0,20	0,20	0,00
MN-1-6-13	54,50	45,50	1,75	5,50	1,75	9,00	0,00	0,00	3,50	3,75	0,50	0,00	0,00	0,00	0,00	0,00	20,70	0,00	8,70	1,50	1,00	0,20	0,20	0,00
MP-2-1-13	42,70	32,50	5,00	2,25	3,00	21,50	0,00	0,00	0,75	10,50	6,50	0,00	0,00	0,50	2,25	0,75	4,70	29,50	0,20	0,00	0,00	0,00	0,50	0,00
MP-2-0-13	28,20	24,25	2,25	0,75	1,00	12,00	0,00	0,00	0,25	3,30	6,25	0,00	0,00	0,25	1,00	0,75	57,20	0,00	2,20	0,00	0,00	0,20	0,00	0,00
2/1/14	66,20	51,75	9,00	4,00	1,50	11,00	0,00	0,25	5,50	4,00	0,75	0,00	0,00	0,50	0,00	0,00	1,20	1,00	19,70	0,00	0,00	0,20	0,50	0,00
2/2/14	73,50	60,75	9,00	2,25	1,50	7,20	0,00	0,00	1,50	4,25	0,50	0,00	0,00	0,50	0,50	0,00	0,50	0,00	18,00	0,00	0,00	0,50	0,20	0,00

Appendix C- Classification

Late Triassic to Late Jurassic

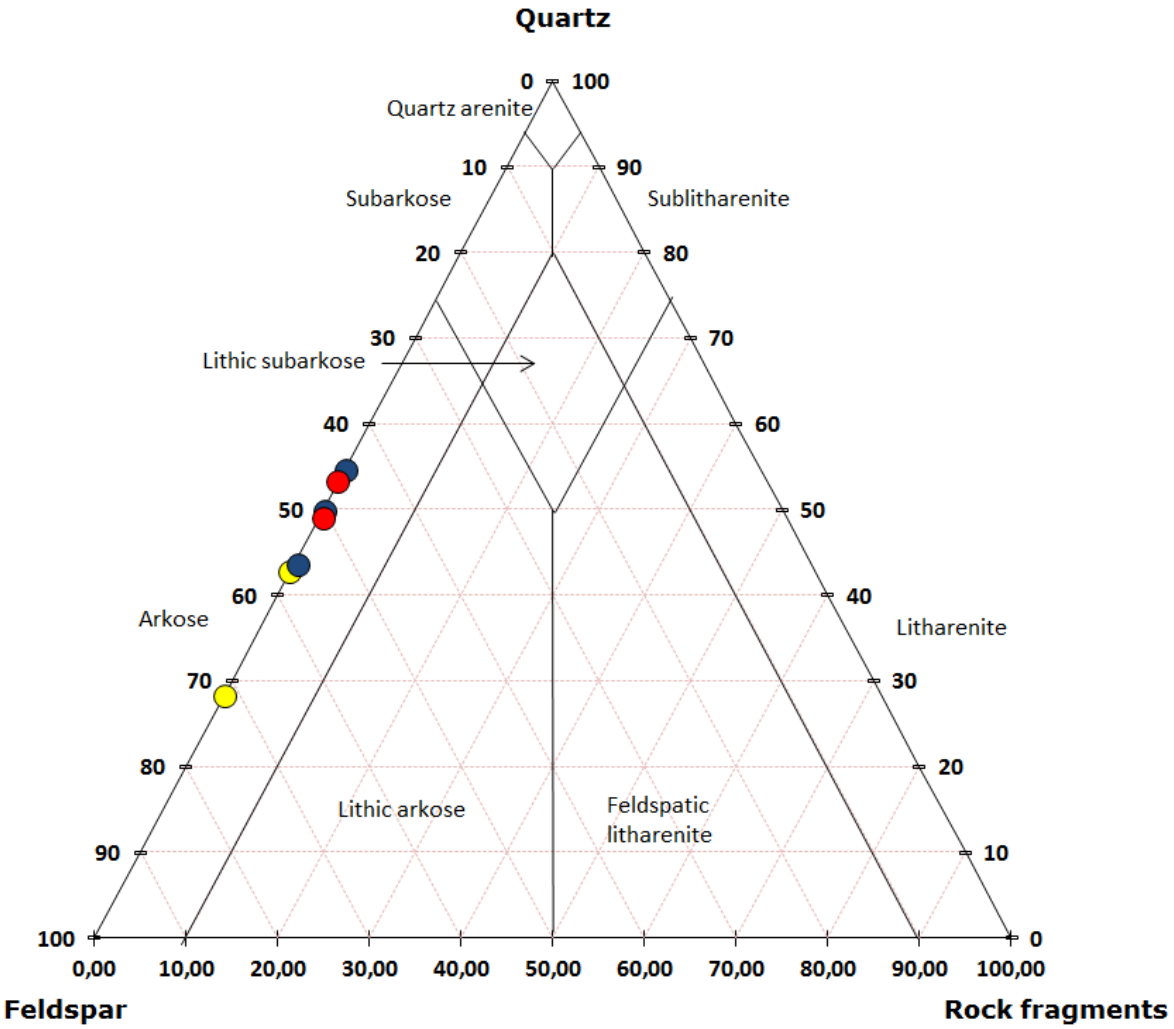

Stratigraphical Unit	Samples	Clay Matrix (%)	Classification
Karoo	MP-2-0-13	57,20	Feldspatic wacke
	MP-2-1-13	4,70	Arkose
Upper Kipatimu Mb.	MN- 1-3-13	0,00	Arkose
	MN-1-6-13	20,70	Feldspatic wacke
	MN-2-1-13	24,50	Feldspatic wacke
Upper Mitole Mb.	NG-1-2-13	5,20	Arkose
	NG-1-5-13	20,50	Feldspatic wacke

Mid Cretaceous

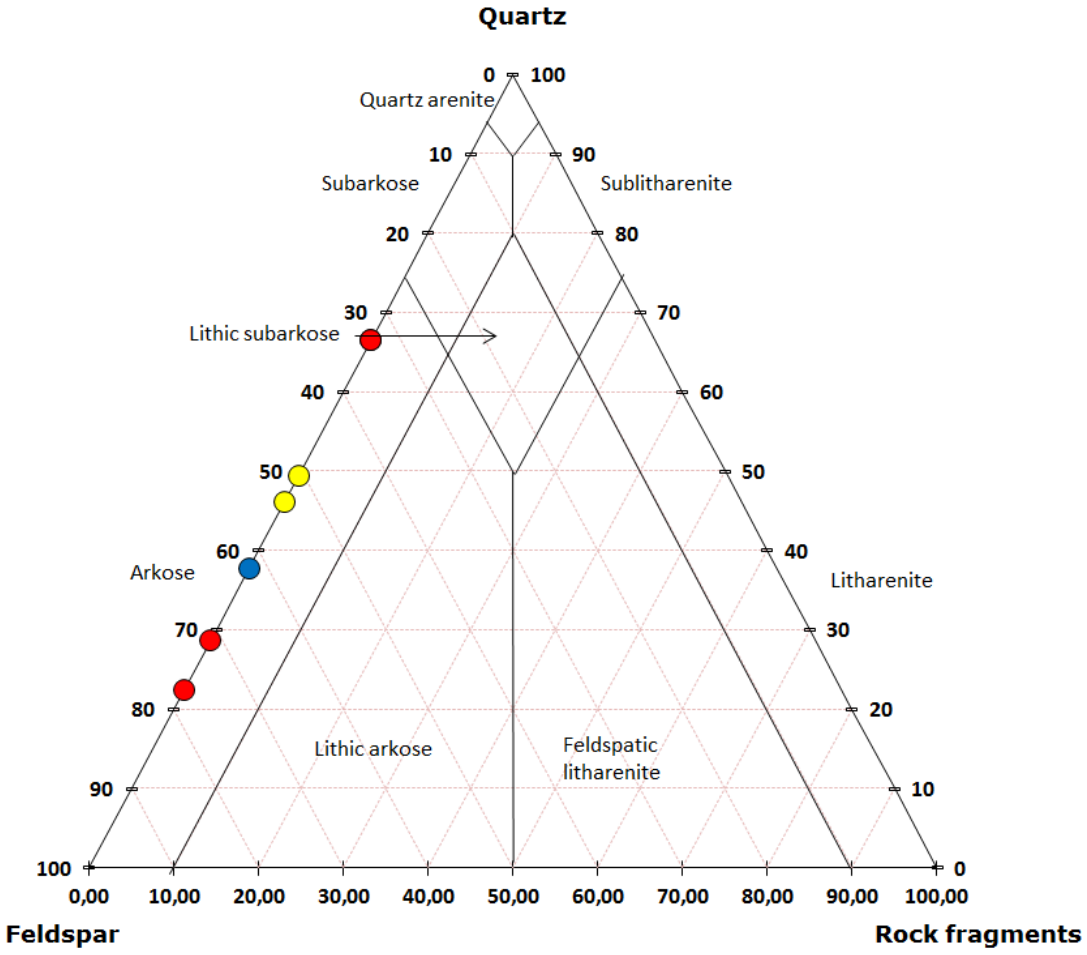

Stratigraphical Unit	Samples	Clay Matrix (%)	Classification
Makonde Fm	MB-1-4-13	5,20	Arkose
	MB-1-7-13	0,00	Arkose
Kihuluhulu Fm.	TDP 24/28/1_ 57-59	0,00	Arkose
	TDP 24/16/3_13-16	0,70	Arkose
	TDP 21/22/2_19-21	0,00	Arkose
	TDP 21/21/1_19-20	65,70	Feldspatic wacke
	TDP 21/17/2_56-58	15,00	Feldspatic wacke

Mid Cretaceous to Recent

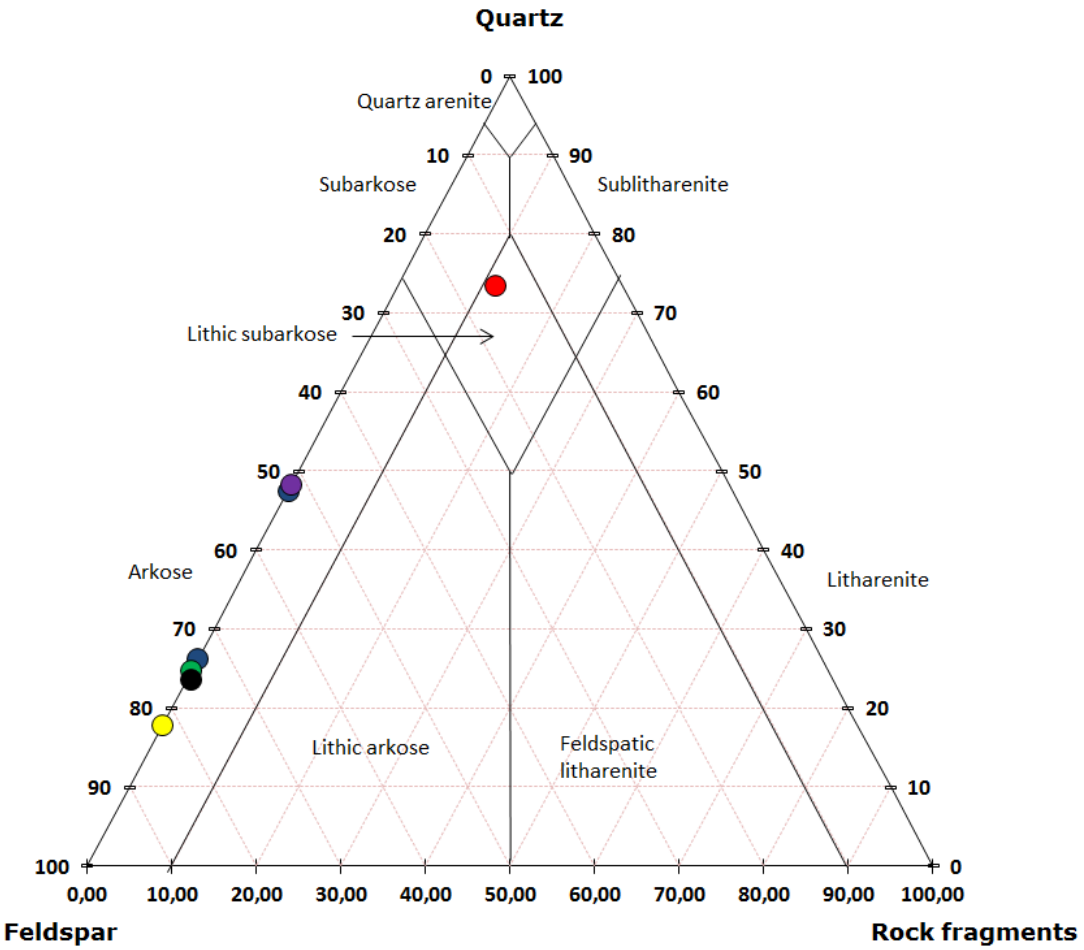

Stratigraphical Unit	Samples	Clay Matrix (%)	Classification
Nangurukuru Fm.	21-7-2012	0,00	Arkose
	TDP 9/13/1_	75,00	Feldspatic Wacke/Mudstone
Kivinje Fm.	TDP 7B/12/2	3,20	Arkose
Masoko Fm	TDP 2/14/2	0,00	Arkose
Pande Fm.	TDP 1/18/1	9,70	Arkose
	TDP 1/20/1	53,70	Feldspatic Wacke
Recent sediment	Matandu River	0,00	Lithic subarkose

Offshore samples

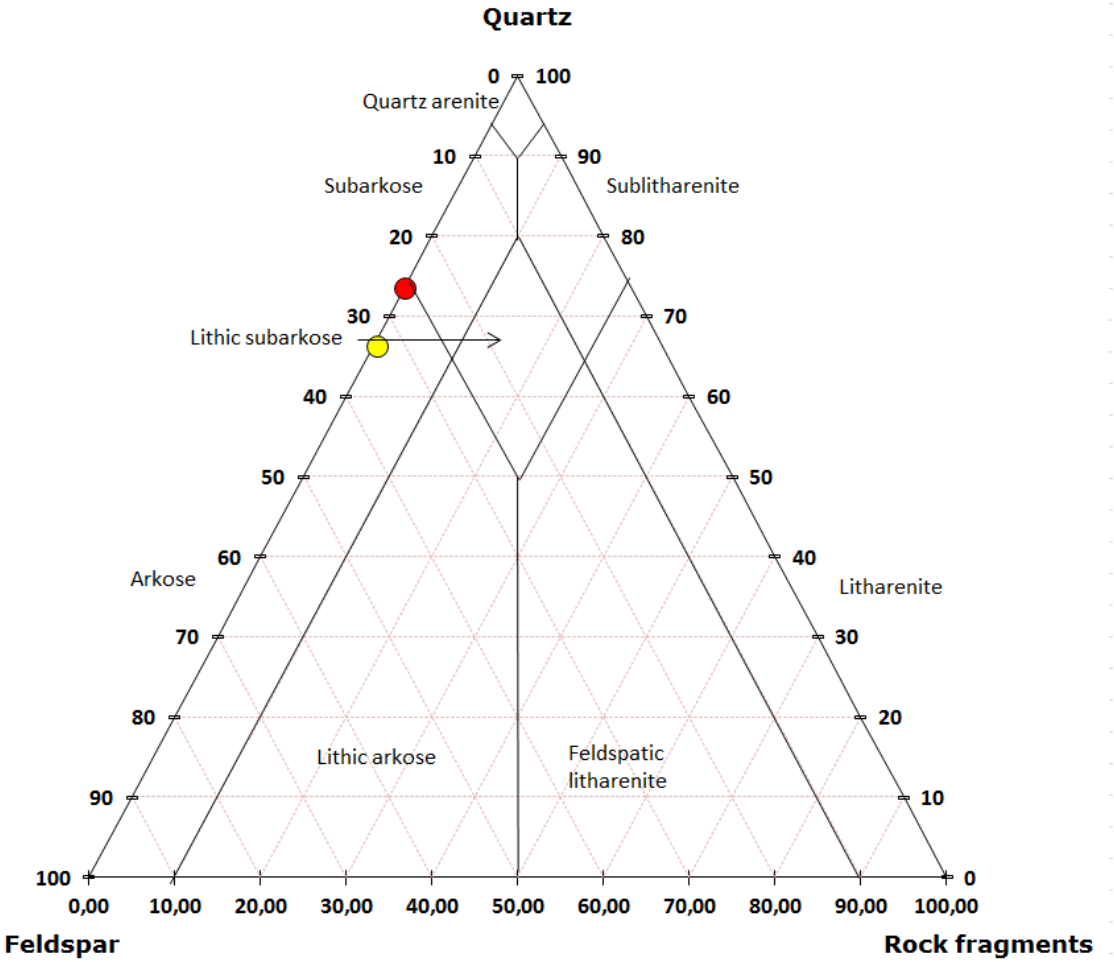

Age	Samples	Clay Matrix (%)	Classification
Paleocene	2/1/14	1,20	Arkose
Cenomanian	2/2/14	0,50	Arkose

X

Appendix D- Conventional heavy mineral analysis

Sample	Andalusite	Anatase	Apatite	Calcic amphibole	Chlor-itoid	Clino pyroxene	Epidote	Gahnite	Garnet	Kyanite	Monazite	Ortho-pyroxene	Rutile	Titanite	Staurolite	Tourmaline	Xenotime	Zircon
BA-2-13	0,00	0,00	10,50	88,50	0,00	0,50	0,00	0,00	0,00	0,00	0,00	0,00	0,00	0,00	0,00	0,00	0,00	0,50
BA-1-13	0,00	0,00	12,50	0,00	0,00	0,00	0,50	0,00	1,00	0,00	1,00	0,00	1,50	0,00	0,00	0,00	0,00	83,50
MP-2-0-13	0,00	0,00	29,00	0,00	0,00	0,00	2,00	0,00	27,00	0,00	0,00	0,00	1,50	33,00	0,00	0,00	0,00	7,50
MP-2-1-13	0,00	0,00	8,50	0,00	0,00	0,00	0,00	0,00	67,00	0,00	0,50	0,00	3,00	12,00	0,00	0,00	0,00	85,00
MN-2-1-13	0,00	2,50	0,00	0,00	0,00	0,00	0,00	0,00	0,00	0,00	0,00	0,00	7,50	0,00	0,00	0,50	0,00	35,00
MN-1-6-13	0,00	0,50	0,00	0,00	0,00	0,00	0,00	0,00	0,00	0,00	0,50	0,00	11,00	0,00	2,50	52,00	0,00	73,00
MN-1-3-13	0,00	0,50	0,00	0,00	0,00	0,00	0,00	0,00	0,00	0,00	3,00	0,00	6,00	0,00	0,00	14,50	0,50	56,00
NG-1-5-13	0,00	2,50	0,00	0,00	0,00	0,00	0,00	0,00	2,00	0,00	7,00	0,00	3,00	0,00	0,50	33,50	0,00	73,00
NG-1-2-13	0,00	0,50	0,00	0,00	0,00	0,00	0,00	0,50	0,00	0,00	3,50	0,00	8,50	0,00	3,00	9,00	0,00	61,00
MB-1-7-13	0,00	0,00	0,00	0,00	0,00	0,00	0,00	0,50	1,50	0,00	13,00	0,00	4,00	0,00	1,50	24,50	0,00	76,00
MB-1-4-13	0,00	2,00	0,00	0,00	0,00	0,00	0,00	0,50	3,50	0,00	3,00	0,00	5,50	0,00	2,00	3,00	0,00	69,00
TDP 24/28/1	0,00	0,00	6,90	0,00	0,00	0,00	0,00	0,00	63,90	0,00	0,00	0,00	1,70	0,00	2,00	14,00	0,50	10,30
TDP 24/16/3	0,00	0,50	23,50	0,00	0,50	0,00	0,00	0,00	48,50	0,00	0,50	0,00	1,50	13,00	10,30	6,90	0,00	7,00
TDP 21/21/1	0,00	0,50	10,50	0,00	0,00	0,00	0,00	0,00	44,00	0,00	0,00	0,00	3,00	13,50	0,50	4,50	0,00	77,50
TDP 21/22/2	0,00	0,00	9,50	0,00	0,00	0,00	0,00	0,00	44,50	0,00	0,00	0,00	2,00	0,00	5,00	12,00	0,00	6,50
TDP 21/17/2	0,00	0,00	13,50	0,00	0,00	2,00	0,00	0,00	38,00	12,00	1,50	0,00	1,00	0,00	5,50	32,00	0,00	23,50
21-7-2012	0,00	0,00	8,50	0,00	0,00	0,00	0,00	0,00	68,50	0,00	0,00	0,00	5,00	0,00	1,00	4,00	0,00	13,00
TDP 9/13/1	0,00	1,00	15,00	0,00	0,00	0,00	0,00	0,00	50,00	0,50	0,00	0,00	3,00	22,50	3,00	1,00	0,00	4,00
TDP 7B/12/2	0,00	0,00	7,00	0,00	0,00	0,00	1,00	0,00	37,50	4,50	0,50	0,00	4,00	29,50	2,00	0,50	0,00	13,50
TDP 2/14/2	0,00	0,00	7,00	0,00	0,00	0,00	45,00	0,00	13,00	1,00	0,00	0,00	1,50	23,50	1,00	5,00	0,00	3,00
TDP 1/20/1	0,50	0,00	9,00	0,00	0,00	0,00	44,00	0,00	27,00	0,50	0,00	0,00	0,00	17,00	0,50	1,00	0,00	0,50
TDP 1/18/1	0,00	0,00	7,00	0,00	0,00	0,00	56,50	0,00	8,50	0,00	0,50	0,00	1,50	15,00	0,00	4,00	0,00	7,00
Matadu River	0,00	0,00	4,00	70,50	0,00	4,00	2,00	0,00	5,00	0,00	0,00	2,50	0,50	0,00	0,00	0,00	0,00	11,00
2/2/14	0,00	0,00	18,00	0,00	0,00	0,00	0,00	0,00	56,00	0,00	0,00	0,00	1,50	0,00	0,50	7,00	0,00	17,00
2/1/14	0,00	0,00	0,50	0,00	0,00	0,00	2,00	0,00	41,50	7,00	1,50	0,00	8,00	12,50	0,00	0,50	0,00	26,50

Appendix E 1- Electron Microprobe Analysis (EMP) of garnet

Wt % from EMP analysis- SAMPLE BA-3-14										
	1	**2**	**3**	**4**	**5**	**6**	**7**	**8**	**9**	**10**
SiO2	37,1113	37,3270	37,2831	37,0657	37,6042	37,2615	37,2524	37,9134	36,7300	37,4883
Al2O3	20,5369	20,3707	20,4782	20,1556	20,3934	20,1949	20,5874	20,5193	20,4623	20,3478
CaO	6,8844	6,5990	6,2619	7,1991	6,9321	7,3151	6,8540	6,3857	6,3463	6,4350
FeO	21,4886	22,3701	22,6493	21,3900	22,3006	21,9501	21,8046	23,5809	23,4953	23,8281
MnO	11,3353	10,4847	10,1951	10,6255	10,4236	10,3747	10,1544	8,2559	8,3084	7,5079
Cr2O3	0,0478	-0,0015	-0,0208	0,0000	0,0045	0,0283	0,0251	0,0016	-0,0203	0,0329
MgO	2,8413	3,0140	3,2201	2,6881	2,7646	2,8254	2,9201	3,7934	3,6884	4,0683
Na2O	0,0227	0,0132	0,0411	0,0242	0,0257	0,0131	0,0169	0,0169	0,0231	0,0084
K2O	-0,0084	-0,0084	-0,0040	0,0114	-0,0059	0,0000	-0,0174	-0,0182	0,0166	0,0108
TiO2	0,0230	0,0400	0,0219	0,0386	0,0141	0,0391	0,0180	0,0188	-0,0008	0,0337
Total	100,2829	100,2087	100,1257	99,1981	100,4567	100,0021	99,6156	100,4675	99,0492	99,7612
Structure formula based on 24 O										
Si	5,9447	5,9767	5,9690	5,9917	6,0030	5,9806	5,9803	6,0119	5,9308	5,9859
Al	3,8776	3,8445	3,8644	3,8404	3,8373	3,8206	3,8956	3,8352	3,8945	3,8296
Ca	1,1816	1,1322	1,0742	1,2470	1,1857	1,2580	1,1790	1,0850	1,0980	1,1010
Fe	2,8788	2,9956	3,0326	2,8918	2,9773	2,9464	2,9274	3,1272	3,1729	3,1820
Mn	1,5380	1,4220	1,3826	1,4549	1,4095	1,4105	1,3808	1,1089	1,1364	1,0155
Cr	0,0091	-0,0003	-0,0039	0,0000	0,0009	0,0054	0,0048	0,0003	-0,0039	0,0062
Mg	0,6786	0,7196	0,7687	0,6479	0,6581	0,6762	0,6990	0,8969	0,8880	0,9686
Na	0,0035	0,0020	0,0064	0,0038	0,0040	0,0020	0,0026	0,0026	0,0036	0,0013
K	-0,0009	-0,0009	-0,0004	0,0012	-0,0006	0,0000	-0,0018	-0,0018	0,0017	0,0011
Ti	0,0055	0,0096	0,0053	0,0094	0,0034	0,0094	0,0043	0,0045	-0,0002	0,0081
Total	16,1166	16,1011	16,0988	16,0881	16,0784	16,1091	16,0720	16,0705	16,1219	16,0993
Mol % end members										
Pyrope	10,7862	11,4606	12,2806	10,3651	10,5545	10,7228	11,2823	14,4132	14,1155	15,4202
Almandine	45,7550	47,7103	48,4488	46,2613	47,7528	46,7244	47,2526	50,2541	50,4332	50,6577
Spessartine	24,4455	22,6483	22,0880	23,2751	22,6066	22,3675	22,2878	17,8201	18,0630	16,1663
Grossular	18,7809	18,0319	17,1614	19,9482	19,0181	19,9501	19,0301	17,4357	17,4532	17,5277
Uvarite	0,1443	-0,0045	-0,0631	0,0000	0,0137	0,0854	0,0771	0,0048	-0,0618	0,0992
Andradite	0,0881	0,1535	0,0843	0,1502	0,0543	0,1497	0,0702	0,0721	-0,0031	0,1289
Alm+Spe	70,2005	70,3586	70,5368	69,5365	70,3595	69,0919	69,5404	68,0742	68,4962	66,8240

Wt % from EMP analysis- SAMPLE BA-3-14 cont.									
	11	**12**	**13**	**14**	**15**	**16**	**17**	**18**	**19**
SiO2	37,2586	37,6189	37,3503	37,2121	37,4279	37,4538	37,5645	37,6320	37,5052
Al2O3	20,4705	20,2933	20,6645	20,1888	20,1010	20,0947	20,4611	20,2434	20,3519
CaO	6,6705	6,6741	6,6566	6,9234	7,3979	7,0217	6,4120	6,1918	6,8591
FeO	23,0607	23,4920	23,7454	21,7482	21,3602	21,5587	22,4148	22,6979	21,9896
MnO	9,2116	8,2152	8,3741	10,6775	10,7126	10,9534	10,2932	10,1463	10,6213
Cr2O3	0,0313	0,0314	0,0125	-0,0283	0,0189	0,0267	0,0094	-0,0172	-0,0157
MgO	3,3486	3,7844	3,6233	2,7284	2,6258	2,8117	3,1524	3,1887	2,9851
Na2O	0,0277	0,0108	-0,0131	0,0100	0,0062	0,0085	0,0208	0,0201	0,0308
K2O	-0,0012	0,0081	-0,0027	-0,0081	-0,0015	-0,0104	-0,0100	0,0008	0,0050
TiO2	0,0234	0,0117	0,0188	0,0133	0,0008	0,0289	0,0226	0,0464	0,0578
Total	100,1019	100,1398	100,4296	99,4652	99,6496	99,9477	100,3408	100,1502	100,3901
Structure formula based on 24 O									
Si	5,9599	5,9955	5,9462	6,0850	6,1050	6,0945	6,0851	6,1053	6,0777
Al	3,8596	3,8122	3,8777	3,3013	3,2788	3,2698	3,3145	3,2842	3,2980
Ca	1,1433	1,1397	1,1355	1,1321	1,2067	1,1426	1,0387	1,0045	1,1115
Fe	3,0850	3,1312	3,1616	3,5563	3,4842	3,5080	3,6310	3,6825	3,5634
Mn	1,2481	1,1091	1,1293	1,7460	1,7474	1,7823	1,6674	1,6461	1,7212
Cr	0,0059	0,0059	0,0024	-0,0069	0,0046	0,0065	0,0023	-0,0042	-0,0038
Mg	0,7987	0,8993	0,8601	0,4462	0,4283	0,4575	0,5107	0,5173	0,4837
Na	0,0043	0,0017	-0,0020	0,0008	0,0005	0,0007	0,0017	0,0016	0,0025
K	-0,0001	0,0008	-0,0003	-0,0007	-0,0001	-0,0008	-0,0008	0,0001	0,0004
Ti	0,0056	0,0028	0,0045	0,0043	0,0003	0,0094	0,0073	0,0151	0,0187
Total	16,1103	16,0984	16,1149	16,2644	16,2556	16,2706	16,2577	16,2526	16,2733
Mol % end members									
Pyrope	12,7042	14,3020	13,6669	6,4867	6,2331	6,6246	7,4469	7,5398	7,0160
Almandine	49,0722	49,7963	50,2369	51,7055	50,7050	50,7941	52,9504	53,6699	51,6829
Spessartine	19,8534	17,6373	17,9439	25,3854	25,4296	25,8071	24,3156	23,9912	24,9636
Grossular	18,1861	18,1254	18,0432	16,4601	17,5612	16,5437	15,1470	14,6407	16,1212
Uvarite	0,0945	0,0944	0,0375	-0,1009	0,0673	0,0944	0,0333	-0,0610	-0,0554
Andradite	0,0896	0,0446	0,0716	0,0632	0,0038	0,1362	0,1068	0,2194	0,2717
Alm+Spe	68,9256	67,4336	68,1808	77,0909	76,1346	76,6012	77,2660	77,6611	76,6465

Wt % from EMP analysis- SAMPLE MP-2-0-13													
	1	**2**	**3**	**4**	**5**	**6**	**7**	**8**	**9**	**10**	**11**	**12**	**13**
SiO2	37,5623	37,4504	37,9002	37,4568	37,8433	38,2675	38,0928	38,2699	38,5126	36,9775	37,6460	37,9236	40,1616
Al2O3	20,9806	20,9024	21,2828	20,6936	21,4554	21,3078	21,1813	21,5788	21,4970	20,5082	20,9020	21,6753	21,6942
CaO	7,0065	5,3624	3,6675	8,0000	2,7024	11,3989	1,8469	7,6826	7,1153	1,7062	14,2901	1,4959	1,1694
FeO	30,4234	27,4718	30,2005	29,8287	31,0390	25,4573	31,0126	25,5892	23,4258	26,2941	22,2326	31,8716	28,5604
MnO	1,4991	4,9497	1,2744	1,2387	1,1971	1,3749	1,0343	0,6626	4,7783	11,8987	4,4738	0,5357	0,3967
Cr2O3	0,0015	0,0277	0,0474	-0,0385	0,0518	0,0660	0,0426	-0,0344	0,0094	0,0121	0,0237	-0,0152	0,1091
MgO	2,5987	3,2133	5,7561	2,7363	5,9173	2,9588	6,4269	6,0607	5,5644	2,8867	0,9322	6,4001	8,5638
Na2O	0,0273	0,0156	-0,0015	0,0039	0,0054	0,0425	0,0316	0,0142	-0,0113	0,0629	0,0000	0,0247	0,0593
K2O	-0,0004	0,0070	-0,0098	0,0004	0,0161	0,0183	0,0075	-0,0035	-0,0066	0,0124	-0,0027	-0,0138	0,0040
TiO2	0,0532	0,0141	-0,0008	0,0968	0,0082	0,0060	0,0208	0,0427	0,0040	0,0073	0,0617	-0,0016	0,0091
Total	100,1523	99,4145	100,1168	100,0167	100,2358	100,8980	99,6973	99,8627	100,8888	100,3660	100,5594	99,8965	100,7275
				Structure formula based on 24 O									
Si	5,9931	6,0066	5,9714	5,9830	5,9595	5,9859	6,0096	5,9658	5,9789	5,9757	5,9656	5,9715	6,1344
Al	3,9456	3,9516	3,9525	3,8961	3,9825	3,9287	3,9388	3,9650	3,9337	3,9065	3,9041	4,0229	3,9058
Ca	1,1978	0,9216	0,6192	1,3692	0,4560	1,9106	0,3122	1,2832	1,1836	0,2954	2,4264	0,2524	0,1914
Fe	4,0596	3,6850	3,9795	3,9847	4,0879	3,3304	4,0918	3,3361	3,0415	3,5538	2,9465	4,1971	3,6484
Mn	0,2026	0,6725	0,1701	0,1676	0,1597	0,1822	0,1382	0,0875	0,6283	1,6288	0,6005	0,0715	0,0513
Cr	0,0003	0,0053	0,0089	-0,0073	0,0097	0,0122	0,0080	-0,0064	0,0017	0,0023	0,0045	-0,0028	0,0198
Mg	0,6182	0,7685	1,3523	0,6517	1,3894	0,6901	1,5118	1,4087	1,2880	0,6956	0,2203	1,5026	1,9504
Na	0,0042	0,0024	-0,0002	0,0006	0,0008	0,0064	0,0048	0,0021	-0,0017	0,0099	0,0000	0,0038	0,0088
K	0,0000	0,0007	-0,0010	0,0000	0,0016	0,0018	0,0008	-0,0003	-0,0007	0,0013	-0,0003	-0,0014	0,0004
Ti	0,0128	0,0034	-0,0002	0,0233	0,0019	0,0014	0,0049	0,0100	0,0009	0,0018	0,0147	-0,0004	0,0021
Total	16,0341	16,0176	16,0523	16,0690	16,0492	16,0497	16,0210	16,0518	16,0543	16,0710	16,0823	16,0171	15,9127
				Mol % end members									
Pyrope	10,1494	12,6890	22,0611	10,5297	22,7603	11,2636	24,9189	23,0214	20,9638	11,2597	3,5453	24,9593	33,2643
Almandine	66,6456	60,8471	64,9218	64,3818	66,9639	54,3568	67,4442	54,5184	49,5022	57,5258	47,4256	69,7151	62,2235
Spessartine	3,3261	11,1037	2,7747	2,7079	2,6158	2,9734	2,2782	1,4298	10,2268	26,3657	9,6657	1,1868	0,8754
Grossular	19,6645	15,2171	10,1010	22,1227	7,4697	31,1834	5,1460	20,9707	19,2638	4,7825	39,0550	4,1922	3,2642
Uvarite	0,0047	0,0870	0,1445	-0,1178	0,1585	0,1998	0,1314	-0,1039	0,0282	0,0375	0,0717	-0,0471	0,3371
Andradite	0,2096	0,0562	-0,0031	0,3759	0,0318	0,0230	0,0814	0,1637	0,0152	0,0287	0,2368	-0,0063	0,0357
Alm+Spe	69,9717	71,9508	67,6965	67,0897	69,5797	57,3301	69,7223	55,9482	59,7290	83,8915	57,0913	70,9020	63,0988

Wt % from EMP analysis- SAMPLE MP-2-0-13 cont.														
	14	**15**	**16**	**17**	**18**	**19**	**20**	**21**	**22**	**23**	**24**	**25**	**26**	**27**
SiO2	37,7704	37,3160	39,0014	37,9207	39,1280	37,9288	39,3823	37,7890	37,1577	37,8401	36,4746	38,2976	39,2354	37,2708
Al2O3	21,4140	21,1321	21,9484	21,3971	22,0323	20,8590	21,9595	20,8022	21,0163	20,8650	20,7375	21,2281	22,1551	20,5110
CaO	3,2617	1,0081	1,1630	6,7819	7,0874	8,0121	3,4162	4,3790	8,6805	6,2829	2,8217	6,7817	1,0778	6,4831
FeO	29,7787	35,3593	26,2188	27,2789	22,6987	26,9244	25,0140	29,9263	28,1872	28,5213	30,4216	26,6240	26,3124	17,8674
MnO	2,6777	0,7283	1,5433	1,9029	0,4387	2,7041	0,3939	1,3556	3,5024	1,7679	8,9596	0,9269	0,4328	16,1746
Cr2O3	0,0916	0,0254	-0,0155	0,0186	0,0886	0,0295	0,0562	-0,0061	-0,0108	0,0000	-0,0181	0,0420	0,0604	-0,0187
MgO	5,1219	4,3198	10,2731	4,5366	8,5025	3,7601	9,8640	5,4139	1,0967	4,9050	1,1077	5,9142	11,0499	1,9618
Na2O	-0,0054	0,0095	0,0074	0,0206	0,0087	0,0484	0,0242	0,0201	0,0571	0,0161	0,0291	0,0347	0,0199	0,0604
K2O	0,0145	0,0023	-0,0048	0,0000	0,0099	0,0066	0,0103	0,0168	0,0112	-0,0008	0,0101	0,0027	-0,0107	0,0062
TiO2	0,0415	0,0299	0,0391	0,0745	0,0462	0,0547	0,0893	0,0815	0,0213	0,0419	0,0127	0,0438	0,0206	0,0136
Total	100,1666	99,9308	100,1743	99,9320	100,0410	100,3277	100,2099	99,7781	99,7196	100,2395	100,5566	99,8958	100,3535	100,3301
Structure formula based on 24 O														
Si	5,9684	5,9789	5,9752	5,9763	5,9803	5,9925	6,0033	5,9886	5,9839	5,9730	5,9408	5,9912	5,9689	5,9880
Al	3,9885	3,9909	3,9635	3,9748	3,9692	3,8845	3,9456	3,8857	3,9892	3,8820	3,9812	3,9143	3,9727	3,8842
Ca	0,5523	0,1731	0,1909	1,1453	1,1607	1,3564	0,5580	0,7436	1,4979	1,0627	0,4924	1,1368	0,1757	1,1161
Fe	3,9354	4,7381	3,3594	3,5955	2,9014	3,5576	3,1889	3,9663	3,7963	3,7652	4,1439	3,4833	3,3477	2,4008
Mn	0,3584	0,0988	0,2003	0,2540	0,0568	0,3619	0,0509	0,1820	0,4778	0,2364	1,2361	0,1228	0,0558	2,2012
Cr	0,0172	0,0048	-0,0028	0,0035	0,0161	0,0055	0,0102	-0,0011	-0,0021	0,0000	-0,0035	0,0078	0,0109	-0,0036
Mg	1,2068	1,0320	2,3468	1,0661	1,9377	0,8858	2,2420	1,2793	0,2633	1,1544	0,2690	1,3795	2,5065	0,4700
Na	-0,0008	0,0015	0,0011	0,0031	0,0013	0,0074	0,0036	0,0031	0,0089	0,0025	0,0046	0,0053	0,0029	0,0094
K	0,0015	0,0002	-0,0005	0,0000	0,0010	0,0007	0,0010	0,0017	0,0012	-0,0001	0,0010	0,0003	-0,0010	0,0006
Ti	0,0099	0,0072	0,0090	0,0177	0,0106	0,0130	0,0205	0,0194	0,0052	0,0100	0,0031	0,0103	0,0047	0,0033
Total	16,0374	16,0256	16,0430	16,0363	16,0351	16,0653	16,0239	16,0685	16,0215	16,0860	16,0686	16,0516	16,0448	16,0699

Wt % from EMP analysis- SAMPLE TDP 24/28/1													
	1	**2**	**3**	**4**	**5**	**6**	**7**	**8**	**9**	**10**	**11**	**12**	**13**
SiO2	38,9547	38,3820	38,2089	38,6841	38,2928	37,9851	37,7567	38,0679	37,4184	39,1460	37,5430	38,6433	39,3198
Al2O3	21,3168	20,6502	21,1378	21,2080	21,3882	20,4438	21,3038	21,5849	21,0884	21,7185	20,7522	21,7859	22,1074
CaO	8,7870	8,9659	8,0106	7,3658	6,9300	9,5622	7,1767	2,0634	7,2744	6,6343	7,2275	9,3473	1,9294
FeO	24,3200	24,5812	26,6971	25,6671	27,8807	25,6857	22,7293	29,8999	30,7197	24,5185	29,3710	23,9814	28,5122
MnO	0,5514	2,2450	1,2813	1,2234	2,2276	3,3722	8,8279	2,4339	2,5973	0,6005	0,6194	1,4432	0,2645
Cr2O3	0,0408	0,0328	-0,0206	0,0281	0,0497	0,0109	0,0093	0,0410	-0,0031	0,1282	0,0062	-0,0358	-0,0262
MgO	6,7159	4,9848	4,8729	6,2651	3,8863	3,1635	2,6318	6,1767	1,1464	7,2715	3,9908	5,6956	8,6460
Na2O	0,0148	0,0203	0,0079	0,0090	0,0218	0,0214	0,0177	0,0038	0,0150	0,0368	0,0000	0,0162	0,0113
K2O	0,0043	0,0012	0,0000	0,0129	0,0092	-0,0004	0,0170	0,0168	0,0213	0,0118	0,0136	0,0111	-0,0022
TiO2	0,0611	0,1264	0,0559	0,0702	0,0191	0,0539	0,0415	0,0039	0,0196	0,0084	0,0186	0,0652	0,0168
Total	100,7668	99,9896	100,2517	100,5336	100,7054	100,2984	100,5116	100,2921	100,2974	100,0745	99,5423	100,9534	100,7790
Structure formula based on 24 O													
Si	5,9934	6,0198	5,9889	5,9992	6,0091	6,0162	5,9859	5,9770	6,0041	6,0277	5,9828	5,9577	6,0199
Al	3,8658	3,8175	3,9052	3,8767	3,9561	3,8166	3,9810	3,9947	3,9885	3,9418	3,8980	3,9590	3,9895
Ca	1,4486	1,5068	1,3454	1,2240	1,1652	1,6228	1,2191	0,3471	1,2507	1,0946	1,2341	1,5441	0,3165
Fe	3,1293	3,2243	3,4996	3,3290	3,6591	3,4023	3,0137	3,9262	4,1224	3,1574	3,9144	3,0921	3,6508
Mn	0,0719	0,2983	0,1701	0,1607	0,2961	0,4524	1,1855	0,3237	0,3530	0,0783	0,0836	0,1885	0,0343
Cr	0,0074	0,0061	-0,0038	0,0052	0,0092	0,0020	0,0017	0,0076	-0,0006	0,0234	0,0012	-0,0065	-0,0048
Mg	1,5407	1,1657	1,1388	1,4487	0,9093	0,7471	0,6221	1,4460	0,2743	1,6695	0,9483	1,3093	1,9737
Na	0,0022	0,0031	0,0012	0,0014	0,0033	0,0033	0,0027	0,0006	0,0023	0,0055	0,0000	0,0024	0,0017
K	0,0004	0,0001	0,0000	0,0013	0,0009	0,0000	0,0017	0,0017	0,0022	0,0012	0,0014	0,0011	-0,0002
Ti	0,0141	0,0298	0,0132	0,0164	0,0045	0,0128	0,0099	0,0009	0,0047	0,0019	0,0045	0,0151	0,0039
Total	16,0738	16,0715	16,0585	16,0625	16,0129	16,0755	16,0236	16,0256	16,0017	16,0014	16,0682	16,0628	15,9853
Mol % end members													
Pyrope	24,8015	18,7088	18,4779	23,4272	15,0465	11,9736	10,2797	23,8951	4,5679	27,7086	15,3291	21,3152	33,0364
Almandine	50,3751	51,7462	56,7816	53,8327	60,5454	54,5288	49,7955	64,8783	68,6549	52,4037	63,2783	50,3388	61,1065
Spessartine	1,1568	4,7866	2,7601	2,5988	4,8995	7,2508	19,5883	5,3489	5,8791	1,2999	1,3516	3,0682	0,5741
Grossular	23,3191	24,1818	21,8287	19,7929	19,2810	26,0082	20,1441	5,7363	20,8291	18,1670	19,9500	25,1381	5,2978
Uvarite	0,1198	0,0979	-0,0621	0,0836	0,1531	0,0328	0,0289	0,1262	-0,0098	0,3886	0,0189	-0,1066	-0,0796
Andradite	0,2277	0,4787	0,2139	0,2649	0,0746	0,2058	0,1636	0,0152	0,0788	0,0323	0,0721	0,2462	0,0648
Alm+Spe	51,5319	56,5329	59,5417	56,4316	65,4449	61,7795	69,3838	70,2273	74,5341	53,7036	64,6298	53,4070	61,6806

Wt% from EMP analysis -SAMPLE TDP 21/17/2											
	1	**2**	**3**	**4**	**5**	**6**	**7**	**8**	**9**	**10**	**11**
SiO2	37,6576	38,1132	37,6234	36,8745	38,5171	39,4168	38,3891	39,0123	37,9054	38,5991	37,5525
Al2O3	20,8108	21,2915	20,9183	20,2367	21,5403	22,4215	21,7633	21,8982	21,0671	21,3737	21,1760
CaO	7,6089	8,0372	7,8370	6,8916	7,4412	6,1088	1,4721	0,9248	6,6655	6,7251	7,4717
FeO	27,3245	26,8062	29,4496	31,4292	24,8804	21,0881	28,3395	27,4836	30,0178	25,2093	29,5157
MnO	2,6651	1,7746	1,8217	2,7903	0,7715	0,4033	0,8369	0,5499	1,2025	1,4130	1,9106
Cr2O3	0,0176	0,0093	-0,0200	0,0091	0,0298	-0,0032	0,0261	0,0092	0,0154	-0,0375	0,0422
MgO	3,5650	3,6534	2,3530	1,2493	6,6432	10,5101	8,6332	10,2224	3,5989	6,9001	2,6147
Na2O	-0,0058	0,0107	0,0093	0,0182	-0,0007	0,0193	0,0249	0,0007	0,0186	0,0089	0,0199
K2O	0,0041	0,0039	0,0039	-0,0015	0,0012	0,0222	0,0104	0,0158	0,0171	0,0020	0,0040
TiO2	0,0131	-0,0214	0,0366	0,0187	0,0716	0,0226	-0,0048	0,0209	0,0552	0,0442	0,1011
Total	99,6608	99,6784	100,0330	99,5162	99,8955	100,0094	99,4908	100,1379	100,5637	100,2379	100,4086
Structure formula based on 24 O											
Si	5,9962	6,0241	6,0056	6,0007	5,9793	5,9597	5,9761	5,9835	5,9922	5,9846	5,9695
Al	3,9059	3,9666	3,9358	3,8817	3,9414	3,9958	3,9933	3,9588	3,9254	3,9061	3,9678
Ca	1,2982	1,3612	1,3404	1,2017	1,2378	0,9897	0,2455	0,1520	1,1290	1,1172	1,2727
Fe	3,6387	3,5434	3,9315	4,2775	3,2302	2,6666	3,6896	3,5254	3,9686	3,2688	3,9240
Mn	0,3595	0,2376	0,2463	0,3846	0,1014	0,0517	0,1104	0,0714	0,1610	0,1856	0,2573
Cr	0,0022	0,0012	-0,0025	0,0012	0,0037	-0,0004	0,0032	0,0011	0,0019	-0,0046	0,0053
Mg	0,8464	0,8610	0,5600	0,3031	1,5377	2,3694	2,0039	2,3378	0,8483	1,5952	0,6198
Na	-0,0018	0,0033	0,0029	0,0057	-0,0002	0,0057	0,0075	0,0002	0,0057	0,0027	0,0061
K	0,0008	0,0008	0,0008	-0,0003	0,0002	0,0043	0,0021	0,0031	0,0034	0,0004	0,0008
Ti	0,0016	-0,0025	0,0044	0,0023	0,0084	0,0026	-0,0006	0,0024	0,0066	0,0052	0,0121
Total	16,0477	15,9966	16,0252	16,0583	16,0398	16,0450	16,0310	16,0357	16,0422	16,0611	16,0353
Mol % end members											
Pyrope	13,7704	14,3458	9,2110	4,9128	25,1294	38,9741	33,1113	38,3867	13,8714	25,8647	10,1748
Almandine	59,1994	59,0393	64,6610	69,3226	52,7887	43,8616	60,9642	57,8868	64,8946	53,0019	64,4221
Spessartine	5,8481	3,9586	4,0511	6,2334	1,6579	0,8496	1,8234	1,1731	2,6330	3,0089	4,2236
Grossular	21,1206	22,6793	22,0461	19,4751	20,2276	16,2788	4,0573	2,4956	18,4621	18,1154	20,8939
Uvarite	0,0360	0,0194	-0,0415	0,0190	0,0598	-0,0063	0,0531	0,0183	0,0315	-0,0745	0,0871
Andradite	0,0255	-0,0424	0,0723	0,0371	0,1366	0,0423	-0,0093	0,0396	0,1073	0,0836	0,1985
Alm+Spe	65,0475	62,9979	68,7121	75,5560	54,4465	44,7112	62,7876	59,0598	67,5276	56,0108	68,6457

Wt % from EMP analysis- SAMPLE 21-7-2012										
	1	**2**	**3**	**4**	**5**	**6**	**7**	**8**	**9**	**10**
SiO2	37,7316	38,4895	38,3999	37,9105	38,1983	38,1584	38,9561	38,0244	35,9939	38,1946
Al2O3	21,4061	21,7374	21,7757	21,4403	21,8490	21,7198	22,0256	21,7238	19,9591	21,7407
CaO	7,6707	12,1170	12,3672	5,8441	1,4899	5,6347	4,4871	6,2260	5,8174	7,5372
FeO	27,0309	21,8486	21,8165	26,9746	29,1456	25,6945	24,3091	26,3355	15,7864	25,5427
MnO	1,6971	0,5440	0,5492	1,7584	2,1837	1,3122	0,6583	1,1881	20,7064	0,7425
Cr2O3	0,0104	0,0213	0,0000	-0,0297	0,0278	0,0522	0,0795	0,0074	-0,0387	0,0075
MgO	4,9058	5,0137	4,9645	5,8369	7,4457	7,0578	9,8110	6,5185	0,8024	5,9580
Na2O	0,0136	0,0153	0,0250	0,0157	-0,0029	-0,0042	-0,0007	-0,0177	0,0275	0,0092
K2O	-0,0033	0,0052	0,0018	0,0089	0,0026	-0,0033	0,0015	-0,0126	0,0054	0,0000
TiO2	0,0446	0,1030	0,0893	-0,0071	0,0018	0,0165	0,0045	0,0139	-0,0015	0,0723
Total	100,5075	99,8949	99,9891	99,7528	100,3415	99,6384	100,3320	100,0073	99,0583	99,8046
Structure formula based on 24 O										
Si	5,9195	5,9673	5,9525	5,9577	5,9536	5,9483	5,9444	5,9303	5,9400	5,9561
Al	3,9584	3,9723	3,9787	3,9715	4,0139	3,9908	3,9616	3,9935	3,8824	3,9961
Ca	1,2895	2,0129	2,0542	0,9841	0,2488	0,9412	0,7337	1,0404	1,0287	1,2594
Fe	3,5466	2,8329	2,8283	3,5453	3,7991	3,3498	3,1023	3,4351	2,1788	3,3312
Mn	0,2255	0,0714	0,0721	0,2341	0,2883	0,1733	0,0851	0,1570	2,8945	0,0981
Cr	0,0019	0,0039	0,0000	-0,0055	0,0051	0,0097	0,0144	0,0014	-0,0076	0,0014
Mg	1,1476	1,1590	1,1475	1,3677	1,7304	1,6405	2,2323	1,5159	0,1974	1,3853
Na	0,0021	0,0023	0,0038	0,0024	-0,0004	-0,0006	-0,0001	-0,0027	0,0044	0,0014
K	-0,0003	0,0005	0,0002	0,0009	0,0003	-0,0003	0,0001	-0,0013	0,0006	0,0000
Ti	0,0105	0,0240	0,0208	-0,0017	0,0004	0,0039	0,0010	0,0033	-0,0004	0,0170
Total	16,1013	16,0466	16,0581	16,0565	16,0395	16,0563	16,0748	16,0729	16,1188	16,0459
Mol % end members										
Pyrope	18,4450	18,9871	18,7407	22,3341	28,4967	26,8129	36,1869	24,6364	3,1383	22,7389
Almandine	57,0044	46,4091	46,1926	57,8921	62,5662	54,7511	50,2905	55,8277	34,6309	54,6783
Spessartine	3,6249	1,1703	1,1778	3,8222	4,7478	2,8320	1,3794	2,5509	46,0067	1,6098
Grossular	20,7254	32,9757	33,5488	16,0694	4,0977	15,3830	11,8933	16,9097	16,3504	20,6717
Uvarite	0,0311	0,0642	0,0000	-0,0904	0,0846	0,1577	0,2332	0,0222	-0,1204	0,0228
Andradite	0,1692	0,3936	0,3401	-0,0274	0,0070	0,0632	0,0167	0,0530	-0,0059	0,2784
Alm+Spe	60,6293	47,5795	47,3704	61,7143	67,3140	57,5831	51,6698	58,3786	80,6376	56,2881

				Wt % from EMP analysis- SAMPLE 21-7-2012 cont.							
	11	**12**	**13**	**14**	**15**	**16**	**17**	**18**	**19**	**20**	**21**
SiO2	37,4589	37,1068	37,5360	36,6673	37,8236	37,2335	37,6039	38,2470	38,2206	39,8109	38,1329
Al2O3	21,3055	21,2928	20,7423	20,8428	21,2587	21,4344	21,2806	21,4400	21,7676	22,5044	21,6729
CaO	5,6853	8,4610	4,5402	1,5097	8,2821	9,9574	2,8756	9,2384	10,0718	6,1214	8,0333
FeO	28,2713	29,2242	30,0717	33,3526	27,6281	26,4195	29,4894	24,7086	24,2164	19,7077	26,2827
MnO	3,3834	1,3078	1,3774	4,9738	0,7347	1,5964	1,3357	0,6529	0,6497	0,6958	1,4359
Cr2O3	0,0338	0,0281	-0,0176	0,0944	0,0372	-0,0075	0,0483	-0,0015	0,0921	-0,0199	0,0806
MgO	3,8500	2,4684	5,3817	2,3358	4,1609	2,5836	6,8748	5,5078	5,1582	11,6697	4,5028
Na2O	-0,0007	-0,0190	-0,0007	0,0259	0,0014	0,0188	0,0116	0,0014	0,0246	-0,0047	0,0100
K2O	0,0048	0,0051	-0,0007	0,0011	0,0077	0,0037	0,0167	-0,0148	0,0041	-0,0109	-0,0018
TiO2	0,0004	0,0082	0,1318	0,0134	0,0841	0,1086	0,0657	0,0552	0,0311	0,0473	0,0646
Total	99,9926	99,8833	99,7621	99,8167	100,0185	99,3482	99,6023	99,8351	100,2361	100,5218	100,2140
Structure formula based on 24 O											
Si	5,9548	5,9297	5,9610	5,9884	6,1100	6,0627	6,1011	6,1663	6,1397	6,3013	6,1305
Al	3,9922	4,0107	3,8826	3,4040	3,4341	3,4902	3,4527	3,4566	3,4967	3,5620	3,4843
Ca	0,9684	1,4488	0,7726	0,2466	1,3379	1,6214	0,4666	1,4894	1,6179	0,9689	1,2915
Fe	3,7587	3,9057	3,9939	5,4471	4,4631	4,3019	4,7846	3,9836	3,8901	3,1193	4,2254
Mn	0,4556	0,1770	0,1853	0,8123	0,1187	0,2599	0,2167	0,1053	0,1044	0,1101	0,2308
Cr	0,0064	0,0053	-0,0033	0,0231	0,0090	-0,0018	0,0118	-0,0004	0,0222	-0,0047	0,0194
Mg	0,9126	0,5882	1,2743	0,3815	0,6722	0,4207	1,1154	0,8880	0,8286	1,8471	0,7239
Na	-0,0001	-0,0029	-0,0001	0,0021	0,0001	0,0015	0,0009	0,0001	0,0020	-0,0004	0,0008
K	0,0005	0,0005	-0,0001	0,0001	0,0006	0,0003	0,0014	-0,0012	0,0003	-0,0009	-0,0001
Ti	0,0001	0,0020	0,0315	0,0044	0,0272	0,0354	0,0213	0,0178	0,0100	0,0150	0,0208
Total	16,0491	16,0649	16,0977	16,3096	16,1729	16,1922	16,1725	16,1054	16,1119	15,9177	16,1273
Mol % end members											
Pyrope	14,9561	9,5995	20,3754	5,5167	10,1412	6,3381	16,8585	13,6956	12,8006	30,5016	11,1167
Almandine	61,6001	63,7463	63,8590	78,7727	67,3367	64,8127	72,3145	61,4400	60,0956	51,5108	64,8879
Spessartine	7,4666	2,8893	2,9625	11,7472	1,7906	3,9163	3,2754	1,6235	1,6123	1,8186	3,5450
Grossular	15,8711	23,6458	12,3526	3,5656	20,1856	24,4276	7,0516	22,9720	24,9943	15,9997	19,8330
Uvarite	0,1044	0,0869	-0,0530	0,3344	0,1360	-0,0276	0,1777	-0,0056	0,3428	-0,0780	0,2985
Andradite	0,0016	0,0322	0,5035	0,0633	0,4099	0,5328	0,3222	0,2745	0,1544	0,2473	0,3190
Alm+Spe	69,0668	66,6356	66,8215	90,5199	69,1273	68,7290	75,5900	63,0634	61,7079	53,3294	68,4329

Wt % from EMP analysis- SAMPLE TDP 9/13/1															
	1	**2**	**3**	**4**	**5**	**6**	**7**	**8**	**9**	**10**	**11**	**12**	**13**	**14**	**15**
SiO2	37,6816	37,9143	37,5391	37,8522	38,4107	37,9352	37,5939	38,1187	37,6344	37,9415	37,62	37,9385	39,1462	38,0466	36,8829
Al2O3	20,6951	21,0056	18,2011	21,1766	21,4118	21,1041	21,1319	21,0107	21,108	21,0213	21,0199	21,4508	22,1995	21,0319	19,8126
CaO	9,1102	7,8427	19,7642	11,6118	5,8749	7,4882	9,2069	5,9237	7,6681	7,2976	6,2297	3,5287	0,9986	7,9045	12,5914
FeO	26,0878	27,9954	7,3937	24,2971	26,0004	26,8887	27,7719	30,4057	28,3073	26,3473	28,5227	27,0262	25,1362	28,211	20,8444
MnO	0,5875	1,1158	16,0421	1,2099	1,4918	0,9506	1,3197	1,1773	0,8849	1,9814	2,73	2,7717	1,7804	1,066	8,336
Cr2O3	0,0271	0,0487	0,0187	0,083	-0,0223	0	0,0089	0,0059	0,1127	-0,003	-0,0708	-0,0074	0,0074	0,0401	-0,0422
MgO	4,2175	3,4984	0,2043	3,0911	6,1516	4,9395	2,5275	3,4143	3,607	4,8166	3,9121	6,4813	10,6556	3,572	0,5168
Na2O	0,0367	-0,0199	0,0253	0,0114	-0,0007	0,0186	0,0015	0,0088	0,0131	0,0144	0,0219	0,0129	0,0368	-0,0145	0,0262
K2O	0,0107	0,0125	-0,0047	0,0316	0,0067	0,0188	0,0121	0,0074	0,0151	0,0446	0,014	0,0204	0,0176	0,0085	0,0025
TiO2	0,0736	0,0309	0,2978	0,0295	0,0075	0,053	0,0791	0,0212	0,0187	0,0221	0,0424	0,0234	0,0217	0,0641	0,1283
Total	98,5278	99,4444	99,4816	99,3942	99,3324	99,3967	99,6534	100,0936	99,3693	99,4838	100,0419	99,2465	100	99,9301	99,0989
Structure formula based on 24 O															
Si	6,0089	6,0246	6,0464	5,9879	6,0196	5,9908	5,9884	6,0465	5,9899	5,9972	5,9758	5,9804	5,9796	6,1456	6,0637
Al	3,8898	3,9342	3,4555	3,9486	3,9552	3,9283	3,9677	3,9283	3,9599	3,9165	3,9356	3,9856	3,9969	3,3973	3,2573
Ca	1,5566	1,3353	3,4110	1,9682	0,9865	1,2671	1,5715	1,0068	1,3077	1,2360	1,0603	0,5960	0,1634	1,2768	2,0701
Fe	3,4792	3,7204	0,9960	3,2145	3,4078	3,5513	3,6998	4,0336	3,7680	3,4829	3,7892	3,5630	3,2111	4,5569	3,4269
Mn	0,0794	0,1502	2,1887	0,1621	0,1980	0,1272	0,1781	0,1582	0,1193	0,2653	0,3673	0,3701	0,2304	0,1722	1,3705
Cr	0,0051	0,0092	0,0036	0,0156	-0,0041	0,0000	0,0017	0,0011	0,0213	-0,0006	-0,0133	-0,0014	0,0013	0,0097	-0,0104
Mg	1,0028	0,8289	0,0491	0,7291	1,4375	1,1631	0,6003	0,8075	0,8560	1,1352	0,9266	1,5234	2,4269	0,5770	0,0850
Na	0,0057	-0,0031	0,0040	0,0017	-0,0001	0,0028	0,0002	0,0014	0,0020	0,0022	0,0034	0,0020	0,0054	-0,0012	0,0022
K	0,0011	0,0013	-0,0005	0,0032	0,0007	0,0019	0,0012	0,0007	0,0015	0,0045	0,0014	0,0021	0,0017	0,0007	0,0002
Ti	0,0177	0,0074	0,0722	0,0070	0,0018	0,0126	0,0190	0,0051	0,0045	0,0053	0,0101	0,0055	0,0050	0,0207	0,0422
Total	16,0462	16,0083	16,2259	16,0379	16,0028	16,0451	16,0278	15,9893	16,0301	16,0445	16,0564	16,0267	16,0219	16,1557	16,3076
Mol % end members															
Pyrope	16,3303	13,6975	0,7301	11,9594	23,8489	19,0012	9,8895	13,4314	14,0866	18,5366	15,0905	25,1524	40,1930	8,7246	1,2165
Almandine	56,6572	61,4804	14,8200	52,7264	56,5377	58,0157	60,9493	67,0891	62,0063	56,8727	61,7108	58,8275	53,1803	68,9050	49,0665
Spessartine	1,2923	2,4818	32,5674	2,6592	3,2855	2,0773	2,9334	2,6310	1,9632	4,3319	5,9823	6,1105	3,8151	2,6037	19,6225
Grossular	25,3492	22,0665	50,7556	32,2844	16,3673	20,7001	25,8878	16,7459	21,5201	20,1821	17,2686	9,8408	2,7068	19,3067	29,6394
Uvarite	0,0835	0,1517	0,0532	0,2554	-0,0688	0,0000	0,0277	0,0185	0,3501	-0,0092	-0,2172	-0,0228	0,0222	0,1469	-0,1490
Andradite	0,2876	0,1221	1,0738	0,1152	0,0293	0,2057	0,3123	0,0841	0,0737	0,0858	0,1650	0,0916	0,0826	0,3131	0,6040
Alm+Spe	57,9495	63,9622	47,3874	55,3857	59,8232	60,0930	63,8827	69,7201	63,9696	61,2046	67,6932	64,9380	56,9954	71,5087	68,6890

Wt % from EMP analysis- SAMPLE TDP 7B/12/2																	
	1	**2**	**3**	**4**	**5**	**6**	**7**	**8**	**9**	**10**	**11**	**12**	**13**	**14**	**15**	**16**	**17**
SiO2	38,2210	37,4476	38,2054	39,3201	38,1115	37,9636	37,9041	37,5549	38,3394	39,1917	39,1138	38,8622	38,9476	38,0141	38,0910	37,7941	39,4566
Al2O3	21,6692	20,9617	21,6450	22,2864	21,2507	21,6044	21,2362	23,7751	21,0767	22,1241	22,0282	21,8429	22,0378	21,0444	21,3078	21,1924	22,1367
CaO	8,0696	5,7799	2,1444	1,8166	6,5850	9,3694	7,8482	23,3445	6,7828	7,5137	7,7810	1,0929	1,3064	6,4047	4,6364	6,5269	1,8005
FeO	25,8472	29,9305	30,9259	24,9244	26,6601	26,9200	28,0446	10,9201	27,1840	23,7295	23,7889	29,8515	23,6444	26,9963	28,7737	27,6036	24,7507
MnO	0,8743	1,9827	1,2811	0,8671	1,3987	0,9045	0,7134	0,2418	0,9879	0,6559	0,6309	1,5476	3,6856	0,6982	0,6381	2,2260	0,8540
Cr2O3	0,0203	0,0076	0,0167	0,0295	0,0481	-0,0109	-0,0093	0,0232	0,0171	-0,0236	0,0079	0,0122	0,0155	-0,0078	0,0430	0,0556	0,0078
MgO	5,3330	3,2035	6,5612	10,9271	5,9102	3,4793	4,1532	0,0109	6,0250	7,4816	7,1941	7,8416	10,5476	6,2844	5,7838	4,3769	11,0069
Na2O	-0,0068	0,0156	-0,0015	0,0183	0,0143	0,0122	0,0053	0,0098	0,0091	0,0184	0,0162	0,0213	0,0096	0,0264	0,0137	0,0146	0,0408
K2O	0,0164	0,0031	0,0165	0,0190	0,0152	0,0074	-0,0058	0,0251	0,0023	0,0161	0,0145	0,0071	0,0083	-0,0027	0,0066	0,0082	0,0131
TiO2	0,0088	-0,0043	0,0153	-0,0016	-0,0040	0,0581	0,0008	0,1711	0,0552	0,0104	0,0188	0,0313	0,0158	0,0079	0,0394	0,0766	0,0242
Total	100,0529	99,3278	100,8099	100,2069	99,9899	100,3078	99,8907	96,0764	100,4794	100,7178	100,5943	101,1107	100,2186	99,4659	99,3335	99,8750	100,0913
Structure formula based on 24 O																	
Si	5,9662	6,0053	5,9633	5,9755	5,9697	5,9659	5,9846	5,9366	5,9796	5,9864	5,9894	5,9953	5,9561	5,9761	6,0073	5,9774	5,9968
Al	3,9869	3,9623	3,9822	3,9921	3,9235	4,0018	3,9521	4,4299	3,8747	3,9833	3,9759	3,9719	3,9724	3,8995	3,9609	3,9506	3,9657
Ca	1,3497	0,9932	0,3586	0,2958	1,1052	1,5777	1,3277	3,9541	1,1335	1,2298	1,2767	0,1807	0,2141	1,0789	0,7835	1,1061	0,2932
Fe	3,3743	4,0142	4,0370	3,1678	3,4925	3,5380	3,7032	1,4437	3,5458	3,0313	3,0465	3,8515	3,0240	3,5494	3,7951	3,6511	3,1460
Mn	0,1156	0,2693	0,1694	0,1116	0,1856	0,1204	0,0954	0,0324	0,1305	0,0849	0,0818	0,2022	0,4774	0,0930	0,0852	0,2982	0,1099
Cr	0,0038	0,0014	0,0031	0,0053	0,0089	-0,0020	-0,0017	0,0043	0,0032	-0,0043	0,0014	0,0022	0,0028	-0,0015	0,0080	0,0104	0,0014
Mg	1,2413	0,7660	1,5270	2,4761	1,3804	0,8153	0,9777	0,0026	1,4011	1,7040	1,6426	1,8038	2,4051	1,4731	1,3601	1,0322	2,4944
Na	-0,0010	0,0024	-0,0002	0,0027	0,0022	0,0019	0,0008	0,0015	0,0014	0,0027	0,0024	0,0032	0,0014	0,0040	0,0021	0,0022	0,0060
K	0,0016	0,0003	0,0016	0,0018	0,0015	0,0007	-0,0006	0,0025	0,0002	0,0016	0,0014	0,0007	0,0008	-0,0003	0,0007	0,0008	0,0013
Ti	0,0021	-0,0010	0,0036	-0,0004	-0,0009	0,0137	0,0002	0,0407	0,0130	0,0024	0,0043	0,0073	0,0036	0,0019	0,0093	0,0182	0,0055
Total	16,0404	16,0135	16,0456	16,0284	16,0685	16,0332	16,0394	15,8484	16,0830	16,0220	16,0226	16,0187	16,0577	16,0741	16,0123	16,0473	16,0203
Mol % end members																	
Pyrope	20,3930	12,6757	25,0382	40,8844	22,3664	13,4464	16,0221	0,0469	22,5007	28,1739	27,1350	29,8263	39,2537	23,7800	22,5130	16,8758	41,2259
Almandine	55,4373	66,4261	66,1943	52,3065	56,5892	58,3537	60,6826	26,3553	56,9416	50,1210	50,3275	63,6854	49,3553	57,2967	62,8194	59,6956	51,9961
Spessartine	1,8993	4,4567	2,7773	1,8430	3,0070	1,9858	1,5634	0,5911	2,0959	1,4032	1,3518	3,3440	7,7920	1,5009	1,4110	4,8757	1,8171
Grossular	22,1748	16,4348	5,8806	4,8844	17,9080	26,0210	21,7572	72,1845	18,2031	20,3331	21,0904	2,9873	3,4938	17,4158	12,9687	18,0843	4,8461
Uvarite	0,0617	0,0239	0,0507	0,0878	0,1448	-0,0335	-0,0285	0,0794	0,0508	-0,0707	0,0237	0,0369	0,0459	-0,0235	0,1331	0,1705	0,0232
Andradite	0,0340	-0,0172	0,0589	-0,0060	-0,0153	0,2266	0,0031	0,7429	0,2080	0,0395	0,0715	0,1201	0,0593	0,0302	0,1547	0,2980	0,0915
Alm+Spe	57,3365	70,8828	68,9716	54,1495	59,5962	60,3395	62,2461	26,9463	59,0375	51,5241	51,6794	67,0294	57,1473	58,7976	64,2304	64,5713	53,8132

Wt % from EMP analysis- SAMPLE TDP 2/14/2															
	1	**2**	**3**	**4**	**5**	**6**	**7**	**8**	**9**	**10**	**11**	**12**	**13**	**14**	**15**
SiO2	38,5235	37,9715	37,7650	37,2986	38,1440	38,7004	38,9126	38,9587	37,7285	38,8170	38,2356	38,1405	38,4305	39,2202	38,527
Al2O3	21,6319	21,4493	21,2884	20,8808	21,4452	21,1674	21,4646	21,7298	20,9818	21,2004	21,0781	21,2559	21,1667	21,7200	38,5270
CaO	9,9925	7,0849	4,8974	3,8996	7,7803	7,2069	6,7068	6,9867	7,0146	6,9256	7,2658	6,6577	6,6163	3,9683	21,5865
FeO	24,5938	27,5450	29,7497	23,0382	26,4120	27,1086	27,0192	26,4840	28,2844	26,3903	29,1032	27,1606	26,4381	25,5895	7,5656
MnO	0,7851	1,3179	2,0629	12,3840	1,2292	0,9032	0,7894	1,3812	1,8968	1,1310	0,7076	1,1380	0,9144	0,6340	25,5519
Cr2O3	0,0030	0,0059	0,0147	-0,0221	0,0105	0,0552	0,0134	0,0478	0,0030	-0,0030	0,0104	0,0104	0,0015	0,0119	1,3275
MgO	5,0079	4,7335	4,2882	1,8924	5,1709	5,6261	5,9180	5,6774	4,2320	5,7290	4,2283	5,4837	6,3905	9,1806	0,0180
Na2O	0,0099	0,0036	0,0212	0,0482	-0,0064	-0,0007	0,0057	0,0078	0,0283	-0,0093	0,0653	0,0050	0,0234	0,0223	5,8742
K2O	0,0052	0,0148	-0,0004	0,0092	-0,0059	0,0092	0,0044	-0,0018	-0,0011	0,0178	0,0111	-0,0059	0,0404	0,0026	-0,0113
TiO2	0,0587	0,0266	0,1968	0,0000	0,0256	0,0518	0,0132	0,0703	0,0631	0,0444	0,0135	0,0634	0,0519	0,0327	-0,0007
Total	100,6115	100,1531	100,2838	99,4288	100,2052	100,8281	100,8473	101,3419	100,2314	100,2431	100,7187	99,9093	100,0736	100,3822	0,0331
Structure formula based on 24 O															
Si	5,9724	5,9669	5,9718	6,0362	5,9669	6,0109	6,0215	6,0022	5,9663	6,0425	6,0028	5,9844	6,1857	6,2549	6,1709
Al	3,9530	3,9729	3,9679	3,9831	3,9542	3,8752	3,9150	3,9461	3,9109	3,8899	3,9005	3,9311	3,4069	3,4639	3,4575
Ca	1,6599	1,1929	0,8298	0,6762	1,3041	1,1994	1,1120	1,1534	1,1886	1,1552	1,2223	1,1193	1,0649	0,6329	1,2118
Fe	3,1888	3,6200	3,9344	3,1181	3,4554	3,5213	3,4967	3,4125	3,7407	3,4357	3,8212	3,5641	4,2554	4,0810	4,0927
Mn	0,1031	0,1754	0,2763	1,6976	0,1629	0,1188	0,1035	0,1803	0,2541	0,1491	0,0941	0,1512	0,1472	0,1011	0,2126
Cr	0,0006	0,0011	0,0028	-0,0042	0,0019	0,0102	0,0025	0,0087	0,0006	-0,0006	0,0019	0,0019	0,0004	0,0028	0,0043
Mg	1,1577	1,1091	1,0111	0,4566	1,2061	1,3029	1,3655	1,3042	0,9979	1,3298	0,9898	1,2829	1,0286	1,4641	0,9409
Na	0,0015	0,0005	0,0033	0,0076	-0,0010	-0,0001	0,0009	0,0012	0,0043	-0,0014	0,0099	0,0008	0,0019	0,0018	-0,0009
K	0,0005	0,0015	0,0000	0,0009	-0,0006	0,0009	0,0004	-0,0002	-0,0001	0,0018	0,0011	-0,0006	0,0033	0,0002	-0,0001
Ti	0,0137	0,0063	0,0468	0,0000	0,0060	0,0121	0,0031	0,0163	0,0150	0,0104	0,0032	0,0150	0,0167	0,0104	0,0106
Total	16,0511	16,0467	16,0442	15,9722	16,0560	16,0516	16,0210	16,0247	16,0783	16,0125	16,0469	16,0501	16,1109	16,0132	16,1003
Mol % end members															
Pyrope	18,9044	18,1675	16,5721	7,6820	19,6547	21,1354	22,4465	21,4676	16,1030	21,8724	16,1403	20,9135	15,7925	23,2682	14,5356
Almandine	52,0727	59,2971	64,4856	52,4551	56,3094	57,1200	57,4811	56,1689	60,3651	56,5119	62,3109	58,0992	65,3352	64,8564	63,2279
Spessartine	1,6836	2,8735	4,5289	28,5585	2,6542	1,9275	1,7009	2,9669	4,1001	2,4530	1,5344	2,4655	2,2597	1,6069	3,2849
Grossular	27,1067	19,5409	13,6008	11,3757	21,2517	19,4558	18,2805	18,9847	19,1805	19,0008	19,9308	18,2463	16,3505	10,0576	18,7210
Uvarite	0,0090	0,0180	0,0452	-0,0714	0,0317	0,1649	0,0404	0,1438	0,0091	-0,0091	0,0316	0,0315	0,0056	0,0452	0,0668
Andradite	0,2236	0,1030	0,7674	0,0000	0,0982	0,1963	0,0505	0,2682	0,2423	0,1710	0,0520	0,2440	0,2565	0,1658	0,1638
Alm+Spe	53,7563	62,1706	69,0145	81,0137	58,9636	59,0475	59,1821	59,1358	64,4652	58,9649	63,8453	60,5647	67,5949	66,4632	66,5128

Wt % from EMP analysis- SAMPLE TDP 1/18/1													
	1	**2**	**3**	**4**	**5**	**6**	**7**	**8**	**9**	**10**	**11**	**12**	**13**
SiO2	38,1253	37,7008	38,6166	38,3307	38,4906	36,6827	37,7410	37,2892	39,1342	38,5062	37,4362	38,2308	36,7715
Al2O3	21,2384	21,4023	21,7487	21,3221	21,5833	20,4760	20,9839	20,8297	22,0947	21,2204	21,1603	21,5045	21,1066
CaO	9,7475	12,8767	6,0668	6,3918	6,1359	0,8550	9,2563	4,5023	1,6218	6,3641	10,7249	10,4778	6,1803
FeO	25,8414	23,2075	26,1758	24,8052	25,3073	28,7917	27,9581	28,4556	26,3231	27,4166	26,7580	22,5487	31,6702
MnO	2,1646	2,5762	0,7457	1,1217	0,7990	11,0350	1,2664	5,4728	0,3359	0,7311	1,9137	0,8410	1,8984
Cr2O3	0,0561	0,0209	0,0839	-0,0059	0,0280	0,0397	0,0248	0,0332	0,1830	-0,0132	0,0427	0,0224	0,0317
MgO	3,3572	2,1413	6,9374	7,8712	7,3407	1,8325	2,4355	2,7989	10,4159	5,9848	1,9400	5,7161	2,2634
Na2O	0,0072	0,0292	0,0035	0,0147	0,0281	0,0640	0,0169	0,0482	0,0376	0,0364	0,0044	-0,0028	0,0261
K2O	-0,0040	0,0018	0,0093	0,0004	0,0241	0,0106	0,0271	0,0055	0,0210	0,0270	0,0139	0,0063	0,0125
TiO2	0,0376	0,0754	0,0650	0,1029	0,0603	0,0162	0,0301	0,0354	0,0172	0,0533	0,0312	0,0331	0,0152
Total	100,5713	100,0320	100,4527	99,9548	99,7973	99,8034	99,7401	99,4708	100,1845	100,3266	100,0252	99,3778	99,9759
Structure formula based on 24 O													
Si	5,9873	5,9531	5,9693	5,9426	5,9725	5,9979	6,0107	6,0071	5,9749	6,0033	5,9588	5,9627	5,9211
Al	3,9314	3,9834	3,9627	3,8964	3,9475	3,9462	3,9391	3,9552	3,9762	3,8996	3,9700	3,9533	4,0060
Ca	1,6402	2,1787	1,0049	1,0618	1,0202	0,1498	1,5796	0,7772	0,2653	1,0631	1,8292	1,7510	1,0663
Fe	3,3940	3,0648	3,3840	3,2163	3,2842	3,9371	3,7239	3,8338	3,3612	3,5748	3,5620	2,9412	4,2650
Mn	0,2879	0,3446	0,0976	0,1473	0,1050	1,5283	0,1708	0,7468	0,0434	0,0965	0,2580	0,1111	0,2589
Cr	0,0104	0,0039	0,0154	-0,0011	0,0052	0,0077	0,0047	0,0063	0,0331	-0,0024	0,0081	0,0041	0,0061
Mg	0,7861	0,5042	1,5990	1,8196	1,6984	0,4468	0,5784	0,6723	2,3712	1,3913	0,4604	1,3293	0,5434
Na	0,0011	0,0045	0,0005	0,0022	0,0042	0,0101	0,0026	0,0075	0,0056	0,0055	0,0007	-0,0004	0,0041
K	-0,0004	0,0002	0,0009	0,0000	0,0024	0,0011	0,0028	0,0006	0,0020	0,0027	0,0014	0,0006	0,0013
Ti	0,0089	0,0179	0,0151	0,0240	0,0141	0,0040	0,0072	0,0086	0,0040	0,0125	0,0075	0,0078	0,0037
Total	16,0470	16,0552	16,0494	16,1092	16,0537	16,0290	16,0197	16,0153	16,0370	16,0469	16,0562	16,0607	16,0759
Mol % end members													
Pyrope	12,8292	8,2460	26,1445	29,0302	27,7199	7,3557	9,5367	11,1218	39,0116	22,6744	7,5171	21,6339	8,8458
Almandine	55,3883	50,1270	55,3302	51,3134	53,6017	64,8224	61,4039	63,4209	55,2984	58,2611	58,1537	47,8669	69,4235
Spessartine	4,6991	5,6358	1,5965	2,3502	1,7140	25,1632	2,8171	12,3541	0,7147	1,5735	4,2124	1,8082	4,2148
Grossular	26,7679	35,6342	16,4301	16,9406	16,6506	2,4663	26,0462	12,8564	4,3651	17,3269	29,8632	28,4972	17,3574
Uvarite	0,1705	0,0640	0,2515	-0,0173	0,0841	0,1268	0,0772	0,1049	0,5452	-0,0398	0,1316	0,0674	0,0985
Andradite	0,1450	0,2930	0,2472	0,3829	0,2298	0,0656	0,1189	0,1419	0,0650	0,2038	0,1220	0,1264	0,0599
Alm+Spe	60,0874	55,7628	56,9267	53,6635	55,3157	89,9857	64,2209	75,7750	56,0131	59,8347	62,3662	49,6751	73,6383

Wt % from EMP analysis- SAMPLE TDP 1/18/1 cont.													
	14	**15**	**16**	**17**	**18**	**19**	**20**	**21**	**22**	**23**	**24**	**25**	**26**
SiO2	38,0407	38,4318	38,3108	38,5960	38,0981	37,5658	36,8682	37,8670	37,9487	39,5667	36,4782	37,6964	39,0319
Al2O3	21,5920	21,5790	21,6690	21,4392	21,5533	21,2159	21,1622	21,3963	21,2169	21,8573	20,5877	21,4478	21,8581
CaO	5,5817	6,3766	8,9839	8,5947	9,1516	1,7873	1,0371	2,2112	6,8604	6,9162	1,2865	1,0830	1,7630
FeO	27,7434	26,6310	24,2076	24,9838	26,5686	30,2270	34,1756	29,9668	27,0688	22,7010	22,8323	32,4084	27,5696
MnO	2,0319	1,0051	1,0124	1,0176	0,8482	1,4903	3,4167	2,1361	1,4983	0,8452	16,5143	1,0802	0,8627
Cr2O3	-0,0088	0,0015	-0,0074	0,0252	-0,0325	-0,0057	0,0000	0,0115	0,0073	0,0254	0,0244	0,0727	0,0247
MgO	5,3659	6,2458	5,9709	5,8372	3,9549	6,8625	3,0807	6,6224	5,3985	8,6237	2,0641	5,9052	8,9375
Na2O	0,0130	0,0746	0,0098	0,0261	0,0222	0,0363	0,0174	0,0269	0,0222	0,0255	0,0068	0,0162	0,0141
K2O	0,0089	-0,0011	-0,0030	-0,0033	0,0221	0,0200	0,0206	0,0137	0,0081	0,0223	0,0026	0,0104	0,0131
TiO2	0,0224	0,0747	0,0208	0,0483	0,0459	0,0189	0,0098	-0,0007	0,0465	0,0630	0,0537	0,0099	0,0608
Total	100,3912	100,4190	100,1747	100,5648	100,2324	99,2184	99,7884	100,2512	100,0757	100,6463	99,8505	99,7303	100,1355
Structure formula based on 24 O													
Si	5,9592	5,9711	5,9475	5,9803	5,9757	5,9549	5,9634	5,9506	5,9596	6,0135	5,9550	5,9748	6,0105
Al	3,9869	3,9518	3,9651	3,9155	3,9848	3,9641	4,0346	3,9631	3,9274	3,9156	3,9615	4,0069	3,9674
Ca	0,9369	1,0616	1,4944	1,4269	1,5381	0,3036	0,1797	0,3723	1,1544	1,1263	0,2250	0,1839	0,2909
Fe	3,6348	3,4604	3,1430	3,2375	3,4852	4,0073	4,6231	3,9383	3,5552	2,8855	3,1173	4,2959	3,5505
Mn	0,2696	0,1323	0,1331	0,1336	0,1127	0,2001	0,4681	0,2843	0,1993	0,1088	2,2836	0,1450	0,1125
Cr	-0,0016	0,0003	-0,0014	0,0046	-0,0060	-0,0011	0,0000	0,0021	0,0014	0,0046	0,0047	0,0137	0,0045
Mg	1,2534	1,4469	1,3821	1,3486	0,9250	1,6220	0,7430	1,5517	1,2641	1,9543	0,5024	1,3956	2,0521
Na	0,0020	0,0112	0,0015	0,0039	0,0034	0,0056	0,0027	0,0041	0,0034	0,0038	0,0011	0,0025	0,0021
K	0,0009	-0,0001	-0,0003	-0,0003	0,0022	0,0020	0,0021	0,0014	0,0008	0,0022	0,0003	0,0011	0,0013
Ti	0,0053	0,0175	0,0049	0,0113	0,0108	0,0045	0,0024	-0,0002	0,0110	0,0144	0,0132	0,0024	0,0141
Total	16,0473	16,0530	16,0699	16,0619	16,0319	16,0631	16,0193	16,0679	16,0767	16,0288	16,0642	16,0217	16,0059
Mol % end members													
Pyrope	20,5528	23,6469	22,4513	21,8839	15,2488	26,4328	12,3497	25,2364	20,4372	32,0697	8,1746	23,1191	34,0618
Almandine	59,6027	56,5525	51,0542	52,5359	57,4576	65,3031	76,8423	64,0518	57,4773	47,3505	50,7182	71,1660	58,9333
Spessartine	4,4212	2,1618	2,1626	2,1673	1,8579	3,2610	7,7808	4,6243	3,2223	1,7856	37,1544	2,4025	1,8678
Grossular	15,3635	17,3489	24,2752	23,1551	25,3568	4,9471	2,9876	6,0553	18,6636	18,4827	3,6614	3,0469	4,8284
Uvarite	-0,0268	0,0045	-0,0221	0,0751	-0,0997	-0,0175	0,0000	0,0349	0,0220	0,0751	0,0769	0,2264	0,0749
Andradite	0,0866	0,2854	0,0789	0,1827	0,1786	0,0735	0,0396	-0,0027	0,1776	0,2364	0,2146	0,0391	0,2338
Alm+Spe	64,0239	58,7143	53,2167	54,7032	59,3155	68,5641	84,6231	68,6761	60,6996	49,1361	87,8726	73,5685	60,8011

Wt % from EMP analysis- SAMPLE 2/1/14																	
	1	**2**	**3**	**4**	**5**	**6**	**7**	**8**	**9**	**10**	**11**	**12**	**13**	**14**	**15**	**16**	**17**
SiO2	38,1853	38,0024	37,2089	37,4673	37,4501	38,8889	38,2394	38,9879	39,0432	37,1527	39,0004	38,3192	37,7360	37,8547	37,5390	38,6780	39,5338
Al2O3	21,3697	21,3908	21,3985	21,2569	21,3075	22,0453	21,5379	22,2225	21,8375	20,0841	22,1506	21,6784	21,1493	20,5856	21,2274	21,6330	22,6114
CaO	2,2078	3,0431	1,4743	1,5585	1,5122	1,3926	3,6707	1,1764	7,2014	10,6526	1,1794	1,5306	7,5849	13,0676	2,8331	2,3967	1,1584
FeO	30,9360	31,4298	30,9915	30,7748	33,9980	27,7204	26,8301	26,7462	25,1903	22,2067	26,2279	31,1054	28,5443	24,9374	32,2258	29,9146	24,3085
MnO	1,3554	0,8954	2,4092	2,3372	1,4943	0,6236	2,6061	0,3787	0,3531	8,8102	0,4200	0,9034	2,1814	1,3079	1,2069	0,7895	0,4479
Cr2O3	0,1261	0,0366	0,0589	0,0636	-0,0253	0,1179	0,0423	0,0631	0,0104	0,0000	0,0401	0,0530	0,0000	0,0164	0,0014	0,1340	-0,0172
MgO	6,0418	5,5815	6,2159	6,1827	4,3707	9,6960	7,2856	10,1253	6,8807	1,2227	10,9974	7,0478	2,7095	1,9932	5,1797	6,8443	12,1738
Na2O	0,0077	-0,0155	0,0109	0,0967	0,0251	0,0052	-0,0007	-0,0096	-0,0084	0,0000	-0,0169	0,0367	0,0217	0,0029	0,0081	0,0023	0,0231
K2O	0,0153	0,0082	-0,0063	0,1503	-0,0093	0,0098	0,0026	0,0036	0,0130	0,0038	0,0059	0,0016	0,0089	0,0022	-0,0030	-0,0016	-0,0052
TiO2	0,0125	0,0432	0,0179	0,0121	-0,0039	0,0467	0,0224	0,0524	0,0975	0,1149	0,0612	0,0207	0,0130	0,0493	-0,0140	0,0286	0,0187
Total	100,2576	100,4154	99,7797	99,9000	100,1195	100,5465	100,2364	99,7466	100,6187	100,2478	100,0660	100,6967	99,9492	99,8170	100,2045	100,4194	100,2533
Structure formula based on 24 O																	
SiO2	1,2709	1,2648	1,2384	1,2470	1,2465	1,2944	1,2727	1,2977	1,2995	1,2366	1,2981	1,2754	1,2560	1,2599	1,2494	1,2873	1,3158
Al2O3	0,6288	0,6294	0,6296	0,6254	0,6269	0,6486	0,6337	0,6539	0,6425	0,5909	0,6517	0,6379	0,6223	0,5139	0,5299	0,5400	0,5644
CaO	0,0394	0,0543	0,0263	0,0278	0,0270	0,0248	0,0655	0,0210	0,1284	0,1900	0,0210	0,0273	0,1353	0,2175	0,0471	0,0399	0,0193
FeO	0,4306	0,4374	0,4313	0,4283	0,4732	0,3858	0,3734	0,3723	0,3506	0,3091	0,3650	0,4329	0,3973	0,4150	0,5363	0,4978	0,4045
MnO	0,0191	0,0126	0,0340	0,0329	0,0211	0,0088	0,0367	0,0053	0,0050	0,1242	0,0059	0,0127	0,0307	0,0218	0,0201	0,0131	0,0075
Cr2O3	0,0025	0,0007	0,0012	0,0013	-0,0005	0,0023	0,0008	0,0012	0,0002	0,0000	0,0008	0,0010	0,0000	0,0004	0,0000	0,0033	-0,0004
MgO	0,1499	0,1385	0,1542	0,1534	0,1085	0,2406	0,1808	0,2512	0,1707	0,0303	0,2729	0,1749	0,0672	0,0332	0,0862	0,1139	0,2026
Na2O	0,0001	-0,0003	0,0002	0,0016	0,0004	0,0001	0,0000	-0,0002	-0,0001	0,0000	-0,0003	0,0006	0,0004	0,0000	0,0001	0,0000	0,0002
K2O	0,0002	0,0001	-0,0001	0,0016	-0,0001	0,0001	0,0000	0,0000	0,0001	0,0000	0,0001	0,0000	0,0001	0,0000	0,0000	0,0000	0,0000
TiO2	0,0003	0,0011	0,0004	0,0003	-0,0001	0,0012	0,0006	0,0013	0,0024	0,0029	0,0015	0,0005	0,0003	0,0016	-0,0005	0,0010	0,0006
total	2,5418	2,5387	2,5156	2,5197	2,5028	2,6067	2,5643	2,6038	2,5994	2,4840	2,6168	2,5632	2,5095	2,4633	2,4687	2,4964	2,5145
Mol % end members																	
Pyrope	23,3608	21,4852	23,8232	23,8213	17,2405	36,2603	27,4836	38,5130	25,9728	4,6219	40,9005	26,9301	10,6578	4,8111	12,5054	17,0242	31,9521
Almandine	67,0910	67,8591	66,6220	66,5060	75,2194	58,1455	56,7687	57,0611	53,3331	47,0833	54,7118	66,6651	62,9761	60,1927	77,8033	74,4083	63,8015
Spessartine	2,9772	1,9580	5,2455	5,1156	3,3485	1,3248	5,5849	0,8183	0,7572	18,9193	0,8874	1,9610	4,8745	3,1569	2,9138	1,9638	1,1756
Grossular	6,1345	8,4179	4,0605	4,3151	4,2865	3,7425	9,9507	3,2155	19,5344	28,9372	3,1521	4,2028	21,4400	31,5419	6,8400	5,9615	3,0404
Uvarite	0,3878	0,1121	0,1796	0,1949	-0,0794	0,3507	0,1269	0,1909	0,0312	0,0000	0,1186	0,1611	0,0000	0,0594	0,0051	0,5000	-0,0677
Andradite	0,0488	0,1678	0,0692	0,0470	-0,0155	0,1762	0,0853	0,2011	0,3714	0,4382	0,2297	0,0798	0,0516	0,2380	-0,0676	0,1423	0,0982
Alm+Spe	70,0681	69,8171	71,8675	71,6216	78,5679	59,4703	62,3535	57,8794	54,0903	66,0026	55,5991	68,6261	67,8506	63,3496	80,7171	76,3721	64,9771

Wt % from EMP analysis- SAMPLE 2/2/14		
	1	2
SiO2	37,6814	38,9334
Al2O3	20,9619	22,0598
CaO	6,6435	1,8822
FeO	30,0272	27,1991
MnO	1,8257	0,5315
Cr2O3	0,0107	-0,0046
MgO	2,8620	9,4871
Na2O	0,0148	0,0074
K2O	-0,0035	0,0075
TiO2	-0,0051	0,0863
Total	100,0188	100,1897
Structure formula based on 24 O		
Si	6,0095	5,9757
Al	3,9405	3,9909
Ca	1,1353	0,3095
Fe	4,0050	3,4914
Mn	0,2466	0,0691
Cr	0,0020	-0,0008
Mg	0,6806	2,1712
Na	0,0023	0,0011
K	-0,0004	0,0007
Ti	-0,0012	0,0199
Total	16,0202	16,0288
Mol % end members		
Pyrope	11,2153	35,8264
Almandine	65,9988	57,6106
Spessartine	4,0643	1,1402
Grossular	18,7084	5,1078
Uvarite	0,0334	-0,0138
Andradite	-0,0202	0,3288
Alm+Spe	70,0631	58,7508

Wt % from EMP analysis- SAMPLE Matandu River	
	1,0
SiO2	37,9163
Al2O3	21,0624
CaO	5,4039
FeO	28,3532
MnO	0,5022
Cr2O3	0,0458
MgO	6,2916
Na2O	0,0244
K2O	0,0018
TiO2	0,0385
Total	99,6401
Structure formula based on 24 O	
Si	5,9664
Al	3,9066
Ca	0,9112
Fe	3,7314
Mn	0,0669
Cr	0,0085
Mg	1,4762
Na	0,0037
K	0,0002
Ti	0,0091
Total	16,0803
Mol % end members	
Pyrope	23,7971
Almandine	60,1510
Spessartine	1,0791
Grossular	14,6881
Uvarite	0,1378
Andradite	0,1469
Alm+Spe	61,2301

Appendix – E2 - Electron Microprobe Analysis (EMP) rutile

	Sample MB-1-4-13					Sample MN-2-1-13							
	WT %												
Elements	**1,00**	**2,00**	**3,00**	**4,00**	**5,00**	**1,00**	**2,00**	**3,00**	**4,00**	**5,00**	**6,00**	**7,00**	**8,00**
Zr	0,05	0,09	0,01	0,06	0,01	0,44	0,01	0,23	0,00	0,11	0,14	0,03	0,01
Cr	0,12	0,07	0,17	0,07	0,00	0,05	0,04	0,15	0,04	0,08	0,06	0,24	0,08
Nb	0,26	0,15	0,09	0,70	0,89	0,38	0,15	0,06	0,05	0,17	0,15	0,10	0,26
Si	0,01	0,01	0,01	0,01	0,01	0,02	0,10	0,03	0,14	0,02	0,03	0,01	0,05
Fe	0,08	0,09	0,54	0,19	0,96	0,15	0,22	0,02	0,24	0,06	0,31	0,13	0,17
Ti	59,90	59,90	59,90	59,90	59,90	59,90	59,90	59,90	59,90	59,90	59,90	59,90	59,90
O	40,00	40,00	40,00	40,00	40,00	40,00	40,00	40,00	40,00	40,00	40,00	40,00	40,00
Total	100,42	100,31	100,71	100,93	101,78	100,94	100,42	100,38	100,38	100,33	100,58	100,41	100,47
	PPM												
Zr	463,00	879,00	102,00	605,00	116,00	4410,00	117,00	2308,00	17,00	1113,00	1356,00	328,00	81,00
Cr	1150,00	655,00	1658,00	677,00	38,00	529,00	356,00	1490,00	443,00	761,00	595,00	2405,00	798,00
Nb	2628,00	1522,00	899,00	7049,00	8916,00	3801,00	1505,00	607,00	485,00	1740,00	1468,00	1036,00	2621,00
Si	91,00	139,00	79,00	118,00	91,00	175,00	966,00	283,00	1426,00	170,00	277,00	110,00	459,00
Fe	821,00	917,00	5401,00	1877,00	9647,00	1466,00	2208,00	158,00	2429,00	554,00	3076,00	1264,00	1693,00
Ti	599000	599000	599000	599000	599000	599000	599000	599000	599000	599000	599000	599000	599000
O	400000	400000	400000	400000	400000	400000	400000	400000	400000	400000	400000	400000	400000